UNIVERSITÀ DEGLI STUDI DI MILANO

Scuola di dottorato di ricerca di Scienze biochimiche, nutrizionali e metaboliche

DOTTORATO DI RICERCA IN BIOCHIMICA
CICLO XXIII

TESI DI DOTTORATO DI RICERCA

Addressing the Molecular Basis of the Interaction Between Glycosaminoglycans, Mimetics and Proteins

Settore BIO/10

Dottorando
Davide Gaudesi

TUTORS:
Prof. Sandro Sonnino
Dott. Marco Guerrini

COORDINATORE DEL DOTTORATO
Prof. Francesco Bonomi

ANNO ACCADEMICO 2009/2010

Table of Content

Table of Content

Abbreviations & Definitions

1. Abbreviations & Definitions

1D	monodimensional
2D	two-dimensional
3D	three-dimensional
1,6 anG_{NS}	N-sulfo-amino-1,6-anhydro-2-deoxy-β-D-glucopyranose
1,6 anM_{NS}	N-sulfo-amino-1,6-anhydro-2-deoxy-β-D-mannopyranose
2,5 anM_{6S}	2,5-anhydro-6-O-sulfo-2-deoxy-β-D-mannopyranose
Aβ	amyloid-β
AT	Antithrombin III
COSY	Correlation Spectroscopy
CS	Chondroitin Sulfate
CW	Continuous-Wave
ΔU	4, 5-unsaturated uronic acid
DLS	Dynamic Light Scattering
DT	relaxation Delay Time
DS	Dermatan Sulfate
FGF(s)	Fibroblast Growth Factor(s)
FGFR(s)	FGF receptor(s)
FID	Free-Induction Decay
Fn	Fourier number
FT	Fourier Transform or Transformation
GAG(s)	Glycosaminoglycan(s)
GalA	Galacturonic acid
GlcA/G	β-D-glucuronic acid
GlcN	α-D-glucosamine
$GlcN_{NAc,6S}/A_{NA}$	N-acetylated, 6-O-sulfated-D-glucosamine
$GlcN_{NS}$	N-sulfated-D-glucosamine
$GlcN_{6S}$	6-O-sulfated-D-glucosamine
$GlcN_{NS,6S}/A$	N, 6-O-disulfated-D-glucosamine
$GlcN_{NS,3,6S}/A^*$	N-sulfated-3,6-O-sulfated-D-glucosamine
IdoA/I	α-L-iduronic acid
$I2_S/I_S$	2-O-sulfated-α-L-iduronic acid
Hep(s)	Heparin(s)
HSQC	Heteronuclear Single Quantum Correlation
INEPT	Insensitive Nuclei Enhancement by Polarization Transfer
LB	Line Broadening
LMWH	Low Molecular Weight Hep
Mn	number-average mean molecular weight
MW	weight-average mean molecular weight
NMR	Nuclear Magnetic Resonance
NOE	Nuclear Overhauser Effect or Enhancement
NOE^{EXP}	experimental NOE value
NOE^{CALC}	theoretical NOE value

NOESY	NOE SpectroscopY
trNOE	transferred NOE
OSCS	OverSulfated CS
PFG	Pulse Field Gradient
rf	radio frequency
ROESY	Rotating frame NOE Spectrosopy
RT	Room Temperature
S/N	Signal-to-Noise ratio
STD	Saturation Transfer Difference
tmix	mixing time
TOCSY	TOtal Correlation SpectroscopY
UFH	Unfractionated Hep
vLMWH	very Low Molecular Weight Hep
WATERGATE	WATER suppression by Gradient Tailored Excitation

Symbols

2. Symbols

$^{1}J_{C\text{-}H}$	one-bond proton-carbon coupling constant
$^{3}J_{H\text{-}H}$	three-bond proton-proton coupling constant
°C	Celsius degree
D	polydispersity (MW/Mn)
d*n*/dc	specific refractive index increment (mL/g)
k_B	Boltzman constant ($(1.38E^{-23}((Kg*m^2)/(sec^2*°K)))$)
K_d	dissociation constant (mM)
k_{off}	unbinding constant (sec^{-1})
λ	laser wavelenght (nm)
n	refractive index
η	viscosity coefficient (Kg/(sec*m))
Θ	scattering angle (90 °)
ppm	parts per million
R_h	hydrodynamic radius (nm)
τ_c	Rotational correlation time

Introduction

3. Introduction

3.1. The extracellular matrix

Cells are not the unique constituent of animal tissues, a major part is filled by a network of macromolecule within the extracellular space, this is called extracellular matrix (ECM) (Fig. 1). ECM is mainly constituted by locally secreted proteins and polysaccharides: (1) polysaccharide chains of the class called glycosaminoglycans (GAGs), which are usually found covalently linked to protein in the form of proteoglycans (PG) and (2) fibrous proteins, including collagen, elastin, fibronectin and laminin, which have both structural and adhesive functions. PG molecules in connective tissue form a highly hydrated, gel-like network in which the fibrous proteins are embedded. The polysaccharide gel resists compressive forces on the matrix while permitting the rapid diffusion of nutrients, metabolites and hormones between the blood and the tissue cells. The collagen fibers both strengthen and help to organize the matrix and rubber-like elastin fibers give it resilience. Finally, many matrix proteins help cells attachment to the appropriate locations (Alberts *et al*., 2002). The complex structure of the ECM is the site in which all inter cellular communication takes place, but that how this is regulated is only now starting to be addressed. This communication must result in all the usual outcomes associated with higher organisms, including cell growth, differentiation and development (Capila and Linhardt, 2002). GAGs (and especially heparan sulfate) are known to be critically involved in most major cellular signaling networks, so understanding the composition of the ECM, their characteristics and interactions will be vital to making progress in this area.

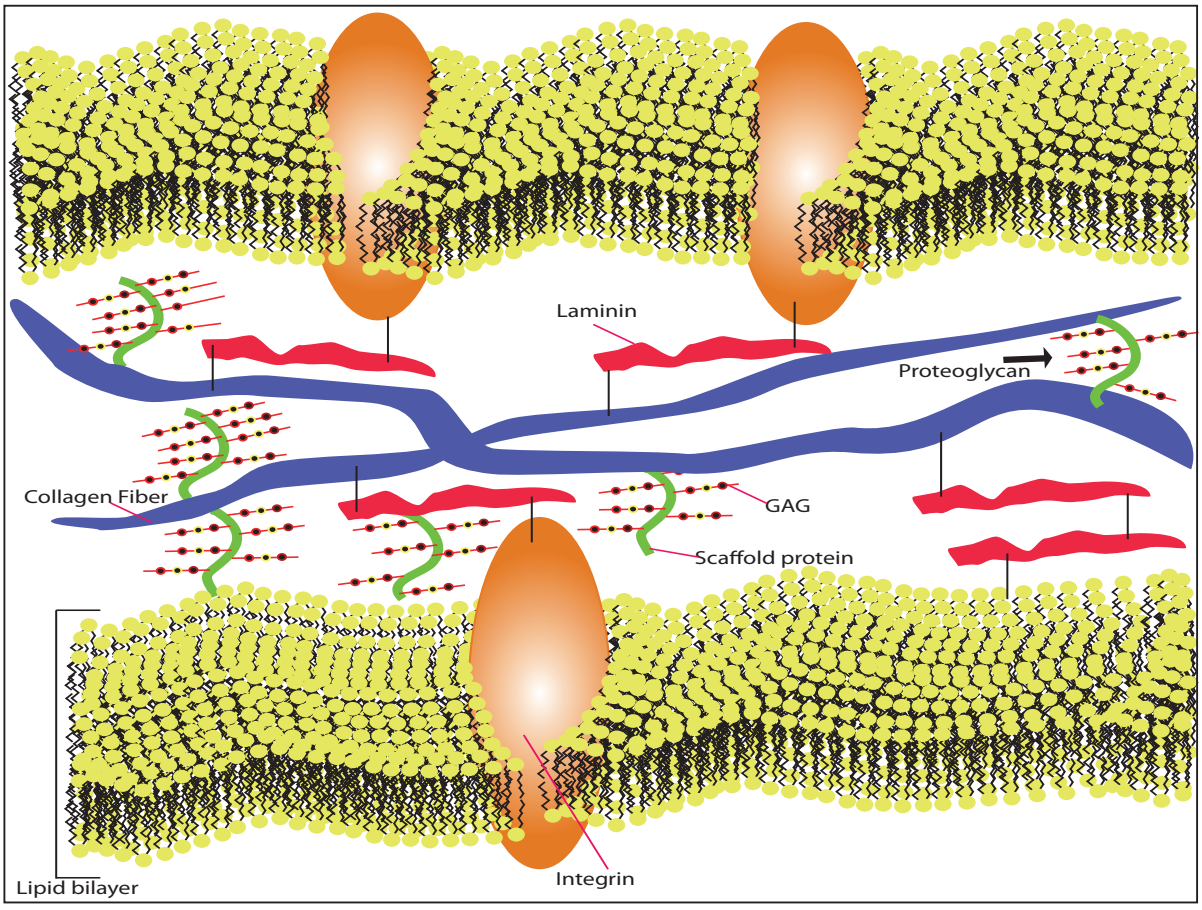

Figure 1. Schematic representation of animal extracellular matrix.

3.1.1. Glycosaminoglycans

Glycosaminoglycans are anionic polysaccharide chains composed by peculiar repeating disaccharide units. One of the two sugars in the repeating disaccharide is always an amino sugar (N-acetylglucosamine or N-acetylgalactosamine), which in most cases is sulfated. The second sugar is usually a uronic acid (glucuronic or iduronic). Because there are sulfate or carboxyl groups on most of their sugars, GAGs are highly negatively charged, for this reason they are the most anionic molecules produced by animal cells. Four main groups of GAGs are distinguished according to their sugars, the type of linkage between the sugars and the number and location of sulfate groups: (1) hyaluronan (hyaluronic acid, HA), (2) chondroitin sulfate (CS), dermatan sulfate (DS), (3) keratan sulfate and (4) heparan sulfate (HS) and heparin (Hep) (Fig. 2).

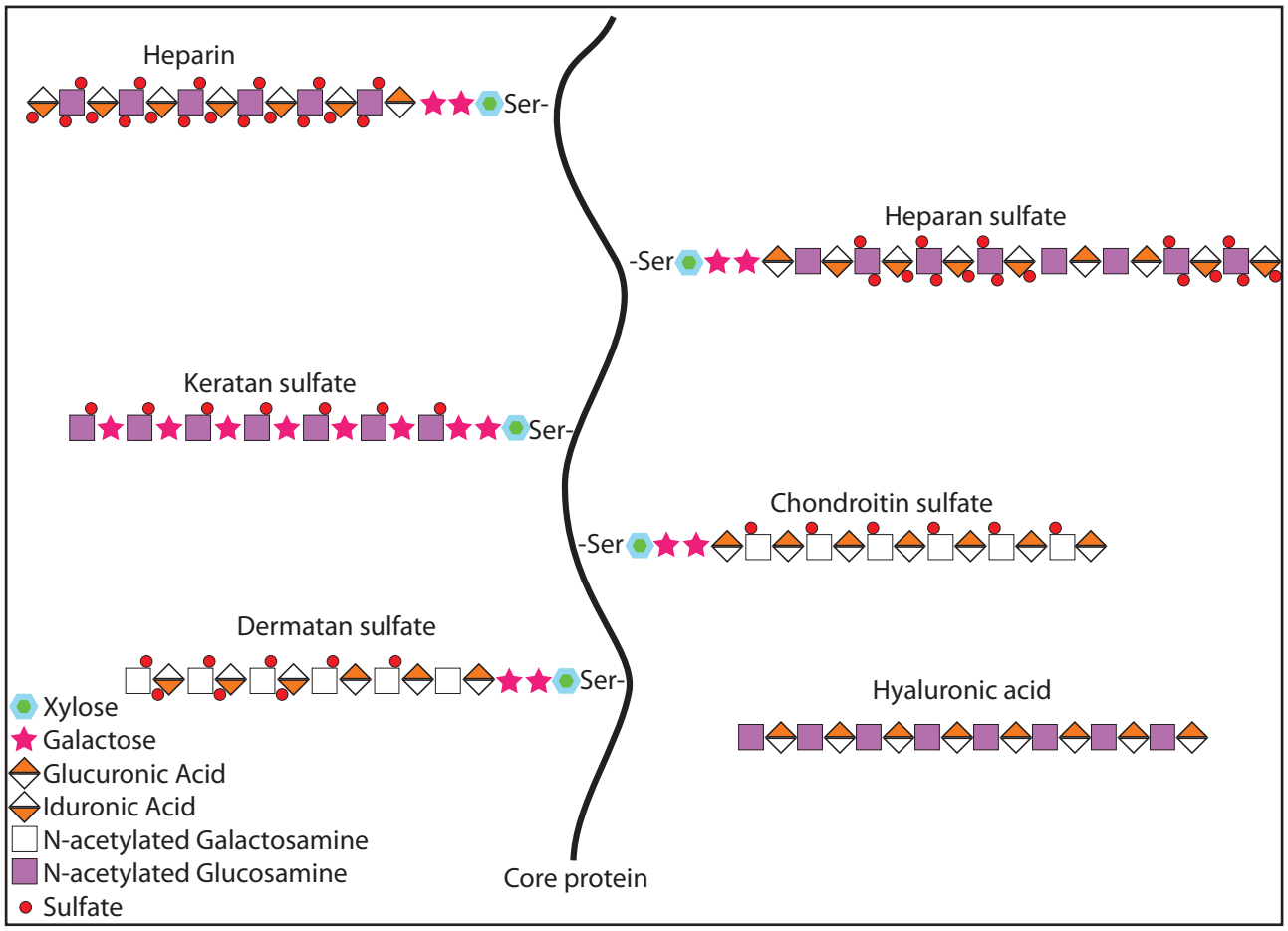

Figure 2. Schematic representation of different glycosaminoglycans .

Since polysaccharide chains are rigid and hydrophilic, GAGs tend to adopt highly extended conformations that occupy a huge volume relative to their mass and they form gels even at very low concentrations. Their high density of negative charges attracts a cloud of cations, most notably Na^+ and Ca^{2+} (Ferro *et al*., 1990; Mulloy and Forster, 2000), that are osmotically active, thus causing large amounts of water to be sucked into the matrix. This creates a swelling pressure, or turgor, that enables the matrix to withstand compressive forces (in contrast to collagen fibrils, which resist stretching forces). The cartilage matrix that lines the knee joint, for example, can support pressures of hundreds of atmospheres in this way. The GAGs in connective tissue usually constitute less than 10% of the

weight of the fibrous proteins, but, because they form porous hydrated gels, the GAG chains fill most of the extracellular space, thus providing mechanical support to the tissue. Due to this important structural function, genetic diseases affecting GAG biosynthesis have severe consequences (i.e. mucopolysaccharidoses), for example in one rare human genetic disease, there is a severe deficiency in the synthesis of the dermatan sulfate. The affected individuals have a short stature, prematurely aged appearance and generalized defects in their skin, joints, muscles and bones. It should be emphasized, that in invertebrates and plants other types of polysaccharides often dominate the extracellular matrix (Alberts *et al*., 2002).

3.1.2. Heparan sulfate/ Heparin

HS family is composed by HS and Hep, molecules sharing some structural features (composed of alternate units of α-D-glucosamine (GlcN) and uronic acid, either β-D-glucuronic acid (GlcA) or α-L-iduronic acid (IdoA), joined together by (1 -> 4) glycosidic linkages. In heparan sulfate the GlcN can be either N-sulfated or N-acetylated (Dreyfuss *et al*., 2009). Cellular localization, their occurrence in the animal kingdom and their biological functions, are the features differentiating them: HS is ubiquitous to the cell surface of both vertebrate and invertebrate species (Cassaro and Dietrich, 1977) (Fig. 3), where Hep is not evolutionary conserved as HS and it is synthesized and stored by mast cells in vertebrates (Nader *et al*., 1999). Furthermore, heparin shows higher degree of sulfation (DoS) (2.3–2.8 sulfates/disaccharide) when compared to HS (0.6–1.5 sulfates/disaccharide) (Dreyfuss *et al*., 2009). HS also has a domain structure of short, highly sulfated regions separated by longer regions of low sulfated, GlcA-rich stretches. Heparin, on the other hand, is richer in IdoA units and lacks this domain structure.

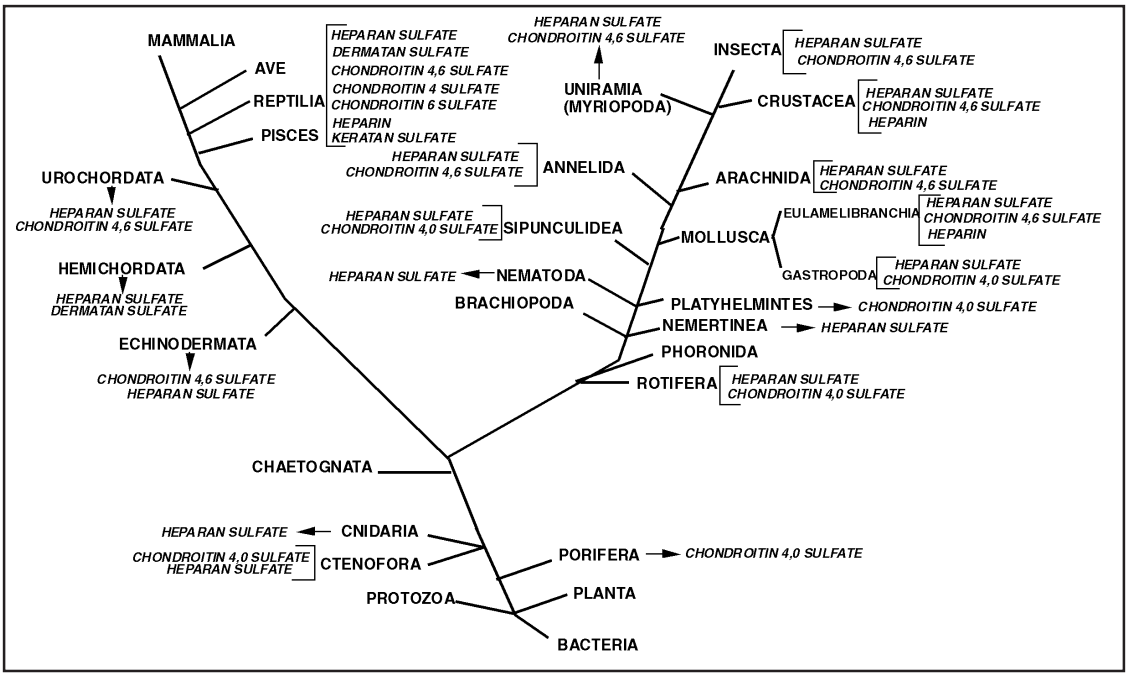

Figure 3. Distribution of sulfated glycosaminoglycans in the animal kingdom (Nader *et al*., 1999).

Negative charge high density and the big structural heterogeneity lead HS/Hep to easily interacts with proteins, such as proteases, growth factors, chemokines, lipid-binding proteins, pathogen proteins,

adhesion proteins and nutritional metabolisms (Capila and Linhardt, 2002; Esko and Selleck, 2002; Lindahl *et al*., 2007; Bishop *et al*., 2007; Ori *et al*., 2008).

3.1.3. HS/Hep biosynthesis and Hep structural properties

HS/Hep, DS and CS are synthesized as proteoglycans, in which they are linked to serine residues in defined core proteins through a glucuronyl-galactosyl-galactosyl-xylosyl tetrasaccharide sequence called linkage region (LR) GlcAβ (1->3) Galβ (1->3) Galβ (1->4) Xylβ-1-O-Ser {LR content varies widely depending on the origin of heparin [i.e. it is lower than 1% in bovine lung heparins and up to 5% in porcine mucosal heparins (Lindahl, 1996; Iacomini *et al*., 1999, 1999)]. There are no evidences for an LR role in biological activities, but some authors suggest an implication in antiangiogenic properties of heparin/HS (Hanhenberger *et al*., 1993)}. Ser residue into the core protein is modified by xylosyltranferase (XylT) in the endoplasmic reticulum (ER) and the cis-Golgi (Esko and Selleck, 2002; Prydz and Dalen, 2000). XylT catalyses the transfer of a Xyl residue through a β-linkage from UDP-Xyl to a Ser residue in the core protein substrates (Fig. 4), the amino acid sequences of which are conserved as Ser-Gly-X-Gly (where Gly and X stand for glycine and any amino acid, respectively) as revealed by comparison with the GAG attachment sites in the core proteins (Esko and Zhang, 1996). Although human and rats β-XylTs have been cloned (Gotting *et al*., 2000), the catalytic role of the second one has not been shown yet and its biological function remain unclear. Subsequently, two Gals are attached to the Xyl residue by galactosyltransferase-I and galactosyltransferase-II (GalT-I and GalT-II) (Fig. 4). GalT-I is one of the seven β1-4GalT family members, which appears to have exclusive specificity for the donor substrate UDP-Gal. On the other hand GalT-II witch transfers Gal from UDP-Gal to a β-linked Gal residue is one of the six β1-3GalT family members (Bai *et al*., 2001). Lastly the LR is completed by the transfers of a GlcA through a β1-3 linkage from UDP-GlcA to Galβ1-3Galβ1-4Xylβ1-O-Ser (Fig. 4), which is catalysed by the glucuronyltransferase-I (GlcAT-1) (Kitagawa *et al*., 1998; Tone *et al*., 1999). Chain polymerisation of the repeating disaccharide region in heparin and HS is evoked by the transfer of the αGlcNAc residue from UDP-GlcNAc to the LR tetrasaccharide, which is mediated by $GlcN_{NAc}$T-I (Fig. 4). The addition of β1-4-linked $GalN_{NAc}$ to the LR by β1-4N- acetylgalactosaminyltransferase-I (GalNAcT-I) initiates the formation of the repeating disaccharide in CS and DS. N-deacetylation and N-sulfation of $GlcN_{NAc}$ residues in heparin and HS are initial modifications of precursor chains and essential for all the subsequent modifications (Fig. 4). Both reactions are catalysed by the bifunctional enzymes $GlcN_{NAc}$ N-deacetylase/N-sulfotransferase (NDSTs). This complex chain of events leads to the synthesis of a wide variety of GAG molecules with different sequences and due to this great varieties they can bind a wide array of ligands mediating and triggering biological functions: cell matrix assembly, cell adhesion (Xian *et al*., 2010), cell/tissue differentiation (Yan and Lin, 2009), cell migration, cell recognition, cell proliferation, cell survival, endocytosis, haemostasis, angiogenesis, defense mechanism (Dreyfuss *et al*., 2009) and inflammation (Li and Vlodavsky, 2009). Heparin is the most homogeneous molecule of the HS/Hep family and its chains are made up of various combinations of building blocks. The distribution of those building blocks generate different charged regions characterised by peculiar disaccharide repeating unit. The less charged sequences are mainly concentrated towards the reducing side of the chains (R) thus the typical disaccharide is GlcA-$GlcN_{NAc}$ (NA domain). On the nonreducing side (NR) there is the highest sulfate groups concentration (NS domain), since the most abundant disaccharide is Ido_{2S}-$GlcN_{NS,6S}$ (TSD). In the middle there is a mixed domain (NA/ NS domain) mainly characterised by a GlcA-

$GlcN_{NS}$ disaccharide repeating unit (Fig. 5), some of the heparin chains contain a specific sequence constituting the antithrombin III (AT) binding domain (AT-bd). This sequence is the pentasaccharide β-D-N-acetylated,6-O-sulfated glucosamine ($GlcN_{NAc,6S}/A_{NA}$)-α(1->4)-D-glucuronic acid (GlcA/G)-β(1->4)-D-N-sulfated,3,6-O-sulfated glucosamine ($GlcN_{NS,3,6S}$/A*)-α(1->4)-D-2-O-sulfated iduronic acid ($IdoA_{2S}/I_S$)-α(1->4)-D-N-sulfated,6-O-sulfated glucosamine ($GlcN_{NS,6S}$/A) (abbreviated in $A_{NA}GA^*I_SA$) shown in Fig. 5. HS/Hep composition varies depending on animal and organ origin and also on the purification procedures (Fig. 5 and Table 1; Loganathan *et al*., 1990; Bianchini, 1997).

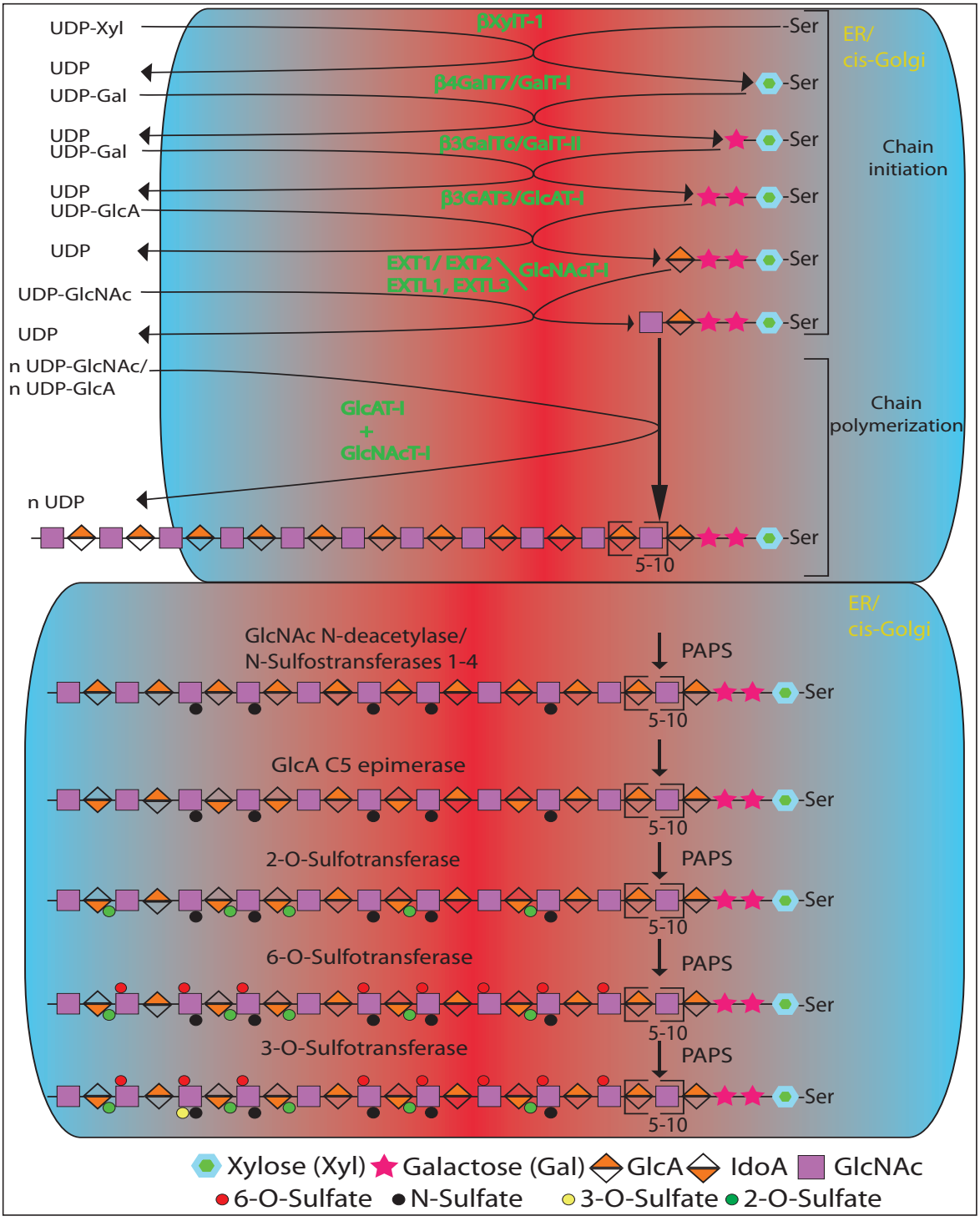

Figure 4. Pathways of heparin/HS biosynthesis. EXT1/EXT2 indicates a heterodimeric complex. XylT= xylosyltransferase; GalT-I= galactosyltransferase-I; GalT-II= galactosyltransferase-II; GlcAT-I= glucoronyltransferase-I; GlcNAcT-I= N-acetylglucosaminyltransferase-I; GlcNAcT-II= N-acetylglucosaminyltransferase-II; GlcA/GlcNacT= GlcA and GlcNAc transferase; PAPS= 3'-phosphoadenosine-5'-phosphosulfate.

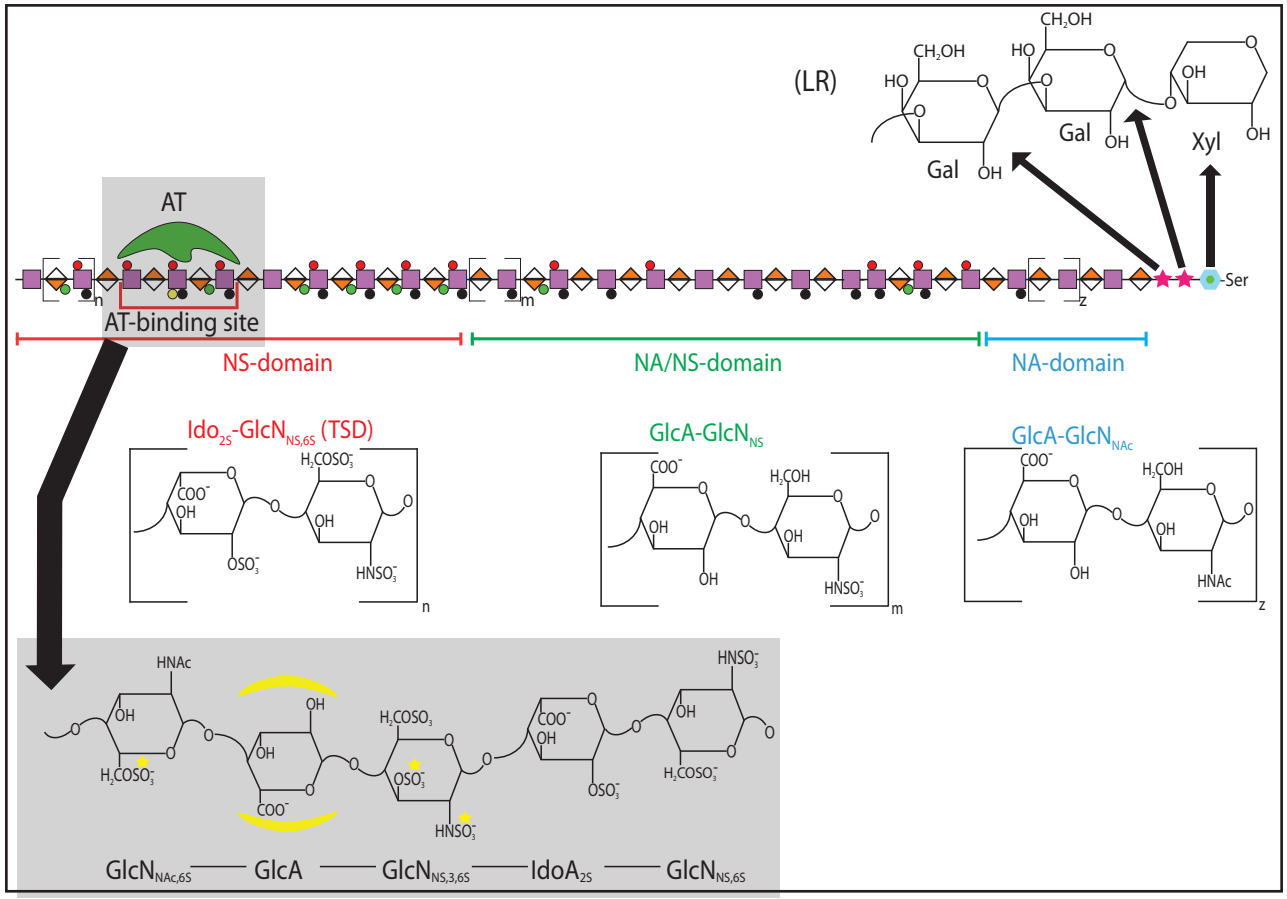

Figure 5. Schematic representation of HS/Hep structure. HS/Hep three domain are shown with their relative disaccharide repeating units, together with the AT-binding domain (AT-bd) [the pentasaccharide β-D-N-acetylated,6-O-sulfated glucosamine ($GlcN_{NAc,6S}/A_{NA}$)-α(1->4)-D-glucuronic acid (GlcA/G)-β(1->4)-D-N-sulfated,3,6-O-sulfated glucosamine ($GlcN_{NS,3,6S}$/A*)-α(1->4)-D-2-O-sulfated iduronic acid ($IdoA_{2S}/I_S$)-α(1->4)-D-N-sulfated,6-O-sulfated glucosamine ($GlcN_{NS,6S}$/A): the yellow stars represent essential sulfate groups and the half moon highlight the essentiality of GlcA]; TSD= trisulfated disaccharide; NS-domain= N-sulfated domain; NA/NS domain= N-acetylated/N-sulfated mixed domain; NA domain= N-acetylated domain; LR= linkage region.

As it was demonstrated, TSD units represent more than 60 % (heparins obtained from porcine mucosa up to 60–75% and heparins obtained from bovine lung up to 85% (Guerrini *et al*., 2001; Sudo *et al*., 2001). TSD characterises the longer segment of NS domain and this segment is often referred to as constituting "regular regions" and is the major contributor to the polyelectrolytic properties of heparin. TSD segments length is known for limited heparin types and only in statistical terms, through oligosaccharides size profiling on oxidated (at nonsulfated uronic acid level) and depolimerised haparin: pig mucosal heparin is statistically characterised by 8-12 TSD units, whereas human fibroblast derived HS is statistically characterised by up to 5 TSD units (Fransson *et al*., 1980; Sjoberg *et al*., 1980).

		Avarage Number in One Heparin Chain			
Species	Tissue	N-acetyl AT Binding site	N-sulfo AT Binding site	Trisulfated Disaccharide	Disulfated Disaccharide
Porcine	intestine	0.5 (0.3-0.7)	0.1	10 (10-15)	1.2 (1-2)
Bovine	lung	0.3	0.3	14	1.0
Bovine	intestine	0.3	0.3	10	1.7
Ovine	intestine	0.7	0.4	11	1.4
Hen	intestine	0.3	0.2	6.7	1.7
Clam	-	0.5	0.4	5.0	1.9

Table 1. Heparin composition from different species and organs. Numbers in parenthesis indicate a range of values typically observed (adapted from Loganathan *et al*., 1990).

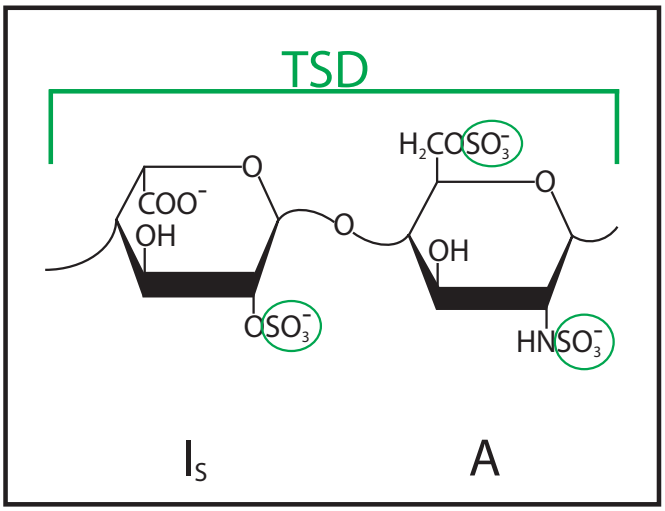

Figure 6. Schematic representation of the typical trisulfated disaccharide (TSD) characterising the NS domain. Sulfate groups (green circles) are highlighted.

3.1.4. GAG sequence conformations: local rigidity and flexibility

Heparin and related polysaccharides tridimensional structures have long been elusive and a matter of controversy (Casu *et al*., 1986). One of the most problematic issue in GAG 3D modeling has been the evaluation of the conformation of their iduronic acid residues, critical to determine the polysaccharide chains conformations. Molecular mechanics studies on monomeric I_S methyl glycoside led to understand that the iduronate ring could be present in three equienergetic conformations: $^1C_4$, $^2S_0$ and $^4C_1$ (Fig. 7) (Ragazzi *et al*., 1986). The $^1C_4$ and $^2S_0$ geometries are similar for the two conformations: helices with regular arrays of three sulfate groups on both sides. However, spacing between sulfate groups on adjacent residues is different for the two local conformations and the sulfate forms cluster in different ways along the chain axis (Fig. 7). The population of individual conformers depends on the structure of neighbouring units and sulfation of the IdoA residue, as suggested by Nuclear Magnetic Resonance (NMR) spectroscopic data (Ferro *et al*., 1986). For example, in heparin/HS the ratio of the $^1C_4$ and $^2S_0$ conformers of the 2-O-sulfated IdoA residue is about 60: 40. When I_S is preceded by a 3-O-sulfated $GlcN_{NS,3S,6S}$ residue, as in the pentasaccharide sequence of the AT-bd, the $^2S_0$ form is more represented than the $^1C_4$ form (Ragazzi *et al*., 1987; Mikhailov *et*

al., 1997). The $^4C_1$ form is selected by I_S when the iduronate residue is located in terminal positions of heparin/HS sequence (Ferro *et al*., 1986). Iduronate position within Hep/Hs sequence is not the only factor affecting the conformational equilibrium, it might also be affected by ionic strength and specific counterions: in fact, it was demonstrated that the equilibrium of the I_S residues of heparin (Ferro *et al*., 1990) and heparin oligosaccharides (Ferro *et al*., 1990; Mulloy and Forster, 2000) is driven by Ca^{2+} ions towards to $^1C_4$ form. IdoA "plasticity" has been suggested to help the most effective docking of the anionic groups of the GAG toward to basic groups of proteins (Mulloy *et al*., 1993), complete conformational maps analysis confirm iduronate capability to assume one out of three (or all three) possible conformations (Ragazzi *et al*., 1986; Casu *et al*., 1988). Moreover, modeling and NMR data (Hricovini *et al*., 2001) indicates that no basic groups in the binding site are within reach of the 2-O-sulphate group of IdoA2-SO_3. Thus this group is not directly involved in the binding process, but appears to be the main driving force affecting the conformational equilibrium in IdoA2-SO_3 towards the skew form (Fig. 8 A) (Hricovini *et al*., 2001). Another important Hep structural features is its linearity that is not continuous, this concept came up as a consequence of crystal structures analysis of heparin oligosaccharide-protein complexes, at the protein- GAG interaction site was noticed a lost of linearity in the polysaccharidic chain and the comparison of "kinks". These kinks seem to be a signature of complex formation, together with a different conformation of an iduronate residue than GAG chain portions not involved in binding (Raman *et al*., 2003). As illustrated in Fig. 8 A, evaluation of the conformation of pentasaccharide complexed with AT in solution has also indicated that the I_S residue is not directly involved in binding, probably GAG molecules use I_S plasticity to drive the preceding trisaccharide sequence (A_{NA}-G-A*) towards the appropriate conformation in order to better fit the protein moiety (Hricovini *et al*., 2001). Notably, Hricovini *et al*. (2001) shown that the IdoA residues, belonging to pentasaccharide flanking sequences, assume different conformations depending their location at the reducing or nonreducing side of the pentasaccharide. These findings suggest that the conformation of the iduronate residues ($^2S_0$ and $^1C^4$ for IdoA located at the nonreducing and reducing side of the $A_{NA}GAI_SA$ sequence) could enhance the AT affinity of $A_{NA}GA^*I_SA$ containing oligosaccharides, either by optimizing contacts between $A_{NA}GA^*I_SA$ and AT or promoting additional contacts involving the $A_{NA}GA^*I_SA$ extensions (Guerrini *et al*., 2008 [b]).

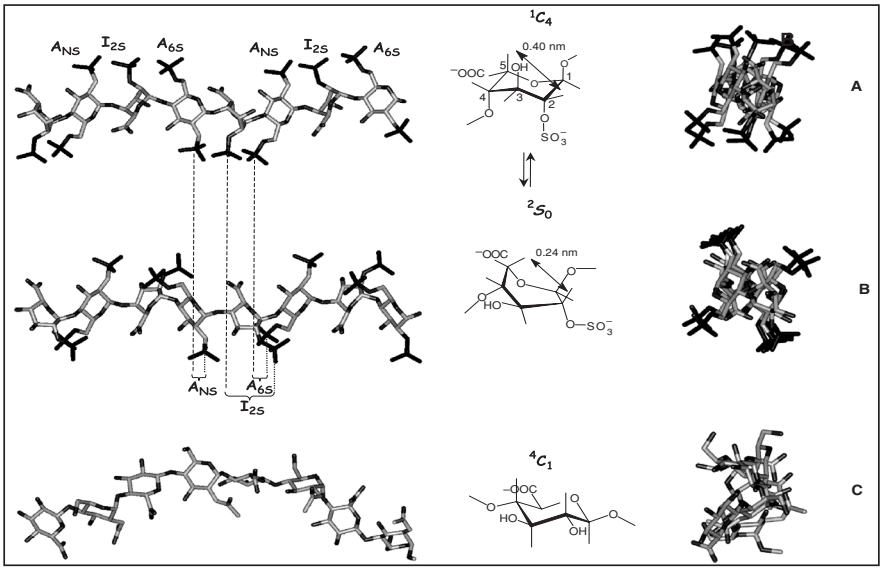

Figure 7. Possible ring conformations of 2-O-sulfated iduronic acid. **A.** I_S $^1C_4$ conformation; **B.** I_S $^2S_0$ conformation; **C.** I_S $^4C_1$ conformation; on the left molecular side view showing the spatial relationship between sulfate groups, in the middle the skeleton representation showing the conformational equilibrium and on the right the axial relationship between saccharidic rings and sulfate groups.

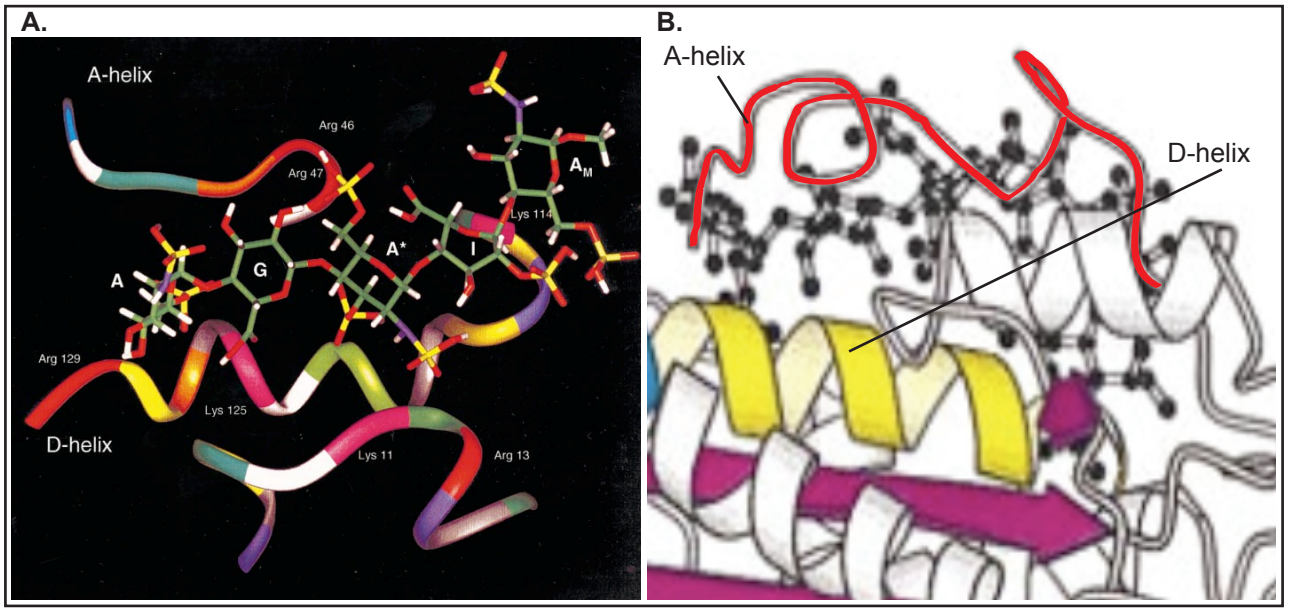

Figure 8. AT-$A_{NA}GA^*I_SA$ complex. **A**. NMR spectroscopy (Hricovini *et al*., 2001): pentasaccharide is represented as sticks, sulfate groups are represented as yellows and red sticks. **B**. X-ray diffraction (modified from Jin *et al*., 1997) :AT-pentasaccharide interaction involve D-helix (yellow) and A-helix (red). The two models mainly diverge for reducent $AN_{NS,6S}$.

3.1.5. Coagulation and heparin

The coagulation cascade is a sequence of enzymatic events. Most plasma coagulation factors circulate as inactive proenzymes (serine proteases) which are synthesized by the liver. These enzymes are proteolitically cleaved, thus inducing their activation, by the activated factors that precede them in the cascade. The cascade is traditionally divided in intrinsic (contact activation) and extrinsic (tissue factor) pathway. The intrinsic pathway is activated by the complex Factor XII (Hageman Factor, FXII), its cofactor high molecular weight kininogen HMWK, collagen and prekallikrein. The complex leads to the activation of FXII that cleaves the Factor XI (FXIa) and the cascade proceeds until the crucial point of Factor X activation (FXa), where the two pathways converge. Stream while the extrinsic pathway is activated *in vivo* by tissue factor (lipoprotein expressed and released by activated leukocytes, activated endothelial cells, subendothelial smooth muscle cells and subendothelial fibroblasts of vascular injury). Although the two pathway converge at FX activation, there is an important interconnection: activated Factor VII (FVII, from extrinsic pathway) participate in the activation of the Factor IX (FIX, intrinsic pathway). When the two pathways converge an important reaction is catalysed which requires activated Factor V (FVa) and FXa: prothrombin (factor II, FII) is cleaved by FXa leading to thrombin formation (FIIa) (Fig. 9). Thombin is a multifunctional enzyme that acts in the coagulation cascade in four important points: 1) it converts fibrinogen into fibrin, causing the formation of insoluble fibers, 2) activates Factor XIII that crosslinked fibrin generating a higly stable clot, 3) increases and accelerates coagulation cascade inducing a positive feedback through activation of FV, FVIII, FXI and 4) it strongly activates platelets, thus causing granules release and platelets aggregation (Fig. 9). Over the last 20 years heparin studies have contributed to elucidate the molecular basis of the anticoagulant and antithrombotic activities of heparin, in particular their inhibition of FXa and thrombin, the final two proteases of the coagulation cascade. Heparin anticoagulant properties are exerted enhancing AT inhibition activity over FXa and thrombin from 300 to 1000 fold and to a minor extent Hep is also capable to accelerate heparin cofactor II (HCFII, which selectively inhibits thrombin). AT

and HCFII are structural homologous (Baglin *et al*., 2002), but where AT binds only heparin, HCFII also binds DS, in fact are involved different polysaccharides sequences as previously shown in Table 2 (Tollefsen, 1992). Anticoagulant effects are also associated with GAG-induced release of tissue factor pathway inhibitor (TFPI) from vascular endothelium (Brooze, 1995; Hoppensteadt *et al*., 2003; Newall *et al*., 2010). The activity of both AT and HCFII is dramatically increased by binding with heparin. Heparin sequences that specifically bind to HCFII have not been identified. In fact, HCFII seems to be bound by heparin rather nonspecifically (Tollefsen, 1992; Bourin and Lindahal, 1999; Petitou, 1988). However, it is reasonable to assume that sequences of the TSD (Fig. 6) are the major sites for HCFII binding. The present informations about the mechanism of the interaction between heparin, AT and thrombin and related structural aspects are largely based on physico-chemical studies of these systems in solution (Olson and Björk, 1992; Olson and Björk, 1992 [b]) and on X-ray diffraction studies (Jin *et al*., 1997; Li *et al*., 2004). Since these studies and their biological implications are covered in other chapters of this thesis, the present chapter briefly discusses only current information on heparin sequences involved in the above interactions and the dependence of these interactions on the size of GAG sequences and the location of active sites in these sequences. The search for minimal sequences binding to AT and HCFII and inducing inhibition of thrombin mediated by these cofactors has led to understanding the size-dependence of GAG activities associated with interaction with the two protease inhibitors. AT-, as well as HCFII-mediated inhibition of thrombin, need relatively long heparin chains as a requisite for binding to both the inhibitor and the enzyme in a ternary complex. The minimum heparin size for significant HCFII binding was a hexasaccharide corresponding to three TSD units; full affinity for HCFII is practically reached at eight monosaccharide residues (Tollefsen, 1992). Thrombin inhibition requires a minimum chain length of 16–18 monosaccharide residues (Laurent, 1978). On the other hand, AT-mediated inhibition of Factor Xa requires only the pentasaccharide sequence of the active site for AT (reviewed in Bourin and Lindahal, 1999, Casu and Lindahl, 2001, Muñoz and Linhardt, 2004).This observation was at the basis of the introduction of low molecular weight heparins (LMWHs) as antithrombotic agents blocking the coagulation cascade at the level of FXa. Low molecular weight heparin are heparin salt having an average MW less than 8000 Da and at least 60% of all molecules must have a MW less than 8000 Da (Linhardt and Gunay, 1999). LMWHs are obtained by chemical or enzymatic depolymerisation of unfractionated heparin (UFH), that introduce modification at the reducing and/or nonreducing end of the obtained molecular species. As a pharmaceutical agent LMWH should respect some rules: a) appropriate MW with a low polydispersity; 2) anti-FXa/ anti-FIIa ratio must be > 1; 3) molecular structure cannot has much artifacts; 4) toxic agent must be eliminated; 5) production reproducibility, minimum number of process steps and high yielding. Nowadays the industrial process are not so performace in respect to all the points, but still high quality LMWH are produced and used for pharmacological treatment (Linhardt and Gunay, 1999). Being only marginally involved in the inhibition of thrombin and in side effects associated with full-length heparin, LMWH species were thought to reduce the hemorrhagic risks. However, the major advantage of LMWHs over conventional heparin for certain therapeutic indications is their better bioavailability. Depolymerisation procedures used for obtaining LMWHs may occasionally cleave the AT-bd, less represented in LMWHs than in conventional heparins (Fareed *et al*., 1999), as observed upon partial digestion with heparinase 1 (Shriver *et al*., 2000; Avci *et al*., 2002). On the other hand, a synthetic pentasaccharide closely reproducing the structure of the AT-bd (as a methyl glycoside, in a variant in which the first GlcN residue is N-sulfated instead of N-acetylated) and based on exclusive inhibition of Factor Xa was proved to be an effective antithrombotic agent (Petitou *et al*., 2004).

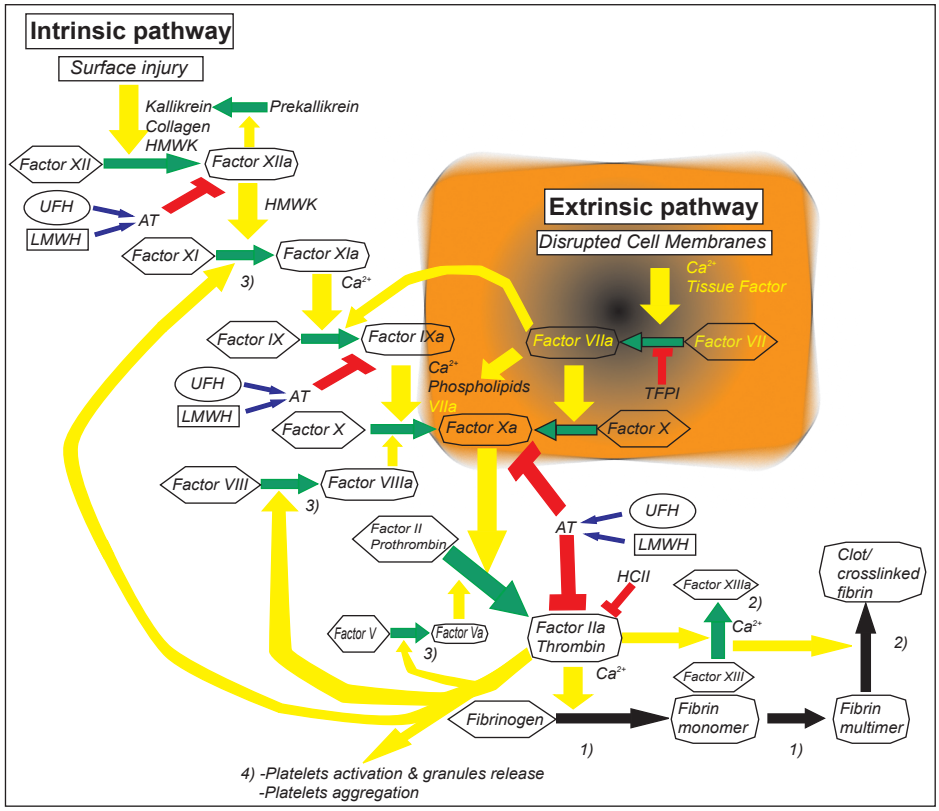

Figure 9. Schematic representation of the coagulation cascade. Intrinsic and extrinsic pathway are shown (the orange box isolates the extrinsic pathway and yellow written molecules belong exclusively to extrinsic pathway). Factor IIa effects are highlighted: 1) conversion from soluble fibrinogen to insoluble fibrin fibers, 2) Factor XIIIa activation and consequent clot formation, 3) activation enhancement of Factor V, Factor VIII and Factor XI, 4) granules release from activated platelets and their aggregation. Green arrows indicate molecular conversion from an inactive to an active form; yellow arrows indicate activation induction; blue arrows indicate acceleration effect over AT, heparin induced; red hammers indicate inhibition effects and black arrows indicate fibrin polymerisation till clot formation. HMWK= high molecular weight kininogen; AT= antithrombin III; HCFII= heparin cofactor II; TFPI= tissue factor pathway inhibitor; UFH= unfractionated heparin; LMWH= low molecular weight haparin.

Synthetic oligosaccharide chemistry has made an important contribution to establish the relationships between structure and AT-mediated activities (van Boeckel and Petitou, 1993; Bauer *et al*., 2002; Petitou *et al*., 2004). A pentasaccharide with an additional 3-O-sulfate group (on the fifth residue) with respect to $A_{NA}GA^{*}I_{S}A$ was shown to be even more active than the natural pentasaccharide (van Boeckel and Petitou, 1993). Moreover, a systematic study of extension of the heparin chain on both sides of the pentasaccharide sequence has confirmed that the chain extension required to bind thrombin in the ternary complex with heparin and AT must be at least 14 monosaccharide residues long and definitely established that such an extension must be toward the nonreducing terminal of the heparin chain (Petitou *et al*., 1999). The actual location of thrombin in the ternary complex was also confirmed by studies using neo-glycoconjugates (Rong *et al*., 1999) and conclusively by X-ray diffraction studies (Iozzo and San Antonio, 2001).

3.2. Heparin as a pharmaceutical agent

Heparin has been used as pharmaceutical agent from the first decades of the last century for the prevention and initial treatment of thrombosis (Murray and Best, 1938; Lam *et al*., 1941). Pharmaceutical grade heparin was derived for decades from different animal sources, mainly bovine lung and porcine intestine (Linhardt and Gunay, 1999), but after the bovine spongiform encephalopathy

(BSE) comparison the European Agency for the Evaluation of Medicinal Products (EMEA) together with the World Health Organization (WHO) decided to apply the “precautionary principle", as a consequence, medications prepared from bovine tissues were forbidden (EMEA, 1998). In the last decade pharmaceutical heparins were most commonly isolated in tons quantities from porcine intestines (Coyne, 1981), generating a big business (Baxter heparin business is $30 million dollar/year; Zoll, Kranz and Borgess, LCC); as a consequence industrial and pharmaceutical heparin production process are tightly guarded. Mainly these production processes are divided in five basic steps: 1) preparation of tissue; 2) extraction of heparin from tissue; 3) recovery of raw heparin; 4) purification of heparin; and 5) recovery of purified heparin. Preparation of the tissue (1) begins with collection at the slaughterhouse, where it remains also for the extraction step (2) and the raw heparin recovery step (3) (Fig. 10 A). The constituents of crude heparin include heparin itself, other related GAGs, including HS, DS, CS and HA and some percentage of nonpolysaccharidic components, such as nucleic acid and proteins. The purification of the resulting raw heparin is performed under current good manufacturing practices (cGMP) conditions and is designed to deal with potential impurities originating from the starting material or introduced during raw heparin extraction (Fig. 10 B). Such impurities may be in the form of other GAGs, extraneous counterions, heavy metals, residual protein or nucleotides, solvent, salts other than heparin, bacterial endotoxins, bioburden and viruses. Specific commercial methods of purifying heparin are tightly guarded industrial secrets set forth in a drug master file submitted to the FDA and foreign regulatory authorities. The yield of USP heparin from American pigs is typically 30,000– 50,000 international unit (IU, IU of heparin is defined as being the required amount of solution to prolong the clotting of 1 ml of whole blood for three minutes), corresponding to ~300 mg per animal; China is the leader state for raw heparin production and export). Small amounts (1–7%) of DS is present in some pharmaceutical grade heparins, but can be virtually eliminated using good manufacturing processes (Linhardt *et al*., 1988; Neville *et al*., 1989).

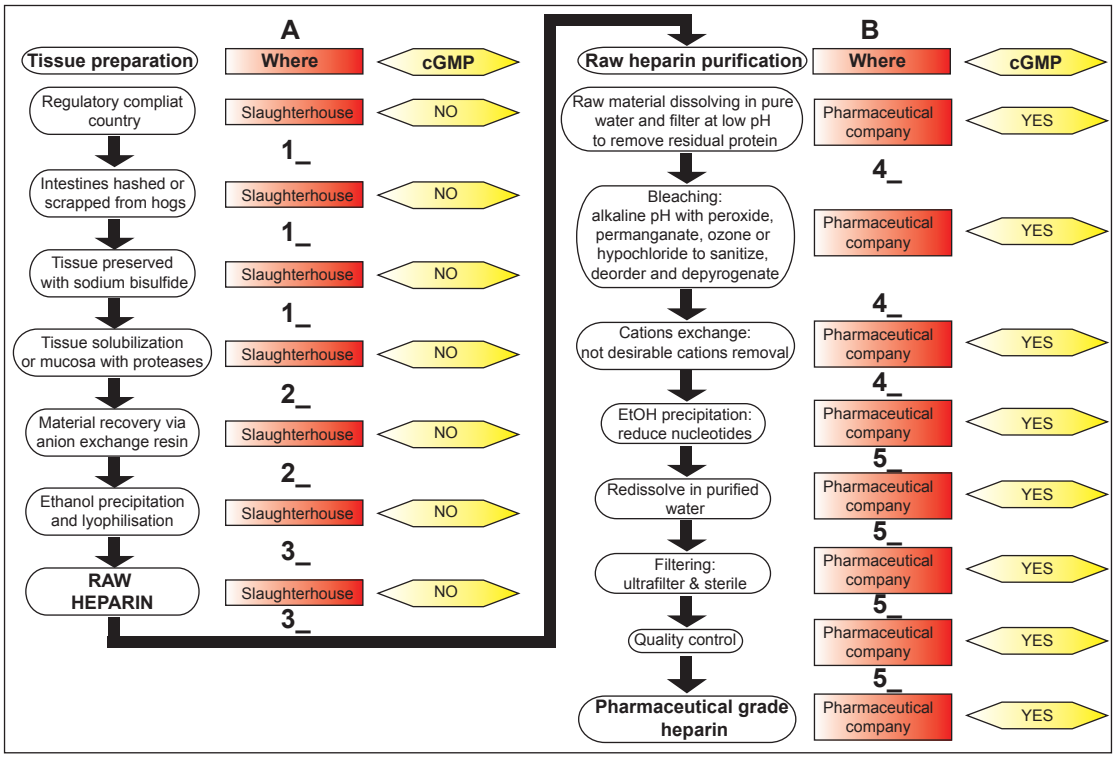

Figure 10. Flow chart of the preparation of heparin from animal tissues. Chart **A** is performed under little or no regulatory control in rural communities while chart **B** is performed under current good manufacturing practices (cGMP) in FDA-inspected facilities.

3.2.1. Heparin crisis

Pharmaceutical heparin security has been an hot topic due to the great difference in quality treatment between no cGMP steps and cGMP steps and quality control procedures applied to certificate heparin. As shown in Fig. 10 A heparin treatment steps are potentially danger for public health, because in the slaughterhouse raw material extraction steps are not subjected to the high quality procedure guaranteed by cGMP, in addiction heparin is a natural occurring molecule derived from a living organism, so naturally existed proteins, nucleic acids, DS and etc impurities are difficult to be removed completely. In late 2007 and into early 2008, a spike in serious allergic-type adverse events was associated with administration of heparin (i.e. heparin crisis), patients became ill with anaphylactoid symptoms, possibly caused by activation of the contact plasma system (WHO, 2008; Guerrini *et al*., 2009; Sasisekharan and Shriver, 2009), whereas, up to heparin crisis, the most serious documented adverse event associated with heparin, aside from a potential bleeding risk, was thrombocytopenia (Battistelli *et al*., 2010; Otis and Zehnder, 2010). Fig. 11 shows the progression of the heparin crisis from the first event until the end of the 2008. It is estimated that several score patients died as a result of this incident and many more suffered illness (246 reported in the USA between January 1st, 2007 and May 31st, 2008; Kishimoto *et al*., 2008; FDA, 2009). This led to a multifaceted investigation into the root cause for this dramatic increase in reactions. Concomitant with the initial identification of the contaminant as "heparin-like" by the US FDA, screening methods were introduced, based on capillary electrophoresis (CE) and proton nuclear magnetic resonance (^{1}H NMR) (FDA, 2008). Subsequently, contaminated heparin lots were detected in a number of countries, including Germany, France, Italy, Japan, Denmark and Australia (Laurencin *et al*., 2008). Following extensive efforts, a major contaminant was identified, over-sulfated chondroitin sulfate (OSCS) (Guerrini *et al*., 2008), which is not a naturally occurring substance. Key to this analysis was the use of multidimensional NMR, including heteronuclear single quantum coherence (HSQC) and heteronuclear multiple bond correlation (HMBC) experiments which determined the sulfation pattern of the disaccharide repeat, the epimeric state of the uronic acid and the glycosidic linkage pattern which characterised the disaccharide repeat as a tetrasulfated chondroitin sulfate-like unit. Ultimate proof-of-structure was obtained when a synthesised version of OSCS matched the HSQC profile of the contaminant in heparin (Fig. 12) (Guerrini *et al*., 2008).

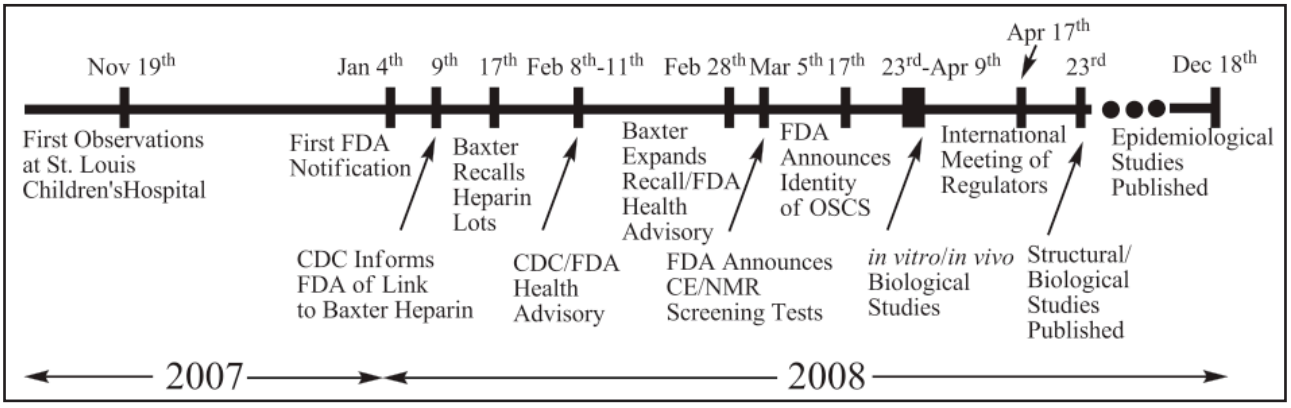

Figure 11. Heparin crisis timeline from the first clinical reports in November 2007 through the epidemiological findings published in December 2008 (Sasisekharan and Shriver, 2009).

In concert with the analytical studies, biological characterisation of the contaminant correlated the presence and extent of contamination with anaphylactoid reactions. It was found that the contami-

nant was capable of activating the contact system both *in vitro* and *in vivo*, using porcines as a model system (Kishimoto *et al*., 2008). In a follow-up study, epidemiological evidences indicated that patients exhibiting the allergic-like symptoms, including hypotension, nausea and shortness of breath were found to likely have received OSCS-contaminated heparin (Blossom *et al*., 2008).Thus, taken together these studies enable some measure of resolution to the heparin crisis and point to the fact that OSCS was likely the causative agent in the onset of anaphylactoid responses in patients. Sufficient proof has been provided that the adverse effects observed for recalled heparins are correlated with their content of OSCS (Kishimoto *et al*., 2008; Blossom *et al*., 2008). No additional serious anaphylactic events have been reported after the discovery of the OSCS contamination. In response to these recent developments, including the development of screening tests for heparin, the United States Pharmacopoeia (USP) and European Pharmacopoeia (EP) requirements for heparin have been revised. The USP has indicated that the monograph for heparin, which currently includes the NMR and CE screening methods, will be further revised to incorporate additional testing. Similarly the EP monograph is also currently undergoing revision.

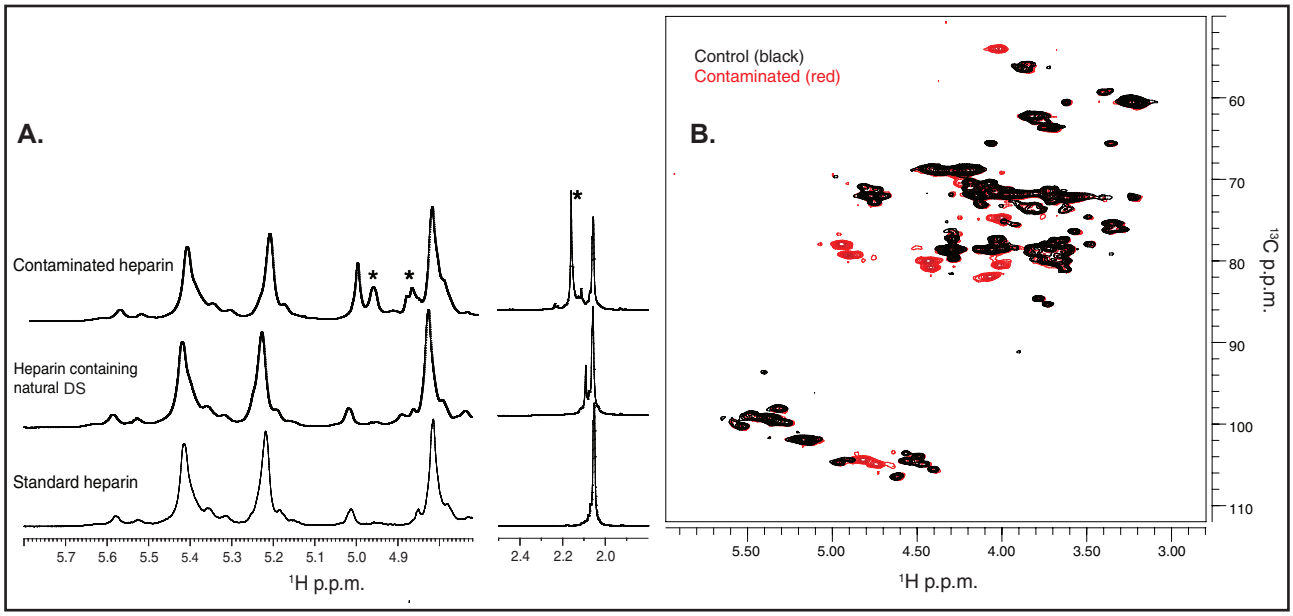

Figure 12. NMR analysis of standard UFH and heparin OSCS contaminated. **A.** ^{1}H spectra overimposition of pure UFH (bottom), natural UFH with natural DS (middle) and UFH with OSCS contamination (upper). **B.** HSQC spectra of UFH (black spectrum) and contaminated heparin with OSCS (red spectrum).

3.2.2. Heparin quality control

Pharmaceutical agents are usually uniquely identifiable molecules, absolutely homogeneous as a consequence of their synthetic origin and for sure, their chemo-physical properties are well documented and easily measurable (i.e. m/z, CD, NMR, HPLC, CE, etc.). Heparin is unlike most modern pharmaceutical agents in that it does not conform to a single, or even a small number, of defined chemical entities but, rather, is inherently variable in structure (chain length varies within sample; sequence varies within a sample, even if chain length is the same; sometimes they are isomeric in terms of uronate and/or sulfate positions). It is important to realise, therefore, that there can be no single, absolute definition by which to decide in favour of acceptance or rejection of a test sample, yet some judgement must still be made by manufacturers and regulatory bodies based on rational measurements, or crite-

ria. All of these variables must be accommodated by a generic analytical method, but what should the analytical testing strategy encompass? Before June 2008 heparin quality control was certified by 1) activity and 2) biochemical contamination assays. 1) activity tests: activated partial thromboplastin time (aPTT is an *in vitro* test to measure thrombus time formation after the addiction of heparin dose to human blood sample; acceptability range is between 30-40 sec), activating clotting time (ACT is an *in vitro* test to measure thrombus time formation after the addiction of heparin dose to human blood sample; acceptability range is between 70-180 sec), anti Factor Xa activity (anti-Xa is an *in vitro* chromogenic test performed on human blood/plasma to measure the anti Factor Xa activity in terms of IU/mg; acceptability range is between 170->190 IU/mg), anti Factor IIa activity (anti-IIa is an *in vitro* chromogenic test performed on human blood/plasma to measure the anti Factor IIa activity in terms of IU/mg; acceptability range is between 170->190 IU/mg); 2) biochemical contamination tests: protein content (acceptable content < 1%), nucleic acid content (acceptable content ~0.3 %) and DS content (acceptable content < 1%). These kind of test are not able to detect tainted substances if that molecules do not change heparin activities, in other worlds they cannot provide any information about structural differences between heparin and an eventual contaminant. One "lesson learned" from heparin crisis is the importance and necessity to get structural and activity informations at the same time to certify complex drug pharmaceutical agents identity, as for heparin. Taking a look to chemical similarities/differences between heparin (Fig. 13 A), CS (Fig. 13 B) and OSCS (Fig. 13 C) could help to understand how much is important this perspective change: 1) heparin is α-D-glucosamine sulfated polysaccharide, whereas chondroitin sulfate is β-D-galactosamine sulfated polysaccharide, as OSCS; 2) heparin anomeric bond connects the iduronate C1 atom to glucosamine through an α-(1->4) covalent bond, whereas chondroitin sulfate connects glucuronate C1 atom to galactosamine through an β-(1->3) covalent bond, as OSCS; 3) heparin amine group of the glucosamine residue is mainly substituted by a sulfate group, whereas chondroitin is exclusively substituted by N-acetyl group, as OSCS; 4) sulfation level are very different, in fact heparin DoS~2.5, CS DoS~2 (Sugumaran and Silbert, 1988) and OSCS DoS~4 (Maruyama, 1998). All these structural features do not alter the activity test results (over sulfation enhances OSCS coagulation activity, Kishimoto *et al*., 2008; Blossom *et al*., 2008), so the absence of any structural analytical test allowed the tainted heparin to be released on the heparin commercial circuit.

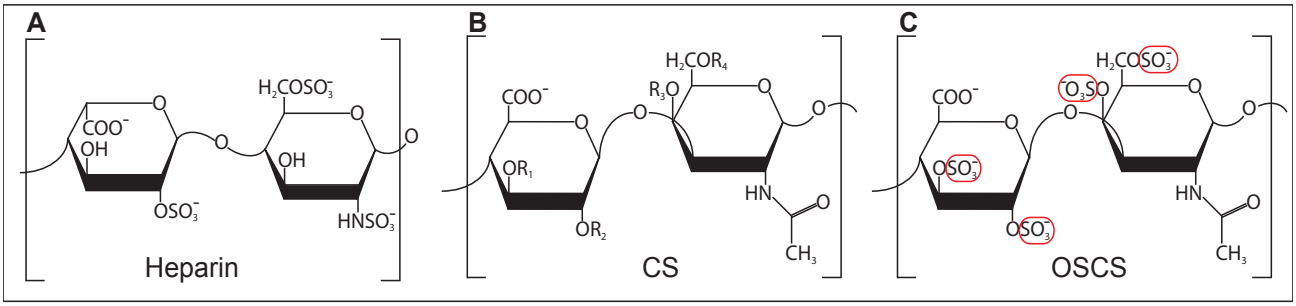

Figure 13. Chemical structures of major repeat units. (**A**–**C**) Schematic of major disaccharide repeat units of heparin (**A**), CS (**B**) and OSCS (**C**). For chondroitin sulfate, R1-R4 can be either sulfated or unsubstituted.

3.3. Heparin the bridge between glycomics and proteomics

The great physiological and biological impact of GAGs and in particular of HS/Hep is mainly ascribed to the big interaction network commonly established by Hep and proteins. The number of proteins

interacting with heparin growth with time and these increasing knowledge highlight its central role in biological phenomena control (Capila and Linhardt, 2002; Esko and Selleck, 2002; Lindahl *et al*., 2007; Bishop *et al*., 2007; Ori *et al*., 2008; Gandhi and Mancera, 2008). Different structural (NMR spectroscopy and X-ray crystallography) and molecular modeling approaches have been used to elucidate the 3D features and structure-activity relationships of protein-GAG interactions (Sasisekharan *et al*., 2006). Table 2 shows a list of heparin-interacting proteins, for the most the crystallized complex with heparin oligosaccharides was resolved (for NCAM (Neural Cell Adhesion Molecule), IL-8 (interleukin-8) and AP-1 (amyloid P-1) the complex with GAGs are not available), optimal length required for binding and their binding affinities can be found in. The most updated list of GAG-binding proteins can be freely consulted at MatrixDB (freely available database focused on interactions established by extracellular proteins and polysaccharides; Chautard *et al*., 2009; MatrixDB) (reviews are Ori *et al*., 2008; Gandhi and Mancera, 2008). Due to their anionic nature, GAGs interact mainly through ionic interactions with basic amino acids: sulfated and carboxylated groups on heparin chains show great affinity for highly positively charged protein surfaces. It was observed that in heparin binding proteins arginine and lysine are 200% and 300 % respectively enriched, compare to the remaining protein sequence (Caldwell *et al*., 1996). The arginine and lysine binding strength were compared and arginine binds 2.5 times more than lysine, in fact arginine establishes a major number of hydrogen bond and electrostatic interactions through its guanidino group with GAG sulfate groups, as a consequence Arg/Lys ratio could define the affinity of a binding site in a protein for GAGs (Hileman *et al*., 1998). Although the importance of electrostatic interactions, proteins-GAGs binding cannot be correctly described without considering all the others interactions involved in. In fact also van der Waals (VDW) forces, hydrogen bonds and hydrophobic interactions are involved in the binding between proteins and GAGs (it was observed that asparagine and glutamine are commonly present in heparin-binding domain and they can establish hydrogen bond; Hileman *et al*., 1998). Polar residues are also important interaction sites, serine and glycine residues provide minimal steric constraints and good flexibility for the interaction with GAGs (Caldwell *et al*., 1996). Protein-GAG interactions seem not to be exclusively dependent from protein aminoacidic sequence and/or electrostatic and non electrostatic interactions. With the exclusion of AT-bd, heparin-binding sites do not show absolute dependency on specific sequences or protein folds. Beside some similarities can be noticed among heparin-binding sites within families of proteins (i.e. FGF families), more often a graded series of activities has been observed, associated with structures possessing little or no apparent similarity in substitution pattern. It now seems likely that it is the combination of overall conformation, charge distribution and flexibility exhibited by a stretch of a GAGs, or a GAG oligosaccharide, that determines the extent of binding or activities. This argument is supported by the observation that comparable structural changes and activities can be induced by other (nonGAGs) sulfated carbohydrates, for example, the effect on angiogenesis induced by a sulfated exopolysaccharide on fibroblast growth factor-2 (FGF-2), or vascular endothelial growth factor (VEGF) (Parish *et al*., 1999; Matou *et al*., 2005). However, by means of pure heparin/HS oligosaccharide standards, minimal binding sequences preferentially recognized by some GAG binding proteins have been defined (Table 3). The interaction between the pentasaccharide and AT is the only real specific binding between a GAG molecule and protein so far described. Thanks to number of analogues of the AT pentasaccharide, the function and essentiality of its functional groups were demonstrated. Lack or modification of one of the essential functional group such as, 6-O-sulfate belong to AN_{NA}, the entire G residue, N-sulfate and 3-O-sulfate belong to A* and the N-sulfate of the reducing glucosamine abolish or drastically reduce the affinity to AT (Petitou *et al*., 2004; van Boeckel and Petitou, 1993). The presence of the heparin

Protein Name	Protein Type	PDB code	GAG binding sequence dimension	K_d	References
NCAM	Adhesion protein	-	5-mer	126 nM	Herndon *et al*., 1999
Fibronectin	Adhesion protein	1FNH	8- to 14-mer	10-100 nM	Sharma *et al*., 1999
IL-8	Chemokine	-	18- to 20-mer	37 μM	Spillmann *et al*., 1998; Krieger *et al*., 2004
Annexin V	Extracellular protein	1G5N	4- to 8-mer	20 nM	Capila *et al*., 2001
AP-1	Glycoprotein	-	4- to 5-mer	μM	Hernaiz *et al*., 2002
FGF-1	Growth factor	1AXM, 2AXM	4- to 6-mer	nM	DiGabriele *et al*., 1998; Guerrini *et al*., 2002
FGF-2	Growth factor	1BFB, 1BFC	4- to 6-mer	nM	Faham *et al*., 1996; Guglieri *et al*., 2008
FGFR-1	Receptor	1FQ9	12-mer	nM	Schlessinger *et al*., 2000
FGFR-2	Receptor	1E0O	12-mer	nM	Pellegrini *et al*., 2000
Thrombin	Serpin/protease	1TB6	16- to 18-mer	nM	Byun *et al*., 1996; Li *et al*., 2004
AT	Serpin	1AZX, 1E03, 1NQ9	5-mer	50 nM	Choay *et al*., 1983; Jin *et al*., 1997; Johnson *et al*., 2003; McCoy *et al*., 2003; Petitou *et al*., 2004
AT/FXa	Serpin/protease	2GD4	5-mer	100–200 nM	Johnson *et al*., 2006

Table 2. Characteristics of some of the known complexes between heparin or heparan sulphate fragments and proteins.

Molecular interactors	Minimal binding sequences	References
Hep: IL-8	I_S-$GlcN_{NS,6S}$-I_S-$GlcN_{NS,6S}$-I_S-$GlcN_{NS,6S}$	Spillmann *et al*., 1998
Hep: Tat	I_S-$GlcN_{NS,6S}$-I_S-$GlcN_{NS,6S}$-I_S-$GlcN_{NS,6S}$	Rusnati *et al*., 1999
Hep: Anexin V	I_S-$GlcN_{NS,6S}$-I_S-$GlcN_{NS,6S}$	Capila *et al*., 2001
Hep: AP-1	I_S-$GlcN_{NS,6S}$-I_S-$GlcN_{NS,6S}$-I_S-$GlcN_{NS,6S}$	Hernaiz *et al*., 2002
Hep: FGF-1	$GlcN_{NS,6S}$-I_S-$GlcN_{NS,6S}$-I_S	Guerrini *et al*., 2002
Hep: FGF-2	$GlcN_{NS}$-I_S-$GlcN_{NS}$-I_S	Guglieri *et al*., 2008
Hep: HCFII	I_S-$GlcN_{NS,6S}$-G-$GlcN_{NAc,6S}$-I-$GlcN_{NS,3,6S}$	Linhardt *et al*., 1986
Hep: heparanase	$GlcN_{NS,6S}$-I-$GlcN_{NAc,6S}$-I-$GlcN_{NS}$-G_{2S}-$GlcN_{NAc,6S}$-I	Li and Vlodavsky, 2009

Table 3. Heparin minimal binding sequences for IL-8, Tat, Anexin V, AP-1, FGF-1, FGF-2 HCFII and heparanase binding. IL-8= interleukin-8; Tat= HIV-1-trans-activating protein; AP-1= amyloid P-1; FGF-1= fibroblast growth factor-1; FGF-2= fibroblast growth factor-2; HCFII= heparin cofactor II.

AT-bd came up from three independent studies in 1976 (Lam *et al*., 1976; Hook *et al*., 1976; Andersson *et al*., 1976), those works clarified that most of the anticoagulant activity of heparin is attributable to species with high affinity (HA) for AT. $A_{NA}GA^*I_SA$ structural elucidation (Casu *et al*., 1981) was a real mile stone for heparin structural research together with the discovery that 3-O-sulfate group from

A* is an essential component of the AT-bd (Lindahl *et al*., 1980). Although the informations about the AT-bd, its location along the heparin chain is still uncertain. Rosenfeld and coworkers suggested that this domain could be located prevalently towards the NR end of the molecule (Rosenfeld *et al*., 1988), others evidences in literature proposed more random distribution (Pejler *et al*., 1987). The binding specificity of pentasaccharide with AT was recently confirmed studying the interaction between $A_{NA}GA^*I_SA$ containing oligosaccharides and the protein. NMR studies on AT-octasaccharides complex shown that (octasaccharides bearing $A_{NA}GA^*I_SA$ towards the reducing or nonreducing end), despite the different location of the pentasaccharide along the chain and the structure of the prolonging saccharide units, the whole pattern of contacts identified in the pentasaccharide-AT complex are maintained for all octasaccharides (Guerrini *et al*., 2008 [b]).

3.3.1. Antithrombin III

Antithrombin III (MW~58000) is the most studied heparin interactors and belong to the serine protease inhibitor (serpin) family. The identification of serpins as a protein family is dated back to the 80s based on the sequence similarities of AT, α1-antitrypsin and ovalbumin (Hunt and Dayhoff, 1980), structure analysis also reveal the similarities between AT, α1-proteinase inhibitor, HCFII and plasminogen activator inhibitor (PAI-1) (Gettins *et al*., 1996; Gettins and Serpin, 2002). Serpins are evolutionary conserved and their implication in different physiological aspects are documented (Fig. 14; Silverman *et al*., 2001). Not all the serpin family members are capable to inhibit serine proteases, some of them show others functions as cell signalling or hormone carriers (Gettins *et al*., 1996). Antithrombin is a major regulator of blood clotting, a plasma protein that inactivates a number of proteinases of the coagulation cascade, especially thrombin and FXa (Olson *et al*., 1993) (Fig. 9). AT inhibition rates are relatively slow under physiological conditions, but the combination of the high plasma concentration (~2.3 mM) and Hep/HS interaction leads to a rapid inactivation of the targets (Damus *et al*., 1973; Rosenberg *et al*., 1973). AT is a glycoprotein with 432 residues and it can be found in two forms: α-antithrombin (major form with four Asn residues glycosylated) and β-antithrombin (minor form and whereas Asn^{135} is not glycosylated). Several AT crystal structures are available and they show 9 α-helices surrounding 3 β-sheets (Schreuder *et al*., 1994; Carrell *et al*., 1994; Skinner *et al*., 1997). Of these secondary structures, two features are striking: a dominant five-stranded β-sheet A approximately in the centre of the inhibitor and an exposed 15-residue sequence containing the reactive bond Arg^{393}-Ser^{394}, the so-called reactive centre loop (RCL) at the ''top'' of the molecule (Fig. 15 A). Two residues, P15-P14 (Gly^{379}-Ser^{380}) at the N-terminal end of the reactive centre loop, are inserted as a short β-strand in-between strands 3 and 4 of β-sheet A in the inhibitor (Fig. 15 A). This feature is called the partial insertion of RCL and undergoes some major changes during the process of proteinase inhibition (see below). The structure of AT cleaved at the reactive bond is similar to intact AT except for the complete insertion of RCL as strand 4a in β-sheet A (Fig. 15 B). This structural change results in the movement of the P1 residue from the ''top'' of the molecule to the ''bottom,'' a distance of approximately 70 Å. This conformational change following cleavage by the target enzyme leads to significant thermodynamic stabilization of the molecule (Bruch *et al*., 1988; Kaslik *et al*., 1997). Crystal structure of the α1-proteinase inhibitor – trypsin complex (Huntington *et al*., 2000) and biochemical results (Plotnick *et al*., 1996; Calugaru *et al*., 2001) indicate that the structural change following cleavage of the P1-P1' bond is critical for the disruption of the catalytic triad of the proteinase, thereby resulting in the inactivation of the enzyme. AT inactivation of thrombin and factor Xa proceeds in similar manner (Björk and Olson, 1997).

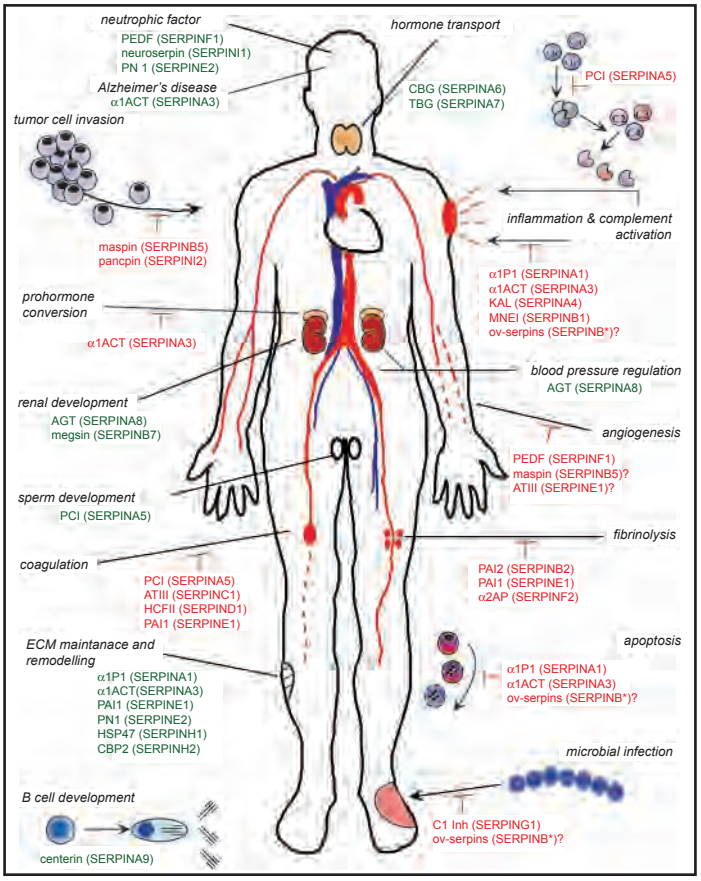

Figure 14. Physiological functions of human serpins. Human serpins are involved in a diversity of biologic functions (italics). For some serpins (red type), their biological functions appear to be related directly to proteinase inhibition. For others (green type), their activity does not require proteinase inhibition, or their role in the biologic process has not been defined (adapted from Silverman *et al*., 2001).

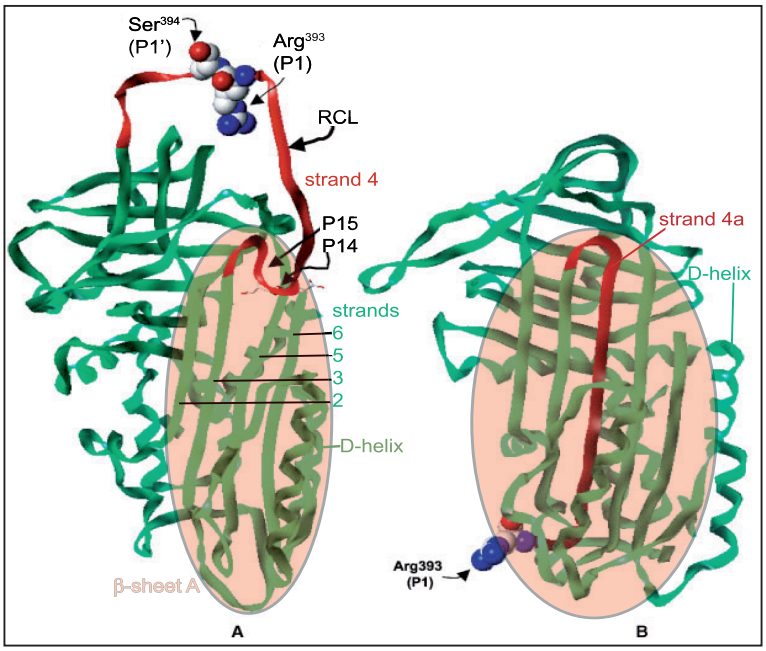

Figure 15. Ribbon diagram of native (A) and cleaved (B) plasma AT. The structure of plasma AT was obtained from PBD (file name '1ath'). The RCL is shown in red. Reactive bond residues Arg^{393} (P1)-Ser^{394} (P10) is shown are space-fill representation, whereas P14-P15 residues (Glu^{381}-Gly^{380}) are shown in capped sticks form. The P1 residue, in an exposed orientation in the native structure, moves from the 'top' of the molecule to the 'bottom' following cleavage with a proteinase. The proteinase, i.e. factor Xa, moves with the P1 residue to the bottom of the inhibitor and gets covalently trapped. RCL is inserted as strand 4 in 6-stranded β-sheet A (adapted from Desai, 2004).

3.3.2. AT is activated by Hep binding

Heparin can activate AT inhibition activity by two mechanisms: a) AT/Hep interaction through $A_{NA}GA^*I_SA$ pentasaccharide (called AT conformational activation) and b) bridging mechanism.
a) AT conformational activation leads to RCL expulsion with a conformational change of the P1-P1' reactive centre (Björk and Olson, 1997; Craig *et al*., 1989; Chuang *et al*., 2001; Olson and Björk, 1992 [b]; Fig. 17 A), the conformational change allows a better recognition from FXa resulting in accelerated cleavage of the P1-P1' bond and rapid formation of the covalent inhibition complex (Fig. 15 B; Fig. 17 A). This mechanism induces a poor acceleration of thrombin inhibition: only twofold (Desai, 2004).
b) after AT bound to Hep pentasaccharide (Fig. 17 A), thrombin interacts and binds to a nonspecific site of the same heparin chain forming the ternary complex AT-Hep-thrombin (Fig. 17 B; Li *et al*., 2004). Heparin bridging guides thrombin to encounter the inhibitor with a diffusion movement, the heparin minimum binding sequence to allow the bridging mechanism was estimated in ~18 residues (Petitou *et al*., 1999; Duchaussoy *et al*., 1999). The bridging mechanism was demonstrated to have an important role also *in vivo*: at physiological Ca^{2+} concentrations UFH enhances FXa inhibition of ~40-fold suggesting that longer chains bind to an exosite on the enzyme (Rezaie *et al*., 1998). Likewise, a bell-shaped dependence of acceleration on the concentration of heparin chains, characteristic of a bridging mechanism, was observed. Mutagenesis of the basic residues in the thrombin heparin-binding site and structural studies of the ternary complex (Jin *et al*., 1997; Li *et al*., 2004; Johnson *et al*., 2006) shown the principal amino acids involved in the bridging mechanism (Fig. 16): Arg^{47}, Lys^{114}, Lys^{125} and Arg^{129} were identified as the most important in the heparin binding site of AT using mutant and recombinant ATs (Sheehan and Sadler, 1994; Ye *et al*., 1994; He *et al*., 1997; Tsiang *et al*., 1997). These basic residues participate in ionic interactions with the negatively charged groups of heparin, as observed in the crystal structure of an AT-pentasaccharide complex. Residues Arg^{129}, Lys^{114} and Arg^{47} are critical for the heparin-induced conformational change of AT, contributing to the resulting AT-Hep high affinity binding (Jin *et al*., 1997; Johnson *et al*., 2003; McCoy *et al*., 2003; Li *et al*., 2004; Johnson *et al*., 2006).

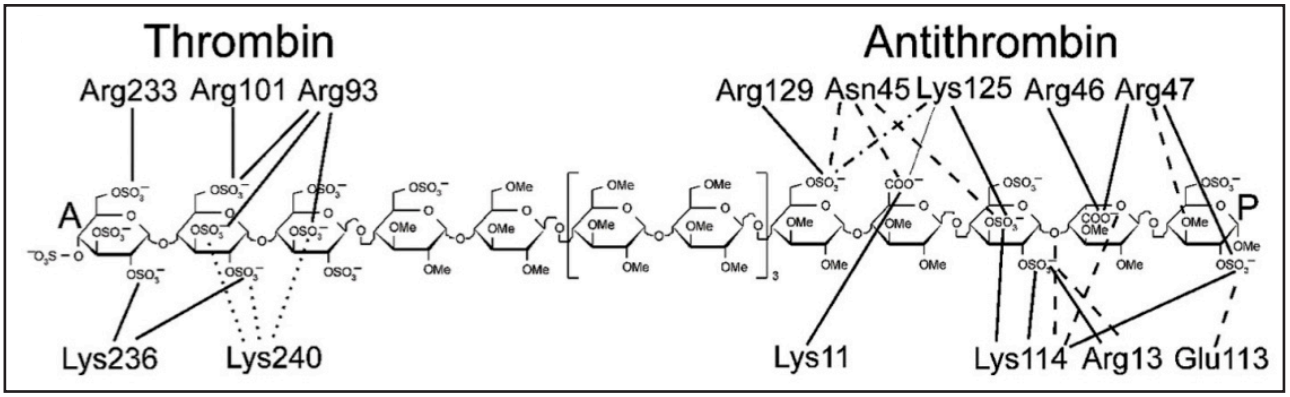

Figure 16. Thrombin and AT interactions established with heparin. Letter code on heparin stands for nonreducing end (A) and reducing end (P). The interactions with thrombin and AT are indicated by lines, with solid lines indicating a salt bridge, dashed lines hydrogen bonds, dashed-dotted lines for water-mediated hydrogen bonds and dotted lines for potential interactions (only for Lys240) (adapted from Li *et al*., 2004).

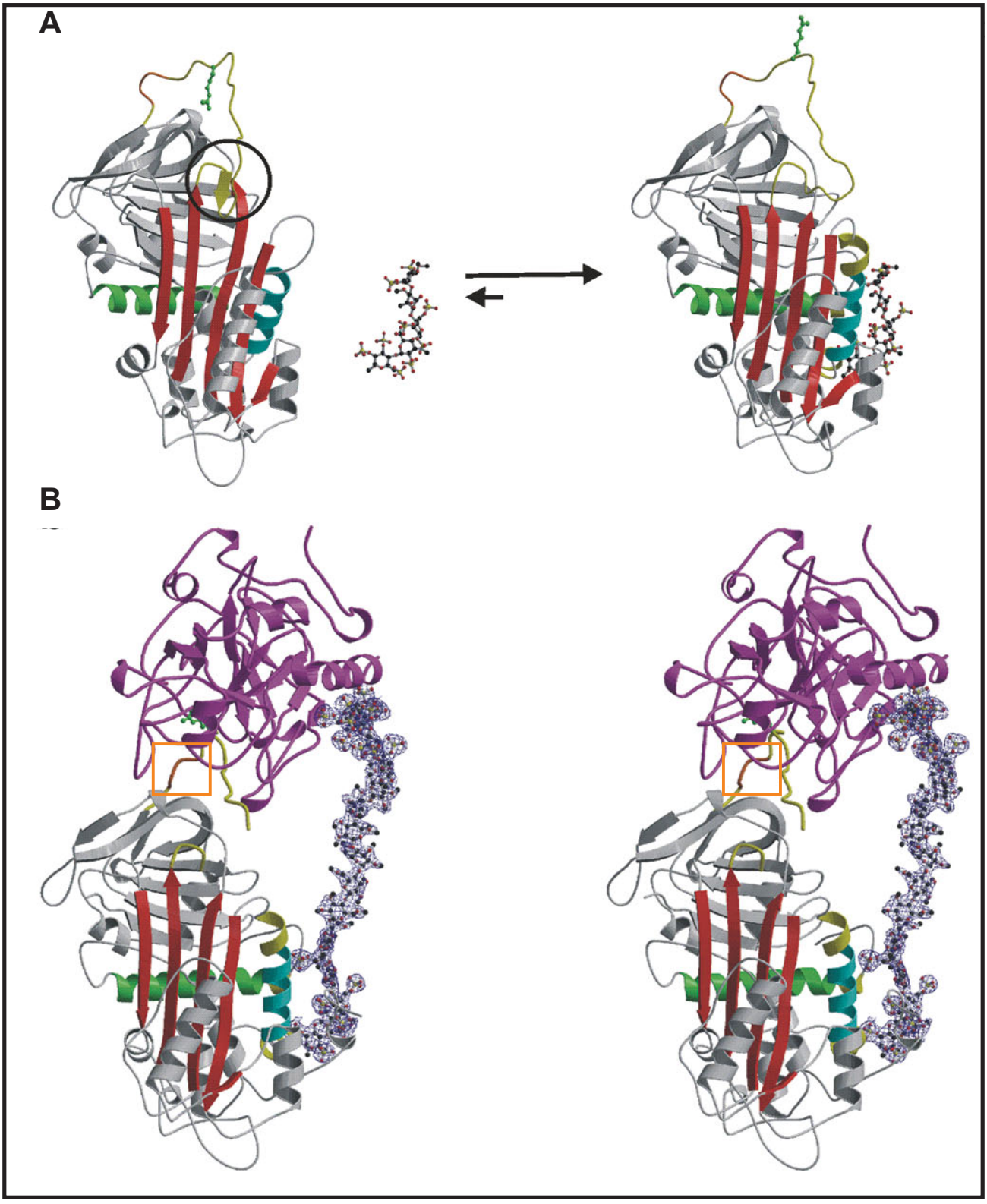

Figure 17. AT/Heparin binding and catalysis of thrombin inhibition by AT. (A) $A_{NA}GA^{*}I_{S}A$ binding to AT induces a conformational change leading to hinge region expulsion (circled) of RCL (yellow) from the central β-sheet A (red) and extension (yellow) of the A and D helices (green and cyan, respectively). As a consequence P1 Arg is liberated (green ball-and-stick). The flexibility of the C-terminal portion of the RCL (P' side) is limited, despite a three-residue insertion (orange square), owing to a tight hydrogen-bonded turn. (**B**) Stereo representation of the crystal structure of the ternary complex between AT (coloured as above), thrombin (magenta) and heparin (ball-and-stick). Thrombin is docked toward the heparin-binding site of AT and makes several exosite interactions. The expulsion of the hinge region is not required to form this complex, but the P' side of the RCL (orange) has been elongated (adapted from Li *et al*., 2004).

3.3.3. The role of extensions of the active pentasaccharide sequence

The major pharmaceutical agents for cardiovascular therapies are UFH and LMWH (Camporese *et al*., 2009), although, as mentioned before, in some cases UFH treatment induced bleeding problem and thrombocytopenia (Battistelli *et al*., 2010; Otis and Zehnder, 2010). The lower molecular size of LMWHs, compared with heparin, involves a more predictable pharmacological action, sustained antithrombotic activity and better subcutaneous bioavailability (Mousa, 2007). LMWHs consist of complex mixture of fragments ranging from tetra to hexadecasaccharides and somewhat higher oligosaccharides (Viskov *et al*., 2009; Bisio *et al*., 2009; Zang *et al*., 2008). Apart from tetrasaccharides, about one out of five chains of LMWHs contain the active sequence $A_{NA}GA^*I_SA$ (Bisio *et al*., 2009), in addiction very little is known about $A_{NA}GA^*I_SA$ flanking sequences. Earlier studies on tetrasaccharides sequences adjacent to the AT-binding site have demonstrated two possible variants of AT-binding sequences, suggesting a possible role of the extensions of these sequences on binding to AT (Loganathan *et al*., 1990). Longer AT-binding sequences, such as decasaccharides, were also previously isolated (Toida *et al*., 1996). The influence of the position of the pentasaccharide sequence along the oligosaccharide chains together with the knowledge of the role of the residues prolonging the active sequence toward both its reducing and nonreducing side are among the major goals of current heparin research (Guerrini *et al*., 2006; Guerrini *et al*., 2008 [b]). Although the active pentasaccharide $A_{NA}GA^*I_SA$ is taken as paradigm for a unique heparin sequence targeting a specific protein (i.e. AT) (Petitou *et al*., 2004), different mechanisms have been proposed for its interaction with AT in terms of position and conformation of sugar residues. The possibility of a shift along the AT D-helix for sequences longer than pentasaccharide was taken into consideration (Belzar *et al*., 2000). Independent crystallographic and NMR studies on the structure of complexes of AT with $A_{NA}GA^*I_SA$ and $A_{NA}GA^*I_SA$-containing oligosaccharides suggested that the position of the pentasaccharide in the protein binding region is unique (Jin *et al*., 1997; Hricovini *et al*., 2001; Li *et al*., 2004; Guerrini *et al*., 2006; Johnson *et al*., 2006; Guerrini *et al*., 2008 [b]). These studies provided information on both the ring conformation of the monosaccharide residues and the geometry of the glycosidic linkages of the AT-bound pentasaccharide. The uronic acid flanking AT-bd or within it strongly affect AT/oligosaccharide complex affinity, as it was demonstrated for the unmodified glucuronic acid residue (Casu and Lindahl, 2001; Petitou *et al*., 2004). The 2-O-sulfate group of the 2-O-sulfated iduronic acid residue was shown to contribute to the binding to AT only indirectly, by favouring the $^2S_0$ conformation of the iduronate ring. Indeed, the 2-OSO_3 group appears to be the main driving force in affecting the shift of the conformational equilibrium of the sulfated iduronate residue towards the skewboat form, thus enhancing dipolar contact between the $A_{NA}GA^*I_SA$ reducing disaccharides with AT aminoacids (Hricovini *et al*., 2001). However, the contribution of the I_S to the AT affinity may be less essential when the size of oligosaccharides is larger than an octasaccharides (Chen *et al*., 2007). Although I_S acts as the major actor for $A_{NA}GA^*I_SA$ binding properties, published data suggest also an important role for 6-O-sulfate group of the A residue at the reducing end of $A_{NA}GA^*I_SA$, in fact its absence in synthetic pentasaccharides results in a decrease in the affinity for AT (van Boeckel and Petitou, 1993). Recently our laboratory in collaboration with Sanofi-Aventis demonstrated the active role of residues prolonging the pentasaccharide sequence toward both its reducing and nonreducing end for some octasaccharides isolated from enoxaparin (Guerrini *et al*., 2006; Guerrini *et al*., 2008 [b]). The affinity of these octasaccharides (Fig. 18) for AT depends not only on the location of the pentasaccharidic sequence $A_{NA}GA^*I_SA$ along the oligosaccharide chain, but may be also strongly affected by the structure of flanking

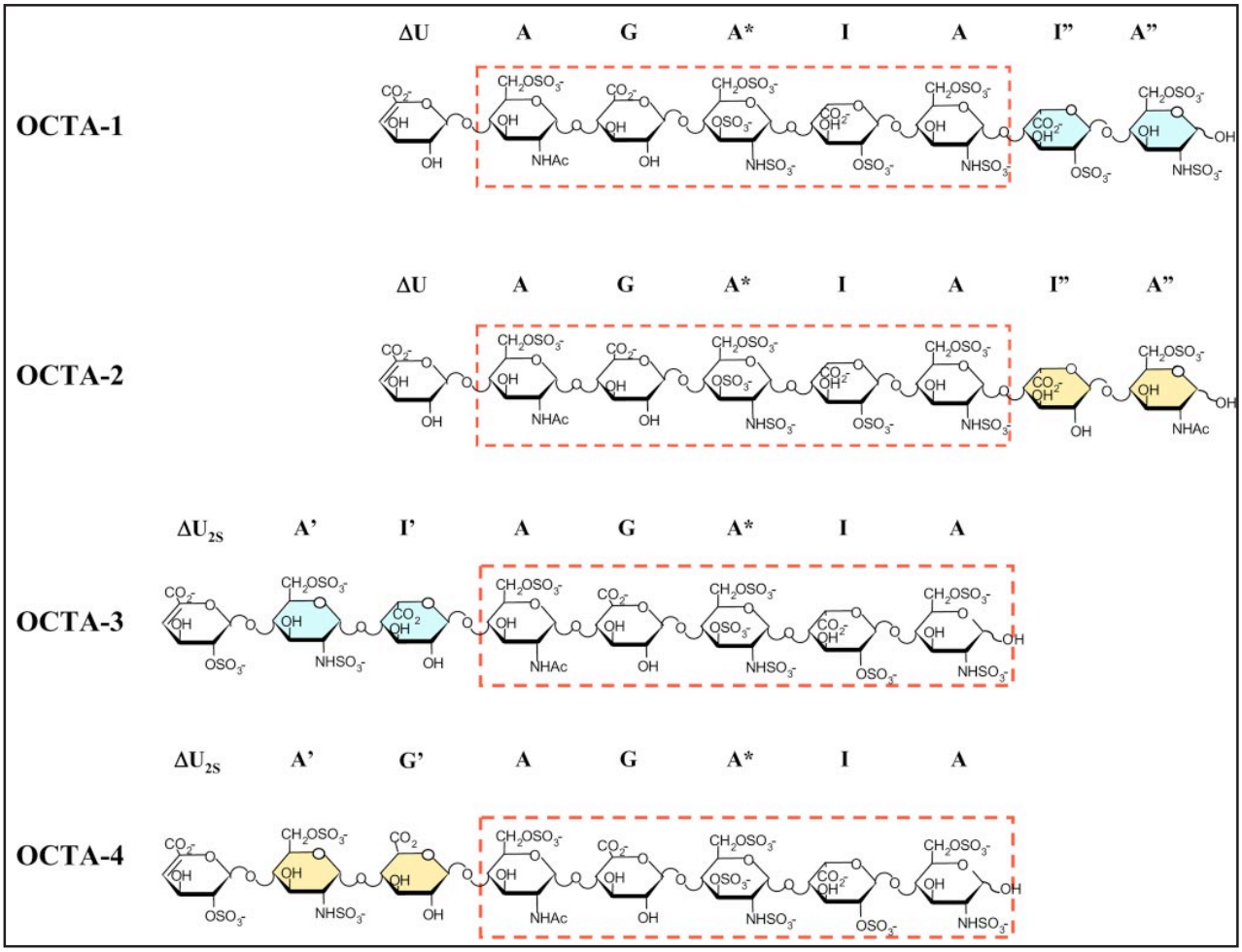

Figure 18. The $A_{NA}GA^*I_SA$ sequence is highlighted in the dashed frame. Reducing end $A_{NA}GA^*I_SA$ extensions of OCTA-1 and OCTA-2 (I"-A") differ in degree of sulfation being trisulfated in OCTA-1 (I_S-$GlcN_{NS,6S}$, in blue) and monosulfated in OCTA-2 (I-$GlcN_{NAc,6S}$, in yellow). Nonreducing end $A_{NA}GA^*I_SA$ extensions of OCTA-3 (in blue) and OCTA-4 (in yellow) differ from each other in the structure of their uronic acid residues, which are the common iduronic acid (I') in OCTA-3 and the unusual glucuronic acid (G') in OCTA-4.

sequences. Notably, the presence of glucuronic acid instead of iduronic acid before the pentasaccharide moiety increases one order of magnitude the affinity toward AT (Guerrini *et al*., 2008 [b]).

3.3.4. Amyloid-β

Heparan sulfate proteoglycans (HSPGs) are involved in many biological process and also in certain neurodegenerative diseases. PGs or GAGs are associated with a variety of amyloid deposits and amyloid-β (Aβ) deposit, this is an amyloidogenesis hallmark and especially for Alzheimer disease (AD) (Castillo *et al*., 1997; van Horssen *et al*., 2003; Watanabe *et al*., 2004; Gruys *et al*., 2006). GAGs are also involved in other neurodegenerative diseases: Gerstmann-Straussler syndrome, Creutzfeldt-Jakob disease, scrapie (Snow *et al*., 1990), mucopolysaccharidoses (Ginsberg *et al*., 1999), Parkinson's disease (Liu *et al*., 2005) and other neuromuscular diseases (Peat *et al*., 2008), all of which share genesis of senile plaques (SPs), cerebrovascular amyloids and neurofibrillary tangles (NFTs) (Perlmutter *et al*., 1990; Su *et al*., 1992; Bame *et al*., 1997; Verbeek *et al*., 1999; van Horssen *et al*., 2003). GAGs pathological functions in these disease is still not clear, suggesting the need for research in this area (Watanabe *et al*., 2004).

3.3.5. Alzheimer disease

Worldwide, approximately 18 million people suffer from Alzheimer's disease, with this number projected to increase to approximately 34 million people by the year 2025 (Hebert *et al*., 2003). It was estimated at least $100 billion as a consequence of direct and indirect annual costs of caring for individuals with Alzheimer's disease in the US alone (Ernst and Hay, 1994). As a prospective, number of patients affected, economical and social impact will dramatically increase in the future, for these reasons therapeutic strategies are growing in interest during the last 20 years. Alzheimer disease is a complex pathology with neurobiological and pathological features: neurologically, first onsets are mild cognitive impairments, deficits in short-term memory, loss of spatial memory and emotional imbalances. The end point of this pathological progression is a total loss of executive function (Pimplikar *et al*., 2009). Pathologically, it is observed the presence of Aβ plaques (Glenner and Wong, 1984) and intracellular tangles of hyperphosphorylated tau protein (Braak and Braak, 1998; Ballatore *et al*., 2007). It is not clear the spatial and temporal connection between dementia and plaques deposition, hyperphosphorylated tau and insoluble tangles are initially observed in the limbic system (entorhinal cortex, hippocampus, dentate gyrus) and then progress to the cortical region, while Aβ plaque deposition starts in the frontal cortex to spread over the entire cortical region. Aβ-peptides are derived from the proteolityc cleavage of the transmembrane amyloid precursor protein (APP, 695 amino acids) (Cole and Vassar, 2008): the β-site APP-cleaving enzyme (BACE 1) operates an extracellular cleavage at Asp^{+1} position of APP, (596-597 of the APP sequence) generating one extracellular big fragment (APPsβ) and another transmembrane fragment (C99). The transmembrane fragment is the substrate of γ-secretase [a protein complex containing presenilin (PS)] that with an intra-membrane cleavage at Val^{+40} or Ala^{+42} position of C99 fragment generates the Aβ-peptides and the amyloid precursor protein intracellular domain (AICD), the first released in the extracellular environment and the second diffuses in the cytol. γ-secretase can generate different peptides [40 amino acids Aβ ($Aβ_{1-40}$) and/or 42 amino acids Aβ ($Aβ_{1-42}$)] depending on the cleavage site (Fig. 19). Presence and accumulation of Aβ-peptides could not be enough to cause AD, because Aβ-peptides were found in both normal and AD brain (Ashall and Goate, 1994).

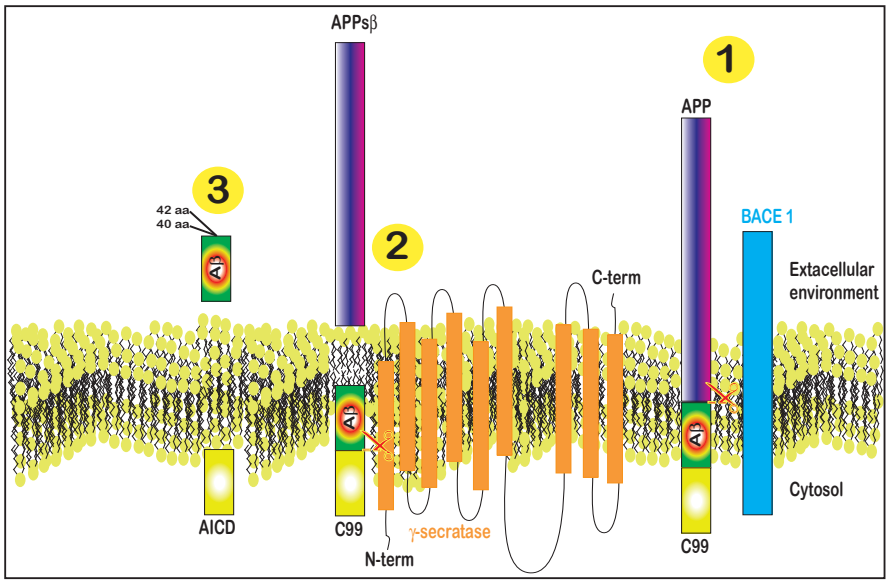

Figure 19. APP processing. BACE1 and the γ-secretase complex sequentially cleave APP to generate Aβ. 1) BACE 1 cleavage of APP, 2) C99 fragment cleavage from γ-secretase complex. 3) Aβ liberation in the extracellular environment and AICD release in the cytosol.

3.3.6. Aβ structure

The high content of amyloidic peptide deposit in the AD brain is a typical hallmark for Alzheimer disease. Hardy and Selkoe (2002) suggested the so called amyloid cascade hypotesis as a model for dementia diseases progression characterised by amyloid deposit: 1) accumulation of missense mutations in APP and/or PS genes causes an hyper synthesis and accumulation of $A\beta_{1-42}$, 2) peptides accumulation induces the condition to trigger amyloid aggregation and fibrils/plaque formation, 3) soluble aggregates start to alterate the synapse functions, 4) amyloid accumulation initiates inflammation (complement system activation and leukocytes recruitment), 5) inflammation side effects cause synaptic and neuritic injury, 6) that, becoming worst, alterate the neuron membrane homeostasis and ions exchange properties, 7) kinases and phosphatases are misregulated leading to the tau protein tangles formation and finally 8) to dementia (neuron dysfunctions and neuron death). Experimental evidences in the last years suggest that the real neurotoxic effects might be caused by soluble aggregates, thus plaques accumulation might be the final consequence of Aβ aggregation (Carotta *et al*., 2006; Pimplikar *et al*., 2009; Kuperstein *et al*., 2010). Different approaches were applied to elucidate the molecular structure (Serpell *et al*., 2000; Tycko, 2006) and mechanism (Harper *et al*., 1999; Aguilar and Small. 2005; Bellesia and Shea, 2009; Di Fede *et al*., 2009) of oligomerisation and fibril formation, nevertheless the fibrillogenesis mechanism is still not completely understood: the first onset is characterised by the formation of small Aβ oligomers (between 6 to 8 unit, called seeds); aggregating seeds organize in a super structure (β-sheet structure) with a β-sheet spacing between 10-11 Å, this generates the fibrillar precursor (protofibrils/protofilaments) with a diameter between 25-30 Å, thus protofibrils assembly leads to the fibril formation (composed by several protofilaments, five or six with a diameter between 60-80 Å). Finally, fibril accumulation causes plaque deposit. Whether these small intermediates interact directly to form protofibrils and then these elongate to form the fully formed fibril, or whether protofilaments are formed first and then associate together remains ambiguous. A schematic representation of the fibrillisation events is shown in Fig. 20.

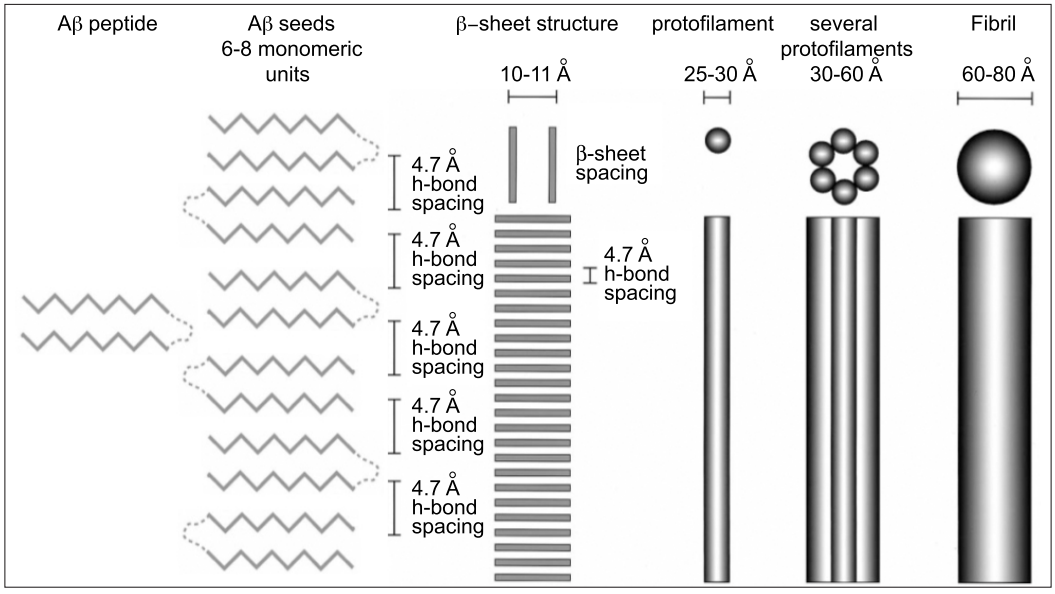

Figure 20. Hierarchy structure of Aβ peptide. The monomer is folded into a double β-strand structure, that interacting each others generate amyloidic fibril.

Structure prediction studies (Soto *et al*., 1994) have indicated that the C-terminal 10 residues and residues 17-21 of Aβ shown the greatest hydrophobicity while the C-terminus (from residue 28) shown a high probability for β-sheet structure. Residues 9-21 shown a lower probability for β-sheet. Two β-turns are predicted between residues 6 and 8 and residues 23 and 27 (Soto *et al*., 1994; Kirschner *et al*., 1987). These characteristics are highlighted in Fig. 21.

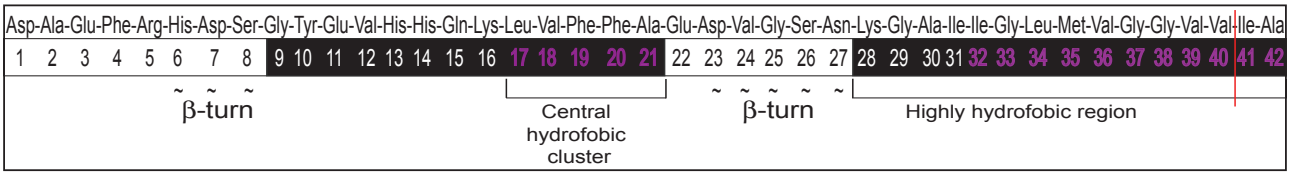

Figure 21. Aβ-peptides aminoacid sequence and predicted structures. On top three letter amino acidic code. The red line indicates $A\beta_{1\text{-}40}$ sequence end.

Recently NMR (Petkova *et al*., 2006; Tycko, 2006; Yu *et al*., 2009) and molecular modeling (Urbanc *et al*., 2004; Urbanc *et al*., 2004 [b]) studies succeeded to solve the Aβ monomer/oligomer structure: secondary structure is characterised by a not ordered region from Asp^1 to Ser^8, two β-strand structures (the first from Gly^9 to Val^{24} and the second from Ile^{32}->Val^{40}/Ile^{42}) and a loop from Gly^{25} to Leu^{31} connecting the first to the second β-strand (Fig. 22 A). NMR measurements indicate in-register parallel alignment of neighbouring peptide chains for residues Val^{12}–Val^{39} and are consistent with disorder in the N-terminal segment; the tertiary structure allows monomer to organize in parallel β-sheet perpendicular to the major protofibril axis (Fig. 22 B, C) and finally the fibril structure is characterised by cross β-structure between protofilaments (Fig. 22 D).

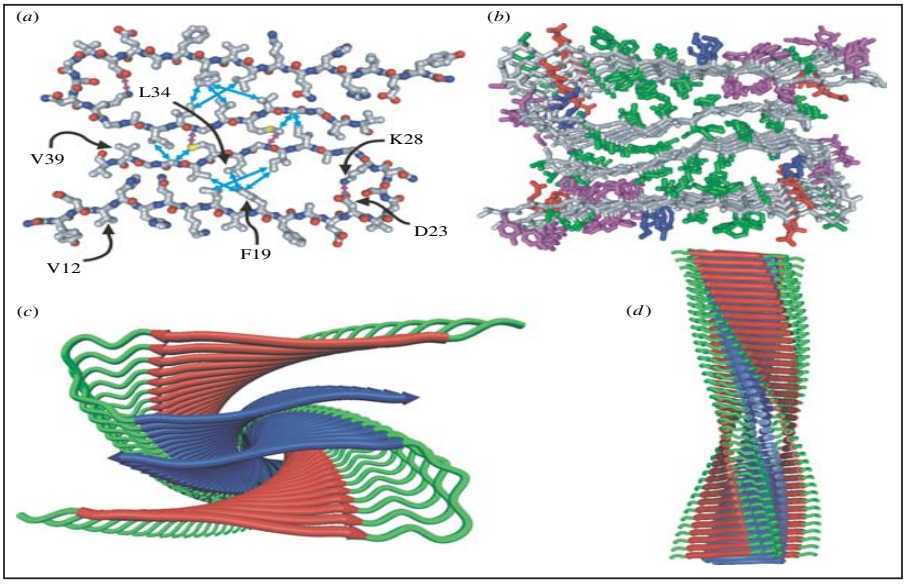

Figure 22. Structural model for the protofilament in $A\beta_{1\text{–}40}$ fibrils (Petkova *et al*., 2006). The long axis of the fibril is perpendicular to the page in panels (a)–(c). The long axis is vertical and parallel to the page in panel (d). (a) All-atom representation of a pair of peptide molecules. Residues Tyr^{10}–Glu^{22} and Ala^{30}–Val^{40} have β-strand conformations, forming two separate in-register, parallel β-sheets. The protofilament is a four-layered β-sheet structure with C2 symmetry about its long axis. Blue double-headed arrows indicate side-chain–side-chain and side-chain–back-bone contacts. Purple double-headed arrows indicate contacts established by measurements of ^{15}N–^{13}C dipole–dipole couplings. (b) Average structure resulting from 10 independent molecular dynamics/energy minimization runs on a cluster of 12 peptide molecules, with interatomic distances and backbone torsion angle restraints dictated by solid-stateNMR data. Hydrophobic, polar, negatively charged and positively charged side-chains are coloured green, purple, red and blue respectively. The four-layered β-sheet structure is stabilized primarily by hydrophobic interactions in the core of the protofilament. Polar and charged side-chains are on the exterior, with the exception of oppositely charged Lys^{28} and Asp^{23} side-chains, which form salt bridges. (c, d) Cartoon representations, with residues Val^{12}–Ala^{21} in red and residues Ala^{30}–Val^{40} in blue (adapted from Tycko, 2006).

3.3.7. Interaction between Aβ and GAG

Aβs and APPβs bind with high affinity to both the core protein and the GAG side chains of vascular heparan sulfate PG (HSPG) (Kjellen and Lindahl, 1991). GAGs, such as KS, DS and CS, have an especially high affinity for Aβs, suggesting that the position and distribution of the sulfate groups on the GAG backbone are important for Aβs–GAG interactions (Narindrasorasak *et al*., 1991; Buee *et al*., 1993 [a],[b]). Aβ-GAG binding site was identified as residues 13–16 (His-His-Gln-Lys) and it represents a unique site for targeting inhibition of Aβ fibril formation (Fraser *et al*., 1992; van Horssen *et al*., 2003). His^{13} in particular is an important residue and is considered critical for GAG interaction (McLaurin and Fraser, 2000). Aβs-GAG interactions have been studied with a variety of biophysical techniques, such as circular dichroism (CD) spectroscopy, fluorescence spectroscopy, NMR spectroscopy, electron microscopy and surface plasmon resonance [SPR, a biosensor technology useful for analyzing the extension and dissociation reaction of proteins (Myszka *et al*., 1999)].Using SPR (Ariga *et al*., 2010), GAGs interaction profiles were studied at pH 4.5 [Aβ-GAG interaction is pH dependent (Brunden *et al*., 1993)] after immobilizing $Aβ_{1–40}$, $Aβ_{1–42}$ and $Aβ_{25–35}$ [$Aβ_{25–35}$ is a small synthetic amyloid composed of 10 amino acids with a very poor aggregation activity, but keeping cytotoxic effect (Forloni *et al*., 1996; Yan *et al*., 1996)] and the results shown that Aβs interact with GAGs with different binding affinities in the following rank order: $Aβ_{1–40} > Aβ_{25–35} > Aβ_{1–42}$. Most recently as further evidence for Aβs-GAG interaction, (Madine, 2009) it was reported a procedure in which a ^{13}C-labeled N-acetyl derivative of the GAG heparin ([^{13}C-CH_3]NAcHP) was used as a probe for analysing protein-GAG interactions in amyloid fibrils using solid-state NMR (ssNMR) spectroscopy. NAcHP emulates heparin by enhancing aggregation and altering the fibril morphology of $Aβ_{1–40}$ and α-synuclein, the major protein component of the Lewy bodies associated with Parkinson's disease. ^{13}C-ssNMR spectra confirmed the presence of [^{13}C-CH_3]NAcHP in $Aβ_{1–40}$ fibril deposits and detected dipolar couplings between the glycan and Arg^5 at the $Aβ_{1–40}$ N-terminus, suggesting that the two species are intimately mixed at the molecular level. That procedure provides a basis for further investigations of polypeptide–glycan interactions within amyloid fibrils.

3.3.8. Can GAG act as therapeutic agents for amyloidogenic disorders?

Potential therapeutic strategies for amyloidosis include reducing the production of amyloidogenic precursor proteins and Aβs, interfering with fibrillogenesis and enhancing amyloid clearance are under consideration (Hirschfield and Hawkins, 2003). Identifying structure–activity relationships between Aβ and different GAGs as well as dependence conditions of GAG binding is necessary for successfully developing and evaluating GAG-specific therapeutic interventions (McLaurin *et al*., 1999). GAGs may act not only to promote fibril formation and aggregation of Aβs, as described above, but also to protect aggregated Aβ from proteolytic degradation (McLaurin *et al*., 1999; Leveugle *et al*., 1998). The latter effect is believed to be competitively inhibited by certain other GAGs. The Aβ -GAG interaction may be mediated by a unique binding site that could serve as a target for inhibiting amyloid formation, either through competition for GAG binding or by specifically targeting the GAG-binding site. As shown above, the His-His-Gln-Lys peptide in Aβ is an essential region for amyloid formation. Drugs targeting that region, therefore, may effectively block the β-structural transition necessary for fibril nucleation. That therapeutic strategy is supported by *in vitro* studies (McLaurin and Fraser, 2000). HSs are known to bind to Aβ and in turn interfere with its fibrillogenesis. HSs are

interesting candidates for therapeutic intervention (Gervais *et al*., 2001), because of the multiple roles that HS plays in organ development and in organ and cell functions. Of course, the potential side effects of targeting HS biosynthesis for therapeutic purposes should be considered. The interaction of HSPGs and GAGs can be inhibited by other sulfated compounds, such as HS, DS and pentosan polysulfate (Leveugle *et al*., 1994). Drugs manufactured by chemical synthesis, isolated from naturally occurring polysaccharides (with or without chemical modification), or manufactured by use of recombinant enzymes (GlcA C5-epimerase; sulfotransferases) with appropriate saccharide substrates should prove useful in inhibiting the binding of HSPGs and GAGs (Kuberan, 2003; Lindahl *et al*., 2007). Knowledge on the role of HSPGs in AD pathology should lead to their therapeutic use (van Horssen *et al*., 2003), especially LMWHs, which can interfere with the interaction between HSPGs and Aβ to stop or prevent amyloidogenesis. Both HSPGs and LMWHs can reduce the progression of inflammation-associated amyloidosis (Kisilevsky *et al*., 1995; Kisilevsky and Svarek, 2002). Several LMWH compounds are reported to have that capability and may provide a potential therapeutic strategy for treating amyloid diseases, especially AD. Zhu *et al*. (2001) reported that dramatic inhibition of amyloidosis was observed after injecting the LMWHs enoxaparin and dalteparin in a amyloid A (AA) amyloidosis mouse model. LMWHs can reverse the process of amyloidosis and inhibit fibril formation by blocking formation of β-pleated structures. GAG mimetics can inhibit this binding and block formation of β-pleated sheets and adherence of disaccharides (Walzer *et al*., 2002) and also efficiently inhibit the stimulatory effect of heparin on APP secretion (Leveugle *et al*., 1994). Small-molecule anionic disulfides (MW 900–1,000) are reported (Kisilevsky *et al*., 1995) to inhibit the *in vitro* acceleration of Aβ fibril formation by HS. Administered orally, these compounds substantially reduced murine splenic AA amyloid progression and also interfered with HS-stimulated β-peptide fibril aggregation. In addition, anionic compounds cross the blood–brain barrier (BBB) *in vivo* and have exhibited protective effects against Aβ-induced cytotoxicity as well as inhibition of the formation of β-pleated sheets (McLaurin *et al*., 1999; Gervais *et al*., 2001; Zhu and Kindy, 2001). These compounds, which have an antiamyloid profile combined with the ability to cross the BBB, are promising therapeutics for amyloid disorders (Gervais *et al*., 2001). Furthermore, an LMWH, 4-deoxy analogue of N-acetylglucosamine, attenuated plaque formation and improved neuropathology of AD in animal models (Kisilevsky and Svarek, 2002; Kisilevsky *et al*., 2003). A beneficial effect of LMWHs (certoparin and C6) as a preventative and/or therapeutic treatment of an Aβ-induced rat model of neuropathology has also been reported (Walzer *et al*., 2002). LMWHs may prevent Aβ from forming its neurotoxic β-pleated sheet conformation *in vivo*, subsequently blocking Aβ-induced neuropathology. In addition, heparin oligosaccharides are known to exhibit antiinflammatory properties as well as inhibitory effects on proteoglycan assembly and may prove useful as neuroprotective agents (Ma *et al*., 2007). Recently, Dudas *et al*. (2008) examined the neuroprotective properties of ''neuroparin'' (C3), a low-molecular-weight GAG (~2.1 kDa), in animal models with characteristic AD lesions. Oral administration of C3 can prevent $A\beta_{25-35}$-induced tau-2 immunoreactivity (Dudas *et al*., 2002). Administration of C3 attenuates AF64A-stimulated (AF64A is the ethylcholine mustard aziridinium ion), low-affinity nerve growth factor receptor-immunoreactive axonal varicosities in the rat septum and also increases dendritic arborization of hippocampal CA1 neurons. For those reasons, C3 may possess neuroprotective properties against many of the characteristic neural lesions in AD. Because C3 can cross the BBB, it could represent an entirely new class of agents that can penetrate the BBB and inhibit Aβ-PG binding for the treatment of neurodegenerative disorders. Phase I clinical studies have, in fact, been completed and proved supportive; the efficacy of one of the compounds is currently being tested in a human phase III trial. For that reason, C3 may prove beneficial in the treatment

of AD and other vascular dementia and senile dementia of the AD type (Ma *et al*., 2003). In addition to C3, a specific disaccharide (CSPG-DS) from the enzymatic degradation of chondroitin sulfate proteoglycan, was found to promote central nervous system recovery by modulating both neuronal and microglial behavior (Rolls, 2004). In neurons, CSPG-DS induced neurite outgrowth and protected against neuronal toxicity and axonal collapse *in vitro*. In light of experimental and clinical results obtained from studies addressing the role of heparan sulfate in amyloid deposition, it is anticipated that additional novel antiamyloid therapeutic targets will be developed by rational design. Li *et al*. (2005) generated transgenic mice that overexpress human heparanase and recently this model demonstrated resistance to amyloid induction (Lindahl *et al*., 2007) further underscores the significance of GAGs in the disease process. Knowledge of GAG involvement in amyloid formation has led to new strategies in drug development for this group of diseases (Kisilevsky *et al*., 1995, 2004; Zhu and Kindy, 2001) and agents that inhibit the interaction between GAGs and fibril protein precursors are presently being tested in trials in human amyloidosis.

Materials & Methods

4. Materials & Methods

4.1. Oligosaccharides purification from pig mucosa heparin with or without standard sulfation pattern

Oligosaccharides tinzaparin derived were prepared from a porcine mucosa tinzaparin Hep with an average Mw of 5500 Da. Two different kind of oligosaccharides were prepared as follows:
a] fractionation and desalting: 150 mg of commercial LMWH (tinzaparin (Tinza), LEO-pharma, Ballerup, Denmark, depolymerised through enzymatic β-elimination (Linhardt, 2001) by the manufacturer) was fractionated using semi preparative size exclusion chromatography, thus, di, tetra, hexa, octa, deca and dodeca-saccharidic fractions were isolated with Bio-gel P (Bio-Rad Laboratories S.r.l, Segrate, Italy) as stationary phase and NH_4Cl 0.25 M as mobile phase. Fractions were desalted with an ultrafiltration step with YC05 Amicon bioseparation filter (Millipore Corporation, Billerica, MA, USA) and with a desalting step through Toyopearl HW-40 (Tosoh Bioscience LLC, Minato-Qu, Tokio, Japan) as stationary phase and 10% EtOH as mobile phase. In the elution profile of tinzaparin it is possible to distinguish 9 peaks (sample codes: decasaccharide [(T) dp10], hexasaccahride [(T) dp 6] and other samples not used during this thesis work), corresponding to oligomers ranging from di to dodecasaccharides and a nonresolved group of peaks in the part of the chromatogram containing higher oligomers. All the intermediate products were checked by ^{13}C NMR analysis. (Table 4).
b] Hep dp 2 was obtained after deaminative reduction of a UFH, fractionated and desalted as previously described (see point **a]**) (Table 4).
Enoxaparin (Enoxa) was supplied by Sanofi-Aventis Pharma (Milan, Italy) as injectable Clexane; Dalteparin (Dalte) was from Pharmacia AB (Stockholm, Sweden) as injectable Fragmin (Table 4).
Octa-3, Octa-5 and Octa-6 were provided by the manufacturer (Sanofi-Aventis, Paris, France) and they were purified as reported in literature (Guerrini *et al*., 2008 [b]) (Table 4; Fig. 18). The table below resume Hep /Hep oligosaccharide codes and features (Table 4) .

Code	Description	MW	Chemical modification	Depolymerisation method	Saccharide sequence	Animal
UFH	Na UFH	17000	NO	NO	$(I_S\text{-}GlcN_{NAc,6S})_{\approx 13}//(I_S\text{-}GlcN_{NS,6S})_{\approx 13}$	*Sus Domesticus*
Hep dp 2	disaccharide Na Hep derived	582	NO	Deaminative reduction	I_S-2,5 anM_{6S}	*Sus Domesticus*
Dalte	Na Fragmin [Dalteparin (LMWH)]	6900	NO	Deaminative reduction	$(I_S\text{-}GlcN_{NAc,6S})_{\approx 3}\text{-}I_S$-2,5 $anM_{6S}//(I_S\text{-}GlcN_{NS,6S})_{\approx 3}\text{-}I_S$-2,5 anM_{6S}	*Sus Domesticus*
Enoxa	Na Clexane [Enoxaparin (LMWH)]	5300	NO	Chemical β-elimination	$\Delta U2_S\text{-}GlcN_{NS,6S}\text{-}(I_S\text{-}GlcN_{NS,6S})_{\approx 7}\text{-}I_S$-2,5 $anM_{6S}//\Delta U2_S\text{-}GlcN_{NS,6S}\text{-}(I_S\text{-}GlcN_{NAc,6S})_{\approx 7}\text{-}I_S$-2,5 anM_{6S}	*Sus Domesticus*
Tinza	Na InnoHep [Tinzaparin (LMWH)]	8300	NO	Enzymatic β-elimination	$\Delta U2_S\text{-}GlcN_{NS,6S}\text{-}(I_S\text{-}GlcN_{NS,6S})_{\approx 10}$	*Sus Domesticus*
(T) dp 6	hexasaccharide Na Tinzaparin derived	2057	NO	Enzymatic β-elimination	$\Delta U2_S\text{-}GlcN_{NS,6S}\text{-}(I_S\text{-}GlcN_{NS,6S})\approx 2$	*Sus Domesticus*
(T) dp 10	decasaccharide Na Tinzaparin derived	4154	NO	Enzymatic β-elimination	$\Delta U2_S\text{-}GlcN_{NS,6S}\text{-}(I_S\text{-}GlcN_{NS,6S})\approx 4$	*Sus Domesticus*
BL Hep	Na Hep	21600	NO	NO	$(I_S\text{-}GlcN_{NS,6S})_{\approx 5}$	*Bos Taurus*
Octa-3	octasaccharide Na Hep derived	2376	NO	Enzymatic β-elimination	$\Delta U2_S\text{-}GlcN_{NS,6S}\text{-}I_S\text{-}A_{NA}\text{-}G\text{-}A^*\text{-}I_S\text{-}A$	*Bos Taurus*
Octa-5	octasaccharide Na Hep derived	2360	NO	Enzymatic β-elimination	$\Delta U2_S\text{-}GlcN_{NS,6S}\text{-}I_S\text{-}A_{NA}\text{-}G\text{-}A^*\text{-}I_S$-1,6 anM_{NS}	*Bos Taurus*
Octa-6	octasaccharide Na Hep derived	2360	NO	Enzymatic β-elimination	$\Delta U2_S\text{-}GlcN_{NS,6S}\text{-}I_S\text{-}A_{NA}\text{-}G\text{-}A^*\text{-}I_S$-1,6 anG_{NS}	*Bos Taurus*

Table 4. Heparin sample and oligosaccharide Hep derived list. Code column contains Ronzoni Institute code, description column gives general information on Hep and oligosacchiaride samples, chemical modification column shows sulfation/acetylation modification done to the specified samples, saccharide sequence column reveals monosaccharide sample sequence compositions and animal column shows binomial system nomenclature Hep animal origin. BL= bovine lung.

4.2. Construction and use of a library of *bona fide* heparin employing 1H NMR and multivariate analysis

4.2.1. Heparin library composition

A library was constructed which contained 28 samples (making a total of 158 spectra) (Table 5), provided by several commercial European manufacturers of heparin and National Institute for Biological Standards and Control (NIBSC) [including the 5th, 6th Hep International Standard and 6th Hep International Standard candidates which, it should be noted, were originally defined in terms of their biological activity, not their structural characteristics]. The commercial Hep samples were considered *bona fide* samples, according to 2009 Pharmacopeial forum, with acceptable content of DS N-acetyl signal [2.08 ± 0.02 ppm; it must be below 1% of the Hep N-acetyl signal (2.05 ± 0.02 ppm)] and current criteria of the manufacturer. For this illustrative example of a Hep library (of necessity, limited in scope), samples have been characterised and selected to represent structural variability arising from the principal European manufacturing processes (including different oxidation levels) related to commercial Heps. The quality of the standard heparin library is critical in any comparison and every effort should be made to include only those samples in which the highest confidence regarding provenance and characteristics can be placed, for whatever purpose the comparison is being made.

4.2.2. 1D and 2D NMR spectroscopy for heparin library

For each Hep samples, 20 mg were dissolved in 0.6 mL of 0.15 mM Na trimethyl-silyl-3-propionic acid (TSP) solution in deuterium oxide. TSP was added both for spectrum calibration and as a control of spectral resolution. 1D and 2D ^{1}H-^{13}C HSQC spectra were measured at 21 °C on a Bruker AVIII-600 instrument (operating at the 600.13 MHz ^{1}H observation frequency) equipped with a cryogenic TXI 5 mM probe (Bruker, Karlsruhe, Germany). Measurements were accepted for Principal Component Analysis (PCA) when the line width of the TSP signal was equal or less than 1 Hz (± 0.1 Hz)). Water presaturation power corresponding to 5 Hz was applied during 12 s of relaxation time. Typically, 32 transients were acquired into 32768 data points covering a spectral width of 10800 Hz. A shifted π/3 squared cosine function was applied before FT and all spectral data sets were processed using TOPSPIN (v. 2.2) software supplied by the manufacturer. The residual water signal lies in a region between about 4.8 ppm and 4.6 ppm, depending on the set temperature (i.e. 21 °C to 40 °C). Within this range the water signal shifts from the region of H5 of iduronate residues (4.75 - 4.86 ppm) to that of the anomeric protons belonging to glucuronic acid and linkage region residues (4.7 - 4.6 ppm). Since the content of linkage region and different glucuronic acid sequences can significantly change within different Hep batches, signal shifting in this region must be accommodated. Water signal at 21 °C is centred at 4.812 (± 0.1 Hz), in this conditions presaturation weakly affects both iduronate signal and linkage region signals. We decided to run ^{1}H NMR at this temperature, in order to collect the most of the informations. ^{1}H-^{13}C HSQC experiments (Palmer *et al*., 1991; Kay *et al*., 1992; Schleucher *et al*., 1994) were acquired with 16 scans for 320 increments in the F1 dimension. The matrix size 1 K x 512 was zero filled 2 K x 1 K by application of a squared cosine function prior to FT. A LB of 1.0 Hz and 0.3 Hz, respectively for F2 and F1, was applied before FT and all spectral data sets were processed using TOPSPIN (v. 2.2) software supplied by the manufacturer. DoS have been calculated as previously described (Guerrini *et al*., 2005). The table below resume Hep codes and features used to build heparin library.

Code	PCA code	Kind	Chemical modification	Animal
G3000	4.1	Na UFH	NO	*Sus Domesticus*
G6686	1.1	Na. Hep. Commercial	NO	*Sus Domesticus*
G6687	1.2	Na. Hep. Commercial	NO	*Sus Domesticus*
G6213	2.1.1	Na. Hep. Commercial	NO	*Sus Domesticus*
G6214	2.1.2	Na. Hep. Commercial	NO	*Sus Domesticus*
G6215	2.1.3	Na. Hep. Commercial	NO	*Sus Domesticus*
G6808	2.2.1	Na. Hep. Commercial (mild oxidation)	$KMnO_4$ oxidation	*Sus Domesticus*
G6812	2.2.2	Na. Hep. Commercial (mild oxidation)	$KMnO_4$ oxidation	*Sus Domesticus*
G6815	2.2.3	Na. Hep. Commercial (mild oxidation)	$KMnO_4$ oxidation	*Sus Domesticus*
G6726	2.3.1	Na. Hep. Commercial (high oxidation)	$KMnO_4$ oxidation	*Sus Domesticus*
G6727	2.3.2	Na. Hep. Commercial (high oxidation)	$KMnO_4$ oxidation	*Sus Domesticus*
G6728	2.3.3	Na. Hep. Commercial (high oxidation)	$KMnO_4$ oxidation	*Sus Domesticus*
A1688	3.1	Na. Hep. Commercial	NO	*Sus Domesticus*
A1689	3.2	Na. Hep. Commercial	NO	*Sus Domesticus*
A1846	3.3	Na. Hep. Commercial	NO	*Sus Domesticus*
A1506	4.2	Na. Hep. Commercial	NO	*Sus Domesticus*
A1618	4.3	Na. Hep. Commercial	NO	*Sus Domesticus*
A1721	4.4	Na. Hep. Commercial	NO	*Sus Domesticus*
A1858	4.5	Na. Hep. Commercial	NO	*Sus Domesticus*
A1922	4.6	Na. Hep. Commercial	NO	*Sus Domesticus*
A1404	5.1	Na. Hep. Commercial	NO	*Sus Domesticus*
A1600	5.2	Na. Hep. Commercial	NO	*Sus Domesticus*
A1774	5.3	Na. Hep. Commercial	NO	*Sus Domesticus*
A1482	6C.1	W candidate for 6°Na Hep. Int. Std.	NO	*Sus Domesticus*
A1483	6C.2	X candidate for 6°Na Hep. Int. Std.	NO	*Sus Domesticus*
A1484	6C.3	Y candidate for 6°Na Hep. Int. Std.	NO	*Sus Domesticus*
A1485	IS6	6°Na Hep. Int. Std.	NO	*Sus Domesticus*
A1487	IS5	5°Na Hep. Int. Std.	NO	*Sus Domesticus*

Table 5. Heparin samples used for ^{1}H NMR spectra acquisition and PCA analysis. PCA code is arbitrary to keep safe manufacturer privacy.

4.2.3. Heparin library analysis by PCA

Before the analysis took place the spectra were aligned, cut to remove the regions containing water and solvent, normalised to the average area under the spectra [the area under the spectra was calculated using the Matlab (R2010a) function trapz (The MathWorks ltd, Cambridge, United Kingdom)], mean-centred and then scaled, using one of these methods: autoscaling, Pareto scaling and Vast scaling. Mean centring removes the first principal component, which otherwise contains the average spectral features. PCA was performed using R (version 2.9.0. R Development Core Team (2010). R: A language and environment for statistical computing. R Foundation for Statistical Computing, Vienna, Austria. ISBN 3-900051-07-0, http://www.R-project.org.), utilising the Princomp algorithim. PCA was performed on a wide spectral region, 6.00-1.95 ppm [with regions 4.912 - 4.730, 3.881 - 3.868, 3.680 - 3.633, 3.363 - 3.355 and 3.010 - 2.220 ppm were excluded].

PCA is a nonparametric technique (i.e. one that does not rely on selecting or defining any values before the analysis begins), which reduces a complicated set of data to a number of lower, independent dimensions, or principal components. These dimensions/principal components explain the overall

variance (Expl. Var.) within the original dataset, with one variable within the dataset being described as a summation of the derived principal components (Eq. 1).

$$X_{ij}=L_{j1}S_{i1}+L_{j2}S_{i2}+\ldots+L_{jp}S_{ip}+E \quad \text{(Eq. 1)}$$

Where X_{ij} is a dataset containing j spectra with i spectral readings (i.e. 1.00 – 2.00 ppm), which can be described as p principal components, where L are the component loadings [related to the spectra] and S are the component scores [related to the spectral features]. The final term, E, is the residual unexplained variance, or error, that cannot be explained by the linear summation.
The proportion of the variance in the data, that is explained by each component, can be analysed through a scree plot (i.e. Fig. 24 A) and the spectral information contained in each component can be extracted and interpreted in the form of component scores which, in this case, will contain features resembling ^{1}H NMR spectra (i.e. Fig. 24 C). For a single contaminant (which does not, by definition, already form part of the library), the variance from the library spectra will be described by one principal component. In the case of multiple, structurally distinct contaminants in the same sample, the variance will also be explained by a single principal component. PCA is unable to distinguish between one or many contaminants in a single sample because it only handles the sum of the spectral features arising from the multiple contaminants, unless the multiple contaminants are also present individually, within the library dataset.
In the analyses conducted here, the datasets were normalised to the average area under the spectra dataset [if not stated otherwise] and mean-centred (Eq. 2) before PCA was employed. This is essential because the first component derived is normally the average of the dataset and would contain a large proportion of the variance, having the effect of swamping the other components.

$$X_{ij}=x_{ij}-x_{avarage\ i} \quad \text{(Eq. 2)}$$

Where X_{ij} and x_{ij} is the dataset after and before treatment and $x_{avarage\ i}$ is the average of the rows for x_{ij}. Autoscaling (Eq. 3), Pareto (Eq. 4) and Vast scaling (Eq. 5) were also employed in some analyses,

$$\text{Autoscaling: } X_{ij}=(x_{ij}-x_{avarage\ i}).\ (x_{sd\ i})^{-1} \quad \text{(Eq. 3)}$$
$$\text{Pareto scaling: } X_{ij}=(x_{ij}-x_{avarage\ i}).\ (\sqrt{x}_{sd\ i})^{-1} \quad \text{(Eq. 4)}$$
$$\text{Vast scaling: } X_{ij}=(x_{ij}-x_{avarage\ i})(x_{sd\ i})^{-1}.\ (x_{avarage\ i}/x_{sd\ i}) \quad \text{(Eq. 5)}$$

Where X_{ij} and x_{ij} are the dataset after and before treatment, $x_{average\ i}$ is the average of the rows for x_{ij} and $x_{sd\ i}$ is the standard deviation of each row. Autoscaling (Eq. 3) normalises the standard deviation to one, therefore the data are compared with respect to correlations, not covariances. A disadvantage of autoscaling is that the data become dimensionless, making it difficult to compare component scores. On the other hand, this does not occur for Pareto scaling (Eq. 4), which normalises to the square root of the standard deviation; the effect being to make large changes less important with respect to small changes in the dataset. Variability stability scaling (Vast scaling), scales on the stability of the variable, selecting for variables with a small standard deviation and placing less importance on variables with large standard deviations. There are no set rules determining when scaling should be used, but mean centring should be used whenever PCA is going to be performed on a dataset. For a protocol to be devised for the automated analysis of pharmaceutical Hep with ^{1}H NMR and multivariate analysis, a clear set of rules will have to be devised regarding which scaling method should be used (van den

Berg *et al*., 2006; Keun *et al*., 2003).

4.2.4. USP NMR protocol (Sodium Heparin Stage 2 monograph)

500 MHz Pulsed (FT) NMR spectrometer, 16 Scans, 90 ° pulse with a 20 sec delay, recorded at a temperature of 25 °C. The N-acetyl peak positions are defined as 2.05 ± 0.02 and 2.16 ± 0.03 ppm, respectively for heparin and OSCS. The positions of H1 of A_{NA}/A [5.42 ppm], H1 of I_S [5.21 ppm], H2 of $GlcN_{NS}$ [3.28 ppm (doublet centred at 3.28 ppm)] and the methyl of $GlcN_{NAc}$ [2.05 ppm] must not differ by more than ± 0.03 ppm. No signals should be present in the ranges 0.10 – 2.00, 2.10 – 3.20 and 5.70 – 8.00 ppm, that have a height greater than 4 % of the mean signal height of H1 of A_{NA}/A [5.42 ppm] and H1 of I_S [5.21 ppm]. There should also be no signal between 3.35–4.55 ppm with a height greater than 200 % signal height of the mean of H1 of A_{NA}/A [5.42 ppm] and H1 of $IdoA_{2S}$ [5.21 ppm], for porcine heparin (i.e. Fig. 34).

4.3. Effects on molecular conformation and anticoagulant activities of 1,6-anhydrosugars at the reducing terminal of antithrombin-binding octasaccharides isolated from low-molecular-weight heparin enoxaparin

4.3.1. AT purification

Antithrombin III (AT; MW= 58000 Da) was purified from a pharmaceutical grade preparation (Kibernin P 1000, ZLB Behring, Milan, Italy). Kibernin P 1000 was dissolved in dH_2O to reach 4 mg/mL and it was loaded on two 10 MWCO Centricon YM-10 (Millipore, Milan, Italy) and they were centrifuged at 5000 rpm, 40 min (flow-through from every single steps were stored and check later to test protein concentration); for every single tube, remaining volume (~0.3 ml) was diluted with 1.7 ml dH_2O and they were centrifuged at 5000 rpm, 40 min; dilution and centrifugation steps were repeated at least 5 times. Finally remaining volume (~0.3 ml) was diluted up to 1 mL with dH_2O, the Centricons were loaded up side down into the centrifuge and they were centrifuged at 2500 rpm, 5 min. Protein concentration was measured by Cary 50 UV-Vis spectrophotometer (Varian, Torino, Italy) at λ= 280 nm.

4.3.2. 1D and 2D NMR spectroscopy for octasaccharide: AT interaction analysis

All mono-dimensional and bi-dimensional NMR spectra were measured at 21 °C, on a Bruker Avance 600 (operating at 600.13 MHz ^1H observation frequency) and Bruker Avance 900 spectrometer (operating at 900.05 MHz ^1H observation frequency) both equipped with a cryogenic TXI 5 mM probe (Bruker, Karlsruhe, Germany). For ^1H detection, 350 μgr of octasaccharide samples were dissolved in D_2O (99.9%) and freeze-dried to remove residual water. After exchanging the samples three times, samples were dissolved in 0.7 mL of 10 mM Na_2HPO_4 pH 7.4, 0.15 M NaCl with 3 mM ethylenediaminetetraacetic acid (EDTA) in D_2O (99.996%) (PBS). For the binding studies, samples were prepared by dissolving 200 μgr and 400 μgr of each octasaccharide sample in the PBS so as to reach

a 1:10 or 1:40 AT/octasaccharide molar ratio for trNOE and STD experiments, respectively. Proton spectra were recorded with presaturation of the residual water signal, with a recycle delay of 8 s and 128 scans. ^{1}H-^{1}H TOCSY (Bax and Davis, 1985; Hwang and Shaka, 1995) spectra were acquired using 32 scans per series of 2K × 512W data points with zero filling in F1 and a shifted squared cosine function was applied prior to FT. For all NOESY and trNOE experiments spectra were recorded using the standard Bruker sequence. Experiments were performed with a total of 48 scans collected for each free-induction decay (matrix 2K × 512 points) and data were zero-filled to 4K × 2K points before FT. Mixing time values of 100, 200 and 300 ms were used. All 1D STD experiments were measured at 900 MHz and it was employed a pulse sequence with spoil sequence to destroy unwanted magnetisation, includes a 25 ms spinlock pulse to eliminate the broad resonances of the protein and water suppression (Mayer and Meyer, 1999). A train of 40 Gaussian-shaped pulses of 50 ms each was applied to produce selective saturation. The on-resonance irradiation was performed at the low field protein resonances (7.25 ppm), whereas the off-resonance control irradiation was performed at 24 ppm. The number of scans and dummy scans were 1024 and 16, respectively. Following saturation time was used: 0.5, 0.8, 1.3, 2 s. All spectra were acquired and processed by TOPSPIN (v. 2.2) software supplied by the manufacturer.

4.3.3. Computational studies on octasaccharide-AT complexes

The octasaccharide models were created by Macromodel version 4.0 (Schrödinger, Mannheim, Germany) starting from previously reported structures (Mulloy *et al*., 1993; Guerrini *et al*., 2008 [b]) where IdoA and I_{2S} are in $^{2}S_{0}$ conformation while glucosamines and glucuronic acid residues are in $^{4}C_{1}$ conformation, as shown from NMR experimental evidences. Molecular Dynamics (MD) simulation of Octa-3, Octa-5 and Octa-6 were performed using AMBER* force field included in MAESTRO 8.0/Macromodel simulation package and macromodel batchmin simulation engine was used for MD trajectory production. Simulation were done on models where each octasaccharide molecule was enveloped by a water molecules layer at least 12 Å wide. To do that, the free code software "solvate-1.0" was used (Helmut Grubmüller and Volker Groll. Theoretical and Computational Biophysic Group, Max Planck Institute, Göttingen, Germany). After a short time MD (about 400 ps) Octa-3, Octa-5, Octa-6 models were checked in each residues conformation to agree qualitatively with the experimental seen. Glycosidic geometries of the I_{S}-1,6-anG/M disaccharides were set according to H1–H4 and H1–H5 inter-residue distances on the basis of values extrapolated from experimental NOE magnitudes. Octa-3, Octa-5 and Octa-6 geometries so obtained were used as ligands for automatic docking octasaccharide/AT complex structure determination. Docking simulations were performed using Autodock-4.2 program (Morris *et al*., 1996; Morris *et al*., 1998). The receptor (AT) geometry was taken from PDB file (Protein Data Bank 1AZX29). Explicit treatment of every hydrogen was used for both ligand and receptor, while atom charges were calculated following Gasteiger approach (Gasteiger, 1980). Ligands were treated as rigid object fixing all glycosidic torsional degrees of freedom, while hexocyclic functional group torsional angles (32 degrees of freedom for each complex) were allowed to move during docking simulation. About 100 complex geometries were generated using a Lamarckian Genetic Algorithm with local search, characterised by the following set of parameter: population size was fixed to 500, maximum number of energy evaluation per run was chosen to be 5 x 106 and 2.7 x 105 maximum generation number. Others parameters are left as default settings. Results were analysed by a fast cluster analysis: generated complex geometries were ranked by a rmsd cut-off of

2.0 Å. After ranking few clusters, with higher score function and/or most 21 populated having the A_{NA}GA*IA sequence in the same position as found in the crystal structure of the pentasaccharide/AT complex (Jin *et al*., 1997), that clusters were considered to fit trNOE data. Less populated clusters, having the octasaccharides moved up toward the nonreducing end by about a disaccharide unit from the normal AT binding site, were also found and considered. To evaluate the ability of all these complex models to interpret the position of the ligand in the AT binding site, the magnitudes of theoretical trNOEs were calculated on different models of octasaccharide/AT complexes using the CORCEMA program (Moseley, 1995). The agreement between the theoretical and experimental trNOEs was evaluated by calculating the fitting quality parameter *R* factors as defined in Eq. 6.

$$R^2 = \frac{\sum_{tmix}(NOE^{EXP}(tmix) - NOE^{CALC}(tmix))^2}{\sum_{tmix}(NOE^{EXP}(tmix))^2} \qquad \text{(Eq. 6)}$$

R-factor values higher than 0.3 are indicative for a pour local structure description. The values of the K_d used to calculate theoretical trNOEs were based on those calculated by equilibrium titration and published data (Guerrini *et al*., 2008 [b]). The correlation times of AT and octasaccharides were considered as isotropic and estimated from the previous data (Hricovini *et al*., 2001; Angulo *et al*., 2005; Guerrini *et al*., 2008 [b]). However, due to the slightly different condition used (temperature and ion strength) the K_d and the off-rate (k_{off}) used in the calculations varied during the optimisation (K_d and k_{off}: 0.1 mM and 50 sec^{-1}, respectively).

4.4. Role of glycosaminoglicans (GAGs) in Alzheimer progression.

4.4.1. Dynamic Light Scattering aggregation kinetics analysis for Aβ interaction with and without GAGs

Experiments were performed on a Viscotek 802 DLS (Malvern Instruments Ltd, Worcestershire, United Kingdom) 90 °angle fixed detector at 25 °C. A 50 mW fiber coupled diode laser, single photon counting module operating at a wavelenght of λ= 830 nm was used as the light source. **Aggregation investigation at different pH**: $A\beta_{1\text{-}40}$ (GenScript USA Inc., Piscataway, NJ, USA) peptide was dissolved in 10 mM NaOH solution pH 11 pre filtered with Anotop 10 filter inorganic membrane with pore of 0.02 μm (Whatman, Maidstone, Kent, United Kingdom). The solution was diluted to a concentration of 23 μM ($MW_{A\beta}$= 4329 Da) in 100 mM Na_2HPO_4+ KH_2PO_4 pH 7 pre filtered with Anotop 10 filter, 5 sec vortex and centrifuge 1000 rpm, 30 sec (for 2 times). All measurements were acquired and processed with Omnisize 3.0 (Malvern Instruments Ltd, Worcestershire, United Kingdom) applying 10 % of laser power for 40 round of scans, 4 sec for each scans; R_h was sampled every hour in triplicate and the average R_h is reported. The first 35 and the last 150 points were manually removed

prior exponential fitting. **Aggregation investigation with different buffers**: $A\beta_{1-40}$ (GenScript USA Inc., Piscataway, NJ, USA) peptide was prepared in two different conditions. Condition A: the peptide was dissolved to a concentration of 0.92 mM in 10 mM NaOH solution pH 11 pre filtered with Anotop 10 filter, 5 sec vortex and centrifuge 1000 rpm, 30 sec (for 2 times). It was diluted to a final concentration of 0.023 mM $A\beta_{1-40}$ in 100 mM TRIS-HCl pH), 0.05% $NaNO_3$ pre filtered with Anotop 10 filter. Condition B: the peptide was dissolved to a concentration of 0.92 mM in 10 mM NaOH solution pH 11 pre filtered with Anotop 10 filter, 5 sec vortex and centrifuge 1000 rpm, 30 sec (for 2 times). It was diluted to a final concentration of 0.44 mM $A\beta_{1-40}$ in 100 mM TRIS-HCl pH), 0.05% $NaNO_3$ pre filtered with Anotop 10 filter. All measurements were acquired and processed with Omnisize 3.0 applying 10 % of laser power for 20 round of scans, 4 sec for each scans; R_h was sampled every hour. The first 25 and the last 150 points were manually removed prior exponential fitting. Sample at 0.023 mM was kept at 37 °C for the entire experimental duration. **Aggregation investigation with or without GAGs**: $A\beta_{1-40}$ (GenScript USA Inc., Piscataway, NJ, USA) peptide was dissolved to a concentration of 23 μM in 10 mM NaOH solution pH 11 pre filtered with Anotop 10 filter, 5 sec vortex and centrifuge 1000 rpm, 30 sec (for 2 times) One fraction was diluted to a final concentration of 0.44 mM $A\beta_{1-40}$ in 50 mM TRIS-HCl pH 7), 0.05% $NaNO_3$ pre filtered with Anotop 10 filter and the remaining fractions were used to get a solution of 0.44 mM $A\beta_{1-40}$, 1:1 final mass ratio with GAGs (Enoxa, Tinza, Dalte, Hep dp 2, (T) dp 6 and (T) dp 10) in 50 mM TRIS-HCl pH 7, 0.05% $NaNO_3$ pre filtered with Anotop 10. All measurements were acquired and processed with Omnisize 3.0 applying 10 % of laser power for 20 round of scans, 4 sec for each scans; R_h was sampled every hour. The first 25 and the last 150 points were manually removed prior exponential fitting. Dynamic light scattering (DLS) is also known as Photon Correlation Spectroscopy. This technique is one of the most popular methods used to determine the size of particles. Shining a monochromatic light beam, such as a laser, onto a solution with spherical particles in Brownian motion causes a Doppler Shift when the light hits the moving particle, changing the wavelength of the incoming light. This change is related to the size of the particle. It is possible to compute the sphere size distribution and give a description of the particle's motion in the medium, thus measuring the diffusion coefficient (D_{coeff}) of the particle and using the autocorrelation function. This method has several advantages: first of all the experiment duration is short and it is almost all automatised so that for routine measurements an extensive experience is not required. Autocorrelation function intensity (Eq. 7) decays as negative exponential (Eq. 8):

$$G = I(T)\,\frac{I(T+t)}{(I(T))^2} \qquad \text{(Eq. 7)}$$

$$G(t) = Ae^{(-2\Gamma t)} + 1 \qquad \text{(Eq. 8)}$$

Where A is amplitude constant, t is the time (sec), Γ is the decay constant (Eq. 9 depending on the D_{coeff} (Eq. 10) and the q factor (Eq. 11):

$$\Gamma = D_{coeff}(t)q^2 \qquad \text{(Eq. 9)}$$

$$D_{coeff} = \frac{k_B T}{6\pi\eta R_h} \quad \text{(Eq. 10)}$$

$$q = \frac{4\pi n(dn/dc)}{\lambda} \sin\frac{\Theta}{2} \quad \text{(Eq. 11)}$$

Omnisize 3.0 calculates the average autocorrelation function through all the selected functions prior data fitting, after that it applies fitting routine called regularisation through a series of negative exponential regression functions. R_h calculation is based on the assumption that the sample contains a single mono-disperse species. In most cases, we do not tend to deal with samples of this type and we need a way of extracting more information from the correlation function. Regularisation is the process in which we model the correlation function to a distribution of particle sizes. In essence, our real correlation function is a combination of a group of virtual mono-disperse functions of differing amplitude. Each virtual function has its own decay rate (which relates to its size) and its own amplitude A (which relates to its contribution to the sum. Regularisation determines the best set of virtual correlation functions that fit the experimental data. So from this collection of functions we can determine the distribution of sizes of particles within a sample. Regularisation tends to over estimate the contribution of the initial and final part of the autocorrelation function, for this reason the first the last data points were manually removed.

Aim of the work

5. Aim of the work

GAGs are some of the most relevant biological molecules, involved in important biological, physiological activities and also used as pharmaceutical agents. GAG research activities oriented to understand their nature, molecular population composition, characterisation, protein-GAG interaction network and putative pharmaceutical properties are essential to develop new drug with a more controlled and described activity. Recently experimental and clinical informations had increased the attention over HS/Hep coagulant and not coagulant activity opening new fields of research oriented to develop new therapeutical strategy involving heparin usage. Heparin mimetics can be extremely helpful from this perspective, due to their controlled nature, molecular features and structure, thus they can be employed as performance drugs. My Ph.D. thesis deals with statistical characterisation of commercial and not commercial pharmaceutical heparin, composition and structural characterisation of heparin mimetics and characterisation of protein-heparin interaction for drug design strategy.
Thesis focus was oriented on three different subject:

1. build a library of accepted and well charaterised heparins, set up a statistical analysis based on a PCA approach to statistically define heparin molecular nature and to develop a new heparin quality control procedure.

2. 1D/2D NMR interaction studies (^{1}H, TOCSY, NOESY, ROESY, trNOE and STD) to understand the importance of $A_{NA}GA^{*}I_{S}A$ flanking residues over AT activation on octasaccharides bearing the pentasaccharide sequence with normal or modified reducent residue in complex with AT.

3. DLS studies on Aβ-heparin or heparin mimetics as a new strategy to counter act Aβ aggregation progression involved in AD and better understand the deep relationship between Aβ peptide and GAGs.

Results & Discussions

6. Results & Discussions

6.1. Construction and use of a library of *bona fide* heparins employing ^{1}H NMR and multivariate analysis

Submitted to The Analyst

6.1.1. Summary

Heparin is one of the most complex pharmaceutical agent on the market. The lack of uniquely/absolute identity for heparin created the condition for the heparin crisis, together with the lack of interest of its structural identity from the international regulatory bodies point of view. One of the most informative methods for the structural analysis of heparin samples is NMR. ^{1}H NMR spectra of heparin are rich in detail and structurally relevant information and they are also highly informative regarding the presence of organic contaminants. Here, a general approach is proposed, based on the comparison of the ^{1}H NMR spectrum of the test heparin to a library of known heparin samples which are of accepted *bona fides*, although any other data, including biological activity, could in principle also be incorporated into the analysis. The second key point is that the limit of sensitivity of such a comparison is also dependent in a fundamental way on the contents of the heparin reference library; the more structurally homogeneous (i.e. the more similar are the ^{1}H NMR spectra of the library components) the greater will be the power of the technique for discerning spectral (i.e. structural) differences between that library and the sample under examination. The composition of the library is therefore a key factor for those interested in making these comparisons, as is the decision regarding which criteria to apply to the question what constitutes *bona fide* heparin? In particular, not only must the provenance and structural quality of the samples be satisfactory, but the defined method of recording the spectrum (i.e. employing a standardised procedure with consistent concentration and magnetic field shimming, etc.) and sample purity (i.e. checking for the presence of salt) must be respected. A general approach for detecting contamination proposed by the USP, for example, have reflected this and the ^{1}H-NMR test for the presence of OSCS in the current USP monograph for Heparin Sodium (Materials and Methods 4.2.4, Pharmacopeial Forum, 2009) pays particular attention to the presence of the N-acetyl signal characteristic of OSCS, which is well-separated from the other signals of heparin. However, it is unlikely that contaminants whose NMR signals lack N-acetyl [$COCH_3$] groups (but which could comprise, for example, sulfated linear polysaccharides such as dextran sulfate, agarose sulfate etc.) would be readily detectable using the proposal by the USP, particularly if these contaminants were present in moderate levels (i.e. 2 - 10 %) and their signals fell under the complex heparin signals between ca. 3.2 - 4.8 ppm (Materials and Methods 4.2.4, Pharmacopeial Forum, 2009). This is because in the USP approach, heparin samples are examined using defined sections of the NMR spectrum *en masse* and are compared with other grouped sections with relatively relaxed intensity criteria [i.e. have a particular defined area; Materials and Methods 4.2.4, Pharmacopeial Forum, 2009 and Fig. 34]. In contrast, approaches employing multivariate analysis of spectra such as the present proposal, do not favour detection of signals in one spectral region over those in another. The practical issues in taking the approach outlined here are two-fold: the first is to establish an example reference library of ^{1}H NMR spectra of recognised heparin samples. It is important to note that this library will inevitably contain intrinsic structural variability. The second is to define a procedure for the objective measure-

ment of the similarity of a test sample with this defined heparin library. One form of multivariate analysis, PCA, has been used to differentiate GAGs (DS from heparin, Ruiz-Calero *et al*., 2000; Ruiz-Calero *et al*., 2002), heparin mixtures have been unravelled (Ruiz-Calero *et al*., 2002 [b]) and heparin from different animal sources analysed (Rudd *et al*., 2009). Beyer *et al*. (2008) proposed the use of PCA to assess the purity of heparin samples and attempted to establish the sensitivity of detection for a particular contaminant (OSCS), using PCA only on the N-acetyl region of the NMR spectra, 2.0 - 2.3 ppm. The power of any of these approaches, however, is fundamentally limited by the nature of the comparison: most have not attempted to define a library of accepted heparins but, rather, make piecemeal comparisons between single samples with and without a contaminant. The ultimate aim of the present work is distinct to these and aims to provide the means of obtaining an objective measure of how similar a test sample is to a group of reference compounds, which has been defined by the user, or analyst, as "heparin". The analysis is free from bias for any particular contaminant and the procedure treats all signals within a spectrum with equal weight. The analysis of a test compound provides a body of information, which can include a measure of the degree of similarity (or difference) between the test sample and the entire contents of the reference library, or any particular selected part of it. This last option allows comparison to be made, for example, with chosen standards, heparins of particular origins, or those derived by particular manufacturing processes.

6.1.2. Heparin library construction

An illustrative library of 28 standard *bona fide* heparin samples from a variety of European manufacturers was assembled and their ^{1}H NMR spectra recorded under standardised conditions (Materials and Methods 4.2.2; 158 spectra in total, arising from distinct preparations and at least 3 repeats for each preparations). Fig. 23 shows the complexity of Hep 1D NMR spectra analysis: contaminats in low amount or tainted molecules with high rate of spectra features similarity cannot be detected by human analysis. The characteristic features of this library and their use for the comparison of a test heparin sample, or number of samples, some containing contaminants, are illustrated (Fig. 24 A, B, C and Fig. 25 and Table 5).

6.1.3. The intrinsic structural variability of heparin samples constituting the library

Multiple ^{1}H NMR spectra of each sample of heparin were recorded and used to form the heparin library. Porcine mucosal intestinal heparin is naturally heterogeneous, through variation in biosynthesis and this heterogeneity can be further increased by structural changes induced by the manufacturing processes. Before a sample was entered in the library it was validated by ^{1}H and ^{1}H-^{13}C HSQC NMR, since the goal was to produce an illustrative (rather than definitive), diverse library covering some of the possible heterogeneity within pharmaceutical heparin. The heterogeneity of the samples can be seen in Fig. 24 A, where 4 components describe the vast majority (> 80 %) of the variability within the library. The discrete spectral features represented by the first two components can be seen in the component score plots (Fig. 24 C and Fig. 25). ^{1}H-^{13}C HSQC spectra of a selection of the heparin samples were recorded to further characterise the library. Most of the HSQC spectra were used to calculate the main amine and uronic signal values together with the mean DoS, applying an established method (Guerrini *et al*., 2005; Table 6 and Table 7). The average DoS for the library was

determined to be 2.45. Principal component analysis of the library was able to discriminate some structural changes related to the manufacturing process; samples with a high DoS (DoS >>2.45) were distinct from samples with a low DoS (DoS <<2.45) (Fig. 24 B), samples with a high level of oxidation were differentiated from those with a standard level of oxidation (Fig. 24 B and Fig. 24 C inset showing signals from oxidation of N-acetyl groups, 2.1 ppm). Moreover, the method can also discriminate different heparin international standards. Analysis was also performed on single samples from each heparin group (Fig. 26); samples were chosen with the best line width at half height. In this analysis there was a good correlation for DoS (component 1 [38.20%] versus component 3 [16.45%]; Fig. 26 C), a good correlation at C6 position of $A6_S$ ([component 1 [38.20 %] versus component 2 [18.90 %] and component 2 [18.90 %] versus component 4 [6.56 %]; Fig. 26 D and Fig. 26 E) and a strong correlation for sulfation at C2 position of $I2_S$ (component 2 [18.90 %] versus component 3 [16.45%]; Fig. 26 F).

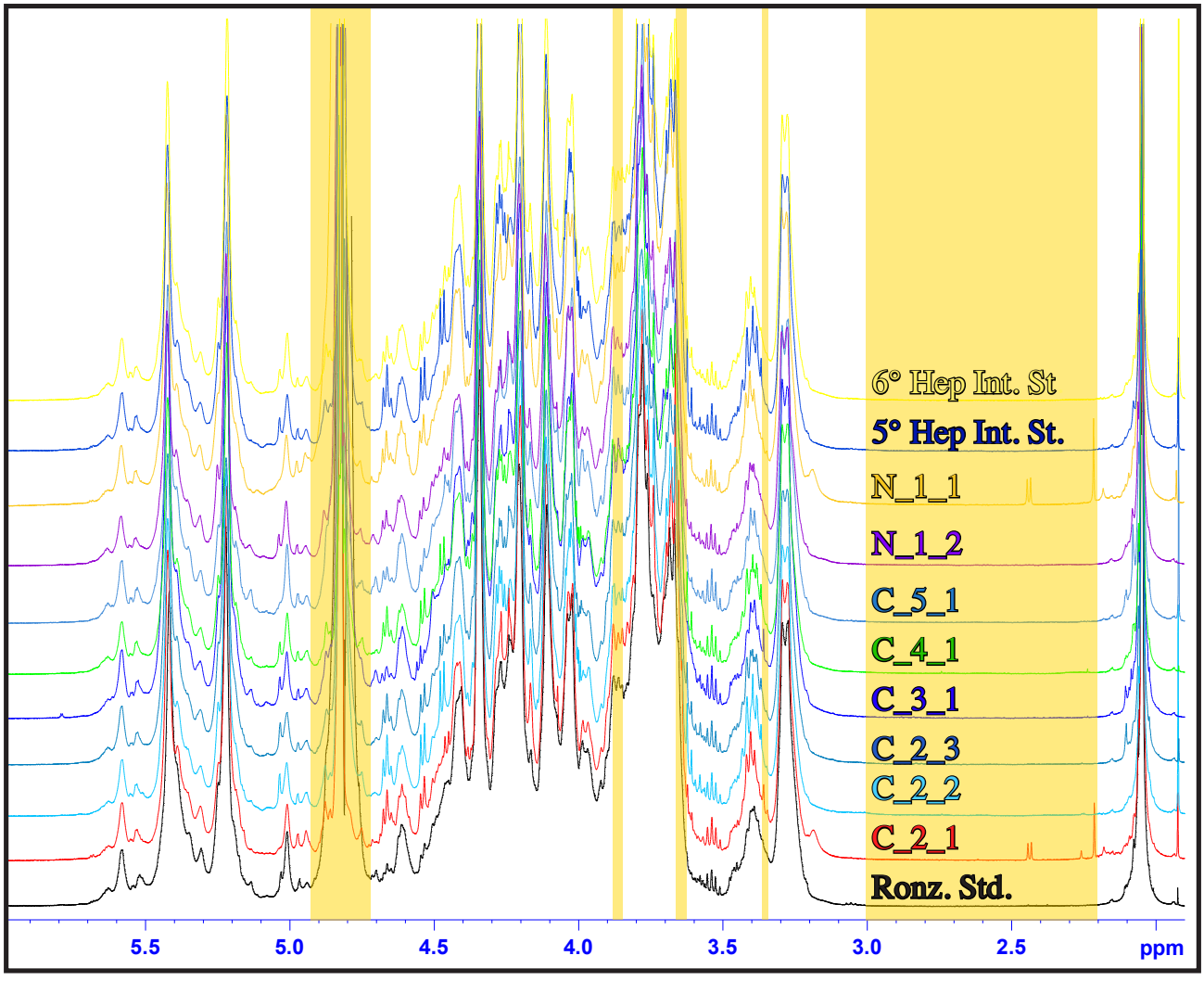

Figure 23. ^{1}H NMR spectra of representative heparins belong to heparin library. It was considered spectra from 6.00 ppm to 1.9 ppm (D_2O, 600MHz, 21 °C). No signals are present outside this region for *bona fide* heparins. Yellow highlighted regions were not considered for PCA.

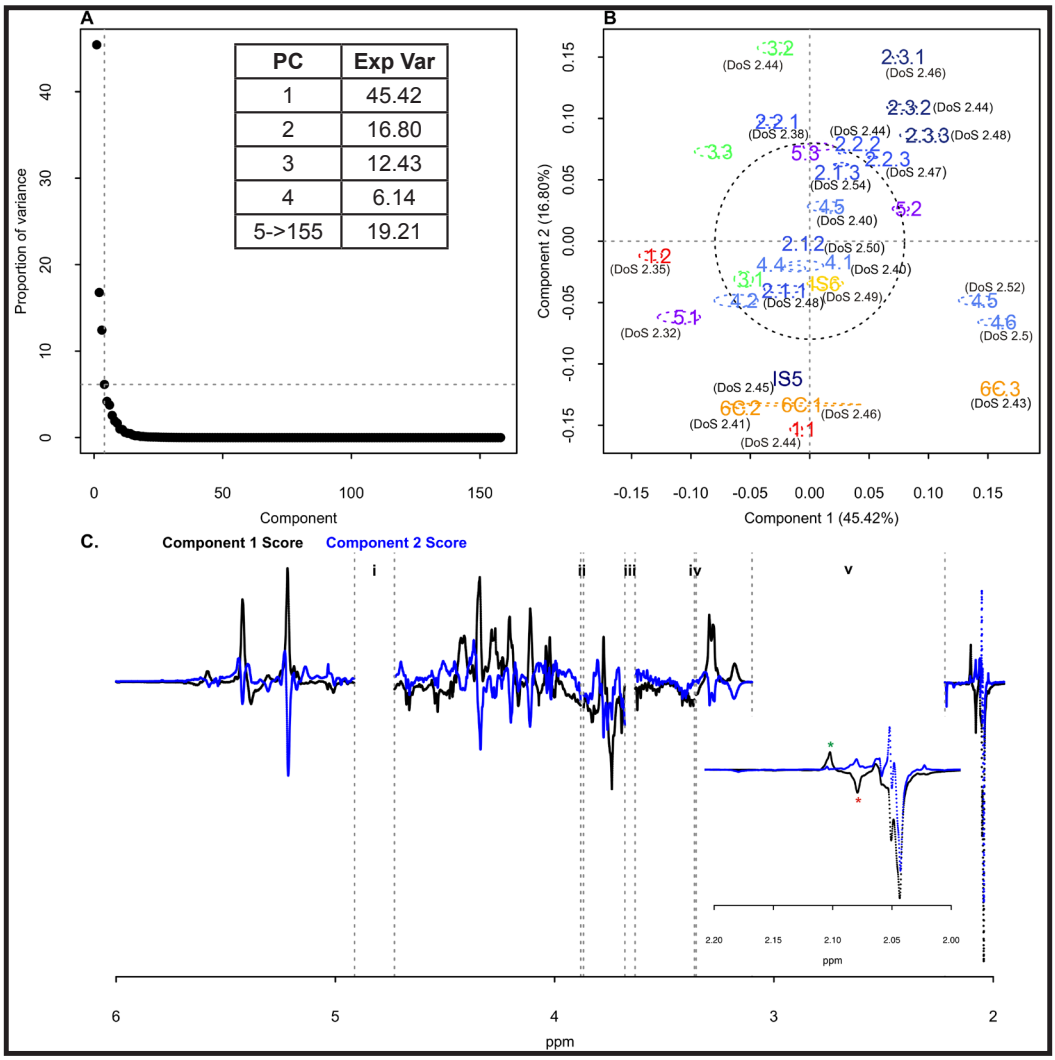

Figure 24. PCA *bona fide* heparin library. **A)** Scree plot, each PC represent a percentage of total variance between different heparin samples. Higher the variance more that PC represent the most of the variances. **B)** Loading plot, in which components 1 and 2 together describe 62.22 % of the variation within the spectra comprising the heparin library (PC $1_{Expl.\ Var.}$= 45.42 %, PC $2_{Expl.\ Var}$= 16.80%. The library contains heparins from 5 manufacturers (labeled 1-5); manufacturer 2 provided: normally (2.1), mildly (2.2) and strongly (2.3) oxidised heparin. Samples labeled 6C were candidates for the 6th International Standard, while IS5 and IS6 are the 5th and 6th International Standard, respectively. The analysis revealed several distinct groups of heparin in the library. Which are plotted as an average of the groups components, 1 and 2, surrounded by an ellipse in which vertical and horizontal dimensions represent the standard deviation of component 2 and component 1, respectively. The black dot and ellipse represent the average position of the heparin library and variation in component 1 and 2, respectively. **C)** Score plots, for component 1 and 2, illustrating the features that differentiate the spectra. The inset contains an expanded view of the N-acetyl region, highlighting the differences in the N-acetyl signal of heparin, but also the presence of dermatan sulfate (red asterisk, ~2.08 ppm) and N-acetyl signals modified through oxidation (green asterisk, ~2.1 ppm). The score plot also shows the 5 regions that were cut before the analysis was performed, labeled i-v. Region i is the water region and regions ii-v contain solvent or signals affected by cations. These were removed in this illustrative example to help simplify the analysis. In a rigorous practical analysis, some of these areas may also be incorporated to provide additional information.

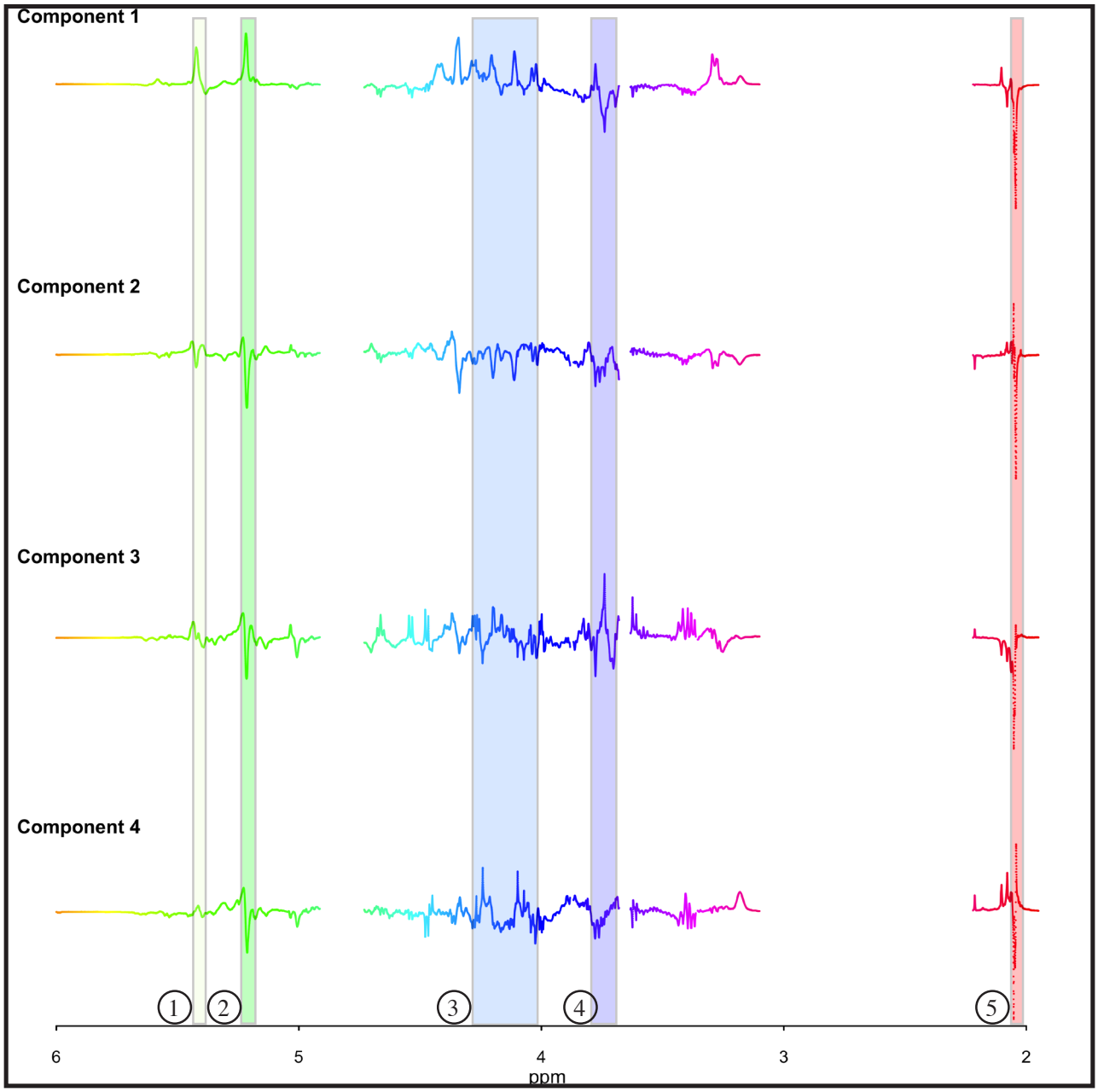

Figure 25. Score plote, for component 1, 2, 3 and 4 illustrating the features that differentiate the spectra at the most (component 1, 2, 3 and 4 together describe > 90% variance of dataset. Component 1 mainly describe variance variations for $COCH_3$ signal, $I2_S$ signal and AN_{NA}/A related signals, A_{TOT} (A_{TOT}= (AN_{NS}, $_{6X}$-I_{2S})+ (AN_{NA}-I)+ (AN_{NA}-G)). Component 2 mainly describe variance variations for $COCH_3$ signal, $I2_S$ signal. Component 3 mainly describe variance variations for AN_{NA}+ A_{6OH} signals. Component 4 mainly describe variance variations for A_{6S} signals. Highlighted regions represent: 1) A_{TOT} signal, 2) $I2_S$ signal, 3) $A6_S$ signal, 4) AN_{NA}+ A_{6OH} signals and 5) $COCH_3$ signal.

Sample code	DoS	AN_{NAc}	H6 A_{6S}	H1 AN_{NS}- G	H1 AN_{NS}- I_{2OH}	H1 A*	H1 AN_{NAc} α red	H1 AN_{NS} α red	H1 AN_{NS} β red	H1 AN_{NS}-I_{2S}
1.1	2,44	11,90	76,50	8,80	7,90	5,30	0,00	0,00	0,00	64,40
1.2	2,35	14,40	76,10	9,60	9,60	4,40	0,90	0,90	0,00	57,50
2.1.1	2,48	11,20	80,00	11,20	9,30	5,60	0,00	2,80	0,00	56,10
2.1.2	2,50	10,70	80,60	8,60	8,60	4,80	0,00	2,90	0,00	61,70
2.1.3	2,54	9,80	82,20	7,10	8,20	5,10	1,00	2,00	0,00	64,70
2.2.1	2,38	12,80	78,10	10,20	8,50	4,20	0,00	1,70	0,00	59,20
2.2.2	2,44	10,70	79,70	9,60	7,80	4,30	0,90	1,70	0,00	60,60
2.2.3	2,47	10,70	80,00	9,50	7,80	5,20	0,00	1,70	0,00	62,60
2.3.1	2,46	10,80	80,60	9,50	8,60	5,70	0,00	1,00	0,00	61,50
2.3.2	2,44	11,60	79,90	10,00	9,10	4,50	0,00	0,90	0,00	60,20
2.3.3	2,48	9,90	79,70	9,40	7,50	4,70	0,00	1,90	0,00	62,70
3.1	N/A	N/A	N/A	N/A	N/A	N/A	N/A	N/A	N/A	N/A
3.2	2,44	12,90	79,90	9,00	9,00	5,40	0,00	1,80	0,00	57,40
3.3	N/A	N/A	N/A	N/A	N/A	N/A	N/A	N/A	N/A	N/A
4.1	2,40	12,90	78,50	10,10	5,50	4,60	1,80	0,70	0,00	63,20
4.2	N/A	N/A	N/A	N/A	N/A	N/A	N/A	N/A	N/A	N/A
4.3	N/A	N/A	N/A	N/A	N/A	N/A	N/A	N/A	N/A	N/A
4.4	N/A	N/A	N/A	N/A	N/A	N/A	N/A	N/A	N/A	N/A
4.5	2,52	9,90	80,60	9,80	7,10	5,40	0,90	0,90	0,00	64,20
4.6	2,50	9,40	77,00	10,40	6,60	4,70	0,00	0,90	0,00	67,00
5.1	2,32	15,90	74,70	10,10	8,40	5,00	0,80	2,50	0,00	53,80
5.2	N/A	N/A	N/A	N/A	N/A	N/A	N/A	N/A	N/A	N/A
5.3	N/A	N/A	N/A	N/A	N/A	N/A	N/A	N/A	N/A	N/A
6C.1	2,46	10,30	77,40	8,00	7,10	5,30	0,90	1,80	0,00	65,80
6C.2	2,41	12,00	76,30	7,60	6,80	5,10	0,80	2,50	0,00	60,90
6C.3	2,43	13,50	77,50	10,50	9,60	4,40	0,90	2,60	0,00	55,80
IS5	2,45	13,50	78,50	8,80	6,10	6,10	0,90	3,50	0,00	58,40
IS6	2,49	10,50	79,60	9,60	7,80	7,00	0,90	1,70	0,00	

Table 6. Principal amines signals express in percentage and mean DoS values of heparin samples belong to *bona fide* library. N/A stands for not acquired HSQC spectra. Values were calculated from ^{1}H-^{13}C HSQC NMR signal integration applying the method reported in Guerrini *et al*., 2005. DoS= degree of sulfation; G= glucuronic acid; I= iduronic acid; AN_{NAc}= H atom linked to N atom belonging to the amine group of $GlcN_{Nac}$ residue; H6 A_{6S}= H atom linked to C6 atom of the saccharidic ring of $GlcN_{NX,6S}$ residue; H1 AN_{NS}-G= H1 atom linked to C1 atom of $GlcN_{NS,6X}$ residue covalently linked to G residue; H1 AN_{NS}-I_{2OH}= H1 atom linked to C1 atom of $GlcN_{NS,6X}$ residue covalently linked to I_{2OH}; H1 A*= H1 atom linked to C1 atom of A*; H1 AN_{NAc} α red= H1 atom linked to C1 atom of α-$GlcN_{NAc}$ residue at the reducing end; H1 AN_{NS} α red= H1 atom linked to C1 atom of α-$GlcN_{NS}$ residue at the reducing end; H1 AN_{NS} β red= H1 atom linked to C1 atom of β-$GlcN_{NS}$ residue at the reducing end; AN_{NS}-I_{2S}= H1 atom linked to C1 atom of $GlcN_{NS}$ residue covalently linked to I_{2S}.

Sample code	H1 I_{2S}	H1 I_{2OH}-A_{6S}	H1 I_{2OH}-A_{6OH}	H1 I_{2S} α red	H1 G- A*	H1 G- AN_{NS}	H1 G-AN_{NAc}	GalU	H2 epox	L.R.
1.1	73,90	6,10	1,70	0,00	2,60	7,00	7,00	0,00	0,00	5,50
1.2	70,70	7,00	2,60	0,00	2,60	8,60	6,00	0,00	0,00	3,70
2.1.1	75,90	5,10	2,10	0,00	3,10	6,20	4,10	0,00	1,00	5,60
2.1.2	77,20	5,00	2,00	0,00	2,00	5,90	5,00	0,00	1,00	5,10
2.1.3	79,60	5,40	2,20	0,00	2,20	6,50	3,20	0,00	0,00	4,70
2.2.1	70,60	5,90	2,00	0,00	2,90	7,80	5,90	0,00	2,90	4,80
2.2.2	73,50	5,90	2,00	0,00	2,90	6,90	4,90	0,00	2,00	4,40
2.2.3	74,10	6,20	2,00	0,00	3,00	7,10	6,10	0,00	0,00	4,00
2.3.1	68,10	4,40	1,80	0,00	2,70	6,20	6,20	0,00	5,30	2,10
2.3.2	70,70	5,20	2,60	33,30	1,70	6,10	7,00	0,00	3,50	1,80
2.3.3	73,20	4,50	1,80	33,30	1,80	5,40	7,10	0,00	3,60	1,80
3.1	N/A	N/A	N/A	N/A	N/A	N/A	N/A	N/A	N/A	N/A
3.2	72,50	6,10	2,60	0,00	2,60	6,10	7,00	0,90	0,00	3,10
3.3	N/A	N/A	N/A	N/A	N/A	N/A	N/A	N/A	N/A	N/A
4.1	71,20	7,20	2,70	0,00	1,80	9,00	5,40	0,00	0,00	2,00
4.2	N/A	N/A	N/A	N/A	N/A	N/A	N/A	N/A	N/A	N/A
4.3	N/A	N/A	N/A	N/A	N/A	N/A	N/A	N/A	N/A	N/A
4.4	N/A	N/A	N/A	N/A	N/A	N/A	N/A	N/A	N/A	N/A
4.5	76,90	6,10	1,70	0,00	1,70	6,20	5,20	0,90	0,00	2,90
4.6	77,50	4,40	2,60	0,00	1,80	6,20	5,30	0,00	0,00	2,30
5.1	70,80	8,00	2,70	0,00	1,80	7,10	6,20	0,90	0,00	4,10
5.2	N/A	N/A	N/A	N/A	N/A	N/A	N/A	N/A	N/A	N/A
5.3	N/A	N/A	N/A	N/A	N/A	N/A	N/A	N/A	N/A	N/A
6C.1	74,30	5,30	2,70	0,00	2,70	6,20	7,10	0,00	0,00	5,80
6C.2	74,50	6,40	2,70	0,00	1,80	6,40	5,50	0,00	0,00	7,90
6C.3	76,70	5,00	2,50	0,00	1,70	5,80	5,80	0,00	0,00	1,30
IS5	76,60	5,60	2,80	0,00	2,80	5,60	3,70	0,00	0,00	6,10
IS6	74,80	7,00	2,60	0,00	2,60	6,10	4,30	0,00	0,00	4,60

Table 7. Principal uronic and linkage region signals values express in percentage of heparin samples belong to *bona fide* library. N/A stands for not acquired HSQC spectra. Values were calculated from ^{1}H-^{13}C HSQC NMR signal integration applying the method reported in Guerrini *et al*., 2005. I= iduronic acid; G= glucoronic acid; H1 I_{2S}= H1 atom linked to C1 atom of $IdoA_{2S}$ residue; H1 I_{2OH}-A_{6S}= H1 atom linked to C1 of $IdoA_{2OH}$ residue covalently linked to $GlcN_{NX,6S}$ residue; H1 I_{2OH}-A_{6OH}= H1 atom linked to C1 atom of $IdoA_{2OH}$ residue covalently linked to $GlcN_{NX,6OH}$ residue; H1 I_{2S} α red= H1 atom linked to C1 atom of α-$IdoA_{2S}$ residue at the reducing end; H1 G-A* = H1 atom linked to C1 atom of G residue covalently linked to A* residue; H1 G-AN_{NS} = H1 atom linked to C1 atom of G residue covalently linked to $GlcN_{NS,6X}$ residue; H1 G-AN_{NAc} = H1 atom linked to C1 atom of G residue covalently linked to $GlcN_{NAc,6X}$ residue; GalU= α-D-galactosyl mannopentaose; H2 epox= H2 atom linked to C2 atom of the residue bearing an epoxy group; L.R.= linkage region.

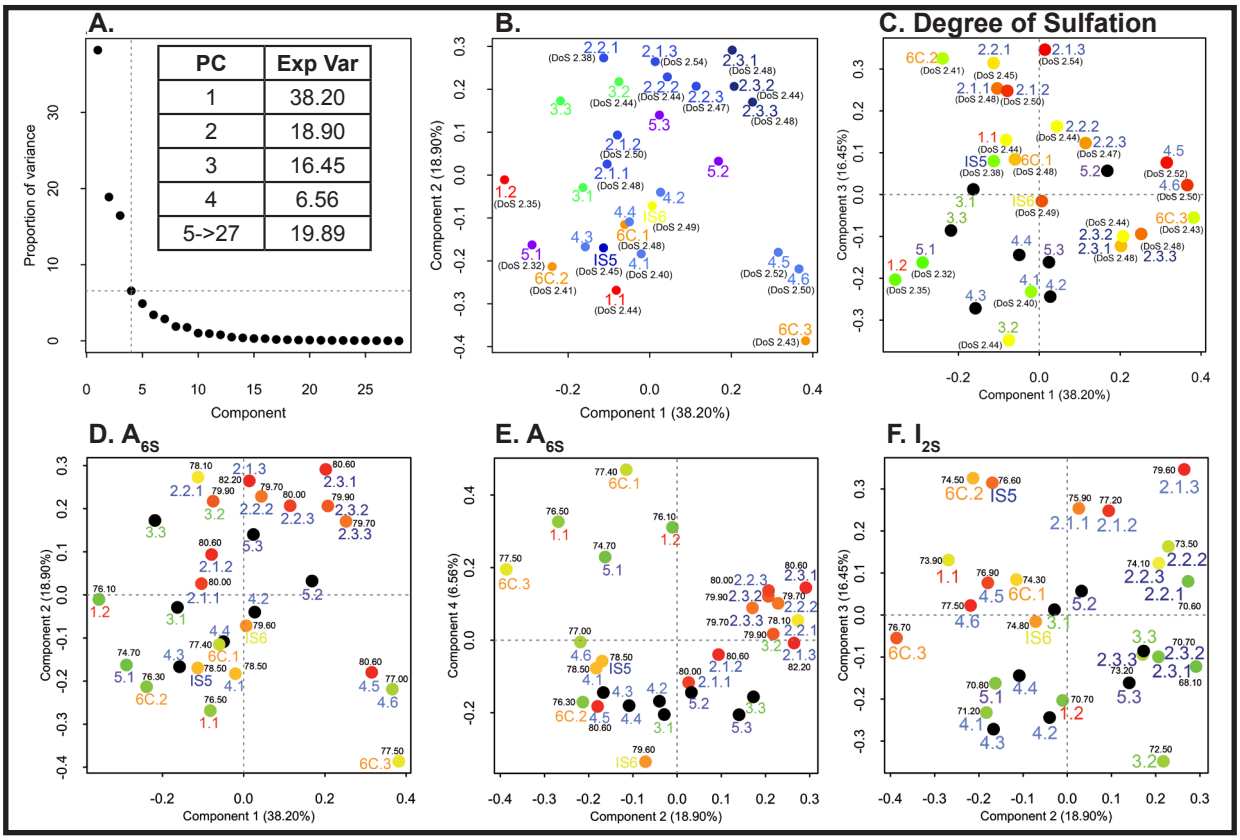

Figure 26. PCA of *bona fide* single spectra Hep library. The same dataset was considered for all 5 analysis. **A)** Scree plot, components 1, 2, 3 and 4 together describe 80.11% of the variation within the spectra comprising the heparin library (PC $1_{Expl.\ Var}$= 38.20 %; PC $2_{Expl.\ Var}$= 18.90%; PC $3_{Expl.\ Var}$= 16.45%; PC $4_{Expl.\ Var}$= 6.56%). **B)** Loading plot, in which components 1 and 2 together describe 57.1 % of the variance within the spectra comprising the heparin library; **C)** Loading plot, for component 1 and 3. Samples characterised by high content of sulfated Hep were discriminated from samples with a low content of sulfated Hep; **D)** Loading plot, for A_{6S} component 1 and 2; more than 50% of samples characterised by high content of GlcN sulfated in C6 were discriminated from other Hep samples; **E)** Loading plot, for A_{6S} component 2 and 4; 100% of samples characterised by high content of GlcN sulfated in sulfated C6 were discriminate from other Hep samples; **F)** Loading plot, for I_{2S} component 2 and 3; samples characterised by high content of sulfated C2 were completely discriminated from the other samples. In panels C, D, E and F: black dots represent samples with no informations available for DoS and sulfation data.

6.1.4. Differentiation of a heparin sample contaminated with a gradient of OSCS from the heparin library

Principal component analysis of a sample sequentially contaminated with OSCS (0.25 - 100 %) and the heparin reference library is shown in Fig. 27 and dataset complexity changes can be appreciated in Table 8, in which the spectral range was 6.00 - 1.95 ppm and the data were mean centred. It can be seen from the loading plots (Fig. 27) that the threshold for differentiation for a single contaminated sample against the heparin library used in this circumstance is ~5 % OSCS; a sample tainted with 3 % OSCS lying within the heparin library cluster and 7 % lying well outside the heparin library area using only components 1 and 2 (Fig. 27). It is also important to state that the 'limit of detection' is also fundamentally limited by the library composition. Three percent contamination is discernable if additional components are used; component 1 Vs component 3, component 1 Vs component 5, component 1 Vs component 6 and component 3 Vs component 6 (Table 8 and Fig. 28).

PC	Exp. Var OSCS 0%	Exp. Var OSCS 0.25%	Exp. Var OSCS 1%	Exp. Var OSCS 3%	Exp. Var OSCS 5%	Exp. Var OSCS 7%	Exp. Var OSCS 15%	Exp. Var OSCS 25%	Exp. Var OSCS 100%
C1	45.42	35.08	34.71	33.66	32.39	30.69	33.70	51.53	91.39
C2	16.80	16.10	16.16	15.98	16.87	19.28	24.73	17.90	3.01
C3	12.43	13.82	13.72	13.55	12.92	12.42	10.24	7.62	1.46
C4	6.14	8.59	8.57	8.85	9.51	10.33	9.18	6.78	1.19
C5	4.18	5.44	5.39	5.69	6.12	6.12	5.09	3.72	0.65
C6	3.76	4.18	4.15	4.17	4.21	4.13	3.40	2.48	0.45
Residual components	11.27	16.79	17.3	18.1	17.98	17.03	13.66	9.97	1.85

Table 8. Change in explained variance values caused by different percentage of OSCS contamination. Dataset complexity decreases as much as OSCS % increases: component 1 explains the 45.42 % of variance without OSCS, but with 100 % OSCS it explains ~90% of variance.

By limiting the analysis to regions of the spectra where isolated spectral features lie, which are specific to the contaminant i.e. the N-acetyl signal of OSCS (2.15 ± 0.02 ppm), it is possible to make the analysis more sensitive. In this case, 1 % OSCS can still be distinguished using components 1 and 2, with 0.25 % lying on the fringe of the heparin library (Fig. 29, the dataset span 2.22 - 1.95 ppm, the area under the spectra were normalised to 1, the dataset was then mean centered and autoscaled). Using fewer components it was possible to differentiate a sample contaminated with 0.25 % OSCS from the heparin library (Fig. 30, component 1 [33.00 %], component 2 [27.30 %], component 3 [11.94 %] and component 4 [6.70 %]).

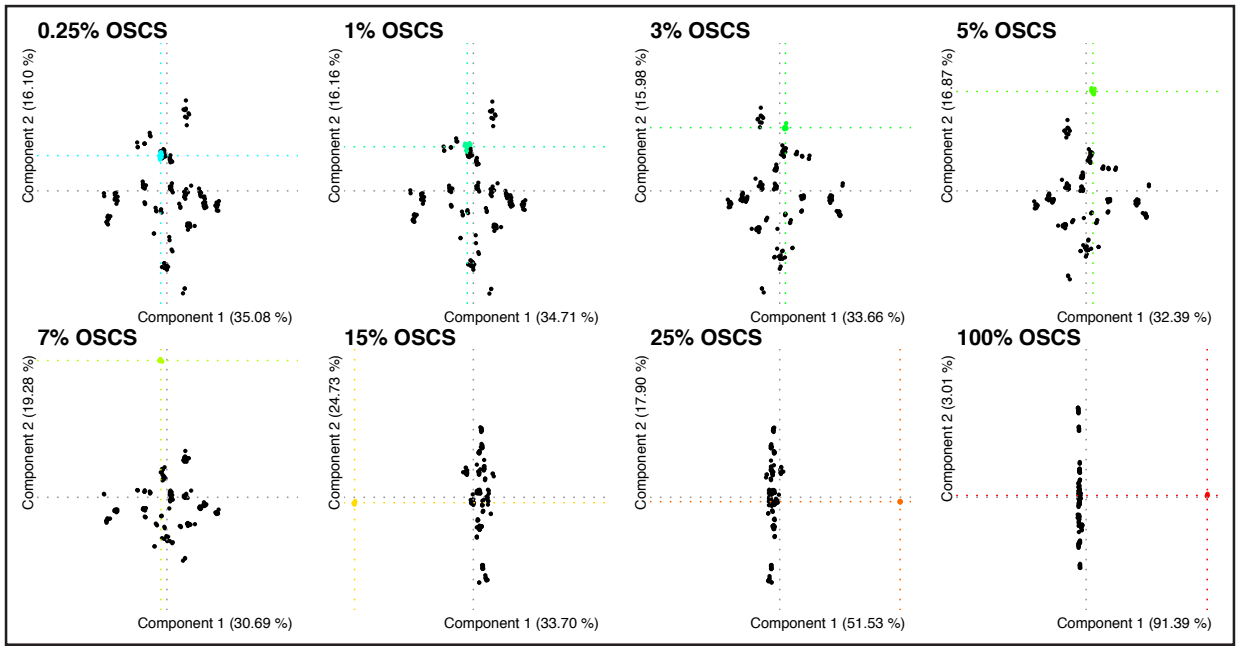

Figure 27. OSCS gradient (coloured circles) compared to the heparin library (black circles). A gradient of OSCS (0.25 % to 100 % w/w) samples compared to a heparin reference library. Note that at 5 % contaminant, test spectra lay outside the body of the heparin reference spectra but, at 3 %, test spectra lay inside. Each PCA was performed with the spectra of the heparin reference library and a single value dilution of OSCS (practically, 3 separate preparations whose spectra were each recorded in triplicate). Prior to PCA, the area of each spectrum was normalised to the average spectral area of the dataset, the dataset was then mean-centered and Pareto scaled. The signals differentiating the heparin library from the OSCS containing samples in the N-acetyl region is a peak at 2.16 ppm, whereas the heparin library is dispersed by signals at ~2.04 ppm (heparin N-acetyl), ~2.08 ppm (dermatan sulfate N-acetyl and ~2.1 ppm (oxidation of heparin N-acetyl) respectively.

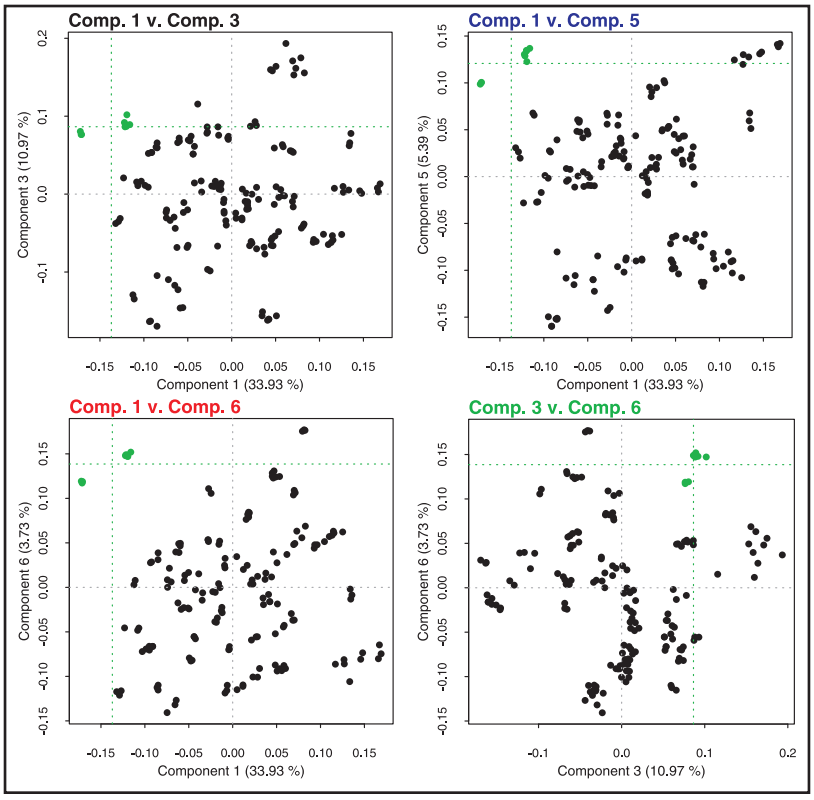

Figure 28. PCA Loading plot for Hep library and 3 % OSCS. Addictional component analysis leads to discerne 3 % OSCS out of the library. Prior to PCA, the area of each spectrum was normalised to the average spectral area of the dataset, the dataset was then mean-centered and Pareto scaled.

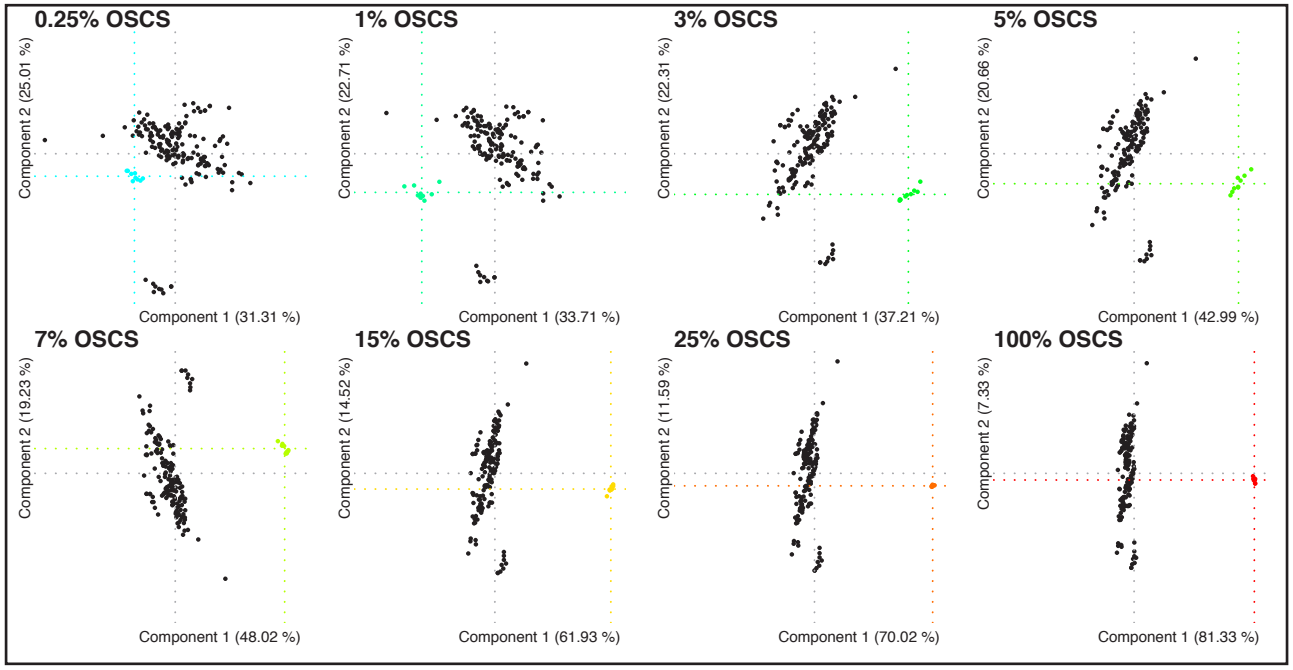

Figure 29. OSCS gradient (0.25-100%) compared to the heparin reference library analysed by PCA of the N-acetyl region (2.22 - 1.95 ppm), the area under the spectra were normalised to the average spectral area, the dataset were then mean-centered and autoscaled. Note that at 1% OSCS the test spectra lay outside the main body of the heparin library; by 0.25%, they lay within the library.

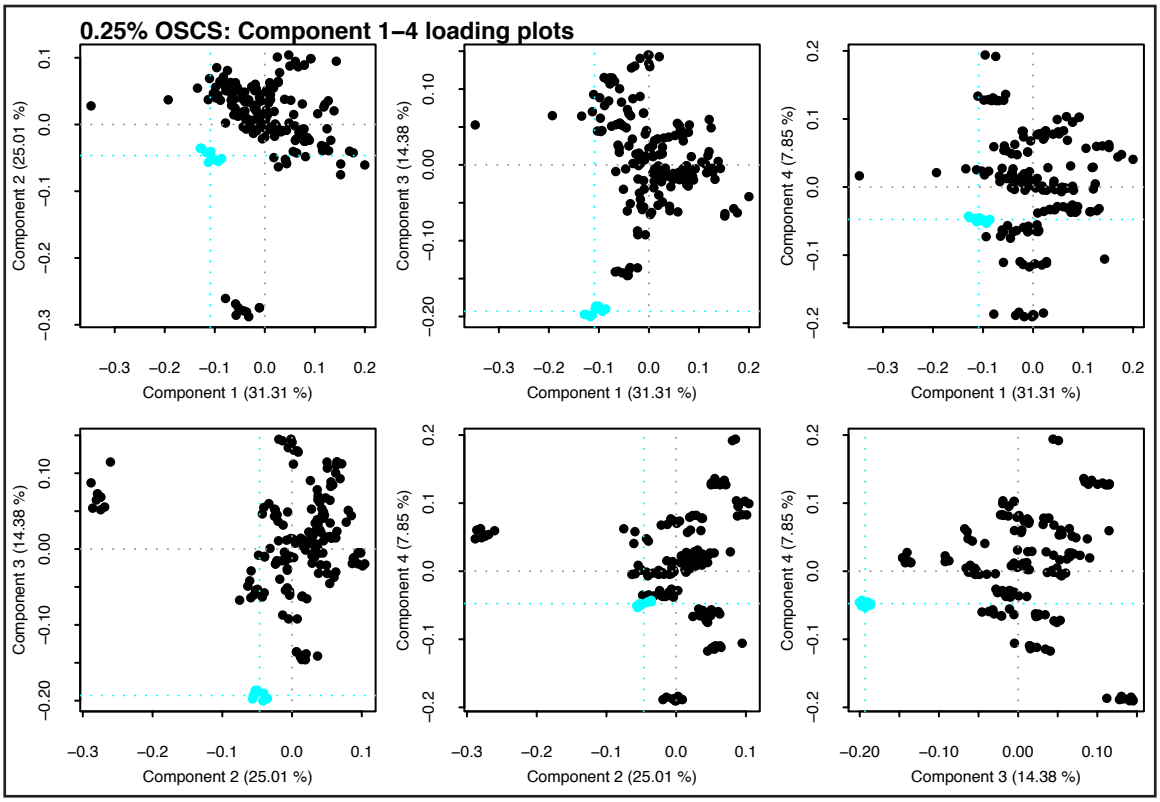

Figure 30. Combinatorial loading plots (components 1-4) derived from the PCA analysis of the OSCS samples with the heparin library, analysis was performed on the N-acetyl region only, the area under the spectra were normalised to the average spectral area, the dataset were then mean-centered and autoscaled.

6.1.5. Detection of non N-acetylated sulfated polysaccharides

Since the recent contamination of heparin with OSCS, many approaches for the detection and analysis of contaminants have been published (Beyer *et al*., 2008; Sitkowski *et al*., 2008; Wang *et al*., 2008; Bairstow *et al*., 2009; Bigler and Brenneisen, 2009; Guerrini *et al*., 2009 [b]; Kakoi *et al*., 2009; Li *et al*., 2009; Liverani *et al*., 2009; Somsen *et al*., 2009; Spencer *et al*., 2009; Trehy *et al*., 2009; Volpi *et al*., 2009; Wielgos *et al*., 2009; Zhang *et al*., 2009; Bednarek *et al*., 2010; Beyer *et al*., 2010; Gemene and Meyerhoff, 2010; Hashii *et al*., 2010; Keire *et al*., 2010; Keire *et al*., 2010 [b]; McKee *et al*., 2010) most of which have concentrated specifically on detection of OSCS. It has been previously shown (Beyer *et al*., 2008; Ruiz-Calero *et al*., 2000; Ruiz-Calero *et al*., 2002; Ruiz-Calero *et al*., 2002 [b]; Rudd *et al*., 2009), that it is possible to differentiate porcine heparin from dermatan sulfate (Fig. 31) and also from bovine lung (BL) heparin (Fig. 32). For both analyses prior mean-centering was employed, the spectral areas were not normalised and no other scaling was used. Here, we show that it is also possible to differentiate samples tainted with non N-acetylated polysaccharides; over sulfated dextran sulfate (OSDxS) and over sulfated agarose sulfate (OSAS) (Table 9; Fig. 33), which is more challenging because the N-acetyl group of contaminating GAGs provided a useful marker signal for ^{1}H NMR that was isolated from other major signals. Samples containing as little as 10 % OSDxS and 10 %OSAS were differentiated from the current heparin library (Fig. 33). The analysis of these samples was performed by normalising the area under the spectra to the average area under the spectra in the dataset, the dataset was then mean-centered, vast scaled and the PCA performed. However, the sample containing 10 % OSAS in Fig. 34 would fail the USP proposed ^{1}H NMR analysis (peak at 2.94 ppm higher than 4 % of comparative signals), whereas OSDxS would pass (FDA, 2009).

PC	Exp. Var Hep library	Exp. Var OSDxS 2%	Exp. Var OSDxS 5%	Exp. Var OSDxS 10%	Exp. Var OSDxS 20%	Exp. Var OSAS 2%	Exp. Var OSAS 5%	Exp. Var OSAS 10%	Exp. Var OSAS 20%
C1	45.42	35.40	35.03	33.22	29.90	35.42	34.84	33.34	32.82
C2	16.80	16.33	16.21	16.43	20.84	16.37	16.29	16.23	16.13
C3	12.43	13.74	13.54	12.68	11.38	13.76	13.51	12.88	12.66
C4	6.14	7.93	7.89	8.33	10.83	7.89	7.69	7.32	8.43
C5	4.18	5.06	4.97	5.93	6.11	5.08	4.99	6.89	7.14
C6	3.76	4.26	4.22	4.64	4.09	4.27	4.28	4.72	4.62
C > 6	11.27	17.28	18,14	18.77	16.85	17.21	18.40	18.62	18.20

Table 9. Principal component Expl. Var. values for heparin library with and without OSDxS and OSAS.

Even though PCA is an independent technique, the quality of the analysis is dependent on the samples within the reference library. The quality of the library clearly influences the ‘limit of detection’, which is something of a misnomer- ‘limit of differentiation’ might be a better term and it is important not to confuse this limit with limits of detection which refer to the much easier task of comparing the spectrum of a single sample of heparin with a spectrum of the same material containing a contaminant. Such a comparison would be expected to be very sensitive. Here, a reference library was employed which encompassed some of the intrinsic natural heterogeneity of porcine intestinal mucosal heparin. If a reference library contains pre-contaminated samples (i.e., the nature of the contaminant is known), this increases the sensitivity of the analysis for that contaminant, as can be seen in the loading plots of Fig. 35, which describes PCA of a heparin library against all the OSCS samples. The samples containing 3 % OSCS clearly lies outside the body of the heparin reference samples (the dataset was normalised to the average area under the spectra and mean-centred before PCA), whereas 5 % lies outside the body of the heparin reference samples if PCA is performed piecemeal with each OSCS contaminated sample (the dataset was normalised to the average area under the spectra, mean-centred and Pareto scaled before PCA). Therefore, if the comparison is required to estimate a known contaminant, rather than assess a general level of similarity between test and library samples, the precise method of the interrogation will change. The inclusion of the contaminants in the library tend to weight the variance in the dataset so that a sample tainted with the included contaminant becomes more likely to be found within the first two components. This changes the question that is being asked from; how similar is the sample heparin to the library? to; how similar is the sample to a library of heparins pre-contaminated with X? These are two distinct analyses. A very useful feature of PCA is that with component loadings (differentiating the variables), PCA produces component scores which contain information about the features making up the components. In this case it is the spectral features that differentiate the contaminated sample from the heparin reference library (Fig. 35).

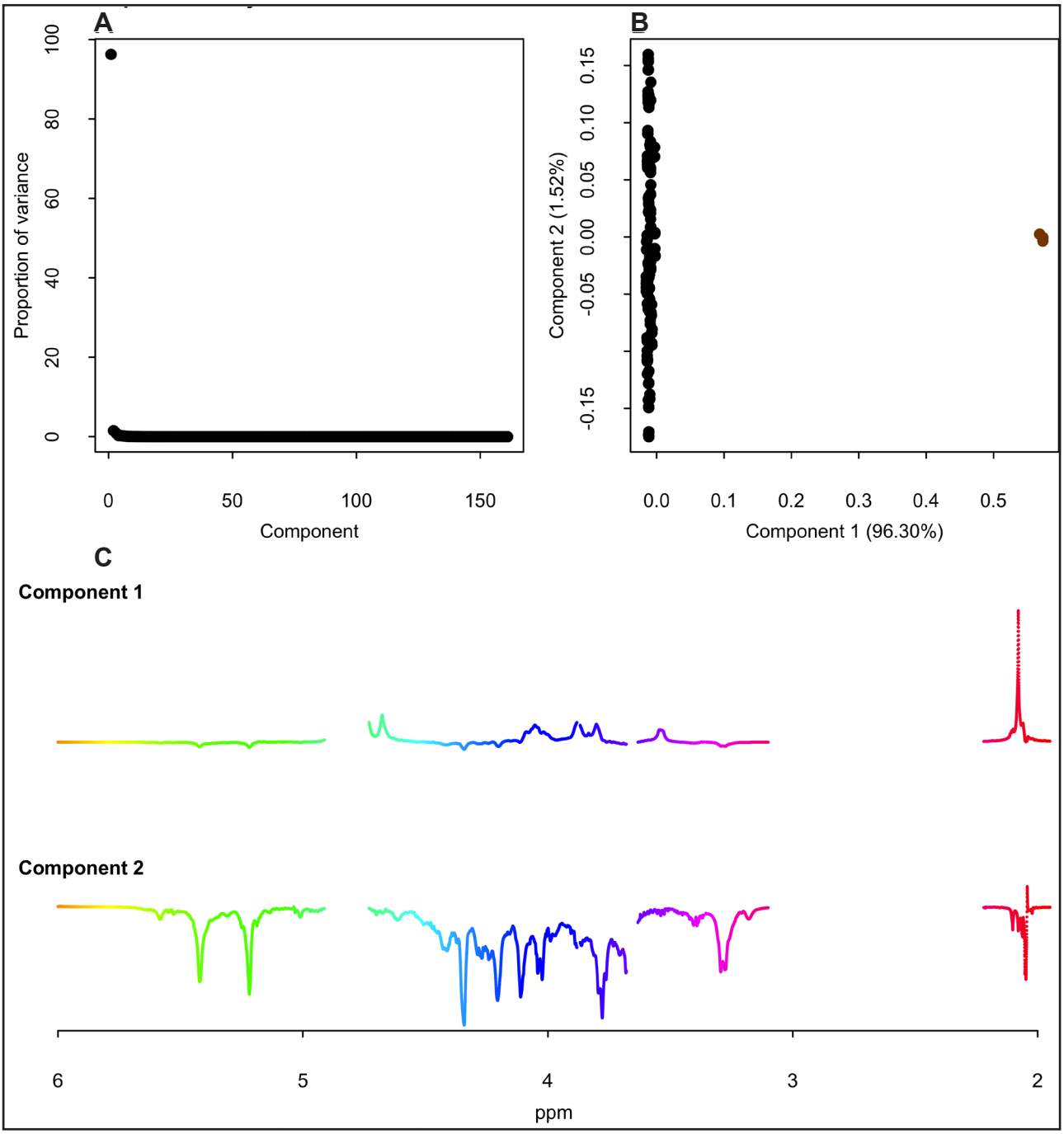

Figure 31. PCA analysis for Hep library and DS. **A)** Scree plot [component 1 (96.30%) and component 2 (1.52 %)]; **B)** Loading plot for componet 1 and componet 2, showing the clear discrimination from DS. **C)** Score plots, for component 1 and 2, illustrating the features that differentiate the spectra. Componet 1 shows that more than 95 % of the variance is described by DS feature (DS peak 2.08 ± 0.02 ppm). The dataset were mean-centered prior analysis.

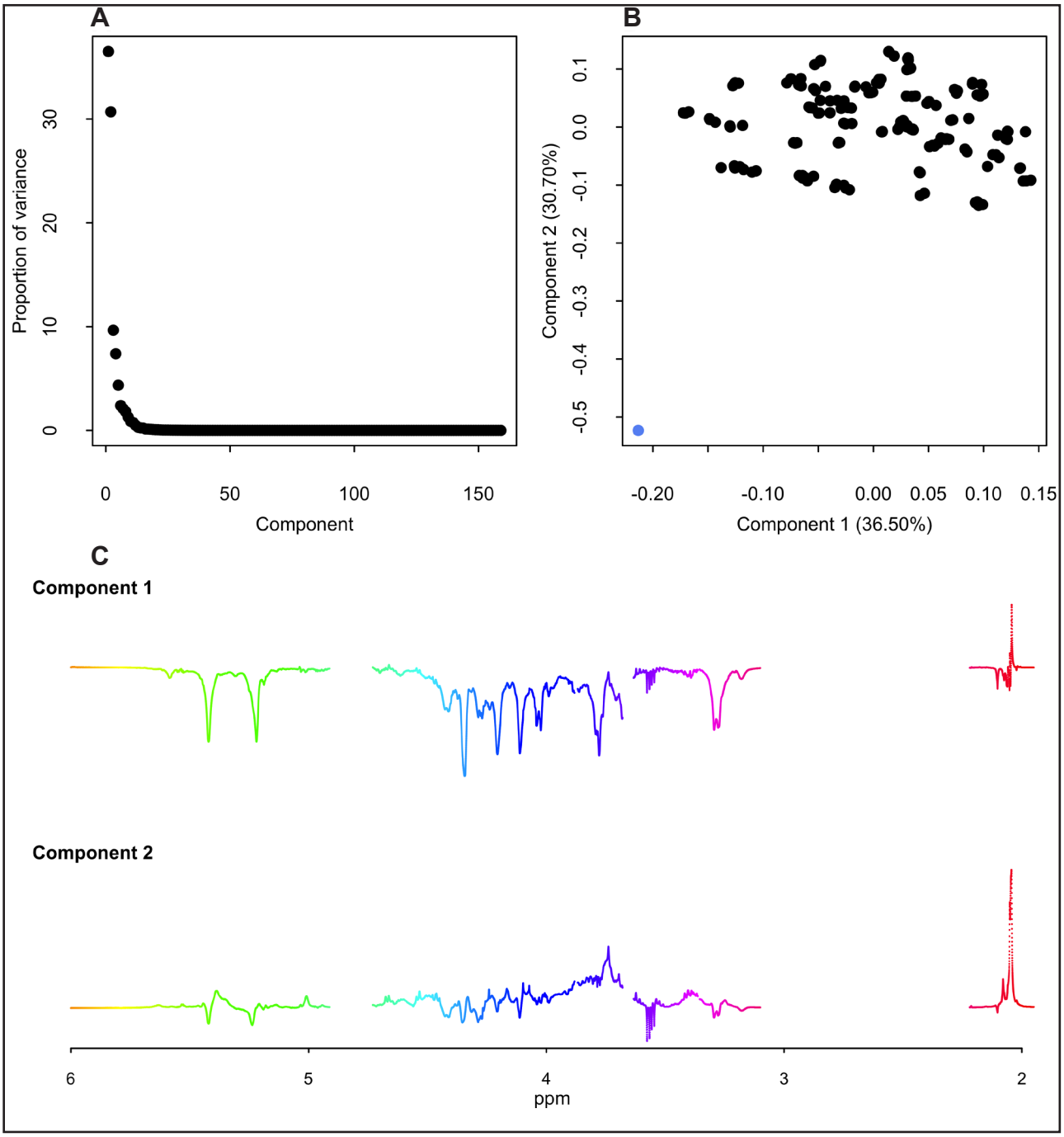

Figure 32. PCA analysis for Hep library and BL 2nd heparin international standard. **A)** Scree plot [component 1 (36.50%) and component 2 (30.70 %)]; **B)** Loading plot for componet 1 and componet 2, showing the clear discrimination from BL 2nd heparin international standard. **C)** Score plots, for component 1 and 2, illustrating the features that differentiate the spectra. Componet 1 shows BL 2nd heparin international standard characteristic spectrum features mainly and component 2 illustrates that pig mucosa heparin is characterised by A_{NA} $COCH_3$ higher content ($COCH_3$ peak 2.05 ± 0.02 ppm). The dataset were mean-centered prior analysis.

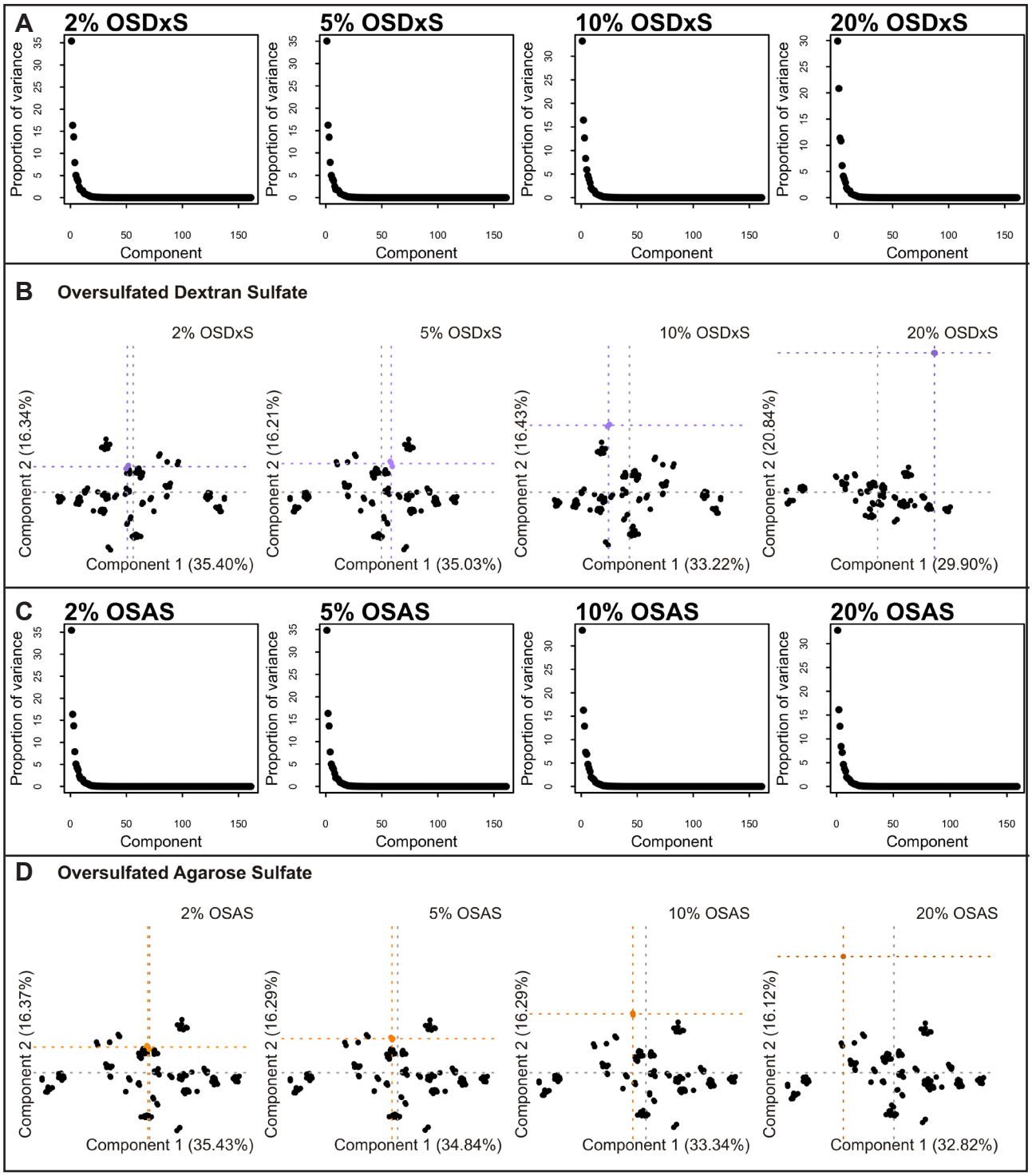

Figure 33. PCA analysis for heparin library with and without OSDxS and OSAS. **A)** Scree plots for heparin library with and without OSDxS gradient (2 %, 5 %, 10 % and 20 % OSDxS). **B)** Loading plots for heparin library with and without OSDxS gradient. **C)** Scree plots for heparin library with and without OSAS gradient (2 %, 5 %, 10 % and 20 % OSAS). **D)** Loading plots for heparin library with and without OSAS gradient. The area under the spectra was normalised to the average area under the spectra in the dataset, the dataset was then mean-centered, pareto scaled prior to PCA analysis. Note that at 10 % of OSDxS and at 10 % of OSAS the test spectra lay outside the main body of the heparin library.

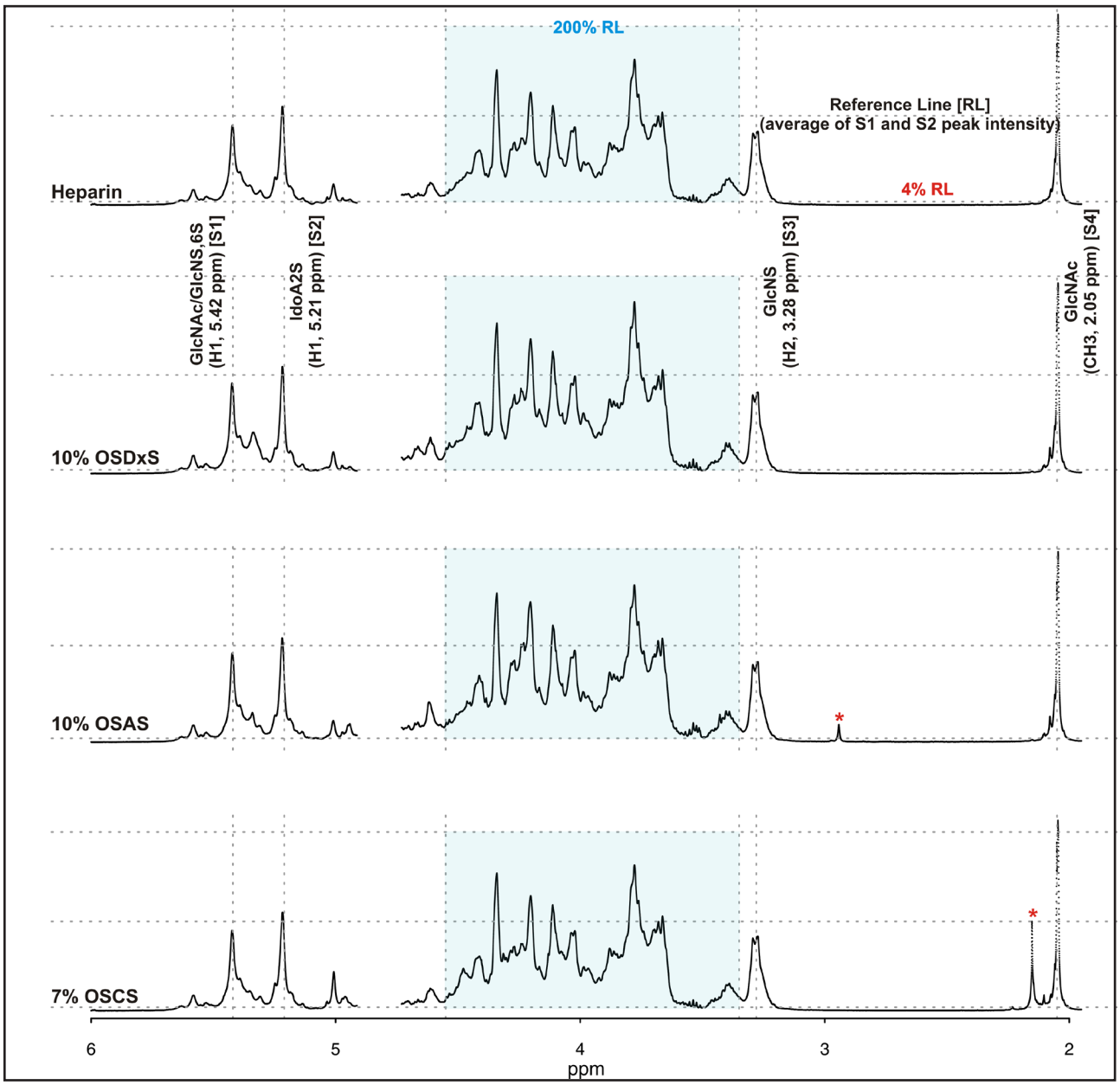

Figure 34. ^{1}H NMR spectra of 4.1 heparin contaminated with 7 % OSCS, 10 % OSAS, 10 % OSDxS, analysed by the method outlined by USP heparin monoscript 2 (Materials and Methods 4.2.4; FDA, 2009) in which signals in broad regions of the spectrum are treated *en masse*. Heparin and 10% OSDxS pass the test, while 10% OSAS and 7% OSCS fail (the spectral features resulting are labeled with a red asterix).

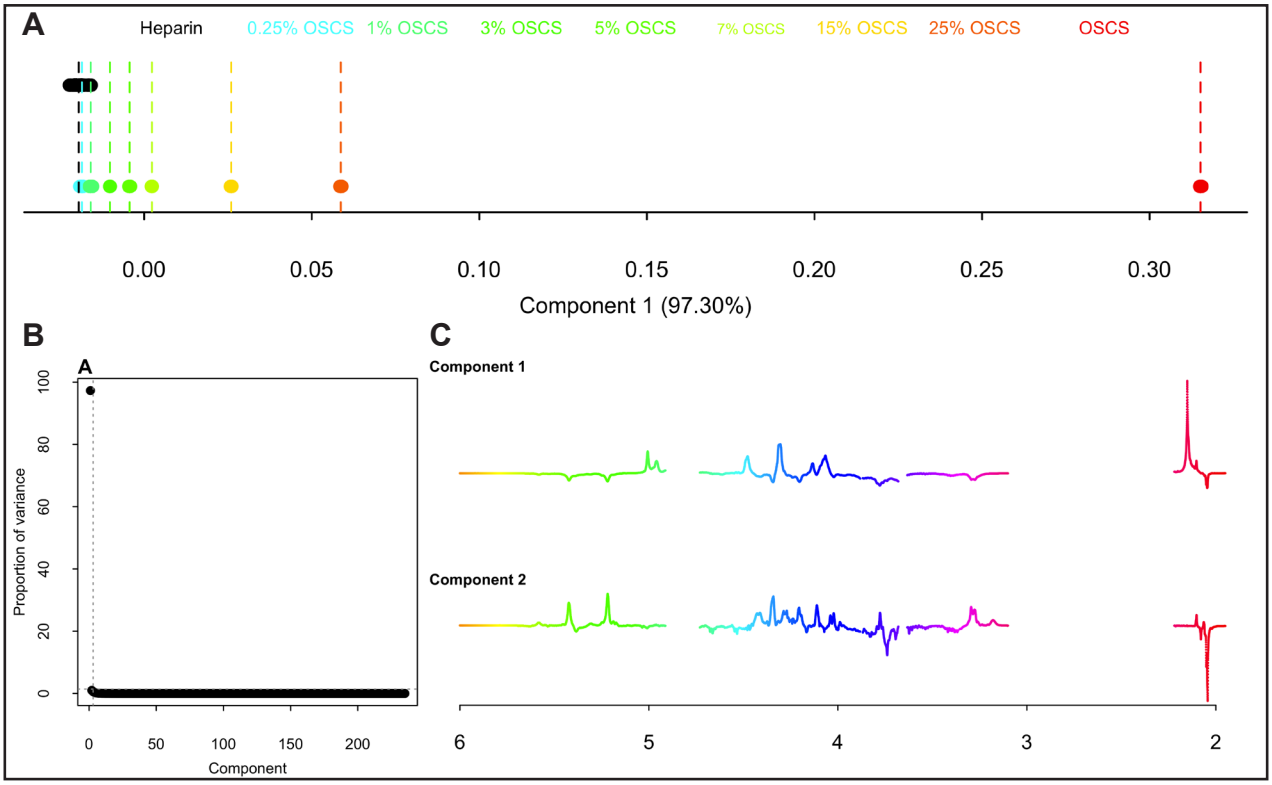

Figure 35. A gradient of OSCS contaminating heparin compared to a heparin library. One component differentiates heparin and OSCS (explaining 97.30 % of the variance). The variation in their spectra defines the intrinsic variability within the heparin library and imposes a fundamental limit on the ability of the comparison to discern spectral differences between the library and any test heparin. B) Scree plot for gradient of OSCS contaminating heparin compared to a heparin library ($PC1_{Expl.\ Var.}$ = 97.30 % and $PC2_{Expl.\ Var.}$ = 1.00 %). C) Score ploat for gradient of OSCS contaminating heparin compared to a heparin library, component 1 and 2. Before PCA the dataset was normalised to the average area under the spectra and mean-centered.

6.1.6. Discussion

A heparin library, comprising common European commercial heparins, was prepared and characterised by ^{1}H and ^{1}H-^{13}C HSQC NMR. Heparins containing modifications induced by the manufacturing processes (over oxidation) were also considered. ^{1}H NMR-PCA can differentiate both OSCS contaminated samples from the library (5 % OSCS for analysis performed on the full spectrum and 1 % OSCS if performed on the N-acetyl region alone) and can also distinguish moderate (10 % OSDxS and 10 %OSAS) contaminated samples, which are not N-acetylated, where the USP NMR identity test cannot. The spectral features that differentiate the contaminated samples from a heparin reference library can be isolated in component score plots and could, if required, be further analysed to help identify the contaminants. The specific question that is being addressed may require a specific set of compounds to be included in the reference library. For example, here, the question asked is how similar is a test heparin sample to the standard reference library of *bona fide* heparin samples under standardised conditions. In this sense, the approach is extremely flexible. One potential development would be to conduct the test of an unknown sample repeatedly against the library, contaminated on each occasion with a different, known contaminant (e.g. OSCS, solvents, protein, lipid etc) in order to facilitate identification of the unknown contaminant. Furthermore, the library could be expanded with samples contaminated in this way provided by the manufacturers, the aim being to cover the heterogeneity of pharmaceutical porcine intestinal mucosal heparins and, possibly, also heparins from other origins, organs and processed by a variety of manufacturing processes. This should provide a better model for the differentiation of heterogeneous heparin samples from contaminated heparin.

6.2. Effects on molecular conformation and anticoagulant activities of 1,6-anhydrosugars at the reducing terminal of antithrombin-binding octasaccharides isolated from low-molecular-weight heparin enoxaparin

Published in J. Med. Chem., 2010, epub ahead of print

6.2.1. Summary

Low molecular weight heparins are widely used in clinics for prevention and treatment of thromboembolism (Gray *et al*., 2008; Linhardt *et al*., 2003). Here, two novel octasaccharides incorporating the active pentasaccharide sequence with a modified aminosugar at the reducing end were isolated from enoxaparin. In these octasaccharides, the most common N-sulfo-6-O-sulfated-glucosamine residue (A) at the reducing end of the $A_{NA}GA^*IA$ sequence (Octa-3 from a previous study) is substituted by a 1,6-anM (Octa-5) and 1,6-anG (Octa-6) residues (Fig. 36) (Guerrini *et al*., 2008 [b]). Partially modified $A_{NA}GA^*I_SA$ sequences are useful models to study the effects of octasaccharides structural variations on AT-binding (Guerrini *et al*., 2008 [b]). Although these two octasaccharides showed significantly lower affinity to AT as well as a reduced anti-FXa activity when compared with the pentasaccharide Fondaparinux (the α- methyl glycoside of a synthetic version of $A_{NA}GA^*I_SA$ with N-SO_3 instead of N-acetyl group at the nonreducing aminosugar residue) and with the $A_{NA}GA^*I_SA$ containing octasaccharides so far described, they display essentially the same anti-FXa activity in plasma and in buffer solution, which supports the concept that they specifically interact with AT. The structure and conformational properties of complexes of Octa-5 and Octa-6 with AT were investigated in solution by saturation transfer difference (STD), transferred nuclear Overhauser effect spectroscopy (trNOESY) NMR experiments, while docking simulation were used to build complex geometries agreeing to the experimental data.

6.2.2. Equilibrium dissociation constants and anti-FXa activity of octasaccharides

Octasaccharides isolation and equilibrium constant measurements were done in collaboration with Prof. Boudier C. (Universite Louis Pasteur, Strasbourg, France). Saturation of constant amounts of AT by increasing quantities of Octa-3, -5, and -6 resulted in a ± 30 % increase of the protein intrinsic fluorescence as observed for the pentasaccharide $A_{NA}GA^*I_SA$ (fondaparinux), the reference product. Fluorescence data were satisfactorily analysed by assuming a 1:1 binding stoichiometry as already reported (Guerrini *et al*., 2008 [b]) to determine the best estimates of the equilibrium dissociation constant (K_d). Its values for the various oligosaccharides: AT pairs are listed in Table 10. We found that in 0.05 M HEPES, 0.1 M NaCl K_d for Octa-5-AT and Octa-6-AT complexes is equal to 0.90 ± 0.08 μM and 1.23 ± 0.06 μM, an affinity about 50- and 10-fold lower than that determined for the fondaparinux and Octa-3 under the same conditions: 0.021 ± 0.001 μM and 0.12 μM, respectively. Because of their moderate affinity, it was not possible to determine K_d for the binding of Octa-5 and -6 to AT in the presence of higher salt concentration. Activity measurements were done in collaboration with Dr. Viskov C. (Sanofi-Aventis, Paris, France). The anti-FXa activity using a purified factor Xa and AT was measured in buffer as well as in human plasma for both octasaccharides. Enoxaparin and the

synthetic pentasaccharide fondaparinux were tested as reference agents (Table 11). A specific activity of 120 anti-FXa IU/mg in buffer was measured for enoxaparin, which is in the known specification range (European Pharmacopea, 2008). The activity of fondaparinux of 810 anti-FXa units/mg is in line with historical data (Herbert *et al*., 1996). The anti-FXa activity in human plasma for enoxaparin and fondaparinux was slightly lower (13 % and 6 %) compared to that in an aqueous buffer solution. In contrast, Octa-5 and Octa-6 shown a lower anti-FXa activity of approximately 50 and 40 anti-FXa IU/mg, respectively, but no difference in their anti-FXa activity in plasma and in aqueous buffer solution.

[NaCl] (M)	Octa-5	Octa-6	Octa-3	Fondaparinux
0.10	0.90	1.23	0.12	0.0207
0.25	>10μM	> 10μM	nd	0.279
0.50	Nd	nd	2,74	3.46

Table 10. Equilibrium dissociation constant Kd (μM) for the interaction of human AT with Octa-5, Octa-6 and Octa-3 oligosaccharides purified from enoxaparin with respect that of the pentasaccharide "Fondaparinux" (ARIXTRA) determined at 25 °C in 0.05 M Hepes, pH 7.4 containing 0.1, 0.25 or 0.5 M NaCl.

Compound	anti-FXa activity (IU/mg)	
	Buffer	Plasma
Enoxaparin	120.0±0.9	104.2±1.3
Fondaparinux	810.1±10.8	761±11.3
Octa-5	51.4±0.8	49.6±0.4
Octa-6	39.6±0.9	39.3±0.8

Table 11. Specific anti-FXa activity measured in human plasma and aqueous buffer solution. Data represent mean ± SEM n=5. Assay calibration was performed against the 2nd international standard for LMWH, code No. 01/608.

6.2.3. NMR characterisation of octasaccharides 5 and 6

The anomeric regions of proton spectra of Octa-5 and Octa-6 are shown in Fig. 37 (for chemical structure of Octa-5 and Octa-6 Fig. 36). Proton and carbon resonances (Table 12 and 13) were assigned using standard homonuclear correlation spectroscopy (COSY) and total correlation spectroscopy (TOCSY) (not shown) and HSQC spectroscopy (Fig. 38 and 39). NOESY experiments were performed to sequentially connect saccharide ring systems (Fig. 40 and Fig. 41). The two octasaccharides, differing in the C2 epimerisation of their 1,6-anydro-hexosamine residues, show significant ^{1}H and ^{13}C chemical shift differences of 1,6-anAS resonances and of the preceding I_S residues (Table 12 and 13). Small differences of proton and carbon chemical shifts found for reducing 1,6-anAS residues with respect to those previously observed for disaccharides, can be ascribed to the different type of uronic acid to which they are linked (Table 12 and Table 13). In fact, the largest differences have been observed for the H4/C4 atoms, which are involved in the linkage with the I residue in octasaccharides and with the 2-O-sulfated 4,5-unsaturated uronic acid (ΔU_{2S}) residues in disaccharides (Table 12 and Table 13) (Mascellani *et al*., 2007). The three bonds proton-proton coupling constants ($^{3}J_{H-H}$)

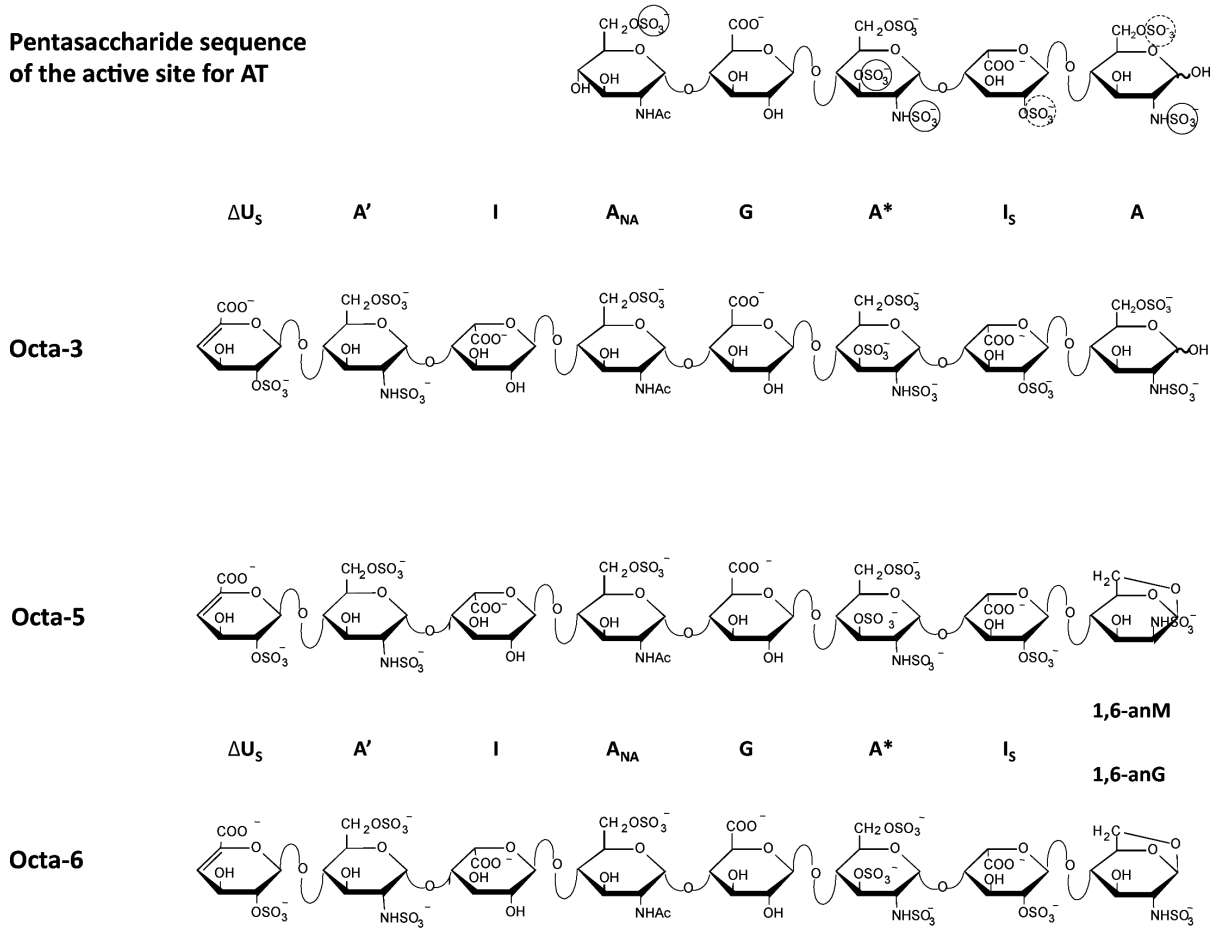

Figure 36. Structure of octasaccharides Octa-5 and Octa-6 in comparison with that of the pentasaccharide sequence of the active site for AT and Octa-3. Groups highlighted in the circles are essential groups for the activation of AT and those highlighted by dashed circles are also important, but not essential contributors to affinity for AT.

of the 1,6-anAS residues, measured on octasaccharides (Table 12), disaccharide and tetrasaccharide models (Table 14) indicate that both these residues assume the $^1C_4$ conformation (Mascellani *et al*., 2007; Cčrny *et al*., 1984).Moreover, the ROESY spectrum indicates a dipolar interaction between H4 and H6a of 1,6-anAS residues, which implies that the 1,6-cycle is located above the pyranose ring (Fig. 42). The conformation of uronate residues within and preceding the $A_{NA}GA^*I_SA$ sequence were analysed by $^3J_{H\text{-}H}$ and NOEs (Table 12 and 15). The measured values of $^3J_{H1\text{-}H2}$ and of $^3J_{H4\text{-}H5}$ of unsaturated uronic acid moiety of both octasaccharides indicated a preferred $^1H_2$ half-chair conformation of such residue, as observed for similar octasaccharides (Guerrini *et al*., 2006). In both octasaccharides, the measured values of $^3J_{H1\text{-}H2}$ and of $^3J_{H4\text{-}H5}$ of sulfated iduronic acid moiety within $A_{NA}GA^*I_SA$ sequence (I_S) are compatible with the presence of both $^1C_4$ and $^2S_0$ forms contributing to the conformational equilibrium of these moieties, similarly to what observed in I_S residues of all previously described octasaccharides in our laboratory (Guerrini *et al*., 2006; Guerrini *et al*., 2008 [b]). However, the $^3J_{H1\text{-}H2}$ and $^3J_{H4\text{-}H5}$ values of I_S measured on Octa-5 ($^3J_{H1\text{-}H2}$ 3.3 Hz and $^3J_{H4\text{-}H5}$ 3.0 Hz) and Octa-6 ($^3J_{H1\text{-}H2}$ 3.1 Hz and $^3J_{H4\text{-}H5}$ 2.9 Hz) spectra are smaller than those measured on Octa-3 ($^3J_{H1\text{-}H2}$ 3.8 Hz and $^3J_{H4\text{-}H5}$ 3.1 Hz) (Guerrini *et al*., 2006), accounting for larger contribution of the $^2S_0$ form to the I_S conformational equilibrium of the latter octasaccharide. This difference suggests that the steric hindrance generated by the reducing bicyclic anhydro ring disfavours the $^2S_0$ form (Table 14 A). In contrast, the nonsulfated iduronic acid residues (I) preceding the $A_{NA}GA^*I_SA$ sequence shows

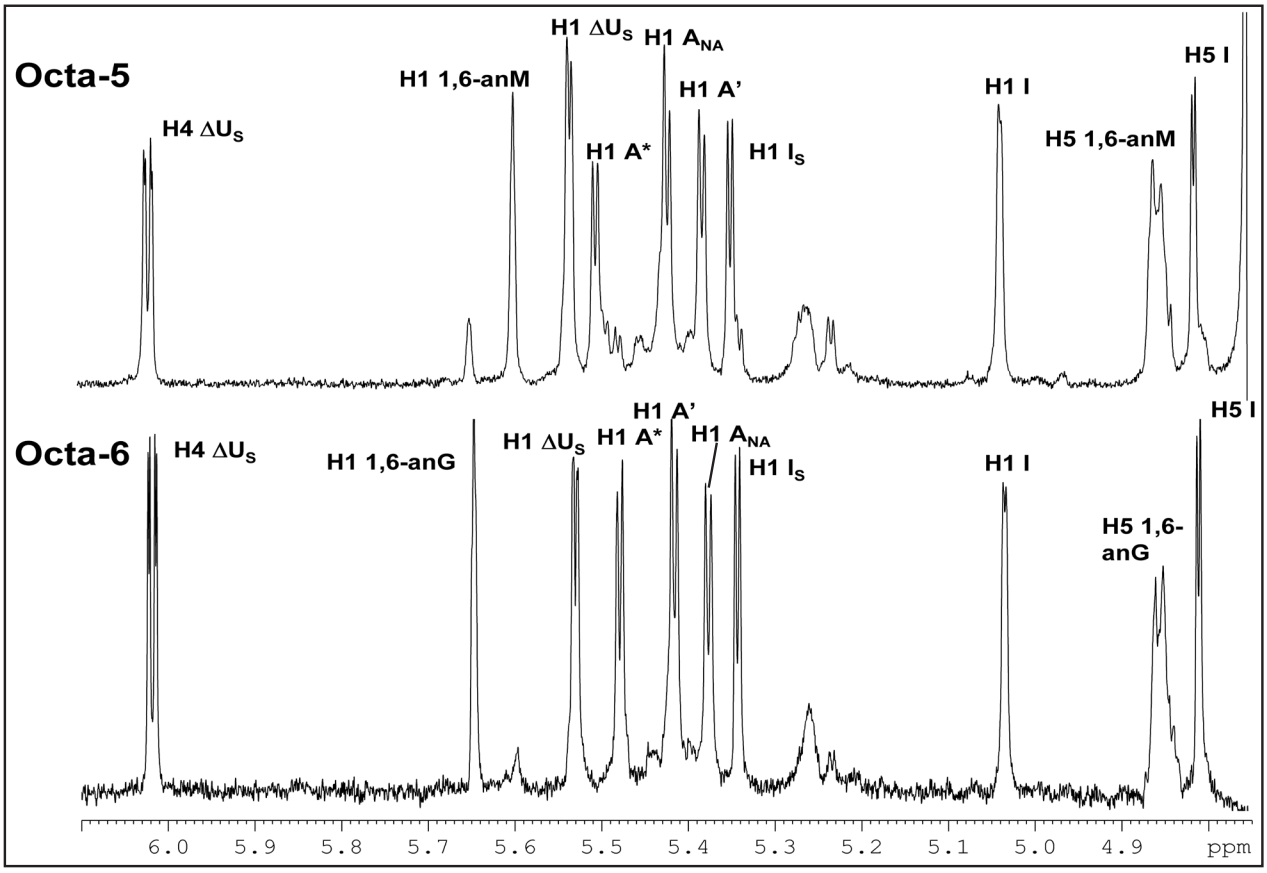

Figure 37. Partial 900 MHz ^{1}H-NMR spectra of Octa-5 and Octa-6.

smaller $^{3}J_{H1\text{-}H2}$ and $^{3}J_{H4\text{-}H5}$ values (Table 12), compatible with a minor contribution of the $^{2}S_{0}$ form. Since the $^{1}C_{4}$ and $^{2}S_{0}$ conformations exhibit distinct H5-H2 distances, the observed NOE value can be considered as marker of the presence of $^{2}S_{0}$ conformation (Ferro *et al*., 1990; Ferro *et al*., 1986). In both octasaccharides, I and I_{S} show detectable H5-H2 NOE, which confirms a contribution of the $^{2}S_{0}$ form to the conformational equilibrium of these residues (Table 15). No significant difference of the conformational equilibrium of I and I_{S} between the two octasaccharides was observed.

A

	ΔU_S	A'	I	A_{NA}	G	A*	I_S	1,6-anM
H1	5.533	5.379	5.038	5.418	4.639	5.503	5.344	5.598
$^3J_{H1-H2}$	*3.1*	*3.9*	*2.3*	*3.8*	*8.2*	*3.5*	*3.3*	*1.9 (1.8)*
H2	4.653	3.311	3.813	3.962	3.414	3.491	4.377	3.503
$^3J_{H2-H3}$								*5.2 (5.4)*
H3	4.353	3.674	4.157	3.798	3.732	4.411	4.237	4.085
$^3J_{H3-H4}$							*3.6*	*(<2)*
H4	6.018	3.866	4.101	3.758	3.82	4.002	4.183	4.011
$^3J_{H4-H5}$	*4.7*		*2.4*				*3.0*	*(1.6)*
H5		4.008	4.811	4.052	3.82	4.169	4.608	4.854
$^3J_{H5-H6a}$								*(0.9)*
$^3J_{H5-H6b}$								*(5.9)*
H6a		4.393		4.367		4.541		4.299
$^3J_{H6a-H6b}$								*(7.8)*
H6b		4.245		4.241		4.284		3.797

B

	ΔU_S	A'	I	A_{NA}	G	A*	I_S	1,6-anG
H1	5.544	5.390	5.046	5.428	4.652	5.491	5.355	5.661
$^3J_{H1-H2}$	*3.0*	*3.8*	*2.1*	*3.9*		*3.5*	*3.1*	*(<2)*
H2	4.666	3.320	3.826	3.970	3.424	3.504	4.407	3.255
$^3J_{H2-H3}$								*(<2)*
H3	4.364	3.686	4.163	3.822	3.744	4.432	4.267	3.948
$^3J_{H3-H4}$								*(<2)*
H4	6.029	3.875	4.112	3.766	3.821	4.003	4.198	3.869
$^3J_{H4-H5}$	*4.7*		*2.4*				*2.9*	*(<2)*
H5		4.010	4.823	4.061	3.821	4.541	4.696	4.868
$^3J_{H5-H6a}$								*(1.2)*
$^3J_{H5-H6b}$								*(5.8)*
H6a		4.402		4.375		4.525		4.261
$^3J_{H6a-H6b}$								*(7.8)*
H6b		4.253		4.253		4.303		3.82

Table 12. Proton chemical shifts (in ppm) and $^3J_{H-H}$ coupling constants (in Hz) of octasaccharide-5 (**A**) and octasaccharide-6 (**B**) residues measured at 30 °C in phosphate buffer 10 mM, pH 7.4 and 0.15 M NaCl with a Bruker Avance 600, 600 MHz. $^3J_{H1-H2}$ couplings in parenthesis were measured on tetra- and disaccharide models having 1,6 anM and 1,6 anG residue at the reducing end respectively (Fig. 43 and Fig. 44; Tab 14)

A

	ΔU_S	A'	I	A_{NA}	G	A*	I_S	1,6anM
C1	100.22	98.48	104.83	99.83	103.86	99.15	102.39	103.76
C2	77.41	60.03	71.40	56.64	76.39	59.45	79.68	55.03
C3	65.67	72.48	70.50	71.40	79.18	79.12	72.57	71.16
C4	108.91	80.97	77.57	80.18	80.1	75.82	78.75	80.83
C5		71.32	71.92	80.1	72.45	72.34	76.48	76.58
C6		69.03		69.03		68.79		67.83

B

	ΔU_S	A'	I	A_{NA}	G	A*	I_S	1,6anG
C1	100.02	98.48	104.83	99.83	103.86	99.29	100.91	104.13
C2	77.41	60.23	71.40	56.64	76.39	59.45	79.12	58.48
C3	65.67	72.48	70.50	71.40	79.18	79.12	72.08	73.02
C4	108.98	80.97	77.67	80.18	80.1	75.82	78.65	79.03
C5		71.58	71.32	72.02	80.1	72.45	72.13	76.24
C6		69.03		69.03		68.79		67.73

Table 13. Carbon chemical shifts (in ppm) of Octa-5 (**A**) and Octa-6 (**B**) measured at 30°C in phosphate buffer 10 mM, pH 7.4 and 0.15 M NaCl with a Bruker Avance 600, 600 MHZ.

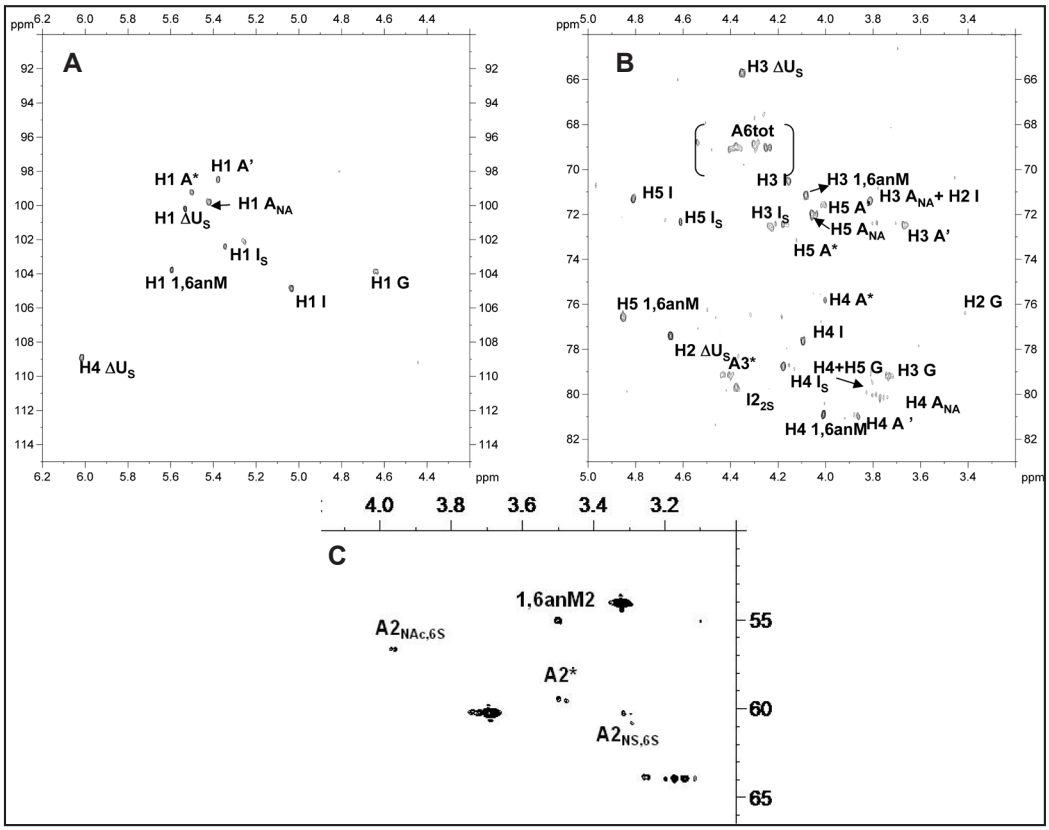

Figure 38. ^{1}H-^{13}C HSQC spectrum of Octa-5 acquired with a Bruker Avance 600, 600 MHz. (**a**) anomeric region, (**b**) ring atoms and (**c**) glucosamine H2/C2 region.

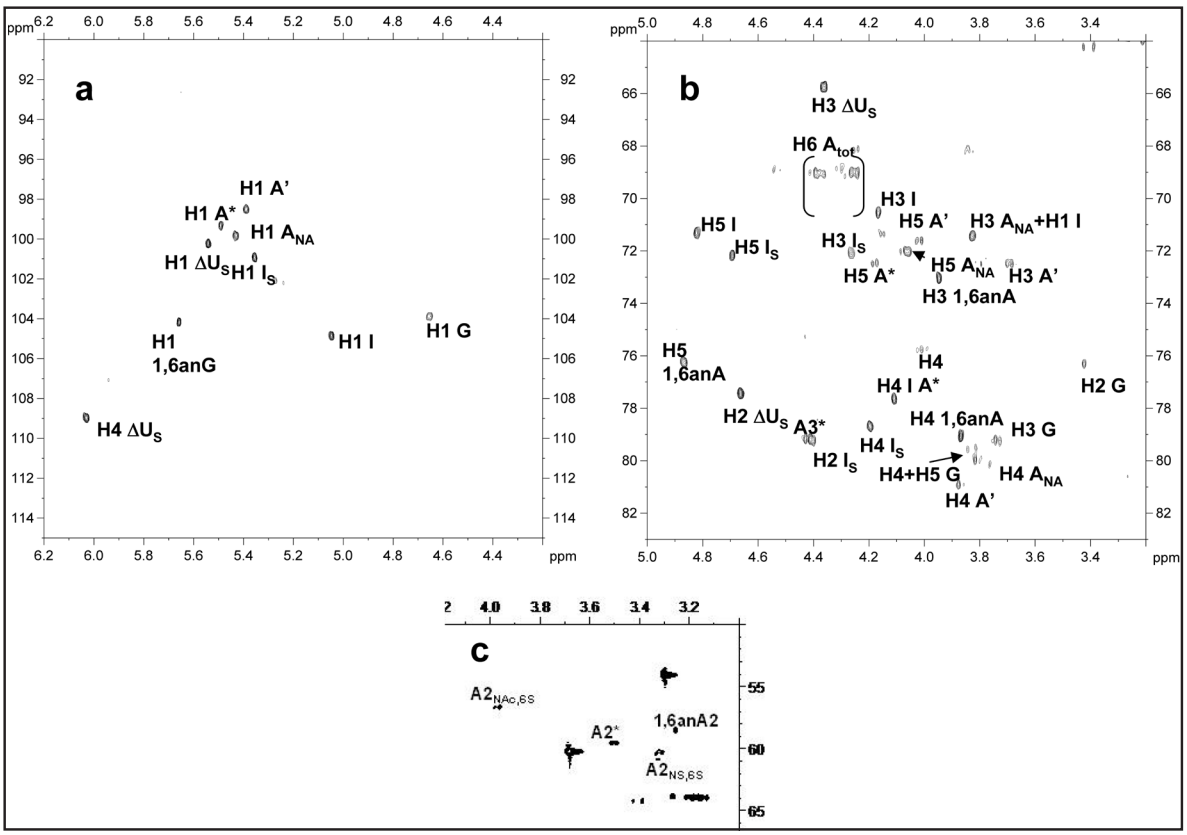

Figure 39. ^{1}H-^{13}C HSQC spectrum of Octa-6 acquired with a Bruker Avance 600, 600 MHz. (**a**) anomeric region, (**b**) ring atoms and (**c**) glucosamine H2/C2 region.

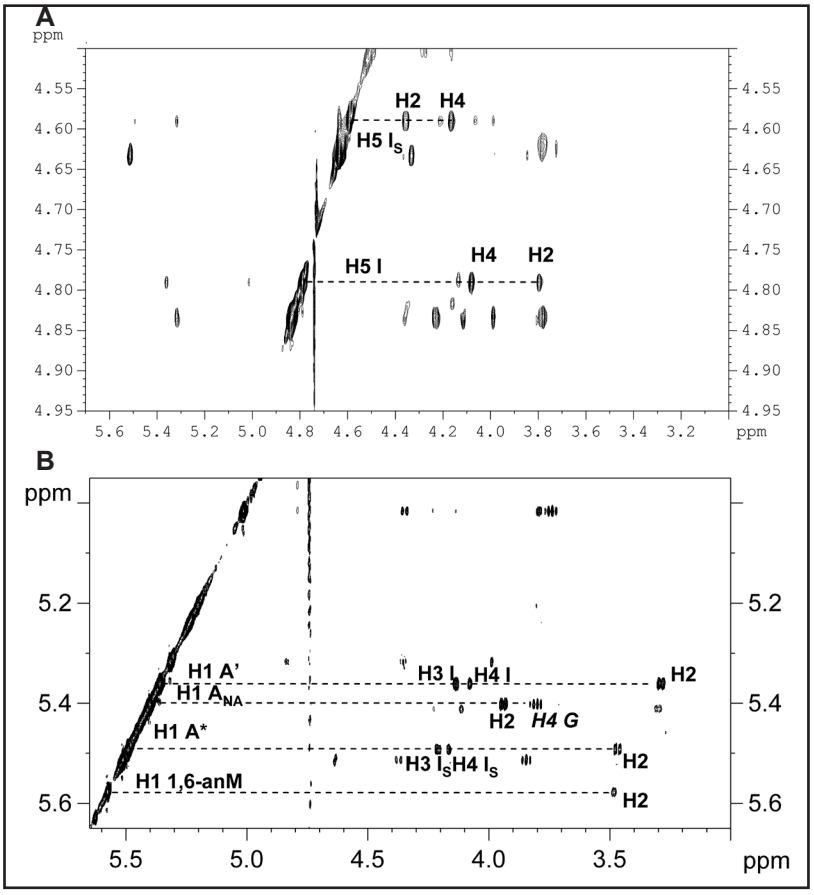

Figure 40. NOESY spectra of Octa-5 acquired with a Bruker Avance 600, 600 MHz. (**A**) H5 I_S region, (**B**) anomeric region.

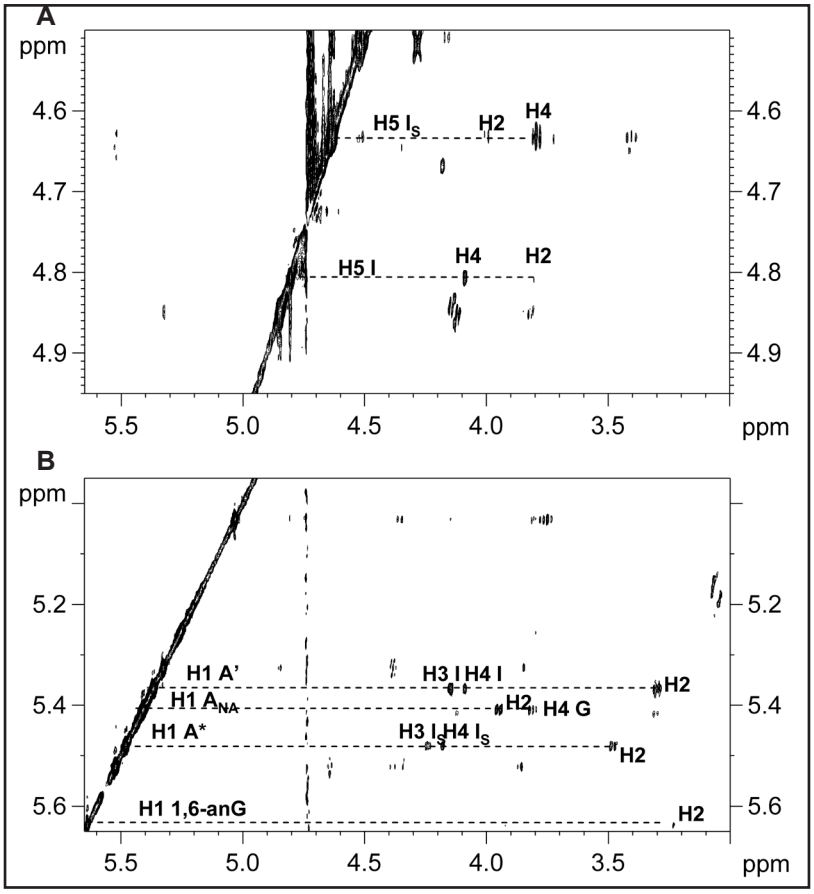

Figure 41. NOESY spectra of Octa-6 acquired with a Bruker Avance 600, 600 MHz. (**A**) H5 I_S region, (**B**) anomeric region.

A

	ΔU_{2S}	A	I_{2S}	1,6 anM_{NS}
H1	**5.513**	**5.383**	**5.531**	**5.568**
$^3J_{H1-H2}$	3.1		2.5	1.8
H2	**4.633**	**3.305**	**4.343**	**3.476**
$^3J_{H2-H3}$			5.0	5.4
H3	**4.316**	**3.666**	**4.253**	**4.049**
$^3J_{H3-H4}$			3.4	~2
H4	**5.922**	**3.844**	**4.103**	**3.988**
$^3J_{H4-H5}$	4.7		2.6	2.8
H5		**4.032**	**4.558**	**4.821**
$^3J_{H5-H6a}$				0.9
$^3J_{H5-H6b}$				5.9
H6a		**4.361**		**4.236**
$^3J_{H6a-H6b}$				7.8
H6b		**4.256**		**3.775**

B

	ΔU_{2S}	1,6 anG_{NS}
H1	**5.636**	**5.636**
$^3J_{H1-H2}$	2.4	~1
H2	**4.652**	**3.197**
$^3J_{H2-H3}$	1.8	1.8
H3	**4.302**	**3.818**
$^3J_{H3-H4}$	4.9	~2
H4	**6.080**	**3.939**
$^3J_{H4-H5}$		nd
H5		**4.843**
$^3J_{H5-H6a}$		1
$^3J_{H5-H6b}$		5.8
H6a		**4.247**
$^3J_{H6a-H6b}$		7.8
H6b		**3.807**

Table 14. Proton chemical shifts (in ppm) and $^3J_{H-H}$ coupling constants (in Hz) of (**A**) ΔU_S-A-I_S-1,6 anM model and (**B**) ΔU_S-1,6 anG model residues. measured at 30 °C in phosphate buffer 10 mM, pH 7.4 and 0.15 M NaCl with a Bruker Avance 600, 600 MHz.

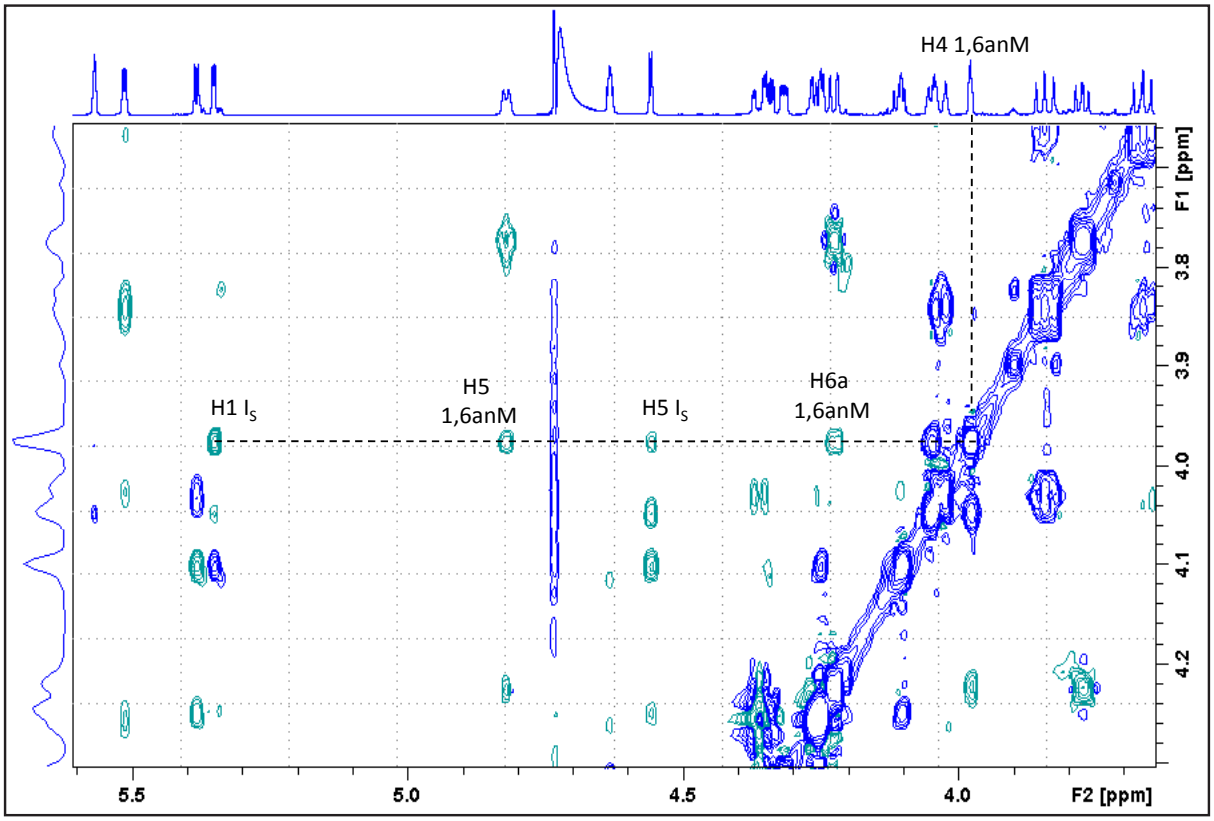

Figure 42. ROESY spectra of ΔU_S-A-I_S-1,6 anM model measured at 30 °C in phosphate buffer 10 mM, pH 7.4 and 0.15 M NaCl with a Bruker Avance 600, 600 MHz.

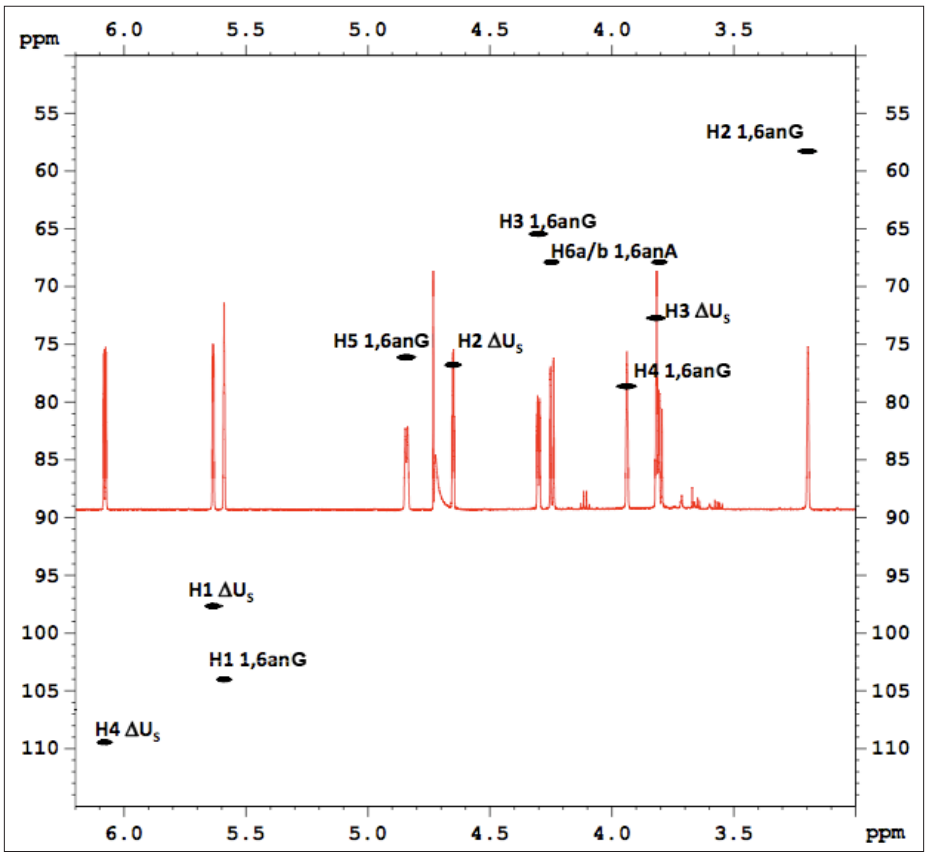

Figure 43. ^{1}H-^{13}C HSQC and ^{1}H spectra superimposition of ΔU_S-1,6 anG model with peak assignment. Spectra were measured at 30 °C in phosphate buffer 10 mM, pH 7.4 and 0.15 M NaCl with a Bruker Avance 600, 600 MHz.

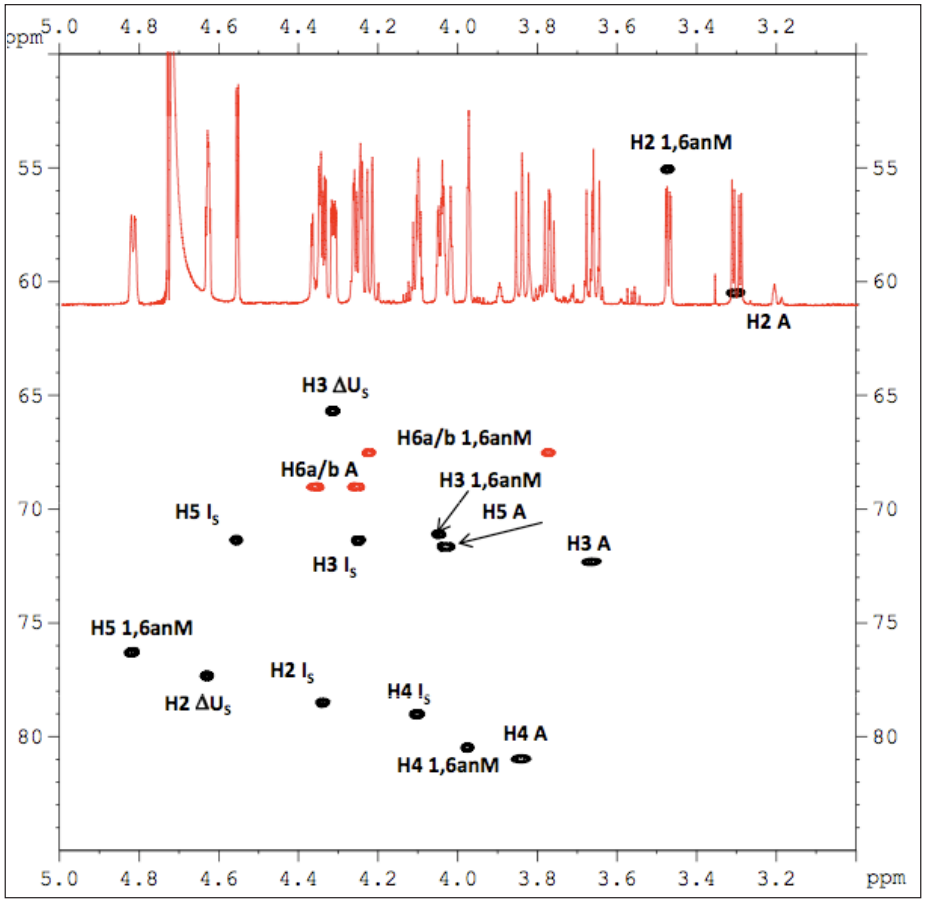

Figure 44. ^{1}H-^{13}C HSQC and ^{1}H spectra superimposition of ΔU_S-A-I_S-1,6 anM model with peak assignment. Spectra were measured at 30 °C in phosphate buffer 10 mM, pH 7.4 and 0.15 M NaCl with a Bruker Avance 600, 600 MHz.

A

		100m	200m	300m
Intra-residue				
H1 ΔU_S	H2	4.7	9.3	18.3 (1.6)
H1 A'	H2	15.2	25.5	37.9 (9.0)
H5 I	H4	15.1	25.2	37.7 (5.9)
	H2	7.0	14.7	23.1 (2.0)
H1 A_{NA}	H2	9.6	16.4	15.6 (7.8)
H1A*	H2	17.7	28.5	44.4 (6.1)
H5 I_S	H4	14.0	26.9	37.5 (5.0)
	H2	11.7	23.0	39.2 (1.6)
H1 1,6-anM	H2	11.8	19.3	30.2 (3.0)
Inter-residue				
H1 ΔU_S	H6 A'	3.0	7.3	12.6 (2.2)
	H6' A'	1.7	4.9	7.8 (0)
	H4 A'	9.2	15.4	24.6 (3.5)
H1 A'	H3 I	16.5	27.3	37.7 (9.4)
	H4 I	9.9	16.3	24.8 (5.2)
H1 I	H4 A_{NA}	16.8	28.7	38.9 (3.4)
H1 A_{NA}	H4 G	17.3	29.7	42.0 (4.5)
H1 A*	H3 I_S	8.7	14.8	23.5 (6.1)
	H4 I_S	5.9	9.2	17.6 (4.4)
H1 I_{2S}	H5 1,6-anM	5.2	10.3	21.8 (2.1)
	H4 1,6-anM	14.0	23.2	39.0 (2.6)

B

		100m	200m	300m
Intra-residue				
H1 ΔU_S	H2	6.4	10.9(nd)	22.1
H1 A'	H2	10.7	19.9(5.4)	32.5
H5 I	H4	11.3	21.5(4.0)	27.7
	H2	5.9	11.1(1.2)	17.5
H1 A_{NA}	H2	9.2	13.6(4.5)	21.6
H1A*	H2	7.8	12.2(4.9)	16.5
H5 I_S	H4	9.7	20.8(3.4)	30.2
	H2	8.9	18.9(1.1)	32.5
H1 1,6-anG	H2	4.0	7.3 (0.8)	12.5
Inter-residue				
H1 ΔU_S	H6 A'	4.4	6.4(1.2)	11.9
	H6' A'	2.5	3.7(nd)	7.4
	H4 A'	8.1	13.8(1.8)	22.6
H1 A'	H3 I	14.0	24.0(6.6)	33.7
	H4 I	8.0	14.4(3.4)	19.8
H1 I	H4 A_{NA}	14.7	27.3(6.3)	41.3
H1 A_{NA}	H4 G	12.3	21.8(2.8)	34.5
H1 A^*	H3 I_S	12.2	28.6(3.5)	38.2
	H4 I_S	9.5	19.4(2.6)	30.1
H1 I_{2S}	H5 1,6-anG	6.4	11.0(1.6)	18.8
	H4 1,6-anG	9.9	16.5(1.5)	29.2

Table 15. Experimental intra- and inter-residues NOESY (in parenthesis) and tr-NOESY values of (**A**) Octa-5 in the complex with AT and (**B**) Octa-6 in the complex with AT at three different mixing times. Spectra were measured at 30 °C in phosphate buffer 10 mM, pH 7.4 and 0.15 M NaCl with a Bruker Avance 600, 600 MHz.

6.2.4. STD experiments

Protocol based on STD NMR spectra is one of the most useful methods to characterise the binding interactions at atomic level of a ligand to a protein target. The experimental protocol is based on the transfer of saturation from the protein to bound ligands that, exchanging into solution between free and bound state, allows to utilize the free ligand signals for detection. The building block of the ligand having the strongest contact to the protein shows the most intense NMR signals, enabling mapping of the ligand's binding epitope (Mayer and Meyer, 2001). The experiments were conducted at the proton frequency of 900 MHz to minimize signals overlapping and at lower sodium chloride concentration (0.15 M instead at 0.5 M) with respect to octasaccharides previously studied (Guerrini *et al*., 2008 [b]). The difference in the conditions setup is due to the lower AT affinity of these octasaccharides. STD spectra of Octa-5/AT and Octa-6/AT complexes in comparison with their corresponding reference spectra are shown in Fig. 45. STD intensities are referred to the most intense STD signal of the spectrum (anomeric protons of A*) and the results are summarised in Table 16.

	H1 ΔU_S	**H4** ΔU_S	**H1** **A'**	**H4** **I**	**H1** **I**	**H1** A_{NA}	**H1** **A***	**H1** I_S	**H4** I_S	***H1*** **1,6-anM/G**	**H3** **1,6-anM/G**	**H2** **1,6-anM/G**	$COCH_3$
Octa-5	61	35	78	70	74	**89**	**100** *(0.25)*	60	66	*39*	48	30	30
Octa-6	55	28	67	59	68	**76**	**100** *(0.23)*	47	nd	*26*	36	nd	28

Table 16. Relative STD intensities at 900 MHz for Octa-5 and Octa-6 bound to AT. The STD NMR values are normalized using the H1 of N-sulfo-3,6-disulfated glucosamine (A*) as a reference (100%). The corresponding fractional STD effect values of A^* are shown in parenthesis (Mayer and Meyer, 2001).

For both octasaccharides the largest STD effects were observed for the anomeric signal of A^* and of the A_{NA} residues within the pentasaccharide sequence (highlighted in bold in Table 16). Weak STD signals were observed for nonreducing ΔU_S residues of all octasaccharides, indicating that this residue is not located in the proximity of the binding region, whereas medium intensity STD signals were observed for the anomeric signal of A' and both H4 and H1 of I, also belonging from the nonreducing extension of the molecule. In contrast of what observed for previously studied octasaccharides (Guerrini *et al*., 2008 [b]), weak STD signals were observed among residues of the $A_{NA}GA^*I_SA$ moiety in both Octa-5 and Octa-6. In fact, whereas the reducing -I_S-A disaccharide unit of $A_{NA}GA^*I_SA$ sequence, similarly to the other pentasaccharide moieties, gave strong STD signals in all previously studied octasaccharides (i.e. Octa-3 and Octa-4, Guerrini *et al*., 2008 [b]), the I_S-1,6-anM and I_S-1,6-anG disaccharides of Octa-5 and Octa-6 show weak STD signals (Table 16). Such an observation is compatible with a minor involvement of this part of the pentasaccharide sequence to the binding with AT. In addition, both octasaccharides shown a small STD effect for the N-acetyl signal at 2.08 ppm, indicating that this group is oriented toward the opposite side of the AT surface, as observed in all previously studied octasaccharides (Guerrini *et al*., 2008 [b]). No particular differences between STD profiles of Octa-5 and Octa-6 were observed. The overall reduction of the STD intensities (about 15-20 %) observed for Octa-6 with respect to Octa-5 is due to a slightly different protein-ligand ratio of the two octasaccharide/AT complexes.

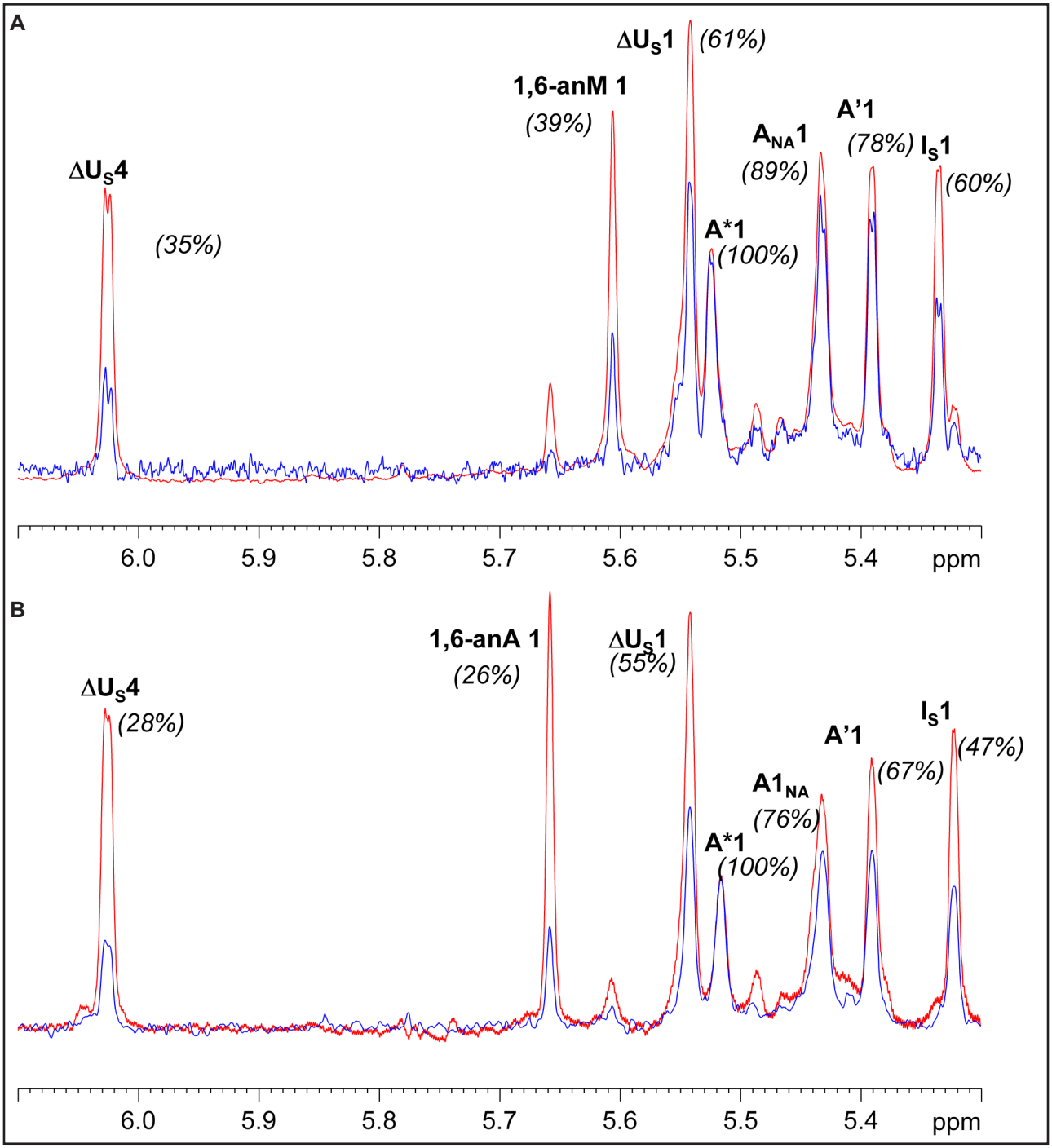

Figure 45. Anomeric region STD spectra of Octa-5/AT (a) and Octa-6/AT (b) complexes measured at 40:1. Reference and STD spectra are shown in red and blue, respectively. Spectra were measured at 30 °C in phosphate buffer 10 mM, pH 7.4 and 0.15 M NaCl with a Bruker Avance 900, 900 MHz.

6.2.5. Conformations of octasaccharide/AT complexes

The increase of the proton linewidth signals observed in the presence of AT, together with a very small variation of chemical shifts, is consistent with an equilibrium regulated by the intermediate dynamic exchange between the free and bound state. The proton NMR spectra of the Octa-5/AT and Octa-6/AT complexes (10:1 molar ratio), in comparison with the corresponding reference spectra, are shown in Fig. 46 and Fig. 47, respectively. In the presence of AT, anomeric signal linewidths (H1) of

A_{NA} and A^* increased considerably in both octasaccharides from 5-7 Hz to 15-18 Hz (A_{NA}) and 17-22 Hz (A^*) respectively, indicating a strong involvement of the corresponding residues in the binding. On the contrary, a smaller increase of linewidths of H4 of unsaturated uronate and H1 of 1,6-anAS residues (from about 3-4 Hz to 5-6 Hz) was observed for both octasaccharides, in agreement with the higher degree of freedom of these residues and their minor involvement in AT binding. Since cross-relaxation rates differ considerably between the free and bound state, there is a great variation in the cross-peak intensities among two-dimensional NOESY (free state) and transferred-NOESY (bound state) (Table 15). The role of the conformational equilibrium of iduronate residues in the binding was also investigated by analysing intra-residue tr-NOE effects. NMR is particularly sensitive to the presence and relative proportion of conformers. In fact, an H2-H5 NOE was exclusively found in the $^2S_0$ conformer and not observed in the $^1C_4$ form (Ferro *et al*., 1990; Ferro *et al*., 1986). Similarly to what observed for the previously studied octasaccharides, the H5-H2/H5-H4 NOE ratio of the 2-O-sulfated iduronate residue within the $A_{NA}GA^*I_SA$ sequence of both Octa-5 and Octa-6 significantly increases in the presence of AT (from 0.3 to 1), indicating that the conformation of this residue is driven toward the pure $^2S_0$ form by the protein binding. On the contrary, a smaller enhancement of H5-H2/H5-H4 NOE ratio (from 0.33 to 0.61) was observed for the I residue, suggesting that in this case AT does not induce a complete $^2S_0$ conformer selection. This result partially contrasts to what observed previously for Octa-3 (Guerrini *et al*., 2006), in which the conformation of the corresponding I residue, present almost exclusively in the $^1C_4$ form in free solution, was completely reversed to $^2S_0$ form in the presence of AT.

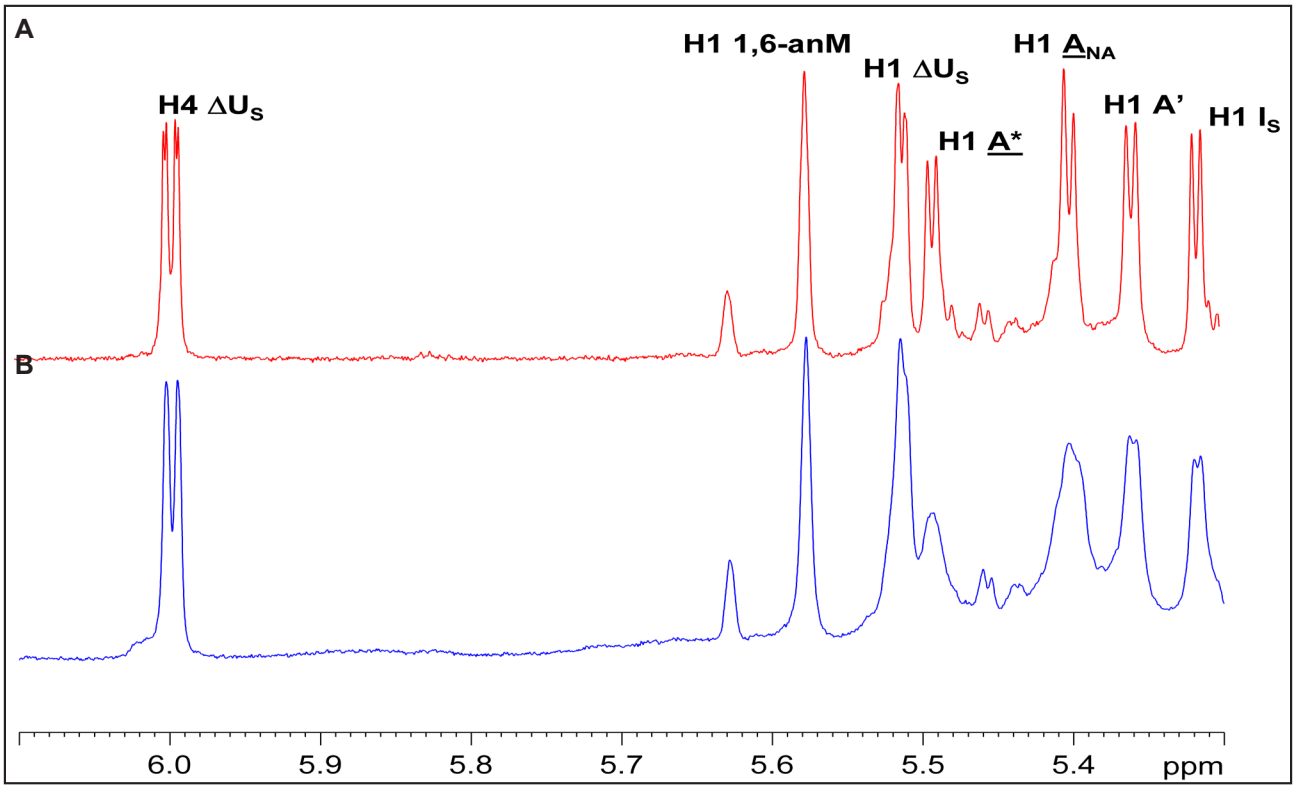

Figure 46. Anomeric region of Octa-5 proton spectra with (**B**) and without AT (**A**) (ligand:AT molar ratio 10:1). Spectra were measured at 30 °C in phosphate buffer 10 mM, pH 7.4 and 0.15 M NaCl with a Bruker Avance 600, 600 MHz.

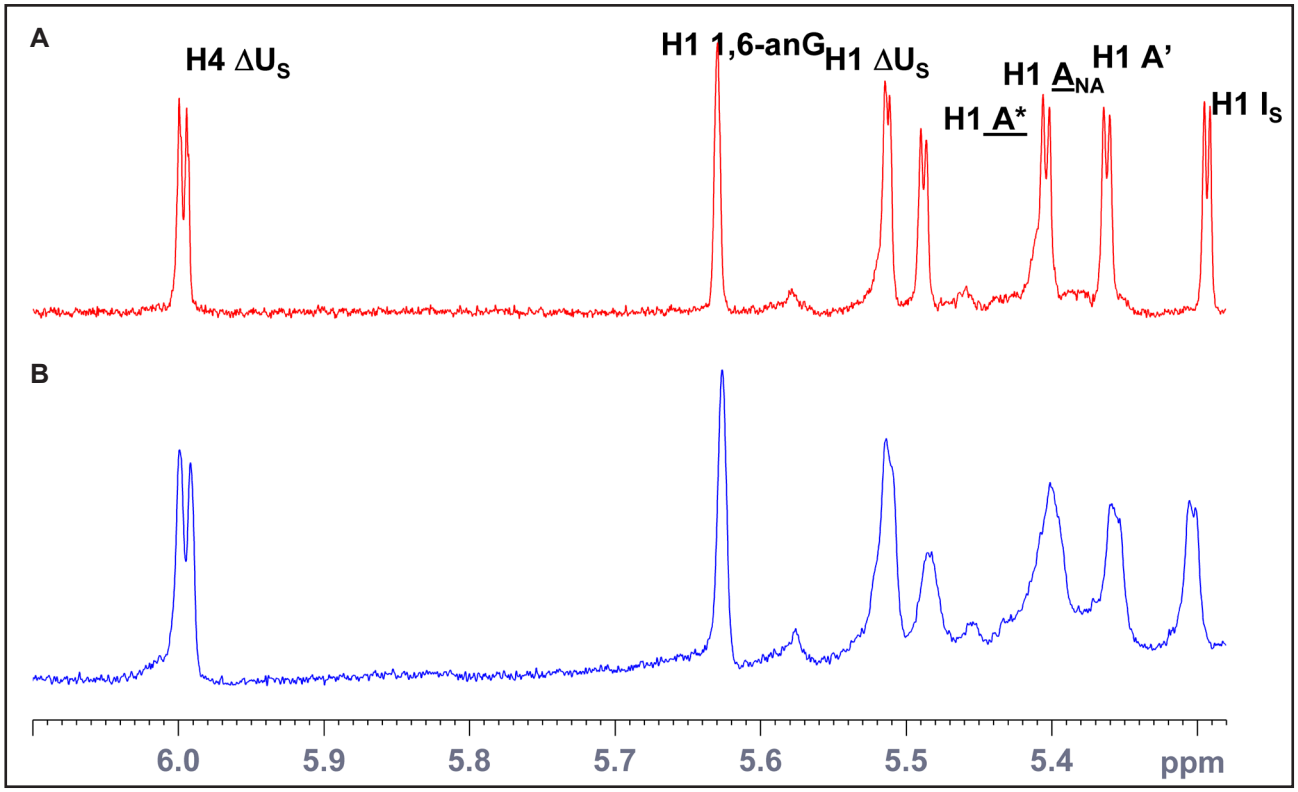

Figure 47. Anomeric region of Octa-6 proton spectra with (**B**) and without AT (**A**) (ligand:AT molar ratio 10:1). Spectra were measured at 30 °C in phosphate buffer 10 mM, pH 7.4 and 0.15 M NaCl with a Bruker Avance 600, 600 MHz.

The observed difference with unmodified octasaccharides could be attributed to the steric hindrance generated by the 1,6 anhydro bicyclic ring which disfavour the $^{2}S_{0}$ form. A qualitative analysis of the inter-residue tr-NOEs, in comparison with NOEs measured in the absence of AT, indicates that no substantial difference in the glycosidic geometries occurred during the binding (Table 15). Molecular dynamics and docking procedures (see experimental section) are used to build models of Octa-5/AT and Octa-6/AT complexes. Docking procedure was repeated also on Octa-3 under the same conditions. Docked structures of octasaccharide/AT complexes having $A_{NA}GA^{*}I_{S}A$ at the same position than observed in crystal structure, together with clusters having shifted structures along the D-helix of AT, were obtained. To estimate the ability of these models to reproduce the average geometries of the octasaccharide/AT complexes indicated by available NMR data, the magnitudes of theoretical tr-NOEs were calculated using the CORCEMA program (Mayer and Meyer, 2001). The agreement between the theoretical and experimental tr-NOEs was estimated by calculating R factors (see Materials and Methods 4.3.3.). More specifically, to evaluate the ability of our models to identify the position of octasaccharide residues along the protein binding region regardless their internal conformation, tr-NOEs of H1-H2 protons cross-relaxing within aminosugar residues were analysed. Complexes having $A_{NA}GA^{*}I_{S}A$ at the same position observed in the structure of pentasacchairide-AT co-crystals (Jin *et al*., 1997), showed a good fitting between theoretical and experimental data, whereas those having shifted structures along the D-helix of AT gave significantly higher R-factors (Table 17). Moreover, in disagreement with STD results, these shifted models present also the octasaccharide rotated along a direction parallel to the D-helix, with the N-acetyl group oriented toward the opposite side of the AT surface (Table 17 and Fig. 48). Docking output models of Octa-5, Octa-6 and Octa-3 that satisfy tr-NOE data take similar positions in the AT binding site (Fig. 49 and Fig. 50). In these assemblies distances between the pentasaccharide moiety and AT are on the average shorter than those between

the nonreducing ΔU_S-A'-I- moiety and the protein binding region, in other words nonreducing moieties are farest than reducing one (Fig. 51). However, whereas distances between the majority of sugar residues of Octa-5 and Octa-6 and the AT interacting aminoacids are similar to those measured for Octa-3, the terminal 1,6-anG/M residues are more distant from Arg^{46} and Arg^{47} than the terminal N-sulfo-glucosamine-6-O-sulfate residue of Octa-3.

	A'	A_{NA}	A*	1,6-anM/G
Octa-3	**0.21(0)**	**0.18(3)**	**0.05(3)**	**0.13(5)**
Octa-5	**0.29(0)**	**0.27(2)**	**0.21(4)**	**0.08(1)**
Octa-5 shifted	**0.28**	0.40	**0.15**	**0.07**
Octa-5 inverted	0.40	0.39	0.50	0.31
Octa-6	**0.22(1)**	**0.13(1)**	**0.31(2)**	**0.04(1)**

Table 17. R-factor average values calculated by fitting between experimental and theoretical tr-NOEs of H1-H2 protons cross-relaxing within hexosamine residues. Values were averaged for different AT-octasaccharide complexes obtained from docking and cluster analysis. Each complex is represented by an ensemble of three or four geometries with an RMSD distance less than 2Å. In brackets the error at the last decimal digit is given by a standard deviation measurement. R-factors calculated on a shifted (Octa-5 shifted) and a inverted (Octa-5 inverted) AT/octasaccharide complexes were also reported. Thin fonts indicate poor fitting with the experimental data.

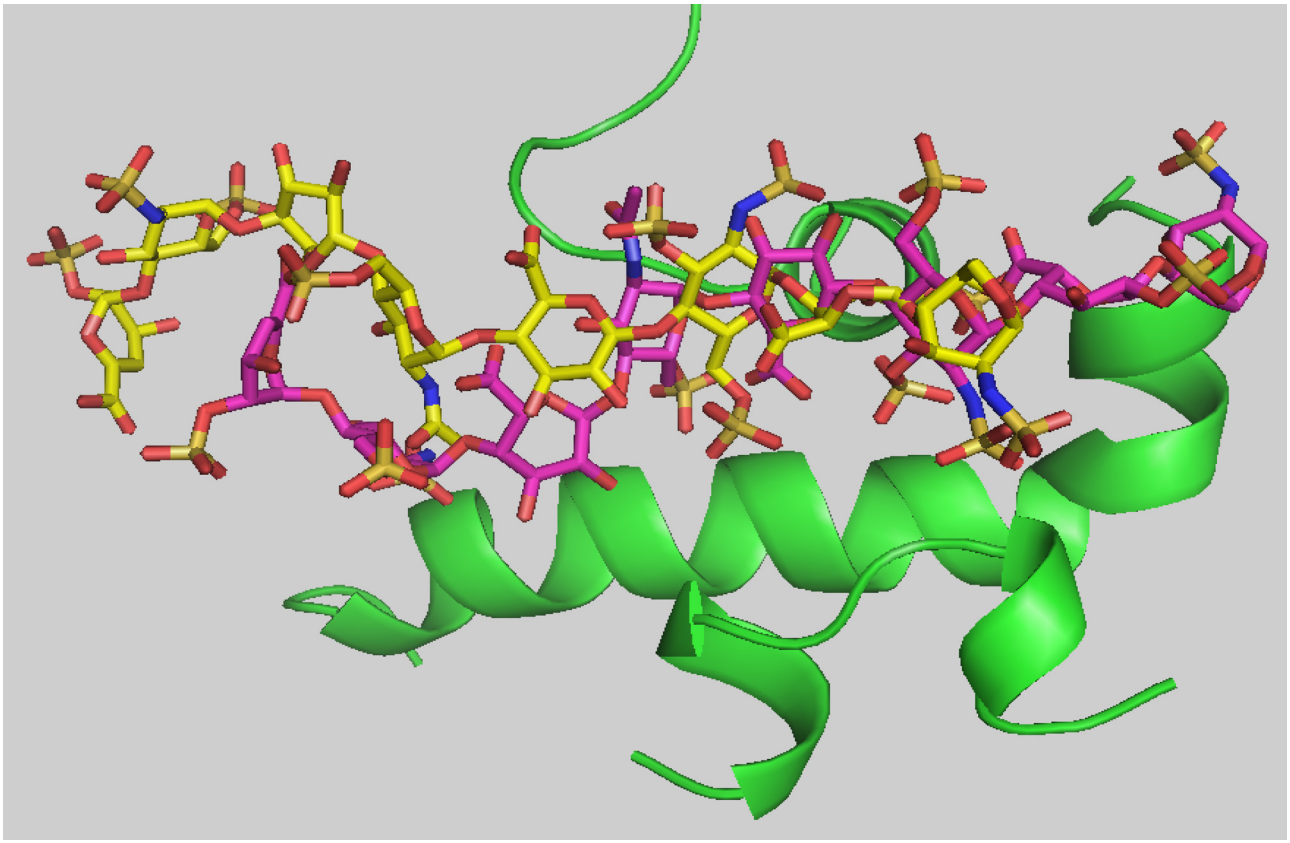

Figure 48. Octa-5/AT complex model obtained by rigid docking simulation, shifted along the AT binding site of about a disaccharide unit length (yellow) with respect to the same molecule having the $A_{NA}GA^*I_SA$ sequence in the original position (pink). The AT binding region is shown in green.

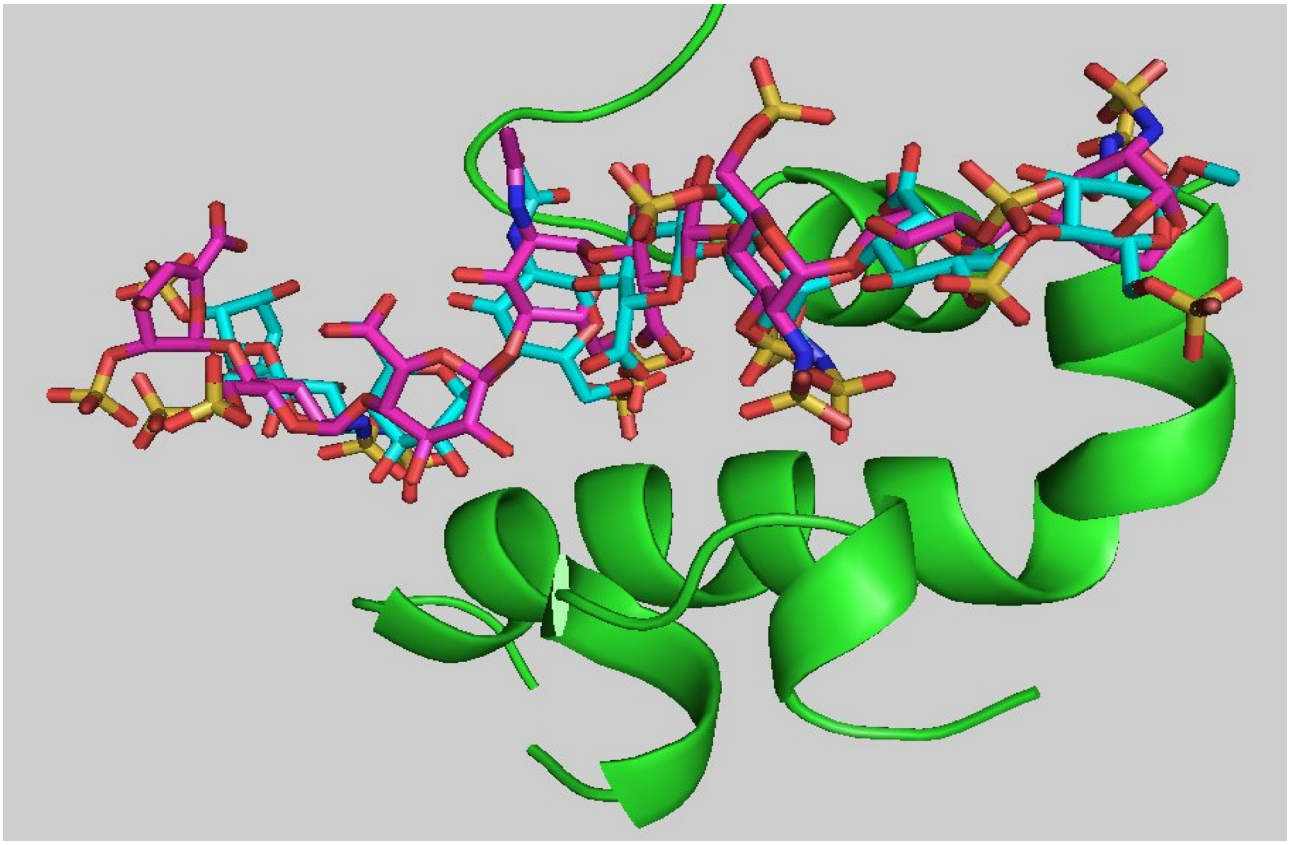

Figure 49. Superimposition of Octa-5/AT (pink) and Octa-3/AT (magenta) model complexes obtained by rigid docking simulation. The AT binding region is shown in green.

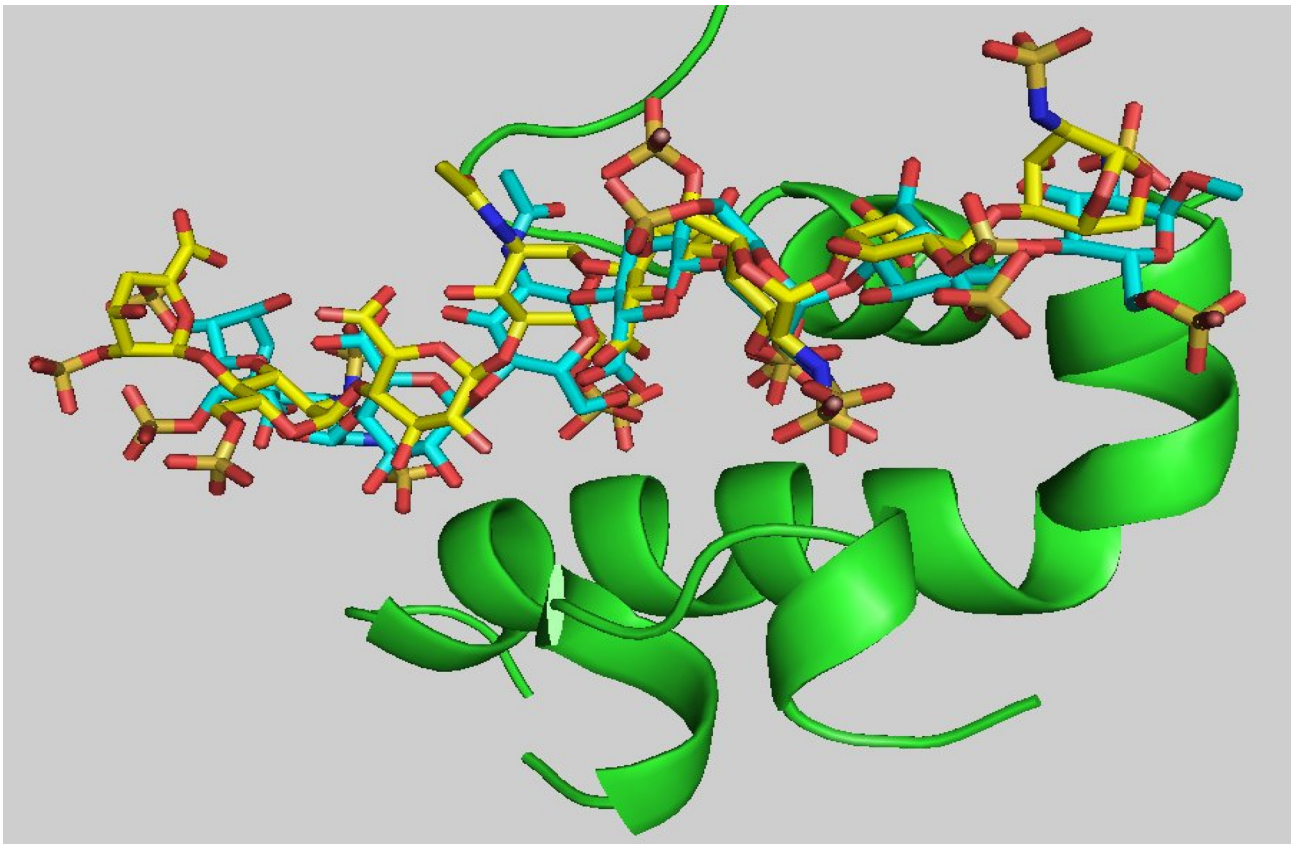

Figure 50. Superimposition of Octa-6/AT (yellow) and Octa-3/AT (magenta) model complexes obtained by rigid docking simulation. The AT binding region is shown in green.

Moreover, the average distance between the N-sulfo group of 1,6-anhydro residues and AT is significantly larger for 1,6-anG than the 1,6-anM (about 0.75 nm versus 0.5 nm), in agreement with the lower affinity observed for Octa-6 (Fig. 51; Table 10). On the contrary, the terminal unmodified residue of Octa-3 shows an average distance from AT comparable to that of the other $A_{NA}GA^{*}I_{S}A$ residues, indicating its stronger involvement in the binding. These results are in a good agreement with the observed STD effects experimentally determined on proton signals of the same residues (Table 16).

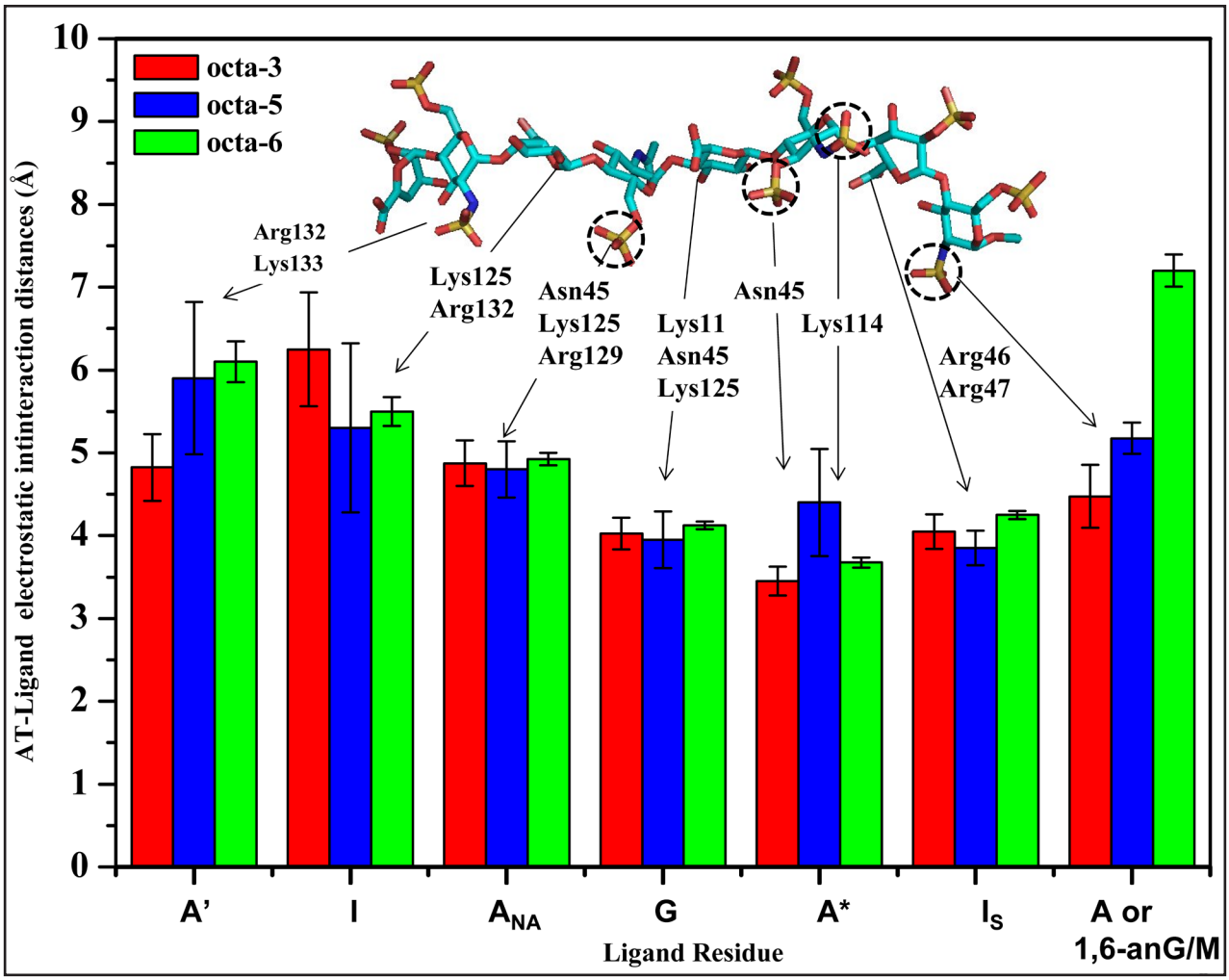

Figure 51. Schematic representation of the individual side chain interactions showing average contact distances between octasaccharide residues and AT (Octa-3, Octa-5 and Octa-6 red, blue and green bars, respectively). Each distance is averaged on two or three ligand–AT contacts on the ensemble of four docking ligand-AT complex generated structures, selected from those that better agree with experimental data (trNOESY). Distance standard deviation is shown on the top of each column. Distances are taken between the heteroatom of the monosaccharide interacting group (-SO_3, -COO or CH-OH) and those of nearest AT aminoacids. Octa-3 structure is shown at the top of the figure with sulfated groups in the $A_{NA}GA^{*}I_{S}A$ sequence essential for AT binding highlighted by dashed circles.

6.2.6. Discussion

In the present work, two novel AT-binding octasaccharides containing an 1,6-anM and 1,6-anG residue, respectively, at the reducing end (Octa-5 and Octa-6) have been isolated from enoxaparin. Even if the presence of terminal 1,6-anhydro rings have been previously described as a major structural fingerprint of enoxaparin (Guerrini *et al*., 2007; Mourier and Viskov, 2005), the present octasaccharides have the peculiarity to bear an 1,6-anM or 1,6-anG instead of the terminal N-sulfo,6-O-sulfoglucosamine of the active pentasaccharide $A_{NA}GA^*I_SA$. The AT binding properties of both Octa-5 and Octa-6 were measured and compared with those previously described for Octa-3 that contains the unmodified pentasaccharide at the reducing end. Fluorescence titrations indicated that the affinity for AT of these octasaccharides is characterised by equilibrium dissociation constants about 10 and 50 fold lower than those measured for Octa-3 and the synthetic pentasaccharide Fondaparinux, respectively (Table 11). Such an evidence confirms that the lack of 6-O sulfo group of the terminal glucosamine residue A of the pentasaccharide sequence $A_{NA}GA^*I_SA$, together with the unusual conformation of the residue bearing the 1,6-anhydro cycle, results in weaker binding to AT. On the other hand, the decreasing in affinity for AT of Octa-5 and Octa-6 with respect to Fondaparinux was much larger than that observed just by the removal of 6-O-sulfo group of the terminal reducing glucosamine of the pentasaccharide (van Boeckel and Petitou, 1993). Although affinity values obtained from the present and previous studies are not directly comparable due to somewhat different experimental conditions, the relatively larger difference found suggested that also the bicyclic structure of the 1,6-anhydro residues might sterically interfere on the interaction with AT. Reduction in AT-binding affinity is correlated with a lower anti-FXa activity of Octa-5 and Octa-6 compared to both Fondaparinux and enoxaparin (Table 11). Importantly, enoxaparin shows a slight decrease in anti-FXa activity (13 %) in human plasma compared to measurement in aqueous buffer solution which could be due to unspecific protein binding (i.e., albumin) of some AT binding components. In contrast, the activities of Octa-5 and Octa-6 are almost the same in plasma and in aqueous solution, suggesting a specific interaction of both compounds with AT (Table 10). This was also confirmed from STD and docking results, showing that the closest contacts with AT involve the residues of the octasaccharide belonging to the sequence $A_{NA}GA^*I_SA$ and correspond to the $A_{NA}GA^*$- moiety for both Octa-5 and Octa-6. On the contrary of what observed for Octa-3 (Guerrini *et al*., 2008 [b]), weaker STD signals for the terminal $-I_S$-1,6-anM/G disaccharides with respect to those of the $-AGA^*$- moiety were observed, indicating a larger distance of these residues from AT. Moreover, only model outputs having the $A_{NA}GA^*I_SA$ sequence in the same position adopted in the pentasaccharide/AT complex can interpret both STD and tr-NOE data (Linhardt and Gunay, 1999). Although our models are not sufficiently accurate to define the complex at atomic level precision due to the lack of suitable molecular dynamic force field description able to satisfy conformational behaviour of highly charged molecules (Forster and Mulloy, 2006), they clearly show that the $-A_{NA}$- G-A*-I_S sequence of the pentasaccharide moiety is in closer contact with AT than the trisaccharide moiety ΔU_S-A'-I- at the nonreducing end and the terminal 1,6an-AS residues at the reducing end (Fig. 51). Beside the larger average distances between AT aminoacids and terminal 1,6-anM/G residue measured for both Octa-5 and Octa-6 with respect to Octa-3, significant differences were found between the two isomers. Octa-6 shows higher averaged distance between the N-SO_3 group of its terminal residue and both Arg^{46} and Arg^{47} with respect to Octa-5 (Fig. 51), paralleling the lower affinity to AT measured for this octasaccharide. The single interaction of the N-SO_3 group in terminal 1,6-anhydro residues is expected to reduce the strength of ionic interac-

tions between the reducing part of the pentasaccharide and AT with respect to unmodified N,6-O-sulfated glucosamine. However, even if the absence of the 6-O-sulfo group in the terminal A residue reduces the affinity to AT (van Boeckel and Petitou, 1993), no ionic interactions have been observed between this group and positively charged aminoacid of AT (Petitou *et al*., 2004; van Boeckel and Petitou, 1993). The observed higher affinity of $A_{NA}GA^*I_SA$ containing oligosaccharides, due also to the contribution of the 6-O-sulfo group on the terminal A residue, can be explained by the increasing of population of the skew $^2S_0$ conformer of the neighbour I_S residue (Ferro *et al*., 1990), as indicated by different $^3J_{H\text{-}H}$ values of I_S measured on Octa-3 with respect to those of Octa-5 and Octa-6 (Guerrini *et al*., 2006). In fact, the higher affinity to AT of an heparin pentasaccharide, bearing an extra sulfate group at C3 of the terminal A residue, was proposed to be the consequence of a high population (about 90%) of the $^2S_0$ conformer (Petitou *et al*., 1991). Moreover, the present results suggest that the manno configuration of the 1,6-anhydro residues promotes a better interaction with AT with respect to the gluco form due to its favourite position of the N-SO_3 group (Fig. 51). Despite their modest anti FXa activity, those 1,6 anhydro modified oligosaccharides display a specific antithrombotic activity which cannot be neglected in the overall biological profile of the LMWH complex mixture. From a practical point of view, since the depolymerisation condition used to prepare enoxaparin strongly affect the content of 1,6-anhydro residues, as well as the relative contents of their manno and gluco epimers, control of the overall composition and activity requires an accurate optimisation of the manufacturing procedures. A more detailed understanding of the role of structural variations on AT binding properties of heparin oligosaccharides may help in the synthesis of ligand analogues and in the design of new LMWHs with an appropriate structure to ensure high affinity to AT. However, structural refinement of the obtained structures by means of methods such as full molecular dynamics simulations or ab-initio calculations is also necessary to fully interpret experimental data.

6.3. Role of glycosaminoglicans in Alzheimer progression

6.3.1. Summary

Proteoglycans are associated with all the types of amyloid deposits in the human body. In particular HS chains, have been reported to be involved in the pathogenesis of Alzheimer's disease, including the genesis of senile plaques, cerebrovascular amyloids and neurofribrillary tangles. Despite the large body of data supporting the importance of HS in amyloidogenesis, little is known about the precise mechanism by which HS promotes amyloid formation and the effect that this GAG has on the various phases of the aggregation process and on the overall aggregation pathway. It has been demonstrated that *in vitro* enoxaparin, a LMWH, is as capable as heparin of attenuating the neurotoxicity and proinflammatory activity of $A\beta_{1\text{-}42}$ (Bergamaschini *et al*., 2002). *In vivo* prophylactic treatment with a clinically relevant dose of enoxaparin reduces reactive astrocytosis and the deposition and total brain concentration of amyloid peptides in two different mouse models (Dudas *et al*., 2002; Bergamaschini *et al*., 2004). Detailed characterisation of HS-oligomers/protein interactions at the molecular level may provide useful information to the generation of drugs against amyloid diseases. In order to unveil the molecular basis of $A\beta_{1\text{-}40}$ -GAG interactions, we followed $A\beta_{1\text{-}40}$ aggregation with and without different heparin oligosaccharides; to identify possible inhibitors of HS, we have undertaken a study on the influence of chain length and detailed structure of heparin oligosaccharides on the aggregation of amyloid peptides. To this purpose, the interaction with amyloid peptides with a number of heparin oligosaccharides systematically differing in molecular size are being investigated using an advanced DLS approache. DLS methods permit to determine the size of molecular aggregates in solution.

6.3.2. Hep, LMWH and derived oligosaccharides preparation and characterisation

Prior to the interaction investigations, a complete NMR characterisation of the GAGs involved was performed. LMWHs were previously characterised by 2D NMR in our laboratory (Bisio *et al*., 2009; for a complete 1D/2D NMR characterisation of UFH and LMWHs see Fig. 52, Fig. 53, Fig. 54 and Fig. 55) and by size exclusion chromatography (SEC, Fig. 56), underlining some interesting features: enoxaparin has the lowest MW and is mainly composed of oligosaccharides with a degree of polymerisation (dp) between 6 and 12; more than the 50 % of tinzaparin is composed of oligosaccharides > dp 18; dalteparin lacks of oligosaccharides < dp 6 with a molecular weight (MW) intermediate between enoxaparin and tinzaparin (Fig. 53). HP-SEC/ TDA analysis shown that: enoxaparin is composed of the lowest percentage of oligosaccharides with MW > 8000 Da (10 %), followed by dalteparin (30 %) and tinzaparin has the highest content of big oligosaccharides compare to the other two LMWHs (46 %) (Fig. 56). In order to obtain oligosaccharides well characterised, one batch of commercial unfractionated heparin (UFH) was depolymerised through deaminative reduction treatment and fractionated by SEC (leading to the purification of oligosaccharides with 2,5 anM_{6S} as reducing end); one batch of commercial LMWH (Tinzaparin) was fractionated by SEC (obtaining oligosaccharides with homogeneous size) and obtaining a complete oligosaccharides panel from disaccharide to dodecasaccharide. Hexasaccharide [(T) dp 6] and decasaccharide [(T) dp 10] derived from tinzaparin, were characterised by 1D and 2D NMR, disaccharide derived from UFH depolymerisation (Hep dp 2) were characterised by 1D and 2D NMR spectroscopy: 1D/2D assignments for

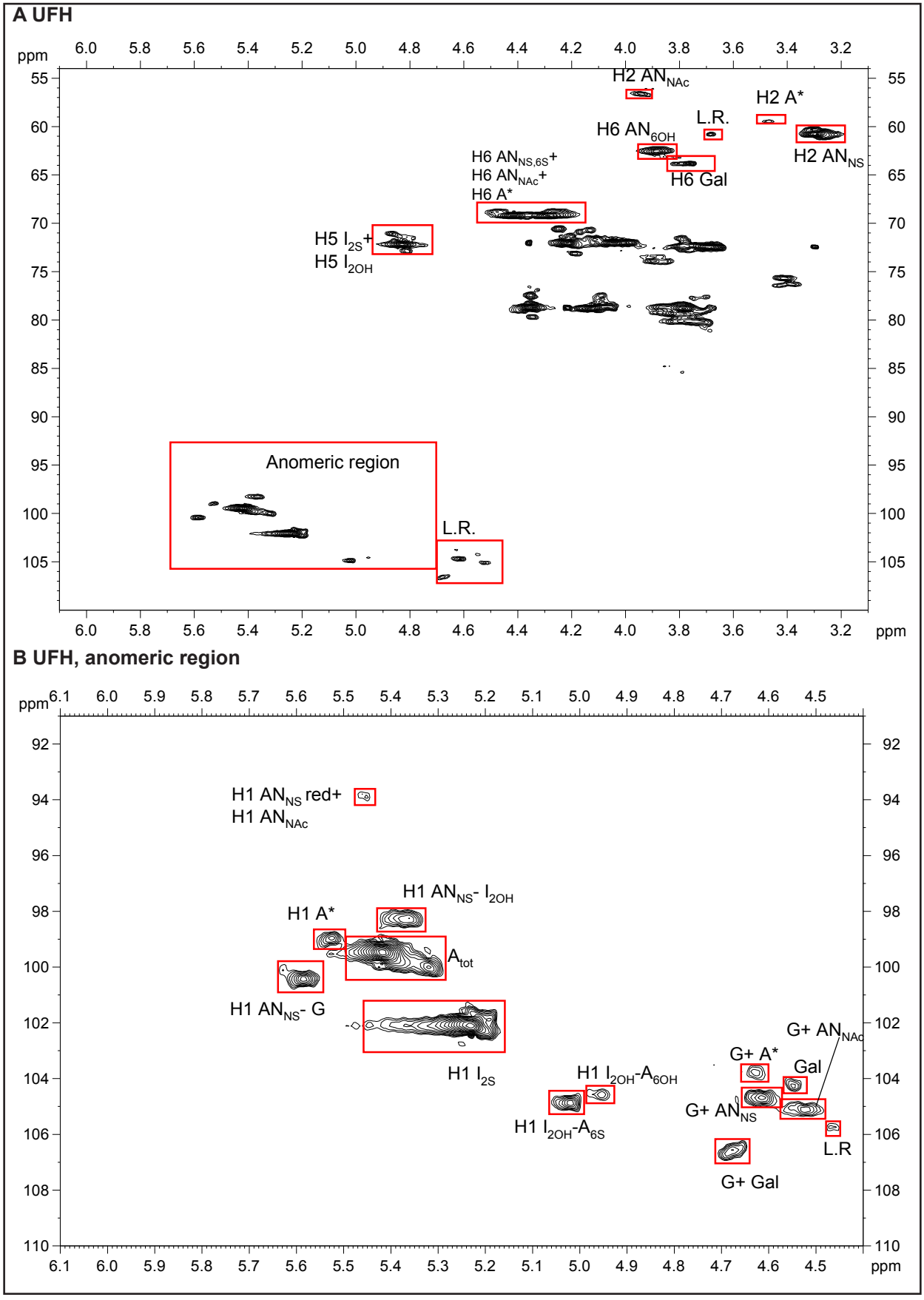

Figure 52. Full assignment of HSQC spectra of UFH. **A** and **B** panels show UFH HSQC full window and anomeric region spectra, respectively; UFH (40 mg/mL in D_2O) spectra were acquired with Bruker Avance 500, 500 MHz spectrometer at 35 °C; L.R= linkage region. H1= H atom links to saccharidic C1 atom; H2= H atom links to saccharidic C2 atom; H3= H atom links to saccharidic C_3 atom; H4= H atom links to saccharidic C4 atom; H5= H atom links to saccharidic C5 atom; H6= H atom links to saccharidic C_6 atom.

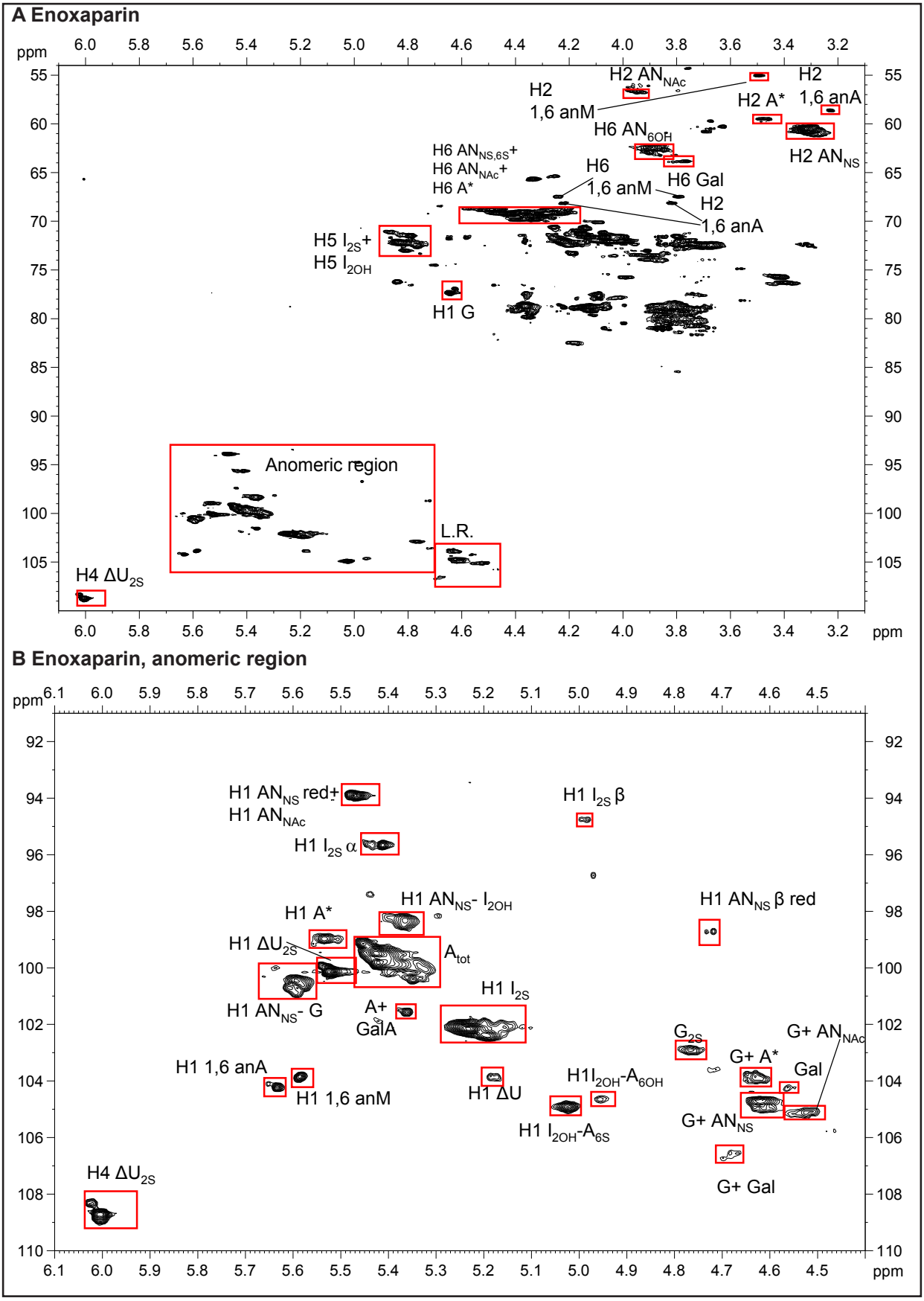

Figure 53. Full assignment of HSQC spectra of enoxaparin **A** and **B** panels show enoxaparin HSQC full window and anomeric region spectra; enoxaparin (40 mg/mL in D_2O) spectra were acquired with Bruker Avance 500, 500 MHz spectrometer at 35 °C; L.R= linkage region. H1= H atom links to saccharidic C1 atom; H2= H atom links to saccharidic C2 atom; H3= H atom links to saccharidic C_3 atom; H4= H atom links to saccharidic C4 atom; H5= H atom links to saccharidic C5 atom; H6= H atom links to saccharidic C_6 atom.

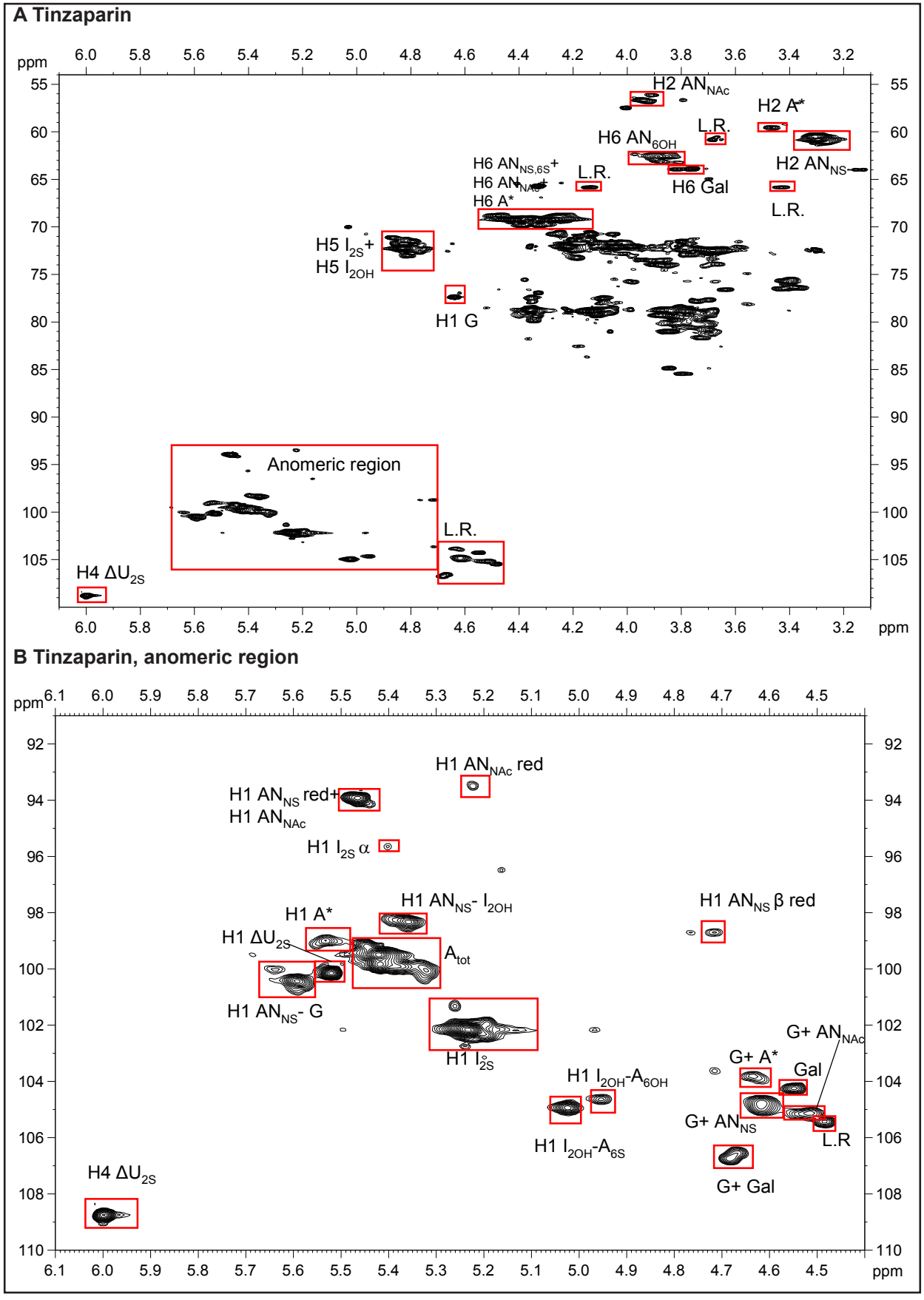

Figure 54. Full assignment of HSQC spectra of tinzaparin. **A** and **B** panels show tinzaparin HSQC full window and anomeric region spectra, respectively; tinzaparin (40 mg/mL in D_2O) spectra were acquired with Bruker Avance 600 spectrometer equipped with cryoprobe at 600 MHz at 30 °C; L.R= linkage region. H1= H atom links to saccharidic C1 atom; H2= H atom links to saccharidic C2 atom; H3= H atom links to saccharidic C_3 atom; H4= H atom links to saccharidic C4 atom; H5= H atom links to saccharidic C5 atom; H6= H atom links to saccharidic C_6 atom.

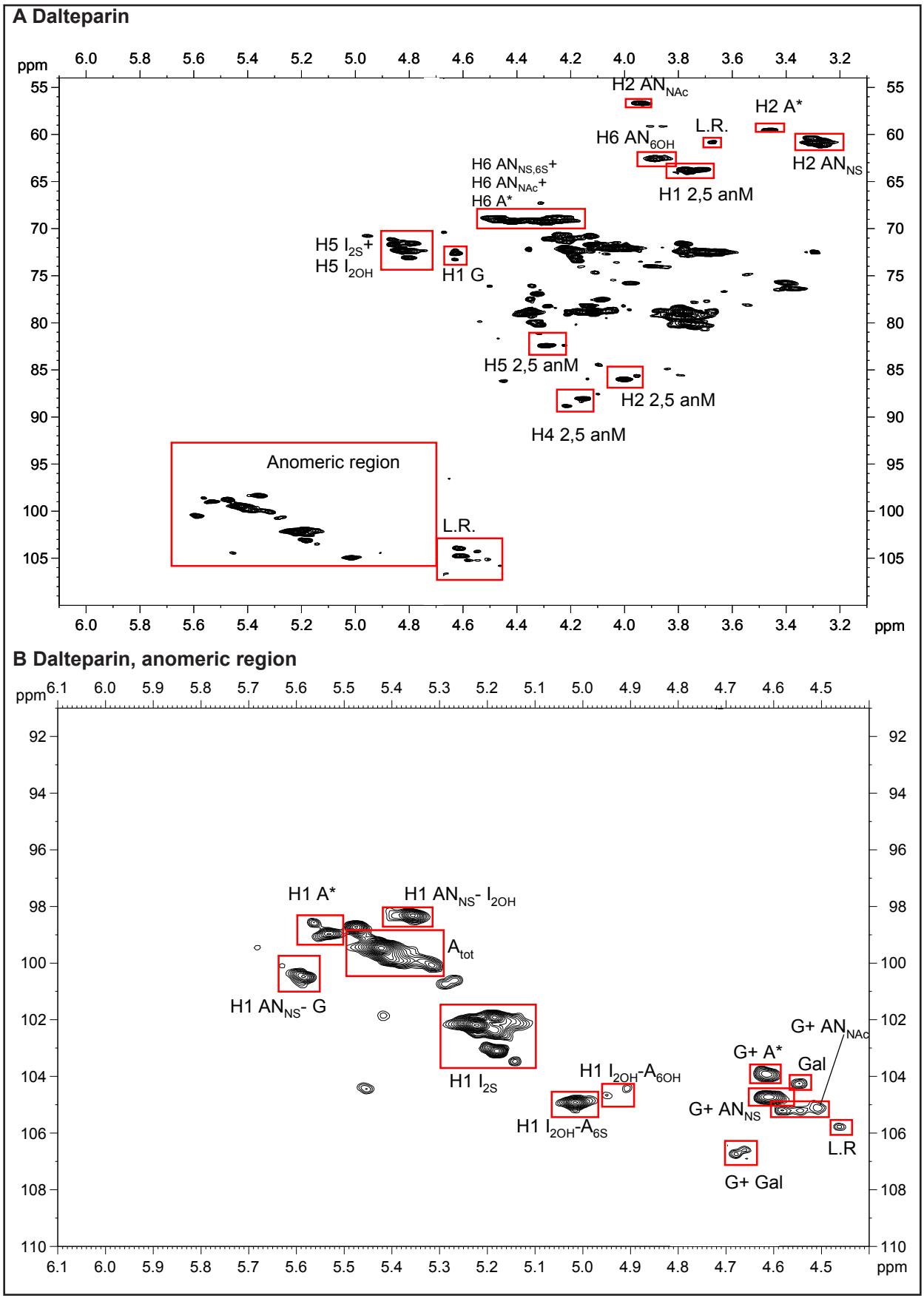

Figure 55. Full assignment of HSQC spectra of dalteparin. **A** and **B** panels show dalteparin HSQC full window and anomeric region spectra, respectively; dalteparin (40 mg/mL in D_2O) spectra were acquired with Bruker Avance 600 spectrometer equipped with cryoprobe at 600 MHz at 21 °C; L.R= linkage region. H1= H atom links to saccharidic C1 atom; H2= H atom links to saccharidic C2 atom; H3= H atom links to saccharidic C_3 atom; H4= H atom links to saccharidic C4 atom; H5= H atom links to saccharidic C5 atom; H6= H atom links to saccharidic C_6 atom.

A

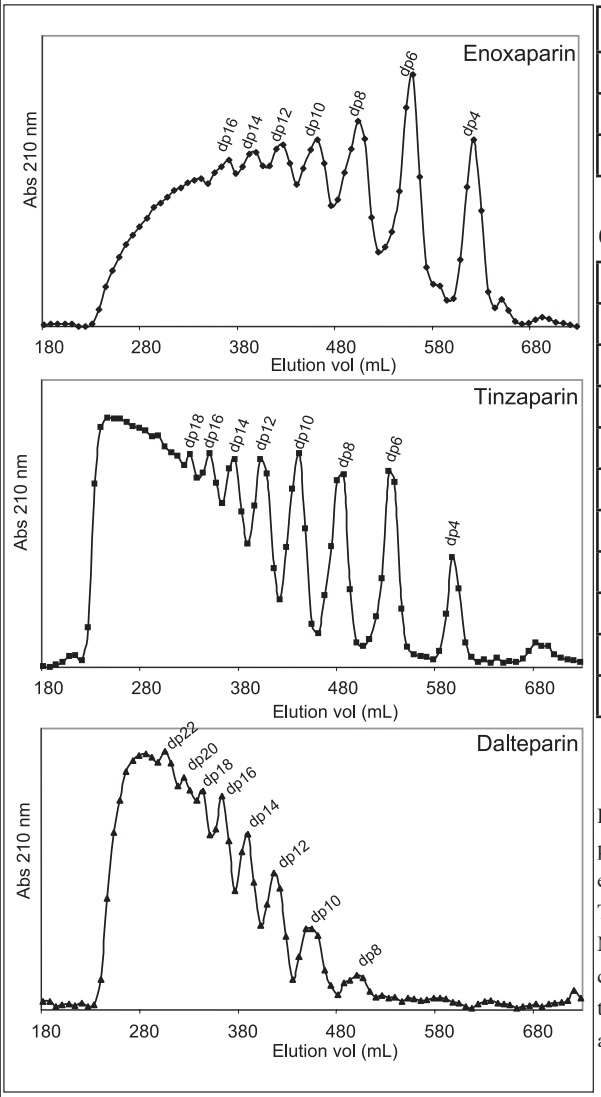

B

LMWH	Mn	MW	D	% > 8000 Da
Enoxaparin	3800	5300	1.30	10
Tinzaparin	5900	8300	1.40	46
Dalteparin	5700	6900	1.22	30

C

Oligosaccharides	Enoxaparin	Tinzaparin	Dalteparin
dp 1 to dp 2	3.6 %	1.6 %	n.d.
dp 3 to dp 4	8.9 %	3.5 %	n.d.
dp 6	10.7 %	4.9 %	n.d.
dp 8	17.8 %	5.1 %	n.d.
dp 10	12.7 %	6.1 %	10.0 %
dp 12	10.1 %	5.1 %	11.0 %
dp 14	0.5 %	7.5 %	9.2 %
dp 16	9.3 %	7.1 %	17.2 %
dp 18	20.4 %	7.6 %	12.6 %
> dp 18	6.0 %	51.5 %	40.0 %

Figure 56. Chromatographic characterisation of LMWH. **A.** Biogel p10 SEC profile of enoxaparin, tinzaparin and dalteparin. **B.** Molecular weight parameters determined via HP-SEC/ TDA for enoxaparin, tinzaparin and dalteparin. The last column reports oligosaccharide percentage composing LMWH with MW > 8000 Da **C.** Evaluation of the relative abundance of the oligosaccharidic components of enoxaparin, tinzaparin and dalteparin (weight %) (n.d. not detected). All the percentages were calculated on the basis of the weight recovery after the biogel p10 column.

Hep dp 2 1D and 1D/2D assignment are shown in Fig. 57, whereas (T) dp 6 and (T) dp 10 1D and 1D/2D assignment are shown in Fig. 58; Hep dp 2 HSQC analysis demonstrated that the sample is a pure solution of disaccharide (there is a single signal in the anomeric region belong to the I_S, see red circled anomeric signal in Fig. 57). Proton spectra of hexasaccharide and decasaccharide tinzaparin derived shown that they are mixture of different sequences and also mixture of hexa/octasaccharide and deca/dodecasaccharide, respectively, with prevalence of hexasaccharide for (T) dp 6 and decasaccharide for (T) dp 10. This reflects tinzaparin heterogeneity. This permit to study the dependency of $A\beta_{1\text{-}40}$-GAGs interaction from GAGs chain length. Actually, the interaction studies of $A\beta_{1\text{-}40}$ with Hep oligosaccharides will give information on the importance of the oligosaccharides length and not on oligosaccharides structures. Informations about oligosaccharidic structure and/or sulfation/acetylation pattern on protein-GAGs interactions can be obtained using homogeneous oligosaccharide, but the isolation of a single molecular population from an heterogeneous pool it is a demanding task and it is out of the objectives of this work.

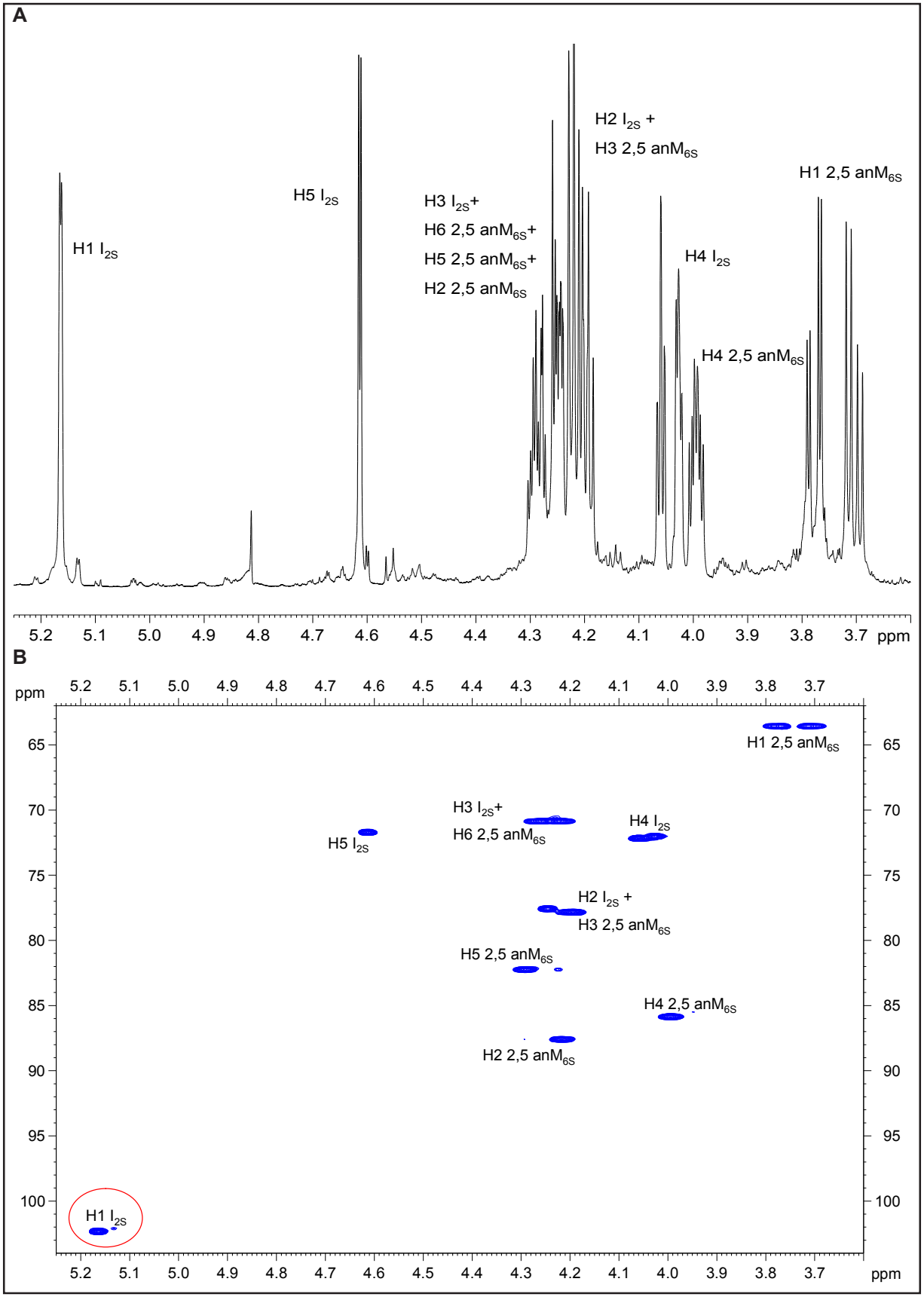

Figure 57. NMR investigation of Hep dp 2. **A** Hep dp 2 ^{1}H spectrum with full peaks assignment; **B** Hep dp 2 ^{1}H -^{13}C HSQC with full peaks assignment; Hep dp 2 (33.5 mg/mL) spectra were acquired with Bruker Avance 600, 600 MHz spectrometer, equipped with cryoprobe at 21 °C. Red circled anomeric signal shows the only anomeric signal, demonstrating disaccharide purity. H1= H atom links to saccharidic C1 atom; H2= H atom links to saccharidic C2 atom; H3= H atom links to saccharidic C_3 atom; H4= H atom links to saccharidic C4 atom; H5= H atom links to saccharidic C5 atom; H6= H atom links to saccharidic C_6 atom.

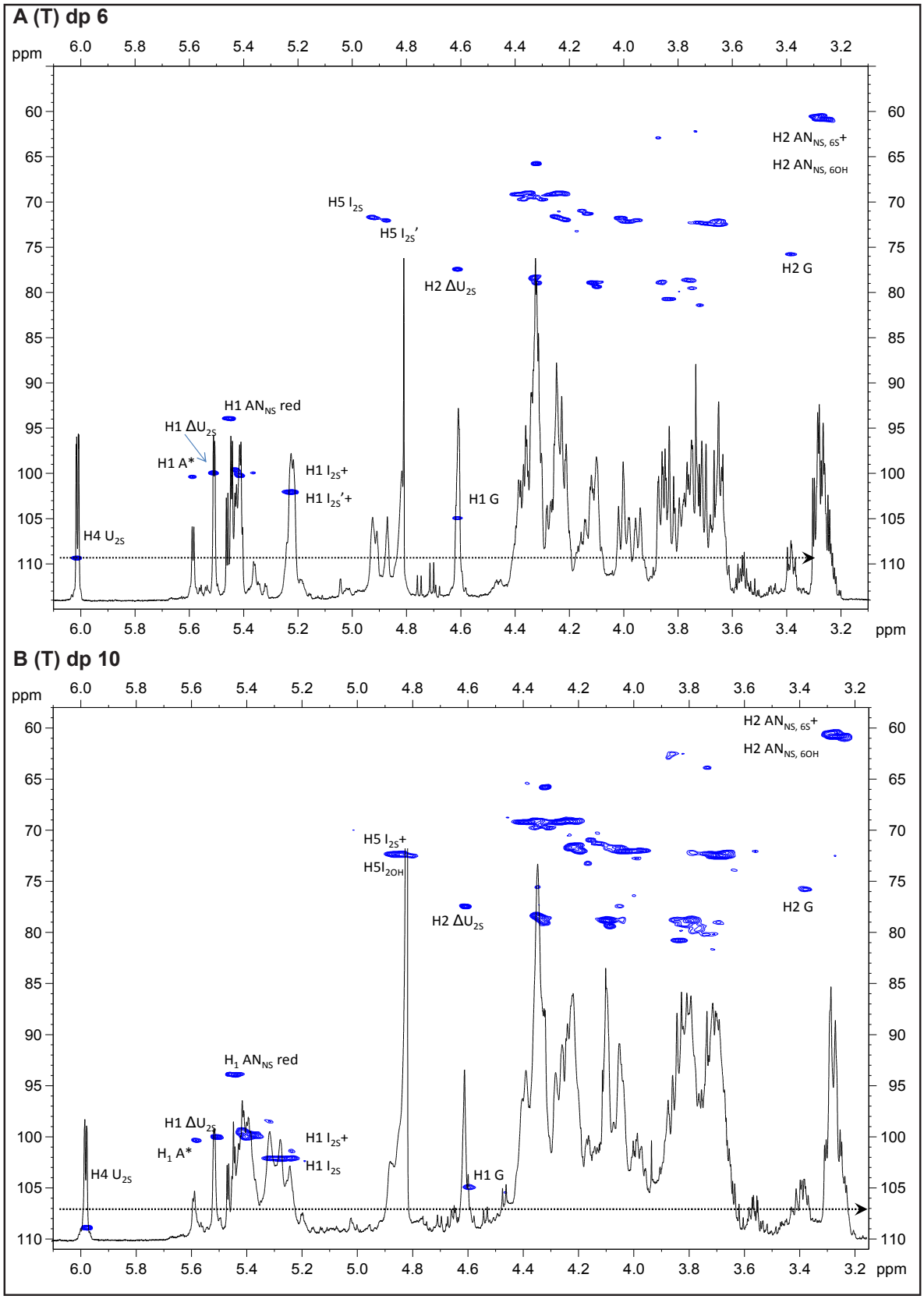

Figure 58. NMR investigation of hexasaccharide [(T) dp 6], decasaccharide [(T) dp 10] tinzaparin derived. **A** (T) dp 6 $^{1}H/^{1}H$-^{13}C HSQC spectra superimposition with anomeric and other majors peaks assignment; **B** (T) dp 10 $^{1}H^{1}H/^{1}H$-^{13}C HSQC spectra superimposition with anomeric and other majors peaks assignment. Hep dp 2 (33.5 mg/mL), (T) dp 6 (11.5 mg/mL) and (T) dp 10 (4.7 mg/mL) spectra were acquired with Bruker Avance 600, 600 MHz spectrometer, equipped with cryoprobe at 21 °C. Dashed arrows are threshold peak intensity levels, below those levels peak signals were not take in account for HSQC. H1= H atom links to saccharidic C1 atom; H2= H atom links to saccharidic C2 atom; H3= H atom links to saccharidic C_3 atom; H4= H atom links to saccharidic C4 atom; H5= H atom links to saccharidic C5 atom; H6= H atom links to saccharidic C_6 atom.

6.3.3. $A\beta_{1-40}$ aggregation kinetics is time dependent and chemo-physical condition dependent

Amyloid peptides tends to form protein aggregations; the properties of this phenomena are time dependent (the probability that two or more monomer of $A\beta_{1-40}$ peptide interact to each other, leading to a dimer or oligomer formation, increases as much as the time pass) and concentration dependent (higher the monomer/oligomer number in the solution higher the probability to have an interaction with the consequence of oligo/polymer formation). It is well known that the transient and prolonged misfolding nature of $A\beta_{1-40}$ makes it difficult to perform proper *in vitro* studies and obtain consistent results (Kim, 2010). From monomers to fibrils, the aggregated form of $A\beta_{1-40}$ is a significant hallmark in the Alzheimer's disease (AD) cascade and becomes the valuable targets for early diagnosis and therapy for AD. Thus, the development of optimised in vitro fibrillogenic conditions to induce the desired $A\beta_{1-40}$ states is essential, as a consequence different solubilisation conditions were tested to obtain the best monomer/polymer ratio as starting point. Information regarding the size of $A\beta_{1-40}$ and the rate of growth can be obtained using laser light scattering (Tomski and Murphy, 1992; Shen *et al*., 1993; Murphy and Pallitto, 2000; Di Fede *et al*., 2009). Dynamic light scattering probes length scales on the order of 0.5- 830 nm, making it appropriate for measuring amyloid aggregates. DLS aggregation kinetics measurements were performed in different chemo-physical condition to demonstrate aggregation state dependency from environmental conditions: hydrodynamic radius (R_h) of 23 μM $A\beta_{1-40}$ in H_2PO_4 and $H(PO_4)_2$ 100mM solutions at a constant temperature of 25 °C at different pH was measured for 75 h (Fig. 55). Acid pH (it means fully protonated protein) protects $A\beta_{1-40}$ from aggregation with an average initial R_h (t_0 R_h)= 61.1 ± 8.5 nm suggesting the presence of a polymer of about 25 units ($A\beta_{1-40}$ monomer R_h= 2.4 ± 0.5 nm), it undergone notable change in molecular population state, nevertheless it did not show reliable sign of aggregation, because after 35 h the system led its stability (t_{35} R_h= 101.9 ± 14.3 nm/final R_h, t_{75} R_h= 120.4 ± 16.8 nm). Neutral pH keeps $A\beta_{1-40}$ in lower aggregation state at starting point (t_0 R_h= 50 ± 0.5 nm), but after 24 h aggregation began. Basic pH brings the system to an intermediate oligomer state (R_h ~85 ± 0.5 nm), but just after 13 h R_h increased showing aggregation (Fig. 59). The differences between the kinetics are explainable as follow: $A\beta_{1-40}$ amino-acid side chains protonation states affect protein folding, $A\beta_{1-40}$ explores different possibilities in order to find the more stable one and when the system reaches the stable condition, the aggregation phenomena starts (between 5 h and 15 h at pH 9, between 25 h at pH 7; a little trend for R_h increasing was measured until 25 h after that the system was stable). $A\beta_{1-40}$ at pH 7 shown higher mobility respect the other two experimental conditions, the aggregation curve slope changed three times during the experiment (it cannot be found a singular regression curve, aggregation curve must be fitted with three different equations: between 0 h and 25 h it is possible to find a 0.75 angular coefficient, between 25 h and 40 h it is possible to find a 11.27 angular coefficient and between 40 h until the end it is possible to find a 5.66 angular coefficient). $A\beta_{1-40}$ aggregation at pH 9 was measurable just after 5 h from experiment beginning, but a constant R_h increase is measurable after 15 h from protein solubilization (see Fig. 59). Aggregation kinetics investigation performed by dynamic light scattering demonstrated how protein protonation state affect the kinetics aggregations, to better understand what happened at molecular level, it is mandatory to analyse $A\beta_{1-40}$ local and total charge profiles, Table 17.

A

	PB pH 2		PB pH 7		PB pH 9	
Time (h)	R_h (nm)	St. Dev.	R_h (nm)	St. Dev.	R_h (nm)	St. Dev.
0	61.1	8.5	34.7	4.9	57.2	8.0
5	97.9	13.7	42.2	5.9	90.0	12.6
10	85.7	12.0	44.6	6.2	92.7	11.0
15	103.6	14.5	39.7	5.6	97.1	12.8
20	110.3	15.4	44.5	6.2	125.5	17.3
25	99.3	13.9	60.7	8.5	130.8	18.3
30	138.6	19.4	117.0	16.4	143.2	18.4
35	101.9	14.3	171.3	24.0	170.4	23.8
40	93.4	13.1	230.4	32.2	210.4	29.4
45	104.7	14.6	253.8	35.5	226.9	31.7
50	92.8	13.0	281.8	26.3	244.9	34.3
55	114.5	16.0	319.7	44.7	272.0	38.0
60	116.0	16.2	348.3	48.7	291.5	40.8
65	117.4	16.4	374.6	52.4	309.5	43.3
70	118.9	16.6	399.0	55.8	326.1	45.6
75	120.4	16.8	421.6	59.0	341.6	47.8

B

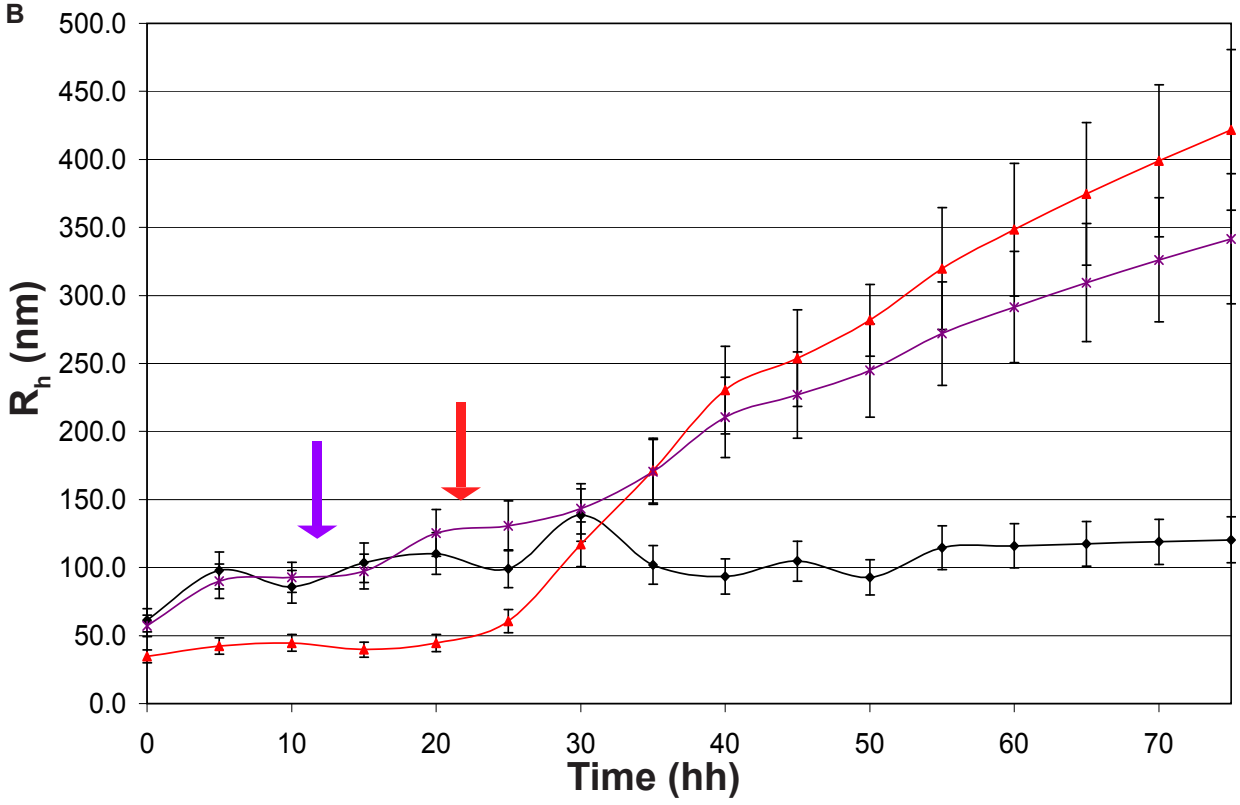

Figure 59. $A\beta_{1\text{-}40}$ aggregation kinetics at different pH. **A** R_h values from DLS measurements. $A\beta_{1\text{-}40}$ (0.1 mg/mL) were kept at 25 °C for the entire experiment duration. **B.** plotted R_h values from DLS measurement of: black line and circles represent $A\beta_{1\text{-}40}$ R_h at pH 2, red line and circles represent $A\beta_{1\text{-}40}$ R_h at pH 7 and purple line and asterisks represent $A\beta_{1\text{-}40}$ R_h at pH 9. The red arrow shows protein aggregation beginning at pH 7 and the purple arrow shows protein aggregation beginning at pH 9. R_h values were sampled every hours and they are the media of three different experiments. $A\beta_{1\text{-}40}$ (23 μM) was kept at 25 °C for the duration of the entire experiment.

	1°	2°	3°	4°	5°	6°	7°	8°	9°	10°	11°	12°	13°	14°	15°	16°	17°	18°	19°	20°	21°	22°	23°	24°	25°	26°	27°	28°	29°	30°	31°	32°	33°	34°	35°	36°	37°	38°	39°	40°	TOT charge
AA	D	A	E	F	R	H	D	S	G	Y	E	V	H	H	Q	K	L	V	F	F	A	E	D	V	G	S	N	K	G	A	I	I	G	L	M	V	G	G	V	V	
Charge pH 2	1		0		1	0	0	1		1	0		0	0		1						0	0			1		1														0	7
Charge pH 4	-1		-1		1	0	-1	1		1	0		0	0		1						0	-1			1		1														-1	1
Charge pH 6	-1		-1		1	-1	-1	1		1	0		-1	-1		1						-1	-1			1		1														-1	-3
Charge pH 7	0		-1		1	-1	-1	1		1	-1		-1	-1		1						-1	-1			1		1														-1	-3
Charge pH 9	0		-1		1	-1	-1	1		1	-1		-1	-1		1						-1	-1			1		1														-1	-3

Table 18. $A\beta_{1\text{-}40}$ sequence charge profiles at different pH. In the second raw it was reported 1-letter aminoacid code, the arbitrary colour code stands for: blue letters represent aminoacid with acid side chains, red letters represent aminoacid with basic side chains, yellow cells represent a positive charge and green cells represent a negative charge.

The peptide is characterised by a neutral region at the C-term except for Val^{40} that acquire a negative charge from pH 4; the N-term part is the most affected by protonation/deprotonation phenomena, in fact high acidity condition (pH ≤ 2) preserves the stability of H-bond so α-helix structure might be favoured [N-term secondary structure is not yet defined, because most of the efforts have been done to understand C-term structure changing (Riek *et al*., 2001; Roychaudhuri *et al*., 2008; Triguero *et al*., 2008)]. This putative structured region does not fit properly with aggregation mechanism, according to DLS data, average R_h did not undergo big changes during experimental time. As much as the pH became neutral/basic, some amino-acid side chains undergo protonation state change: Asp^1, Glu^3, Arg^5, His^6, Glu^7, Ser^8, Tyr^{10}, Glu^{11}, His^{13}, His^{14}, Lys^{16}, Glu^{22} and Asp^{23}; this leads to N-term internal charge neutralisation and H-bond destabilisation that became more pronounced at pH 7 caused to the absence of local charge on Asp^1 and to the sequence of positive and negative charges characterising the peptide from Glu^3 to Glu^{11} (neutral pH induces the formation of different salt bridges through peptide at N-term segment: Glu^3- Arg^5, Arg^5 - His^6, Asp^7- Ser^8, Tyr^{10}- Glu^{11} and His^{14}- Lys^{16}). It was shown that Asp^{23} is a key residue for the formation of the β-structure (Petkova *et al*., 2002; Urbanc *et al*., 2004; Urbanc *et al*., 2004 [b]), in fact Asp^{23} deprotonation induced by neutral pH creates the condition for salt bridges formation (Asp^{23}-Lys^{28}), this induces folding rearrangement leading to β-structure formation and stabilisation, protecting $A\beta_{1\text{-}40}$ in a pro-aggregation condition. According to DLS data amino-acids deprotonation (neutral condition) causes R_h increase (pro-aggregation condition) due to H-bond breakage and α-helix destabilisation after amino-acids deprotonation (the following amino-acids are deprotonated at pH 7: Glu^3, His^6, Asp^7, Glu^{11} and His^{14}). Aggregation in basic condition happened at faster rate, anyway there is no change in charge profile (Table 17), this could be due to dramatically change in chemical equilibrium between the structures explored by molecules, in fact R_h increase at pH 9 was triggered in the half time compare to the DLS aggregation kinetics at pH 7 (Fig. 55). Together this data shown that $A\beta_{1\text{-}40}$ aggregation is time dependent and chemo-physical dependent, moreover they demonstrated what is the best chemo-physical condition to study the alteration of $A\beta_{1\text{-}40}$ aggregation: buffer solution at pH 7 allows to measure peptide aggregation (starting from 25 h), the initial and final monomer/oligomer dimensions are in the order of magnitude to eventualy show aggregation perturbations by external agents (Hep and mimetics) and it gives the opportunity to study *in vitro* an *in vivo* phenomena in reliable conditions (pH and salt concentration).

6.3.4. Experimental condition affects $A\beta_{1-40}$ aggregation kinetics

Aggregation is a concentration dependent phenomenon, for this reason protein concentration at starting point is extremely important for kinetics; to test the reliability of previously shown aggregation data, experimental conditions were changed and aggregation progression was measured by DLS: recently it was shown that is possible follow a fast aggregation kinetics using NaOH (as solubilisation solution) and TRIS-HCl pH 7 (as buffer solution) at 37 °C with a low aggregation state as starting point (Di Fede *et al*., 2009), so $A\beta_{1-40}$ was prepared in NaOH 10mM, TRIS-HCl 100 mM, pH 7 and aggregation kinetics was followed for 75 h and later on compared to $A\beta_{1-40}$ aggregation in PB. Two preparations were tested: 23 μM $A\beta_{1-40}$ in NaOH 10mM, TRIS-HCl 100 mM, pH 7 and 462 μM $A\beta_{1-40}$ in NaOH 10mM, TRIS-HCl 100 mM, pH 7 (Fig. 60). The first interesting thing is that change in solubilization condition led to a better oligomer stabilisation: t_0 R_h are different in the three different conditions, but, at the same concentration, TRIS solubilisation shown a more pronounced effect over aggregation protection compare to PB solubilisation (the starting aggregation state is higher for TRIS solubilisation (23 μM $A\beta_{1-40}$ in PB t_0 R_h= 34.7 nm; 23 μM Aβ in TRIS t_0 R_h= 162.8 nm). Aggregation progression profiles are completely different, in fact the fold aggregation state (f.a.s., ratio between t_{75} R_h and t_0 R_h) of $A\beta_{1-40}$ solubilsed in PB is much higher than the f.a.s., of $A\beta_{1-40}$ solubilsed in TRIS (23 μM $A\beta_{1-40}$ in PB f.a.s.= 12.4, whereas 23 μM $A\beta_{1-40}$ in TRIS f.a.s.= 2.03). Notably, higher temperature does not seem to affect TRIS aggregation protection (aggregation experiment of 23 μM $A\beta_{1-40}$ in TRIS was performed at 37 °C; higher temperature means more kinetics energy, this condition should induce a pro-aggregation condition, because $A\beta_{1-40}$ monomer-monomer interactions happened at higher ratio) (Fig. 60). As it shown in Fig. 60 $A\beta_{1-40}$ at low or high concentration is stable at least for 40 h if it is buffered with a TRIS solution, instead the aggregation started after only 25 h in PB; also see Fig. 59). $A\beta_{1-40}$ at higher concentration shown a completely different aggregation behaviour, because the t_0 R_h of 462 μM $A\beta_{1-40}$ buffered with TRIS was an intermediate value compare to t_0 R_h of 23 μM $A\beta_{1-40}$ conditions (Fig. 60). It was stable for the first 40 h, but between 45 h and 55 h it shown a dramatic R_h increase showing a clear hallmark of fast and complete aggregation. This last condition ($A\beta_{1-40}$ 462 μM, NaOH 10 mM, TRIS-HCl pH 7, 25 °C) was selected to performed amyloid interaction studies with GAGs. In this condition protein stability is guaranteed for 40 h (much more than the 24 h need from the peptide to aggregate in the PB solubilisation condition), the inhibition or attenuation of the aggregation induced by an external agents (as Hep or mimetics/derivatives) must continues over this lag time phase, assuring the efficacy of the treatment. Taken together the solubility investigations suggest that a better experimental setting to study $A\beta_{1-40}$ aggregation progression is represented by a not phosphated buffer with higher $A\beta_{1-40}$ starting concentration.

A

	[Aβ]= 23 μM PB pH 7		[Aβ]= 23 μM TRIS pH 7		[Aβ]= 462 μM TRIS pH 7	
Time (h)	R_h (nm)	St. Dev	R_h (nm)	St. Dev	R_h (nm)	St. Dev
0	34.7	4.9	162.8	22.8	57.8	8.1
5	42.2	5.9	169.0	23.6	96.6	13.5
10	44.6	6.2	230.9	32.3	109.9	15.4
15	39.7	5.6	251.1	35.1	124.1	17.4
20	44.5	6.2	265.4	37.1	136.6	19.1
25	60.7	8.5	276.6	38.7	150.3	21.0
30	117.0	16.4	285.6	40.0	176.3	24.7
35	171.3	24.0	293.3	41.0	169.7	23.7
40	230.4	32.2	300.0	42.0	180.0	25.2
45	253.8	35.5	305.9	42.8	187.2	26.2
50	281.8	26.3	311.1	43.5	946.4	132.4
55	319.7	41.3	315.9	44.2	2453.2	343.1
60	348.3	42.1	320.2	44.8	2784.1	389.4
65	374.6	43.0	324.2	45.3	3088.5	432.0
70	399.0	43.9	327.9	45.9	3370.1	471.3
75	421.6	44.7	331.3	46.3	3632.8	508.1

B

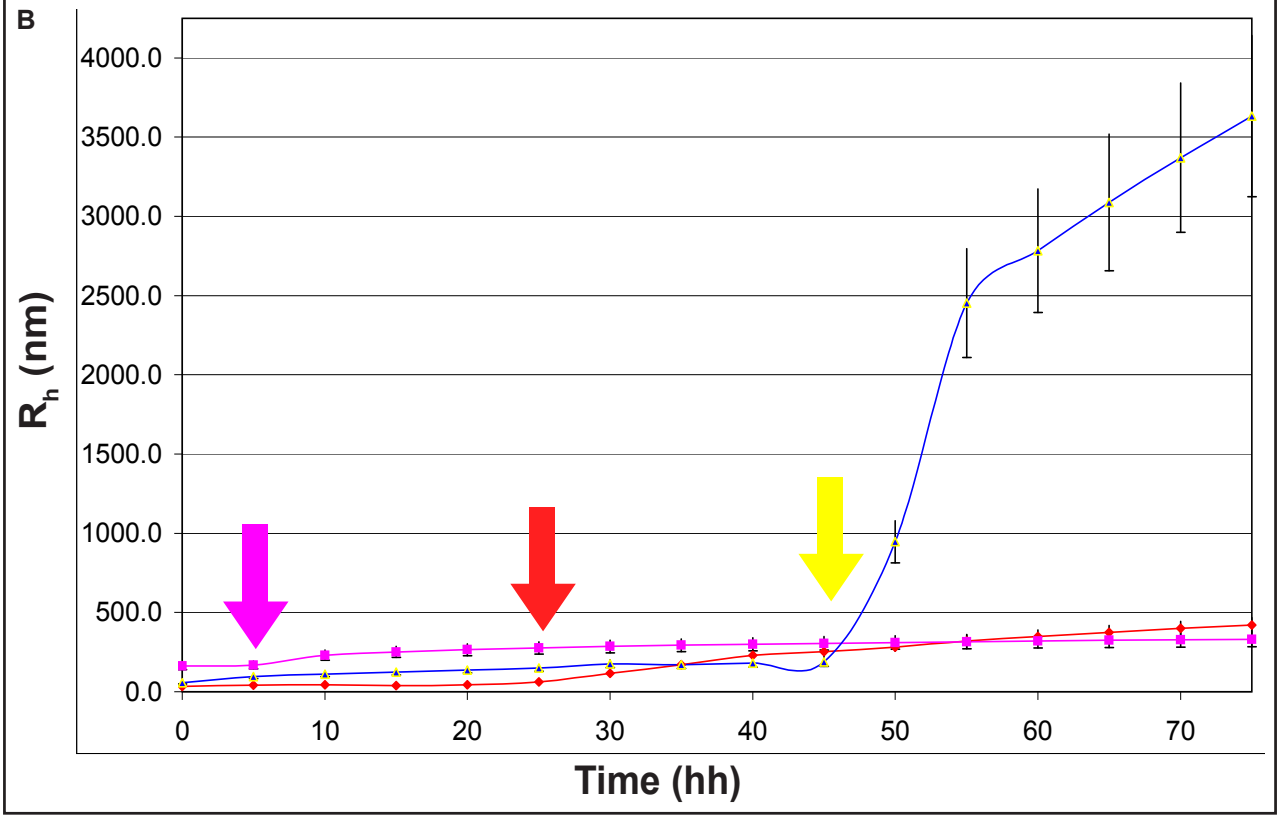

Figure 60. $A\beta_{1-40}$ aggregation kinetics in different conditions: **A** R_h values from DLS measurements in 2 different buffer conditions (PB and TRIS) and at 2 different concentrations (23 μM and 462 μM); **B** plotted R_h values from DLS measurements in 3 different conditions; red line and triangles represent R_h values for 23 μM $A\beta_{1-40}$ dissolved in PB, purple line and squares represent R_h values for 23 μM $A\beta_{1-40}$ dissolved in TRIS and yellow line and triangles represent R_h values for 462 μM $A\beta_{1-40}$ dissolved in TRIS; red arrow shows aggregation starting point for $A\beta_{1-40}$ in PB, purple arrow shows aggregation starting point for $A\beta_{1-40}$ in TRIS (23 μM $A\beta_{1-40}$) and yellow arrow shows aggregation starting point for $A\beta_{1-40}$ in TRIS (462 μM $A\beta_{1-40}$). During all the experimental time the sample was kept at 25 °C apart $A\beta_{1-40}$ 23 μM in TRIS, because it was kept at 37 °C.

6.3.5. Amyloid peptide aggregation is affected by heparin and heparin like molecules interaction

The next step was to follow the $A\beta_{1-40}$ aggregation with or without heparin and mimics. As it has been reported free sulfated molecules partially inhibit the aggregation phenomenon (Fraser *et al*., 1992; Kisilevsky *et al*., 1995; Kisilevsky and Svarek, 2002), thus using the previously described Hep, LMWH and oligosaccharide Hep derived, we demonstrated the efficacy and reliability of this new treatment. It was used an UFH, three different kind of LMWH (Enoxa, Tinza and Dalte; all described and characterised in session 6.3.2) and three different oligosaccharides [Hep dpm 2, (T) dp 6 and (T) dp 10) derived from tinzaparin depolymerisation; all described and characterise in session 6.3.2]. In that experimental conditions, heparin was able to counteract amyloid aggregation, t_{75} R_h values with and without heparin were sensibly different, thus supporting a theoretical starting point (in the presence of UFH, t_{75} R_h of $A\beta_{1-40}$ was reduced to the 16 % compare to t_{75} R_h of $A\beta_{1-40}$ alone; Fig. 62, panel A and B): f.a.s. of $A\beta_{1-40}$ alone increases more than 62 times during the experimental time (Table 19). DLS results show that more the GAG length increase more its properties resemble UFH aggregation attenuation properties, in fact tinzaparin that is characterised by oligosaccharides > 8000 Da (see Fig. 56 B) shown an attenuation effect comparable to UFH, whereas enoxaparin and dalteparin strongly attenuate the aggregation progression (Fig. 62, panel A and B; Table 19). This approach allows to focus the attention on oligosaccharide dimension effect.

Treatment	t_0 R_h	t_{75} R_h	F.a.s.	Δ f.a.s.
$A\beta_{1-40}$	57.8	3632.8	62.8	1
+ UFH	63.7	606.2	9.5	6.6
+ Enoxaparin	32.7	182.4	5.6	11.2
+ Tinzaparin	27.9	447.1	16.0	3.9
+ Dalteparin	32.4	169.7	5.2	12.0
+ Disaccharide	49.5	179.0	3.6	17.4
+ Exasaccharide	51.7	199.4	3.8	16.5
+ Decasaccharide	45.3	126.5	2.8	22.4

Table 19. Initial and final hydrodynamic radius values for $A\beta_{1-40}$ with or without UFH, LMWH and Hep mimetics/derivatives and relatively fold aggregation state values (f.a.s.). Δ f.a.s. is the ratio $A\beta_{1-40}$ f.a.s./ treatment f.a.s.

As it was shown in section 6.3.2., enoxaparin, tinzaparin and dalteparin are characterised by different oligosaccharidic composition and DLS data shown that they differently contribute to amyloid aggregation. Those different effects might related to the LMWHs oligosaccharidic composition, thus to test if different oligosaccharides could induce different effects over $A\beta_{1-40}$ aggregation, it were selected oligosaccharides with homogeneous length and used them for interaction studies with $A\beta_{1-40}$ (oligosaccharides were previously characterised in section 6.3.2.). It was measured a comparable effect for hexasaccharide and disaccharide, that it was much stronger than UFH effect (Table 19; Fig. 63, panel A and B). Interestingly, a stronger inhibition effect was also shown by the decasaccharide (Fig. 63, panel A and B). Oligosaccharides attenuate aggregation as enoxaparin and dalteparin (Table 19), this suggests that LMWH effectivenss could driven by just a part of the oligosaccharide population

composing the LMWH. In particular the subpopulation of small chain oligosaccharides that cannot act as UFH (enoxaparin and dalteparin are mainly composed of oligosaccharides < 8000 Da ~dp 22), these oligosaccharides could interfere in the early and late fibril formation stage (for a schematic representation of plaque formation state Fig. 20) and as a consequence of their limited dimensions, they cannot act as $A\beta_{1\text{-}40}$ aggregation site. This resulted in a stronger aggregation attenuation effect. The consideration that hexasaccharide and disaccharide shown weaker effects over aggregation attenuation, suggests that anti-aggregation oligosaccharides might be able to exert a certain bridge effect. In fact smaller chain oligosaccharides (< dp 10/12) are able to interfere with the aggregation phenomenon, but they form soluble aggregates less stable than the one generate by the presence of bigger oligosaccharides. During aggregation lag phase (from 0 h to 48 h) amyloidic seeds and protofilaments tend to reach the stability and without any agents, attenuating the aggregation, the system can overcome this step accessing to the exponential fibril formation step (Fig. 60, Fig. 62 and Fig. 63 blue aggregation profile). Oligosaccharides could interfere soon after seeds formation (t_0 R_h with and without GAGs are comparable) stabilizing soluble aggregates (like soluble protofilaments, R_h< 200 nm) and avoiding bigger aggregates formations, whereas with UFH just a weak aggregation attenuation can be observed (Fig. 62). Fig. 61 represents a model for $A\beta_{1\text{-}40}$ aggregation interference caused by GAGs.

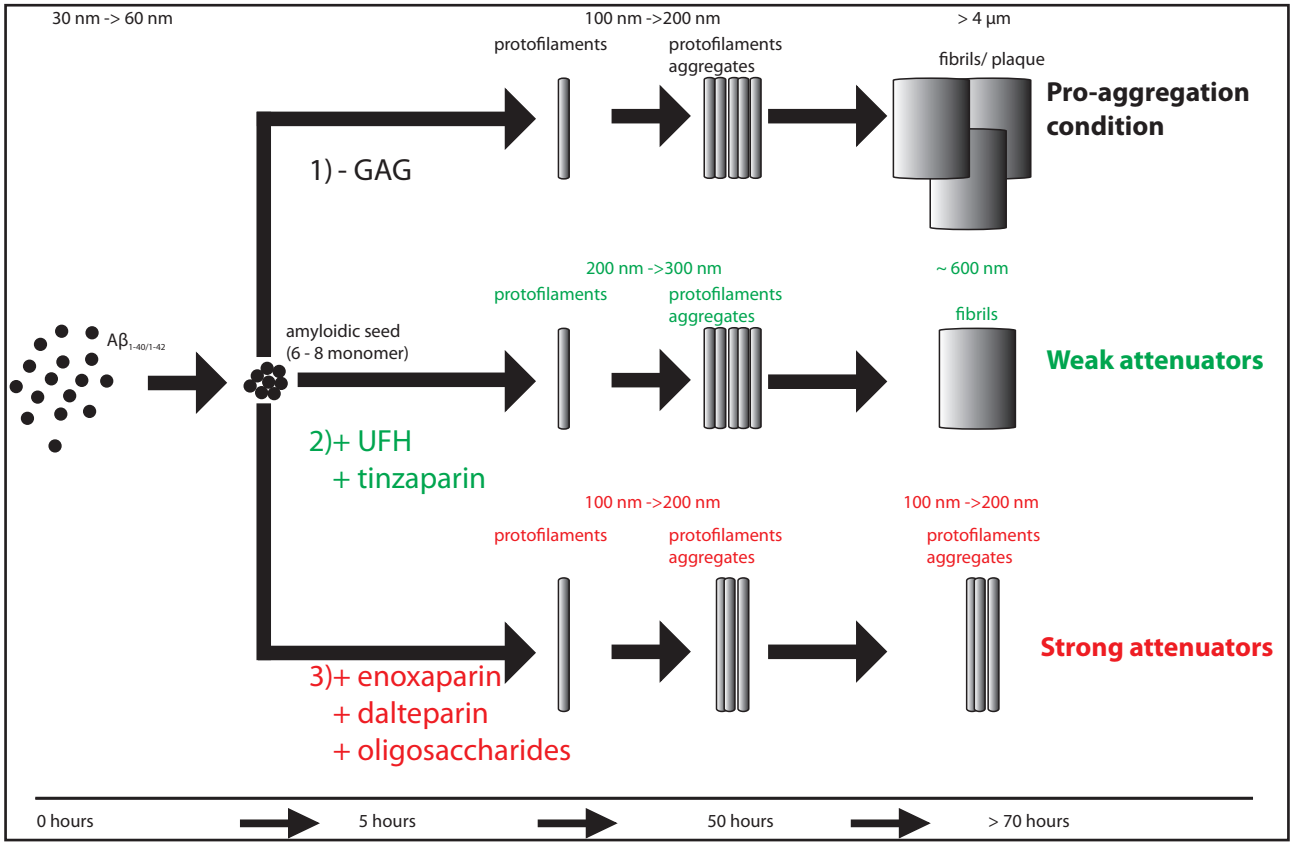

Figure 61. Model of the possible attenuation of Aβs aggregation by UFH, LMWH and oligosaccharides. 1) Amyloid aggregation without GAGs proceeds until fibril formation causing plaque accumulation. 2) Heparin and/or tinzaparin mildly attenuate Aβs aggregation and fibril formation still occurs. 3) Oligosaccharides (dp 6 < X < dp 12) and/or LMWHs characterised by anti-aggregation oligosaccharides (dp < 22) are able to strongly attenuate amyloid aggregation with no fibrils formation.

A

	$A\beta_{1-40}$		+ UFH (Heparin)		+ Enoxaparin		+ Tinzaparin		+ Dalteparin	
Time (h)	R_h (nm)	St. Dev	R_h (nm)	St. Dev	R_h (nm)	St. Dev	R_h (nm)	St. Dev	R_h (nm)	St. Dev
0	57.8	8.1	63.7	3.2	32.7	1.6	27.9	1.4	32.4	1.6
5	96.6	13.5	111.0	15.5	49.7	7.0	64.1	9.0	44.4	6.2
10	109.9	15.4	150.4	21.0	59.9	8.4	92.2	12.9	53.0	7.4
15	124.1	17.4	173.5	24.3	69.3	9.7	106.5	14.9	62.0	8.7
20	136.6	19.1	169.5	23.7	80.0	11.2	118.8	16.6	69.2	9.7
25	150.3	21.0	188.9	26.4	92.5	12.9	135.3	18.9	77.2	10.8
30	176.3	24.7	219.2	30.7	97.6	13.7	170.4	23.8	88.9	12.4
35	169.7	23.7	245.5	34.3	107.0	15.0	184.5	25.8	97.9	13.7
40	180.0	25.2	274.8	38.4	116.5	16.3	199.9	28.0	106.9	14.9
45	187.2	26.2	223.2	31.2	128.8	18.0	216.9	30.3	110.4	15.4
50	946.4	132.4	307.8	43.0	128.0	17.9	303.6	42.5	126.7	17.7
55	2453.2	343.1	385.7	53.9	144.7	20.2	353.0	49.4	133.8	18.7
60	2784.1	389.4	431.9	60.4	154.2	21.6	371.9	52.0	142.8	20.0
65	3088.5	432.0	483.5	67.6	163.6	22.9	393.6	55.1	151.8	21.2
70	3370.1	471.3	594.0	83.1	174.8	24.4	418.5	58.5	160.0	22.4
75	3632.8	508.1	606.2	84.8	182.4	25.5	447.1	62.5	169.7	23.7

B

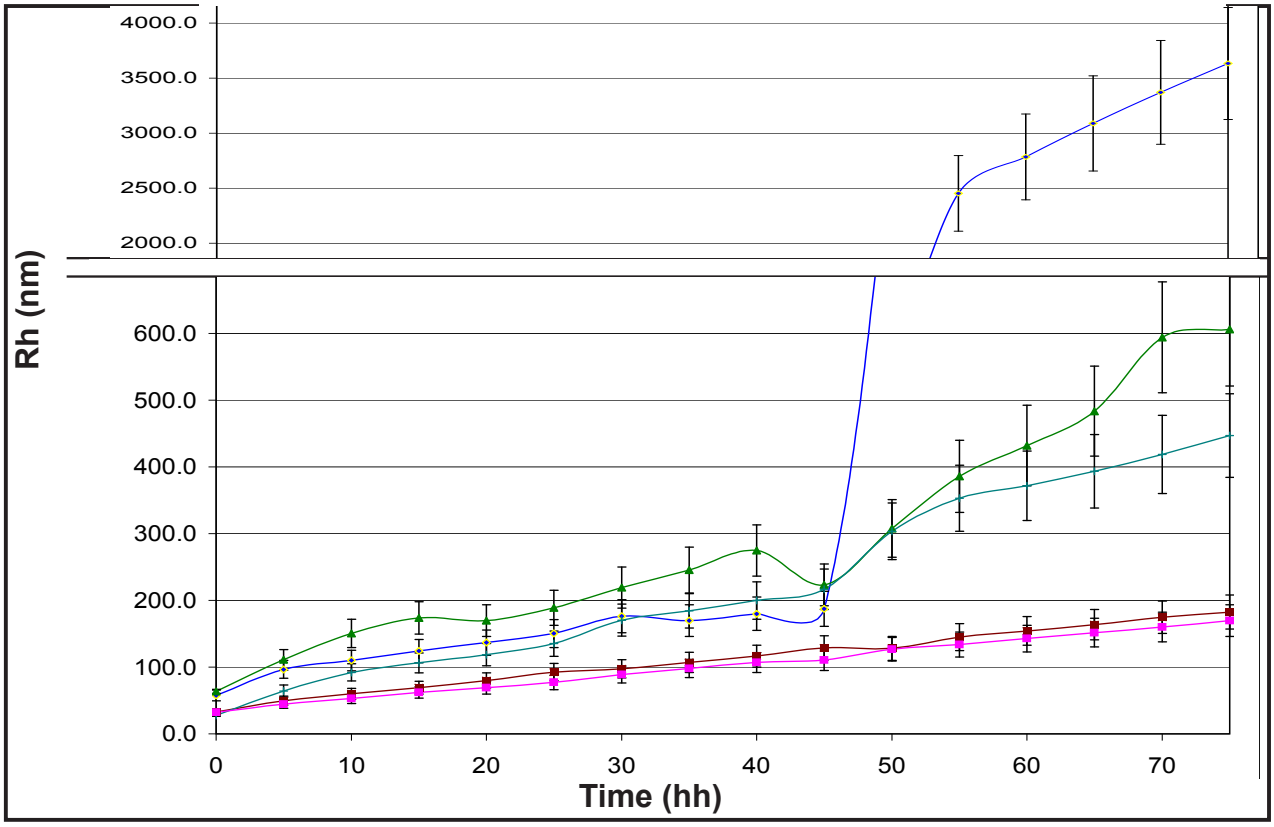

Figure 62. $A\beta_{1-40}$ aggregation kinetics with and without Hep/LMWH. **A** R_h values from DLS measurements of $A\beta_{1-40}$ with and without UFH and LMWHs. **B** plotted R_h values from DLS measurements of $A\beta_{1-40}$ with and without UFH and LMWH; yellow line and circles represent $A\beta_{1-40}$ aggregation trend alone; green line and scores represent $A\beta_{1-40}$ aggregation trend with UFH; clear blue line and squares represent $A\beta_{1-40}$ aggregation trend with tinzaparin; brown line and scores represent $A\beta_{1-40}$ aggregation trend with enoxaparin; clear purple line and squares represent $A\beta_{1-40}$ aggregation trend with dalteparin. During all the experimental time the sample was kept at 25 °C.

A

	$A\beta_{1-40}$		+ Hep dp 2 (Disaccharide)		+ (T) dp 6 (Hexasaccharide)		+ (T) dp 10 (Decasaccharide)	
Time (h)	R_h (nm)	St. Dev	R_h (nm)	St. Dev	R_h (nm)	St. Dev	R_h (nm)	St. Dev
0	57.8	8.1	49.5	2.5	51.7	2.6	45.3	2.3
5	96.6	13.5	67.3	9.4	70.7	9.9	58.0	8.1
10	109.9	15.4	80.2	11.2	72.4	10.1	64.0	8.9
15	124.1	17.4	90.2	12.6	78.2	10.9	68.8	9.6
20	136.6	19.1	98.4	13.8	84.5	11.8	73.6	10.3
25	150.3	21.0	95.4	13.3	91.3	12.8	78.4	11.0
30	176.3	24.7	119.8	16.8	113.0	15.8	83.2	11.6
35	169.7	23.7	119.3	16.7	106.6	14.9	88.0	12.3
40	180.0	25.2	125.9	17.6	115.2	16.1	92.8	13.0
45	187.2	26.2	119.3	16.7	124.5	17.4	97.6	13.7
50	946.4	132.4	137.0	19.2	134.5	18.8	102.4	14.3
55	2453.2	343.1	146.6	20.5	145.4	20.3	107.2	15.0
60	2784.1	389.4	153.9	21.5	157.1	22.0	112.0	15.7
65	3088.5	432.0	161.7	22.6	169.8	23.7	116.9	16.3
70	3370.1	471.3	149.2	20.9	142.3	19.9	110.1	15.4
75	3632.8	508.1	179.0	25.0	199.4	27.9	126.5	17.7

B

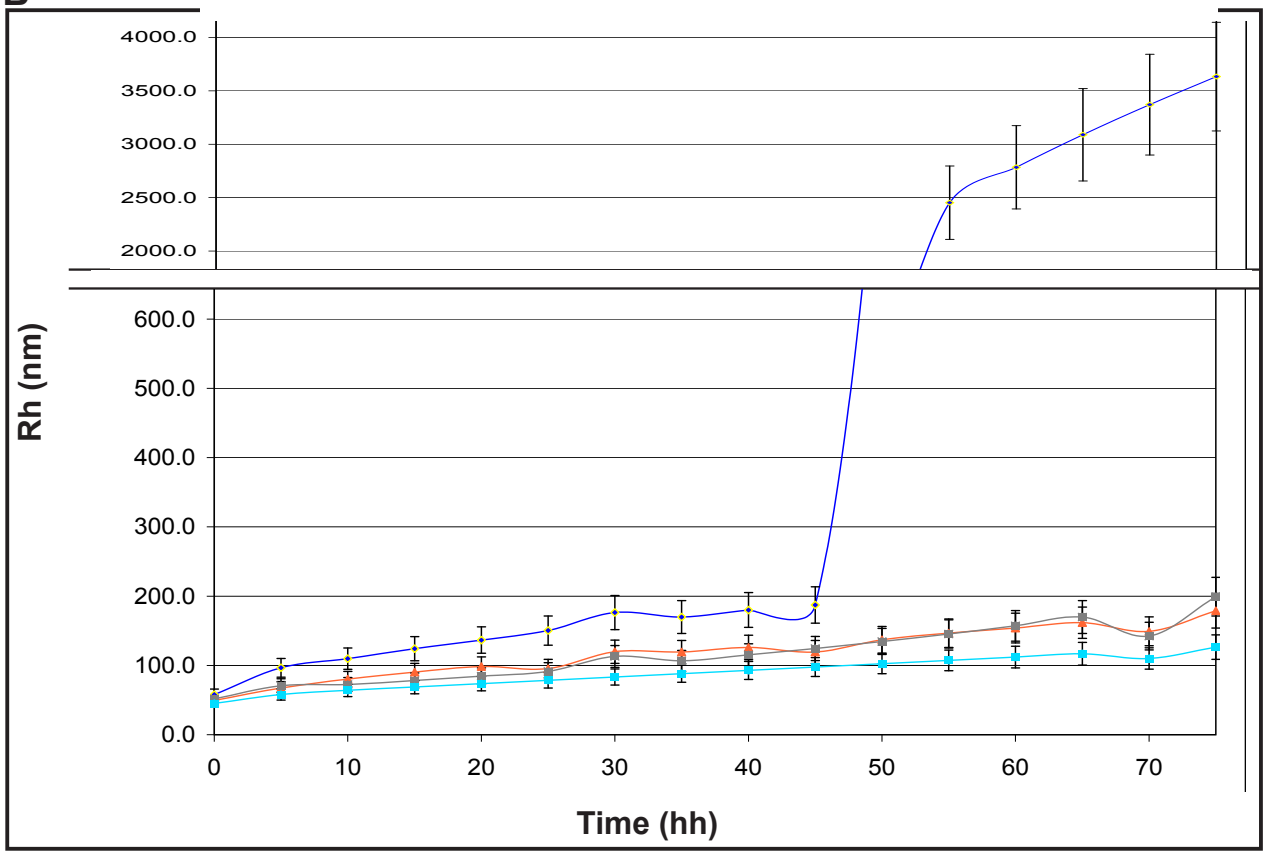

Figure 63. $A\beta_{1-40}$ aggregation kinetics with and without Hep mimetics/derivatives. **A** R_h values from DLS measurements of $A\beta_{1-40}$ with and without oligosaccharides. **B** plotted R_h values from DLS measurements of $A\beta_{1-40}$ with and without oligosaccharides; yellow line and circles represent $A\beta_{1-40}$ aggregation trend alone; orange line and squares represent $A\beta_{1-40}$ aggregation trend with Hep dp 2; grey line and squares represent $A\beta_{1-40}$ aggregation trend with (T) dp 6; azure line and triangles represent $A\beta_{1-40}$ aggregation trend with (T) dp 10. During all the experimental time the sample was kept at 25 °C.

6.3.6. Discussion

A complete DLS study was performed and through it was demonstrated that DLS is a reliable technique to measure changes in $A\beta_{1-40}$ fold aggregation state. Following aggregation kinetics it was possible to test chemo-physical and experimental conditions effects on the $A\beta_{1-40}$ aggregation properties, in fact the protein behaved differently changing the pH of the solution [this suggests that protonation state is strictly related to the conformational change involved in fibril formation (Petkova *et al*., 2006; Tycko, 2006; Yu *et al*., 2009)]. $A\beta_{1-40}$ shown changing in aggregation properties related to the buffer and protein concentration (the protein underwent aggregation phenomena only after stabilisation of internal salt bridges and secondary structures stabilization and aggregation seed formation). $A\beta_{1-40}$ aggregation is characterised by a lag phase (molecules explore different conformations and create the aggregation seed reaching a soluble protofilaments state condition), an exponential phase (the real aggregation step) and a final plateau representing the end of the aggregation (fibrils/ little plaque). An external agent can perturb this chain of events and it should inhibit or dramatically attenuate aggregation, thus leading to the formation of little soluble aggregates. DLS measurement demonstrated that UFH and tinzaparin attenuate aggregates formation and the final aggregate dimensions are sensibly smaller than aggregate dimensions in the presence of $A\beta_{1-40}$ alone (heparin weekly attenuate fibril formation and no plateau was reached in the experimental conditions): enoxaparin and dalteparin are capable to cause a stronger attenuation of amyloid aggregation than UFH and tinzaparin, in fact the final aggregation state is smaller in the presence of this two LMWHs than in the presence of tinzaparin. Importantly a protofibrillar condition is stabilized by enoxaparin and dalteparin. According to LMWHs chromatographic characterisation this effect seems MW related (Fig. 56). Hexasaccharide and disaccharide shown a comparable attenuation effect as enoxaparin and dalteparin, suggesting that LMWHs attenuation effects could be driven by a subpopulation of oligosaccharides (strong attenuators, Fig. 61). Soluble aggregates and protofilaments were of lower dimensions in the presence of decasaccharide: strong attenuators seem to stabilise amyloid aggregates in the protofibril forms (100-200 nm in diameter). Recently Hoshi, M. *et al*. (2010) suggested that amyloids toxicity could be driven by amylospheroid (ASPD, amyloidic spheroid moiety ranging from 4 nm to 18 nm in diameter and ~30 KDa MW; MTT viability test were performed on primary cultures from rat septum regions showing that isolated ASPD inhibits MTT activity), with high stability (2 months at 4 °C, Hoshi, 2010). According to our data, strong GAGs attenuators inhibit ASPD stabilisation, forcing the system to stay in an higher f.a.s, but probably with less toxic aggregates. The molecular mechanism is still not clear, thus further studies will help enlightening it. LMWHs are mixture of oligosaccharides, we wondered whether the equilibrium between different molecular populations (sequence composition, sulfation/acetylation content) could be a key parameter to understand this phenomenon. Using selected oligosaccharides is possible to avoid to consider the contemporary effect of different molecular population on the same compounds. In addiction selected oligosaccharides chemically modified in specific oligosaccharidic position (reducing or nonreducing residues and/or sulfation/acetylation pattern) could help to understand the molecular basis behind this phenomenon. Such an experimental strategy could lead to a better drug design approach.

Conclusions

7. Conclusions

GAGs are polyelectrolites with a central biological relevance of which the HS/Hep family recover an important role contributing to regulate exchanges between the outer cell space (the extracellular matrix) and the inner cell space (cytosol) through GAG binding proteins. This Ph.D. thesis was oriented to understand not clear aspects of Hep defined as a pharmaceutical agent, as an AT interactor and as amyloidic protein interactor that have not been cleared so far:

→ Heparin was statistically described throughout s heparin library which was prepared and characterised using by 1H and ^{1}H-^{13}C HSQC NMR**.** Common European commercial heparins and heparin containing modifications induced by the manufacturing process (over oxidation) were also considered. PCA is able to differentiate both polluted N-acetylated molecules from the library and can also highlights non N-acetylated contaminated samples, whereas the USP NMR identity test failed. Our data demonstrate how NMR in combination with chemometrics techniques as PCA can be used as a reliable quality control procedure to certify pharmaceutical heparin, and hopefully this approach could help to avoid an eventual new heparin crisis. In the next future the heparin library will be expanded reaching a total number of 100 heparins as the final library and different pollutants like solvents (EtOH, peracetic acid, acetone, MetOH, etc.) and organic/biological molecule (amino acids, lipids, etc) will be considered. The feasibility of the method suggests the possibility to expand the library with samples provided by the manufacturers with the aim to cover the heterogeneity of pharmaceutical porcine intestinal mucosal heparin and, possibly, also heparins from other origins, organs and processed by a variety of manufacturing processes.

→ Two octasaccharides isolated from low-molecular-weight heparin enoxaparin bearing a 1,6-anhydrosugars at the reducing terminal were investigated (Octa-5 and Octa-6). Combinatory approach of NMR and docking studies demonstrated that Octa-5 and Octa-6 interact differently with AT clarifying that at molecular basis. According to affinity data Octa-5 and Octa-6 equilibrium dissociation constants to AT are lower of 43 fold and 59 fold than fondaparinux, respectively. STD data shown that the closest contacts with AT involve the residues of the octasaccharide belonging to the sequence $A_{NA}GA^{*}I_{S}A$ and correspond to the $A_{NA}GA^{*}$-moiety for both Octa-5 and Octa-6. On the contrary of what was observed for Octa-3, weaker STD signals for the terminal -I_{S}-1,6-anM/G disaccharides with respect to those of the -$A_{NA}GA^{*}$- moiety were observed, indicating a larger distance of these residues from AT. The investigations underline that the manno configuration of the 1,6-anhydro residues promotes a better interaction with AT with respect to the gluco form due to its favourite position of the N-SO_3 group. A more detailed understanding of the role of structural variations on AT binding properties of heparin oligosaccharides may help in the synthesis of ligand analogues and in the design of new LMWHs with an appropriate structure to ensure high affinity to AT

→ Aβ aggregation properties with and without Hep and its fractions or mimetics/derivatives were described by DLS approach. The protein is strongly affected by the chemo-physical environmental condition (pH 2 is a anti-aggregation condition; pH 7 keeps the system stable for 24 h, but after that the aggregation starts exponentially; pH 9 is an unstable condition and after 15 h aggregation exponential starts) and by the buffer condition (PB shown a low stabilization effect over the aggregation phenomenon, whereas TRIS was able to counteract the aggregation progression for a longer time). DLS data also demonstrated that $A\beta_{1\text{-}40}$ aggregation is strongly affected by heparin presence (aggregation proceeds much slower with heparin), but LMWHs and Hep oligosaccharides shown a much stronger effect over the aggregation. DLS investigation qualitatively demonstrated the effect of sulfated molecules over amyloidosis progression, but it cannot give any information about structural features involved in this phenomenon. Thus future NMR interaction studies and DLS investigation involving modified GAGs could help in understanding the molecular basis of Aβs-GAGs interactions.

References

8. References

1. Aguilar, M. I.; Small, D. H.; Surface plasmon resonance for the analysis of beta-amyloid interactions and fibril formation in Alzheimer's disease research. Neurotox, Res., 2005, 7 (1-2), 17-27.
2. Alberts, B.; Johnson, A.; Lewis, J.; Raff, M.; Roberts, K.; Walter, P.; The Extracellular Matrix of Animals. Molecular biology of the cell- fourth edition. Molecular Biology of The Cell, fourth edition, Garland Science, 2002, 190-192.
3. Andersson, L. O.; Barrowcliffe, T.W.; Holmer, E.; Johnson, E. A.; Sims, G. E. C.; Anticoagulant properties of heparin fractionated by affinity chromatography on matrix-bound antithrombin III and by gel filtration. Thromb. Res., 1976, 9, 575–583.
4. Angulo, J.; Hricovıni, M.; Gairi, M.; Guerrini, M.; de Paz, J. L.; Ojeda, R.; Martín-Lomas, M.; Nieto P.; Dynamic properties of biologically active synthetic heparin-like hexasaccharides. Glycobiology. 2005, 15, 1008–1015.
5. Ariga, T.; Miyatake, T.; Yu, R. K.; Role of proteoglycans and glycosaminoglycans in the pathogenesis of Alzheimer's disease and related disorders: amyloidogenesis and therapeutic strategies--a review. J. Neurosci. Res., 2010, 88 (11), 2303-2315.
6. Ashall, F.; Goate, A. M.; Role of the beta-amyloid precursor protein in Alzheimer's disease. Trends. Biochem. Sci., 1994, 19 (1), 42-46.
7. Avci, F. Y.; Karst, N. A.; Linhardt, R. J.; Synthetic oligosaccharides as heparin-mimetics displaying anticoagulant properties. Curr. Pharmac. Design, 2003, 9, 2323–2335.
8. Bae, J.; Desai, U. R.; Pervin, A.; Caldwell, E. E.; Weiler, J. M.; Linhardt, R. J.; Interaction of heparin with synthetic antithrombin III peptide analogues. Biochem. J., 1994, 301 (Pt 1), 121-129.
9. Baglin, T.P.; Carrell, R.W.; Church, F. C.; Esmon, C.T.; Huntington, J.A.; Crystal structures of native and thrombin-complexed heparin cofactor II reveal a multistep allosteric mechanism. Proc. Natl. Acad. Sci. USA, 2002, 99, 11079–11084.
10. Bai, X.; Zhou, D.; Brown, J.R.; Crawford, B. E.; Hennet, T.; Esko, J.D.; Biosynthesis of the linkage region of glycosaminoglycans: cloning and activity of galactosyltranferase II, the sixth member of the β1,3-galactosyltranferase family (β3GalT6). J. Biol. Chem. 2001, 276, 48189-48195.
11. Bairstow, S.; McKee, J.; Nordhaus, M.; Johnson, R.; Identification of a simple and sensitive microplate method for the detection of oversulfated chondroitin sulfate in heparin products. Anal. Biochem., 2009, 388 (2), 317-21.
12. Ballatore, C; Lee, V. M.; Trojanowski, J. Q.; Tau-mediated neurodegeneration in Alzheimer's disease and related disorders. Nat. Rev. Neurosci., 2007, 8 (9), 663-672.
13. Bame, K. J.; Danda, J.; Hassall, A.; Tumova, S.; Abeta(1-40) prevents heparanase-catalyzed degradation of heparan sulfate glycosaminoglycans and proteoglycans in vitro. A role for heparan sulfate proteoglycan turnover in Alzheimer's disease. J. Biol. Chem., 1997, 272 (27), 17005-17011.
14. Battistelli, S.; Genovese, A.; Gori, T.; Heparin-induced thrombocytopenia in surgical patients. Am. J. Surg., 2010, 199 (1), 43-51.
15. Bauer, K. A.; Hawkins; D.V.; Peters, P, C.; Petitou, M.; Herbert, J-M,; van Boeckel, C. A. A.; Fondaparinux, a synthetic pentasaccharide: the first in a new class of antithrombotic agents-the

selective factor Xa inhibitors. Card. Drug Reviews 2002, 20, 37–52.
16. Bax, A. and Davis, D. G.; Practical aspects of two-dimensional transverse NOE spectroscopy. J. Magn. Res., 1985, 63, 207-213.
17. Bax, A. and Davis, D. G.; MLEV-17-Based Two Dimensional Homonuclear Magnetization Transfer Spectroscopy. J. Magn. Res., 1985, 65, 855-860.[b]
18. Bednarek, E.; Sitkowski, J.; Bocian, W.; Mulloy, B.; Kozerski, L.; An assessment of polydispersed species in unfractionated and low molecular weight heparins by diffusion ordered nuclear magnetic resonance spectroscopy method. J. Pharm. Biomed. Anal., 2010, 53 (3), 302-308.
19. Bellesia, G.; Shea, J. E.; Effect of beta-sheet propensity on peptide aggregation. J. Chem. Phys., 2009, 130 (14), 145103 (1-10).
20. Belzar, K. J.; Dafforn, T. R.; Petitou, M.; Carrell, R. W.; Huntington, J. A.; The effect of a reducing-end extension on pentasaccharide binding by antithrombin. J. Biol. Chem., 2000, 275, 8733– 8741.
21. Bergamaschini, L.; Donarini, C.; Rossi, E.; De Luigi, A.; Vergani, C.; De Simoni, M. G.; Heparin attenuates cytotoxic and inflammatory activity of Alzheimer amyloid-beta in vitro. Neurobiol. Aging, 2002, 23 (4), 531-536.
22. Bergamaschini, L.; Rossi, E.; Storini, C.; Pizzimenti, S.; Distaso, M.; Perego, C.; De Luigi, A.; Vergani, C.; De Simoni, M. G.;. Peripheral treatment with enoxaparin, a low molecular weight heparin, reduces plaques and beta-amyloid accumulation in a mouse model of Alzheimer's disease. J Neurosci., 2004, 24 (17), 4181-4186.
23. Beyer, T.; Diehl, B.; Randel, G.; Humpfer, E.; Schafer, H.; Spraul, M.; Schollmayer, C.; Holzgrabe, U.; Quality assessment of unfractionated heparin using (1)H nuclear magnetic resonance spectroscopy. J. Pharm. Biomed. Anal., 2008, 14 (1), 13-19.
24. Beyer, T.; Matz, M.; Brinz, D.; Radler, O.; Wolf, B.; Norwig, J.; Baumann, K.; Alban, S.; Holzgrabe, U.; Composition of OSCS-contaminated heparin occurring in 2008 in batches on the German market. Eur. J. Pharm. Sci., 2010, 40, 4, 297-304.
25. Bianchini, P.; Liverani, L.; Mascellani, G.; Parma, B.; Heterogeneity of unfractionated heparins studied in connection with species, source and production processes. Semin. Thromb. Hemost., 1997, 23 (1), 3-10.
26. Bigler, P.; Brenneisen, R.; Improved impurity fingerprinting of heparin by high resolution. 1H NMR spectroscopy. J. Pharm. Biomed. Anal., 2009, 49 (4), 1060-1064.
27. Bishop, J. R.; Schuksz, M.; Esko, J. D.; Heparan sulphate proteoglycans fine-tune mammalian physiology. Nature, 2007, 446 (7139), 1030-1037.
28. Bisio, A.; Vecchietti, D.; Citterio, L.; Guerrini, M.; Raman, R.; Bertini, S.; Eisele, G.; Naggi, A.; Sasisekharan, R.; Torri, G.; Structural features of low-molecular-weight heparins affecting their affinity to antithrombin. Thromb. Haemost., 2009, 102 (5), 865-873.
29. Björk, I.; Olson, S.T.; Antithrombin: A bloody important serpin. In: Church, F.C.; Cunningham, D.D.; Ginsburg, D.; Hoffman, M.; Tollefsen, D.M.; Stone, S.R.; editors. Chemistry and biology of serpins. New York: Plenum Press, 1997, 17–33.
30. Blossom, D. B.; Kallen, A. J.; Patel, P. R.; Elward, A.; Robinson, L.; Gao, G.; Langer, R.; Perkins, K. M.; Jaeger, J. L.; Kurkjian, K. M.; Jones, M.; Schillie, S. F.; Shehab, N.; Ketterer, D.; Venkataraman, G.; Kishimoto, T. K.; Shriver, Z.; McMahon, A. W.; Austen, K. F.; Kozlowski, S.; Srinivasan, A.; Turabelidze, G.; Gould, C. V.; Arduino, M. J.; Sasisekharan, R.; Outbreak of adverse reactions associated with contaminated heparin. N. Engl. J. Med., 2008, 359 (25), 2674-2684.

31. Bourin, M.C,; Lindahl U. Glycosaminoglycans and the regulation of blood coagulation. Biochem. J., 1999, 289, 313–330.
32. Braak, H.; Braak, E.; Evolution of neuronal changes in the course of Alzheimer's disease. J. Neural. Transm. Suppl., 1998, 53, 127-140.
33. Brooze, G.I.; Tissue factor pathway inhibitor. Thromb. Haemost. 1995, 74, 90–93.
34. Bruch, M.; Weiss, V.; Engel, J.; Plasma serine proteinase inhibitors (serpins) exhibit major conformational changes and a large increase in conformational stability upon cleavage at their reactive sites. J. Biol. Chem., 1988, 263, 16626–16630.
35. Brunden, K. R.; Richter-Cook, N. J.; Chaturvedi, N.; Frederickson, R. C.; pH-dependent binding of synthetic beta-amyloid peptides to glycosaminoglycans. J. Neurochem., 1993, 61 (6), 2147-2154.
36. Buee, L.; Ding, W.; Anderson, J. P.; Narindrasorasak, S.; Kisilevsky, R.; Boyle, N. J.; Robakis, N. K.; Delacourte, A.; Greenberg, B.; Fillit, H. M.; Binding of vascular heparan sulfate proteoglycan to Alzheimer's amyloid precursor protein is mediated in part by the N-terminal region of A4 peptide. Brain. Res., 1993, 627 (2), 199-204.
37. Buee, L.; Ding, W.; Delacourte, A.; Fillit, H.; Binding of secreted human neuroblastoma proteoglycans to the Alzheimer's amyloid A4 peptide. Brain. Res., 1993, 601, (1-2), 154-63 [b].
38. Byun, Y.; Jacobs, H. A.; Kim, S. W.; Mechanism of thrombin inactivation by immobilized heparin. J. Biomed. Mater. Res., 1996, 30, 4, 423-427.
39. Caldwell, E. E.; Nadkarni, V. D.; Fromm, J. R.; Linhardt, R. J.; Weiler, J. M.; Importance of specific amino acids in protein binding sites for heparin and heparan sulfate. Int. J. Biochem. Cell. Biol., 1996, 28 (2), 203-216.
40. Calugaru, S.V.; Swanson, R.; Olson, S.T.; The pH dependence of serpin-proteinase complex dissociation reveals a mechanism of complex stabilization involving inactive and active conformational states of the proteinase which are perturbable by calcium. J. Biol. Chem., 2001, 276, 32446–32455
41. Camporese, G.; Bernardi, E.; Noventa, F.; Update on the clinical use of the low-molecular-weight heparin, parnaparin. Vasc. Health Risk Manag., 2009, 5, 819-831.
42. Capila, I.; Hernaiz, M. J.; Mo, Y. D.; Mealy, T. R.; Campos, B.; Dedman, J. R.; Linhardt, R. J.; Seaton, B. A.; Annexin V--heparin oligosaccharide complex suggests heparan sulfate--mediated assembly on cell surfaces. Structure, 2001, 9 (1), 57-64.
43. Capila, I.; Linhardt, R. J.; Heparin-protein interactions. Angew. Chem. Int. Ed. Engl., 2002, 41 (3), 391-412.
44. Cardin, A. D.; Weintraub, H. J.; Molecular modeling of protein-glycosaminoglycan interactions. Arteriosclerosis, 1989, 9 (1), 21-32.
45. Carrell, R.W.; Stein, P.E.; Fermi, G.; Wardell, M.R.; Biological implications of a 3 A˚ structure of dimeric antithrombin. Structure, 1994, 2, 257–270.
46. Carrotta, R.; Di Carlo, M.; Manno, M.; Montana, G.; Picone, P.; Romancino, D.; San Biagio, P. L.; Toxicity of recombinant beta-amyloid prefibrillar oligomers on the morphogenesis of the sea urchin Paracentrotus lividus. FASEB J., 2006, 20 (11), 1916-1917.
47. Cassaro, C. M.; Dietrich, C. P.; Distribution of sulfated mucopolysaccharides in invertebrates. J. Biol. Chem., 1977, 252 (7), 2254-2261.
48. Castillo, G. M.; Ngo, C.; Cummings, J.; Wight, T. N.; Snow, A. D.; Perlecan binds to the beta-amyloid proteins (A beta) of Alzheimer's disease, accelerates A beta fibril formation and maintains A beta fibril stability. J. Neurochem., 1997, 69 (6), 2452-2465.

49. Casu, B.; Oreste, P.; Torri, G.; Zoppetti, G.; Choay, J.; Lormeau, J. C.; Petitou, M.; Sinay, P.; The structure of heparin oligosaccharide fragments with high anti-(factor Xa) activity containing the minimal antithrombin III-binding sequence. Chemical and 13C nuclear-magnetic-resonance studies. Biochem J., 1981, 197 (3), 599-609.
50. Casu, B.; Choay, J.; Ferro, D.R.; Gatti, G.; Torri, G.; Petitou, M.; Sinaÿ, P.; Controversial glycosaminoglycan conformations. Nature, 1986, 322, 215-16.
51. Casu, B.; Petitou, M.; Provasoli, M.; Sinay, P.; Conformational flexibility: a new concept for explaining binding and biological properties of iduronic acid-containing glycosaminoglycans. Trends. Biochem. Sci., 1988,13 (6), 221-225.
52. Casu, B.; Lindahl, U. Structure and biological interactions of heparin and heparan sulfate. Adv. Carbohydr. Chem. Biochem., 2001, 57, 159–206.
53. Casu, B.; Structure and active domains of heparin. Chemistry and Biology of Heparin and Heparan Sulfate. Elsevier Ltd., 2005, chap. 1, 1-26.
54. Černy, I.; Buděšinsky, M.; Trnka, T.; Černy, M. Preparation of 2-amino-1,6-anhydro-2,3-dideoxy-β-L-arabino-hexopyranose. 1H- and 13C-n.m.r. spectra of deoxy derivatives of 2-amino-1,6-anhydro-2-deoxy-D-glucose and 2-amino-1,6-anhydro-2-deoxy-D-mannose. Carbohydr. Res., 1984, 130, 103–114.
55. Chautard, E.; Ballut, L.; Thierry-Mieg, N.; Ricard-Blum, S.; MatrixDB, a database focused on extracellular protein-protein and protein-carbohydrate interactions. Bioinformatics, 2009, 25, 690-691.
56. Chen, J.; Jones, C. L.; Liu, J. Using an enzymatic combinatorial approach to identify anticoagulant heparan sulfate structures. Chem. Biol., 2007, 14, 986-993.
57. Choay, J.; Petitou, M.; Lormeau, J. C.; Sinay, P.; Casu, B.; Gatti, G; Structure-activity relationship in heparin: a synthetic pentasaccharide with high affinity for antithrombin III and eliciting high anti-factor Xa activity. Biochem. Biophys. Res. Commun., 1983, 116, 492-499.
58. Chuang, Y-J.; Swanson, R.; Raja, S.M.; Olson, S.T.; Heparin enhances the specificity of antithrombin for thrombin and factor Xa independent of the reactive center loop sequence. Evidence for an exosite determinant of factor Xa specificity in heparin-activated antithrombin. J. Biol. Chem., 2001, 276, 14961–14971.
59. Cole, S. L.; Vassar, R.; The role of amyloid precursor protein processing by BACE1, the beta-secretase, in Alzheimer disease pathophysiology. J. Biol. Chem., 2008, 283 (44), 29621-29625.
60. Contaminant detected in heparin material of specified origin in the USA and in Germany; serious adverse events reported; recall measures initiated. World Health Organization Alert No. 118 (7 March 2008) <http://www.who.int/medicines/publications/drugalerts/Alert_118_Heparin.pdf>.
61. Coyne, E.; Heparin – past, present and future, Elsevier, Amsterdam, 1981, 9–17.
62. Craig, P.A.; Olson, S.T.; Shore, J.D.; Transient kinetics of heparin-catalyzed protease inactivation by antithrombin III. Characterization of assembly, product formation and heparin dissociation steps in the factor Xa reaction. J. Biol. Chem., 1989, 264, 5452–5461.
63. Damus, P. S.; Hicks, M.; Rosenberg, R. D.; Anticoagulant action of heparin. Nature, 1973,246 (5432), 355-357.
64. Deakin, J. A.; Blaum, B. S.; Gallagher, J. T.; Uhrín, D.; Lyon, M. The binding properties of minimal oligosaccharides reveal a common heparan sulfate/dermatan sulfate-binding site in hepatocyte growth factor/scatter factor that can accommodate a wide variety of sulfation pat-

terns. J. Biol.Chem., 2009, 284, 6311-6321.
65. Desai, U. R.; New antithrombin-based anticoagulants. Med. Res. Rev., 2004, 24 (2), 151-181.
66. Di Fede, G.; Catania, M.; Morbin, M.; Rossi, G.; Suardi, S.; Mazzoleni, G.; Merlin, M.; Giovagnoli, A.R.; Prioni, S.; Erbetta, A.; Falcone, C.; Gobbi, M.; Colombo, L.; Bastone, A.; Beeg, M.; Manzoni, C.; Francescucci, B.; Spagnoli, A.; Cantù, L.; Del Favero, E.; Levy, E.; Salmona, M.; Tagliavini, F.; A Recessive Mutation in the APP Gene with Dominant-Negative Effect on Amyloidogenesis. Science, 2009, 323, 1473-1477.
67. DiGabriele, A. D.; Lax, I.; Chen, D. I.; Svahn, C. M.; Jaye, M.; Schlessinger, J.; Hendrickson, W. A.; Structure of a heparin-linked biologically active dimer of fibroblast growth factor. Nature, 1998, 393, 6687, 812-817.
68. Dreyfuss, J. L.; Regatieri, C. V.; Jarrouge, T. R.; Cavalheiro, R. P.; Sampaio, L. O.; Nader, H. B.; Heparan sulfate proteoglycans: structure, protein interactions and cell signaling. An. Acad. Bras. Cienc., 2009, 81 (3), 409-429.
69. Duchaussoy, P.; Jaurand, G.; Driguez, P. A.; Lederman, I.; Ceccato, M. L.; Gourvenec, F.; Strassel, J. M.; Sizun, P.; Petitou, M.; Herbert, J. M.; Assessment through chemical synthesis of the size of the heparin sequence involved in thrombin inhibition. Carbohydr. Res., 1999, 317 (1-4), 85-99.
70. Dudas, B.; Cornelli, U.; Lee, J.M.; Hejna, M.J.; Walzer, M.; Lorens, S.A.; Mervis, R.F.; Fareed, J. and Hanin, I.; Oral and subcutaneous administration of the glycosaminoglycan C3 attenuates Abeta(25-35)-induced abnormal tau protein immunoreactivity in rat brain. Neurobiol. Aging, 2002, 23, 97–104.
71. Dudas, B.; Rose, M.; Cornelli, U.; Pavlovich, A.; Hanin, I.; Neuroprotective properties of glycosaminoglycans: potential treatment for neurodegenerative disorders. Neurodegener. Dis., 2008, 5 (3-4), 200-205.
72. Ernst, R. L.; Hay, J. W.; The US economic and social costs of Alzheimer's disease revisited. Am. J. Public Health, 1994. 84 (8), 1261-1264.
73. Esko, J.D.; Zhang, L.; Influence of core protein sequence on glycosaminoglycan assembly. Curr. Opin. Struct. Biol., 1996, 6, 663-670.
74. Esko, J. D.; Selleck, S. B.; Order out of chaos: assembly of ligand binding sites in heparan sulfate. Annu. Rev. Biochem., 2002, 71, 435-471.
75. European Agency for the Evaluation of Medicinal Products, Commetee for proprietary medicinal products (CPMP). Note for guidance on minimising the risk of transmitting animal spongiform encephalopathy agent via medicinal products. 1998, CPMP/BWP/1230/98 corr.
76. Faham, S.; Hileman, R. E.; Fromm, J. R.; Linhardt, R. J.; Rees, D. C.; Heparin structure and interactions with basic fibroblast growth factor. Science, 1996, 271, 5252, 1116-1120.
77. Fareed, J.; Haas, S.; Sahahara, E.; Differentiation of low molecular-weight heparins, applied and clinical considerations. Semin. Thromb. Hemost., 1999, 3, 1–147.
78. Ferro, D.R.; Provasoli, A.; Ragazzi. M.; Torri, G.; Casu, B.; Gatti, G.; Jacquinet, J. C.; Sinay, P.; Petitou, M.; Choay, J.; Evidence for conformational equilibrium of the sulfated L-iduronate residue in heparin and in synthetic heparin mono- and oligo-saccharides: NMR and force-field studies. J. Am. Chem. Soc., 1986, 108, 6773-6778.
79. Ferro, D. R.; Provasoli, A.; Ragazzi, M.; Casu, B.; Torri, G.; Bossennec, V.; Perly, B.; Sinaÿ, P.; Petitou, M.; Choay, J. Conformer populations of L-iduronic acid residues in glycosaminoglycan sequences. Carbohydr. Res., 1990, 195,157-167.
80. Forloni, G.; Bugiani, O.; Tagliavini, F.; Salmona, M.; Apoptosis-mediated neurotoxicity in-

duced by beta-amyloid and PrP fragments. Mol. Chem. Neuropathol., 1996, 28 (1-3), 163-171.
81. Forster, M.; Mulloy, B.; Computational approaches to the identification of heparin-binding sites on the surfaces of proteins. Biochem. Soc. Trans., 2006, 34 (Pt 3), 431-434.
82. Fransson, L. A.; Sjoberg, I.; Havsmark, B.; Structural studies on heparan sulphates. Characterization of oligosaccharides; obtained by periodate oxidation and alkaline elimination. Eur. J. Biochem., 1980, 106 (1), 59-69.
83. Fraser, P. E.; Nguyen, J. T.; Chin, D. T.; Kirschner, D. A.; Effects of sulfate ions on Alzheimer beta/A4 peptide assemblies: implications for amyloid fibril-proteoglycan interactions. J. Neurochem., 1992, 59 (4), 1531-1515.
84. Fromm, J. R.; Hileman, R. E.; Caldwell, E. E.; Weiler, J. M.; Linhardt, R. J.; Pattern and spacing of basic amino acids in heparin binding sites. Arch. Biochem. Biophys., 1997, 343 (1), 92-100.
85. Gandhi, N. S.; Mancera, R. L.; The structure of glycosaminoglycans and their interactions with proteins. Chem. Biol. Drug, Des., 2008, 72 (6), 455-482.
86. Gasteiger, J. and Marsili M.; Iterative partial equalization of orbital electronegativity - A rapid access to atomic charges. Tetrahedron, 1980, 30, 3219-3228.
87. Gemene, K. L.; Meyerhoff, M. E.; Reversible detection of heparin and other polyanions by pulsed chronopotentiometric polymer membrane electrode. Anal. Chem., 2010, 82 (5), 1612-1615.
88. Gervais, F.; Paquette, J.; Morissette, C.; Krzywkowski, P.; Yu, M.; Azzi, M.; Lacombe, D.; Kong, X.; Aman, A.; Laurin, J.; Szarek, W. A.; Tremblay, P.; Targeting soluble Abeta peptide with Tramiprosate for the treatment of brain amyloidosis. Neurobiol. Aging., 2007, 28 (4), 537-547.
89. Gettins, P. G. W.; Patston, P. A.; Olson, S. T.; Serpins: structure, function and biology. New York. R. G. Landes, Company, 1996.
90. Gettins, P.G.W.; Serpin structure, mechanism and function. Chem. Rev., 2002, 102, 4751–4803.
91. Ginsberg, S. D.; Galvin, J. E.; Lee, V. M.; Rorke, L. B.; Dickson, D. W.; Wolfe, J. H.; Jones, M. Z.; Trojanowski, J. Q.; Accumulation of intracellular amyloid-beta peptide (A beta 1-40) in mucopolysaccharidosis brains. J. Neuropathol. Exp. Neurol., 1999, 58 (8), 815-824.
92. Glenner, G. G.; Wong, C. W.; Alzheimer's disease: initial report of the purification and characterization of a novel cerebrovascular amyloid protein. Biochem. Biophys. Res. Commun., 1984, 120 (3), 885-890.
93. Gotting, C.; Kuhn, J.; Zhan, R.; Brinkmann, T.; Kleesiek, K.; Molecular cloning and expression of human UDP-d-xylose: proteoglycan core protein β-D-xylosyltranferase and its first isoform XT-II. J. Mol. Biol., 2000, 304, 517-528.
94. Gray, E.; Mulloy, B.; Barrowcliffe, T. W. Heparin and low-molecular-weight heparin. Thromb. Haemost., 2008, 99, 807-818.
95. Gruys, E.; Ultee, A.; Upragarin, N.; Glycosaminoglycans are part of amyloid fibrils: ultrastructural evidence in avian AA amyloid stained with cuprolinic blue and labeled with immunogold. Amyloid, 2006, 13 (1), 13-19.
96. Guerrini, M.; Bisio, A.; Torri, G.; Combined quantitative (1)H and (13)C nuclear magnetic resonance spectroscopy for characterization of heparin preparations. Semin. Thromb. Hemost., 2001, 27 (5), 473-482.
97. Guerrini, M.; Agulles, T.; Bisio, A.; Hricovini, M.; Lay, L.; Naggi, A.; Poletti, L.; Sturiale, L.;

Torri, G.; Casu, B.; Minimal heparin/heparan sulfate sequences for binding to fibroblast growth factor-1. Biochem. Biophys. Res. Commun., 2002, 292 (1), 222-230.

98. Guerrini, M.; Naggi, A.; Guglieri, S.; Santarsiero, R.; Torri, G.; Complex glycosaminoglycans: profiling substitution patterns by two-dimensional nuclear magnetic resonance spectroscopy. Anal. Biochem., 2005, 337 (1), 35-47.
99. Guerrini, M.; Guglieri, S.; Beccati, D.; Torri, G.; Viskov, C.; Mourier, P. Conformational transitions induced in heparin octasaccharides by binding with antithrombin III. Biochem. J., 2006, 399, 191-198.
100. Guerrini, M.; Guglieri, S.; Naggi, A.; Sasisekharan, R.; Torri, G. Low molecular weight heparins: structural differentiation by bidimensional nuclear magnetic resonance spectroscopy. Semin. Thromb. Hemost., 2007, 33, 478-487.
101. Guerrini, M.; Beccati, D.; Shriver, Z.; Naggi, A.; Viswanathan, K.; Bisio, A.; Capila, I.; Lansing, J. C.; Guglieri, S.; Fraser, B.; Al-Hakim, A.; Gunay, N. S.; Zhang, Z.; Robinson, L.; Buhse, L.; Nasr, M.; Woodcock, J.; Langer, R.; Venkataraman, G.; Linhardt, R. J.; Casu, B.; Torri, G.; Sasisekharan, R.; Oversulfated chondroitin sulfate is a contaminant in heparin associated with adverse clinical events. Nat. Biotechnol., 2008, 26 (6), 669-75.
102. Guerrini, M.; Guglieri, S.; Casu, B.; Torri, G.; Mourier, P.; Boudier, C.; Viskov, C.; Antithrombin-binding octasaccharides and role of extensions of the active pentasaccharide sequence in the specificity and strength of interaction. J. Biol. Chem., 2008, 283, 26662-26675. [b]
103. Guerrini, M.; Shriver, Z.; Bisio, A.; Naggi, A.; Casu, B.; Sasisekharan, R.; Torri, G.; The tainted heparin story: an update. Thromb. Haemost., 2009, 102 (5), 907-911.
104. Guerrini, M.; Zhang, Z.; Shriver, Z.; Naggi, A.; Masuko, S.; Langer, R.; Casu, B.; Linhardt, R. J.; Torri, G.; Sasisekharan, R.; Orthogonal analytical approaches to detect potential contaminants in heparin. Proc. Nat. Acad. Sci. U S A, 2009, 106 (40), 16956-16961 [b].
105. Guglieri, S.; Hricovini, M.; Raman, R.; Polito, L.; Torri, G.; Casu, B.; Sasisekharan, R.; Guerrini, M.; Minimum FGF2 Binding Structural Requirements of Heparin and Heparan Sulfate Oligosaccharides As Determined by NMR Spectroscopy. Biochemistry, 2008, 47 (52), 13862–13869.
106. Gutierrez, M.; Llobera, A.; Vila-Planas, J.; Capdevila, F.; Demming, S.; Buttgenbach, S.; Minguez, S.; Jimenez-Jorquera, C.; Hybrid electronic tongue based on optical and electrochemical microsensors for quality control of wine. Analyst. 2010, 135 (7), 1718-1725.
107. Hanhenberger, R.; Jakobson, Å.M., Ansari. A.; Wehler, T.; Svahn, C.M.; Lindahl, U.; Low-sulfated oligosaccharides derived from heparan sulfate inhibit normal angiogenesis. Glycobiology, 1993, 3, 567–573.
108. Hardy, J.; Selkoe, D. J.; The amyloid hypothesis of Alzheimer's disease: progress and problems on the road to therapeutics. Science, 2002, 297 (5580), 353-356.
109. Harper, J. D.; Wong, S. S.; Lieber, C. M.; Lansbury, P. T., Jr.; Assembly of A beta amyloid protofibrils: an in vitro model for a possible early event in Alzheimer's disease. Biochemistry, 1999, 38 (28), 8972-8980.
110. Hashii, N.; Kawasaki, N.; Itoh, S.; Qin, Y.; Fujita, N.; Hattori, T.; Miyata, K.; Bando, A.; Sekimoto, Y.; Hama, T.; Kashimura, M.; Tatsumi, M.; Mabuchi, K.; Namekawa, H.; Sakai, T.; Hirose, M.; Dobashi, S.; Shimahashi, H.; Koyama, S.; Herr, S. O.; Kawai, K.; Yoden, H.; Yamaguchi, T.; Heparin identification test and purity test for OSCS in heparin sodium and heparin calcium by weak anion-exchange high-performance liquid chromatography. Biologicals, 2010, 38, 5, 539-543.

111. He, X.; Ye, J.; Esmon, C. T.; Rezaie, A. R.; Influence of arginines 93, 97 and 101 of thrombin to its functional specificity. Biochemistry, 1997, 36 (29), 8969-8976.
112. Herbert, J.M.; Herault, J. P.; Bernat, A.; Van Amsterdam,R. G. M.; Vogel, G. M. T.; Lormeau, J. C.; Petitou, M.; Meuleman, D. G. Biochemical and pharmacological properties of SA-NORG3232701. Circ. Res., 1996, 79 (3), 590–600.
113. Hebert, L. E.; Scherr, P. A.; Bienias, J. L.; Bennett, D. A.; Evans, D. A.; Alzheimer disease in the US population: prevalence estimates using the 2000 census. Arch. Neurol., 2003, 60 (8), 1119-1122.
114. Hernaiz, M. J.; LeBrun, L. A.; Wu, Y.; Sen, J. W.; Linhardt, R. J.; Heegaard, N. H.; Characterization of heparin binding by a peptide from amyloid P component using capillary electrophoresis, surface plasmon resonance and isothermal titration calorimetry. Eur. J. Biochem., 2002, 269 (12), 2860-2867.
115. Herndon, M. E.; Stipp, C. S.; Lander, A. D.; Interactions of neural glycosaminoglycans and proteoglycans with protein ligands: assessment of selectivity, heterogeneity and the participation of core proteins in binding. Glycobiology, 1999, 9 (2), 143-155.
116. Hileman, R. E.; Fromm, J. R.; Weiler, J. M.; Linhardt, R. J.; Glycosaminoglycan-protein interactions: definition of consensus sites in glycosaminoglycan binding proteins. Bioessays, 1998, 20 (2), 156-167.
117. Hirschfield, G. M.; Hawkins, P. N.; Amyloidosis: new strategies for treatment. Int. J. Biochem. Cell Bio., 2003, 35 (12), 1608-1613.
118. Hook, M.; Bjork, I.; Hopwood, J.; Lindahl, U.; Anticoagulant activity of heparin: separation of high-activity and low-activity heparin species by affinity chromatography on immobilized antithrombin. FEBS Lett., 1976, 66, 90–93.
119. Hoppensteadt, D.A.; Fareed, J.; Kaiser, B.; Tissue factor inhibitor: potential implications in the treatment of cardiovascular disorder. In: Sasahara AA, Loscalzo J, eds. New Therapeutic Agents in Thrombosis and Thrombolysis. New York: Marcel Dekker, 2003, 231–300.
120. Hoshi, M.; Sato, M.; Matsumoto, S.; Noguchi, A.; Yasutake, K.; Yoshida, N.; Sato, K.; Spherical aggregates of -amyloid (amylospheroid) show high neurotoxicity and activate tau protein kinase Iglycogen synthase kinase-3. Proc. Natl. Acad. Sci. USA, 2010, 100 (11), 6370 – 6375.
121. Hricovini, M.; Guerrini, M.; Bisio, A.; Torri, G.; Petitou, M. and Casu, B.; Conformation of heparin pentasaccharide bound to antithrombin III. Biochem. J. 2001, 359, 265–272.
122. Hricovini, M.; Guerrini, M.; Bisio, A.; Torri, G.; Naggi, A.; Casu, B.; Active conformations of glycosaminoglycans. NMR determination of the conformation of heparin sequences complexed with antithrombin and fibroblast growth factors in solution. Semin. Thromb. Hemost. 2002, 28 (4), 325-334.
123. Hunt, L. T.; Dayhoff, M. O.; A surprising new protein superfamily containing ovalbumin, antithrombin-III and alpha 1-proteinase inhibitor. Biochem. Biophys. Res. Commun., 1980, 95 (2), 864-871.
124. Huntington, J.A.; Read, R.J; Carrell, R.W.; Structure of a serpin – protease complex shows inhibition by deformation. Nature, 2000, 407, 923–926.
125. Hwang, T. L. and Shaka, A. J.; Water Suppression That Works. Excitation Sculpting Using Arbitrary Wave-Forms and Pulsed-Field Gradients. J. Magn. Res., Series A, 1995, 112, 275-279.
126. Iacomini, M.; Casu, B.; Guerrini, M.; Naggi, A.; Pirola, A.; Torri, G.; ‘‘Linkage region’’ sequences of heparins and heparan sulfates: detection and quantification by nuclear magnetic resonance spectroscopy. Anal. Biochem., 1999, 274, 50–58.

127. Inoue, Y and Nagasawa, K; Selective N-desulfation of heparin with dimethyl sulfoxide containing water or methanol. Carbohydr. Res, 1976, 46 (1), 87-95.
128. Iozzo, R.V.; San Antonio, J.D.; Heparan sulfate proteoglycans: heavy hitters in the angiogenesis arena. J. Clin. Inv., 2001, 108, 349–335.
129. Jeske, W.P.; Neville, B.; Ma, Q.; Hoppensteadt, D.A.; Fareed, J.; Effect of 1,6-anhydro bicyclic ring structure on the pharmacokinetic and pharmacodynamic behaviour of low molecular weight heparin. Blood (ASH Annual Meeting Abstracts) 2004, 104, Abstract 1868.
130. Jin, L.; Abrahams J.P.; Skinner R.; Petitou M.; Pike R.N. and Carrell R.W.; The anticoagulant activation of antithrombin by heparin. Proc. Natl. Acad. Sci. U.S.A., 1997, 94, 14683–14688.
131. Johnson, D. J.; Huntington, J. A.; Crystal structure of antithrombin in a heparin-bound intermediate state. Biochemistry, 2003, 42 (29), 8712-8719.
132. Johnson, D. J.; Li, W.; Adams, T. E.; Huntington, J. A.; Antithrombin-S195A factor Xa-heparin structure reveals the allosteric mechanism of antithrombin activation. EMBO J., 2006, 25 (9), 2029-2037.
133. Jolliffe, I. T.; Principal component analysis. 2nd ed. 2002, Springer, New York, 1-487.
134. Kakoi, N.; Kinoshita, M.; Kawasaki, N.; Yamaguchi, T.; Hayakawa, T.; Kakehi, K.; Capillary electrophoresis analysis of contaminants in heparin sodium for the Japanese pharmacopoeia purity test. Yakugaku Zasshi, 2009, 129 (10), 1255-64.
135. Kaslik, G.; Kardos, J.; Szabó, E.; Szilágyi, L.; Závodsky, P.; Westler, W.M.; Markley, J.L.; Gráf, L.; Effects of serpin binding on target proteinase: Global stabilization, localized increased structural flexibility and conserved hydrogen bonding at the active site. Biochemistry, 1997, 36, 5455–5464.
136. Kay, L.; Keifer, P. and Saarinen, T.; Pure absorption gradient enhanced heteronuclear single quantum correlation spectroscopy with improved sensitivity. J. Am. Chem. Soc., 1992, 114, 26, 10663-10665.
137. Keire, D. A.; Trehy, M. L.; Reepmeyer, J. C.; Kolinski, R. E.; Ye, W.; Dunn, J.; Westenberger, B. J.; Buhse, L. F.; Analysis of crude heparin by (1)H NMR, capillary electrophoresis and strong-anion-exchange-HPLC for contamination by over sulfated chondroitin sulfate. J. Pharm. Biomed. Anal., 2010, 51 (4), 921-926.
138. Keire, D. A.; Mans, D. J.; Ye, H.; Kolinski, R. E.; Buhse, L. F.; Assay of possible economically motivated additives or native impurities levels in heparin by (H) NMR, SAX-HPLC and anticoagulation time approaches. J. Pharm. Biomed. Anal., 2010, 52 (5), 656-664 [b].
139. Keun, H. C.; Ebbels, T. M. D.; Antti, H.; Bollard, M. E.; Beckonert, O.; Holmes, E.; Lindon, J. C. and Nicholson, J. K.; Improved analysis of multivariate data by variable stability scaling: application to NMR-based metabolic profiling. Anal. Chim. Acta, 2003, 490 (1-2), 265-276.
140. Kim, H. Y.; Kim, Y. S.; Han, G. H.; Kim, D. J.; Regulation of in vitro Abeta1-40 Aggregation Mediated by Small Molecules. J. Alzheimers Dis., 2010.
141. Kirschner, D. A.; Inouye, H.; Duffy, L. K.; Sinclair, A; Lind, M.; Selkoe, D. J.; Synthetic peptide homologous to beta protein from Alzheimer disease forms amyloid-like fibrils in vitro. Proc. Natl. Acad. Sci. U S A, 1987, 84 (19), 6953-6957.
142. Kishimoto, T. K.; Viswanathan, K.; Ganguly, T.; Elankumaran, S.; Smith, S.; Pelzer, K.; Lansing, J. C.; Sriranganathan, N.; Zhao, G.; Galcheva-Gargova, Z.; Al-Hakim, A.; Bailey, G. S.; Fraser, B.; Roy, S.; Rogers-Cotrone, T.; Buhse, L.; Whary, M.; Fox, J.; Nasr, M.; Dal Pan, G. J.; Shriver, Z.; Langer, R. S.; Venkataraman, G.; Austen, K. F.; Woodcock, J.; Sasisekharan, R.; Contaminated heparin associated with adverse clinical events and activation of the contact

system. N. Engl. J. Med., 2008, 358 (23), 2457-67.
143. Kisilevsky, R.; Lemieux, L. J.; Fraser, P. E.; Kong, X.; Hultin, P. G.; Szarek, W. A.; Arresting amyloidosis in vivo using small-molecule anionic sulphonates or sulphates: implications for Alzheimer's disease. Nat. Med., 1995, 1 (2), 143-148.
144. Kisilevsky, R.; Szarek, W. A.; Novel glycosaminoglycan precursors as anti-amyloid agents part II. J. Mol.Neurosci., 2002, 19 (1-2), 45-50.
145. Kisilevsky, R.; Szarek, W. A.; Ancsin, J.; Bhat, S.; Li, Z.; Marone, S.; Novel glycosaminoglycan precursors as anti-amyloid agents, part III. J. Mol. Neurosci., 2003, 20 (3), 291-297.
146. Kisilevsky, R.; Szarek, W. A.; Ancsin, J. B.; Elimova, E.; Marone, S.; Bhat, S.; Berkin, A.; Inhibition of amyloid A amyloidogenesis in vivo and in tissue culture by 4-deoxy analogues of peracetylated 2-acetamido-2-deoxy-alpha- and beta-d-glucose: implications for the treatment of various amyloidoses. Am. J. Pathol., 2004, 164 (6), 2127-2137.
147. Kitagawa, H.; Tone, Y.; Tamura, J.; Neumann, K.W.; Ogawa, T.; Oka, S.; Kawasaki, T.; Sugahara, K.; Molecular cloning and expression of glucuronyltranferase I involved in the biosynthesis of glycosaminoglycan-protein linkage region of proteoglycans. J. Biol. Chem., 1998, 273, 6615-6618.
148. Kjellen, L.; Lindahl, U.; Proteoglycans: structures and interactions. Annu. Rev. Biochem., 1991, 60, 443-475.
149. Krieger, E.; Geretti, E.; Brandner, B.; Goger, B.; Wells, T. N.; Kungl, A. J.; A structural and dynamic model for the interaction of interleukin-8 and glycosaminoglycans: support from isothermal fluorescence titrations. Proteins, 2004, 4, 768-775.
150. Kuberan, B.; Lech, M. Z.; Beeler, D. L.; Wu, Z. L.; Rosenberg, R. D.; Enzymatic synthesis of antithrombin III-binding heparan sulfate pentasaccharide. Nat. Biotechnol., 2003, 21 (11), 1343-1346.
151. Kuperstein, I.; Broersen, K.; Benilova, I.; Rozenski, J.; Jonckheere, W.; Debulpaep, M.; Vandersteen, A.; Segers-Nolten, I.; Van Der Werf, K.; Subramaniam, V.; Braeken, D.; Callewaert, G.; Bartic, C.; D'Hooge, R.; Martins, I. C.; Rousseau, F.; Schymkowitz, J.; De Strooper, B.; Neurotoxicity of Alzheimer's disease Abeta peptides is induced by small changes in the Abeta42 to Abeta40 ratio. 2010, EMBO J., 29 (19), 3408-3420.
152. Lam, C. R.; Heparin Administration: Methods and Results in Thirty Cases.. Ann. Surg., 1941, 114 (2), 205-11.
153. Lam, L.H.; Silbert, J.E.; Rosenberg, R.D.; The separation of active and inactive forms of heparin. Biochem. Biophys. Res. Comm. 1976, 69, 570–577.
154. Lane, D. A.; Denton, J.; Flynn, A. M.; Thunberg, L.; Lindahl, U. Anticoagulant activities of heparin oligosaccharides and their neutralization by platelet factor 4. Biochem. J., 1984, 218, 725-732.
155. Laurencin, C. T.; Nair, L.; The FDA and safety--beyond the heparin crisis. Nat. Biotechnol., 2008, 26 (6), 621-623.
156. Heparin Sodium Stage 2 Monograph. Pharmacopeial Forum. 2009, 35 (5), 1085-1088.
157. Laurent, T.C.; Tengblad, A., Thunberg L, Höök M, Lindahl U. The molecular-weight dependence of the anticoagulant activity of heparin. Biochem. J., 1978, 175, 691–701.
158. Leveugle, B.; Scanameo, A.; Ding, W.; Fillit, H.; Binding of heparan sulfate glycosaminoglycan to beta-amyloid peptide: inhibition by potentially therapeutic polysulfated compounds. Neuroreport, 1994, 5 (11), 1389-1392.
159. Leveugle, B.; Ding, W.; Laurence, F.; Dehouck, M. P.; Scanameo, A.; Cecchelli, R.; Fillit, H.;

Heparin oligosaccharides that pass the blood-brain barrier inhibit beta-amyloid precursor protein secretion and heparin binding to beta-amyloid peptide. J. Neurochem., 1998, 70 (2), 736-744.

160. Li, B.; Suwan, J.; Martin, J. G.; Zhang, F.; Zhang, Z.; Hoppensteadt, D.; Clark, M.; Fareed, J.; Linhardt, R. J.; Oversulfated chondroitin sulfate interaction with heparin-binding proteins: new insights into adverse reactions from contaminated heparins. Biochem. Pharmacol., 2009, 78 (3), 292-300.
161. Li, J. P.; Galvis, M. L.; Gong, F.; Zhang, X.; Zcharia, E.; Metzger, S.; Vlodavsky, I.; Kisilevsky, R.; Lindahl, U.; In vivo fragmentation of heparan sulfate by heparanase overexpression renders mice resistant to amyloid protein A amyloidosis. Proc. Natl. Acad. Sci. U S A, 2005, 102 (18), 6473-6477.
162. Li, J. P.; Vlodavsky, I.; Heparin, heparan sulfate and heparanase in inflammatory reactions. Thromb. Haemost., 2009, 102 (5), 823-828.
163. Li, W.; Johnson, D.J.D.; Esmon, C.T.; Huntington, J.A.; Structure of the antithrombin-thrombin-heparin ternary complex reveals the antithrombotic mechanism of heparin. Nature Str. Mol. Biol., 2004, 11, 857–862.
164. Lindahl, U.; Bäckström, G.; Thunberg, L.; Leder, I.G.; Evidence for a 3-O-sulfated d-glucosamine residue in the antithrombin-binding sequence of heparin. Proc. Natl. Acad. Sci. USA, 1980, 77, 6551–6555.
165. Lindahl, U.; Further characterization of the heparin–protein linkage region. Biochim. Biophys. Acta, 1996, 130, 368–382.
166. Lindahl, U.; Heparan sulfate-protein interactions--a concept for drug design? Thromb. Haemost., 2007, 98 (1), 109-115.
167. Lindahl, U.; Li, J.P.. Interaction between heparan sulfate and proteins - Design and functional implications. Int. Rev. Cell Biol., 2009, 276, 105-159.
168. Linhardt, R. J.; Rice, K. G.; Merchant, Z. M.; Kim, Y. S.; Lohse, D. L.; Structure and activity of a unique heparin-derived hexasaccharide. J. Biol. Chem., 1986, 261 (31), 14448-14454.
169. Linhardt, R. J.; Rice, K. G.; Kim, Y. S.; Lohse, D. L.; Wang, H. M.; Loganathan, D.; Mapping and quantification of the major oligosaccharide components of heparin. Biochem. J., 1988, 254, 781–787.
170. Linhardt, R. J.; Gunay, N. S. Production and chemical processing of low molecular weight heparins. Semin. Thromb. Hemost., 1999, 25 (Suppl 3), 5–16.
171. Linhardt, J.R; Analysis of Glycosaminoglycans with Polysaccharide Lyases. Curr. Prot. Mol. Bio., 2001, 17.13B.1-17.13B.16.
172. Linhardt, R. J. Heparin: Structure and Activity. J. Med. Chem., 2003, 46, 2551-2554.
173. Liu, I. H.; Uversky, V. N.; Munishkina, L. A.; Fink, A. L.; Halfter, W.; Cole, G. J.; Agrin binds alpha-synuclein and modulates alpha-synuclein fibrillation. Glycobiology, 2005, 15 (12), 1320-31.
174. Liverani, L.; Mascellani, G.; Spelta, F.; Heparins: process-related physico-chemical and compositional characteristics, fingerprints and impurities. Thromb. Haemost., 2009, 102 (5), 846-53.
175. Loganathan, D.; Wang, H. M.; Mallis, L. M.; Linhardt, R. J.; Structural variation in the antithrombin III binding site region and its occurrence in heparin from different sources. Biochemistry, 1990, 29 (18), 4362-4368.
176. Low molecular mass heparin. European Pharmacopoeia 01/2008:0828, 6.0 ed.; European Directorate for the Quality of Medicine & HealthCare, January, 2008, Strasbourg.

177. Ma, Q.; Cornelli, U.; Hanin, I.; Jeske, W. P.; Linhardt, R. J.; Walenga, J. M.; Fareed, J.; Lee, J. M.; Heparin oligosaccharides as potential therapeutic agents in senile dementia. Curr. Pharm. Des., 2007, 13 (15), 1607-1616.
178. Ma, Q.; Schultz, C.; Neville, B.; Jeske, W.; Hoppensteadt, D.; Cornelli, U.; Lee, J.; Lorens, S.; Hanin, I.; Fareed, J.; Pharmacodynamics and pharmacokinetics of C3, a heparin-derived oligosaccharide mixture, in nonhuman primates. 2003, Thromb. Res., 2003, 112 (4), 249-255.
179. Madine, J.; Clayton, J. C.; Yates, E. A.; Middleton, D. A.; Exploiting a (13)C-labelled heparin analogue for in situ solid-state NMR investigations of peptide-glycan interactions within amyloid fibrils. Org. Biomol. Chem., 2009, 7 (11), 2414-2420.
180. Maruyama, T.; Toida, T.; Imanari, T.; Yu, G.; Linhardt, R. J.; Conformational changes and anticoagulant activity of chondroitin sulfate following its O-sulfonation. Carbohydr. Res., 1998. 306 (1-2), 35-43.
181. Mascellani, G.; Guerrini, M.; Torri, G.; Liverani, L.; Spelta, F.; Bianchini, P. Characterization of di- and monosulfated, unsaturated heparin disaccharides with terminal N-sulfated 1,6-anhydro-β-D-glucosamine or N-sulfated 1,6-anhydro-β-D-mannosamine residues. Carbohydr. Res., 2007, 342, 835-842.
182. Matou, S.; Colliec-Jouault, S.; Galy-Fauroux, I.; Ratiskol, J.; Sinquin, C.; Guezennec, J.; Fischer A.M.; Helley, D.; Effect of an oversulfated exopolysaccharide on angiogenesis induced by fibroblast growth factor-2 or vascular endothelial growth factor in vitro. Biochem. Pharmacol., 2005, 69., 751-759.
183. MatrixDB website <http://matrixdb.ibcp.fr/index.html>
184. Mayer, M. and Meyer, B.; Characterization of Ligand Binding by Saturation Transfer Difference NMR Spectroscopy. Angew. Chem. Int. Ed., 1999, 38, 12, 1784-1788.
185. Mayer, M.; Meyer, B. Group epitope mapping by saturation transfer difference NMR to identify segments of a ligand in direct contact with a protein receptor. J. Am. Chem. Soc., 2001, 123, 6108-6117.
186. McCoy, A. J.; Pei, X. Y.; Skinner, R.; Abrahams, J. P.; Carrell, R. W.; Structure of beta-antithrombin and the effect of glycosylation on antithrombin's heparin affinity and activity. J. Mol. Biol., 2003, 326 (3), 823-833.
187. McKee, J.; Bairstow, S.; Szabo, C.; Ray, J.; Wielgos, T.; Hu, P.; Chess, E.; Nordhaus, M.; Hai, T.; Campbell, J.; Donovan, S.; Riedel, N.; Cammack, J.; Johnson, R.; Viseux, N.; Structure Elucidation and Biological Activity of the Oversulfated Chondroitin Sulfate Contaminant in Baxter Heparin. J. Clin. Pharmacol., 2010.
188. McLaurin, J.; Franklin, T.; Zhang, X.; Deng, J.; Fraser, P. E.; Interactions of Alzheimer amyloid-beta peptides with glycosaminoglycans effects on fibril nucleation and growth. Eur. J. Biochem., 1999, 266 (3), 1101-1110.
189. McLaurin, J.; Fraser, P. E.; Effect of amino-acid substitutions on Alzheimer's amyloid-beta peptide-glycosaminoglycan interactions. Eur. J. Biochem., 2000, 267 (21), 6353-6361.
190. Mikhailov, D.; Linhardt, R. J.; Mayo, K. H.; NMR solution conformation of heparin-derived hexasaccharide. Biochem. J., 1997, 328 (1), 51-61.
191. Morris, G. M.; Goodsell, D. S.; Huey, R.; Olson, A.J.; Distributed automated docking of flexible ligands to proteins: parallel applications of AutoDock 2.4. J. Comput. Aided Mol. Des., 1996, 10, 293–304.
192. Morris, G. M.; Goodsell, D. S.; Halliday, R. S.; Huey, R.; Hart, W. E.; Belew, R. K.; Olson, A. J.; Automated docking using a Lamarckian genetic algorithm and an empirical binding free energy

function. J. Comp. Chem., 1998, 19 (14), 1639-1662.
193. Moseley, H. N.; Curto, E. V. and Krishna N. R.; Complete relaxation and conformational exchange matrix (CORCEMA) analysis of NOESY spectra of interacting systems; two-dimensional transferred NOESY. J. Magn. Reson. Ser. B, 1995, 108, 243–261.
194. Motamedi-Shad, N.; Monsellier, E.; Chiti, F.; Amyloid formation by the model protein muscle acylphosphatase is accelerated by heparin and heparan sulphate through a scaffolding-based mechanism. J. Biochem., 2009, 146 (6), 805-814. [a]
195. Motamedi-Shad, N.; Monsellier, E.; Torrassa, S.; Relini, A.; Chiti, F.; Kinetic Analysis of Amyloid Formation in the Presence of Heparan Sulfate. J. Biol. Chem., 2009, 284 (43), 29921-29934. [b]
196. Mourier, P.; Viskov, C. US. Patent 2005/0119477 A1; Chem. Abstr. 142:89363.
197. Mousa, S. A. Heparin and low molecular weight heparin in thrombosis and inflammation: emerging link. Semin. Thromb. Hemost., 2007, 33 (5), 524-533.
198. Mulloy, B.; Forster, M. J.; Jones, C. and Davies, D. B.; NMR molecular modeling studies of the solution conformation of heparin. Biochem. J., 1993, 293, 849–858.
199. Mulloy, B.; Forster, M. J.; Conformation and dynamics of heparin and heparan sulfate. Glycobiology, 2000, 10 (11), 1147-1156.
200. Muñoz, E.M.; Linhardt. R.J.; Heparin-binding domains in vascular biology. Arter. Thromb. Vasc. Biol., 2004, 24, 1549–1557.
201. Murphy, R. M.; Pallitto, M. M.; Probing the kinetics of beta-amyloid self-association. J. Struct. Biol., 2000, 130 (2-3), 109-122.
202. Murray, G. D.; Best, C. H.; The Use of Heparin in Thrombosis. Ann. Surg., 1938, 108 (2), 163-77.
203. Myszka, D. G.; Wood, S. J.; Biere, A. L.; Analysis of fibril elongation using surface plasmon resonance biosensors. Methods Enzymol., 1999, 309, 386-402.
204. Nader, H. B.; Chavante, S. F.; dos-Santos, E. A.; Oliveira, T. W.; de-Paiva, J. F.; Jeronimo, S. M.; Medeiros, G. F.; de-Abreu, L. R.; Leite, E. L.; de-Sousa-Filho, J. F.; Castro, R. A.; Toma, L.; Tersariol, I. L.; Porcionatto, M. A.; Dietrich, C. P.; Heparan sulfates and heparins: similar compounds performing the same functions in vertebrates and invertebrates? Braz. J. Med. Biol. Res., 1999, 32 (5), 529-538.
205. Narindrasorasak, S.; Lowery, D.; Gonzalez-DeWhitt, P.; Poorman, R. A.; Greenberg, B.; Kisilevsky, R.; High affinity interactions between the Alzheimer's beta-amyloid precursor proteins and the basement membrane form of heparan sulfate proteoglycan. J. Biol. Chem., 1991, 266 (20), 12878-12883.
206. Neville, G. A.; Mori, F.; Holme, K. R; Perlin, A. S.; Monitoring the purity of pharmaceutical heparin preparations by high-field 1H-nuclear magnetic resonance spectroscopy. J. Pharm. Sci., 1989, 78, 101–104.
207. Newall, F.; Johnston, L.; Summerhayes, R.; Lane, G.; Cranswick, N.; Monagle, P.; Ignjatovic, V.; Novel interactions between UFH and TFPI in children. Br. J. Haem., 2010, 151, 376–380.
208. Olson, S. T.; Björk, I.; Role of protein conformational changes, surface approximation and protein cofactors in heparin-accelerated antithrombin-proteinase reaction. In: Lane, D.A., Björk, I., Lindahl, U., eds. Heparin and Related Polysaccharides. New York: Plenum Press, 1992, 155–166.
209. Olson, S. T.; Björk, I.; Sheffer, R.; Craig, P.A.; Shore, J.D.; Choay, J.; Role of antithrombin-binding pentasaccharide in heparin acceleration of antithrombin-proteinase reaction. Resolution

of the antithrombin conformational change contribution to heparin rate enhancement. J. Biol. Chem., 1992, 267, 12528–12538 [b].

210. Olson, S. T.; Björk, I.; Shore, J. D.; Kinetic characterization of heparin-catalyzed and uncatalyzed inhibition of blood coagulation proteinases by antithrombin. Methods. Enzymol., 1993, 22, 525-559.
211. Ori, A.; Wilkinson, M. C.; Fernig, D. G.; The heparanome and regulation of cell function: structures, functions and challenges. Front. Biosci., 2008, 13, 4309-4338.
212. Otis, S. A.; Zehnder, J. L.; Heparin-induced thrombocytopenia: current status and diagnostic challenges. Am. J. Hematol., 2010, 85 (9), 700-706.
213. Palmer, A. G.; Cavanagh, J.; Wright, P. E. and Rance, M.; Sensitivity improvement in proton-detected two-dimensional heteronuclear correlation NMR spectroscopy. J. Magn. Res., 93 (1), 151-170.
214. Parish, C.R.; Freeman, C.; Brown, K.J.; Francis, D.J.; Cowden, W.B.; Identification of sulfated oligosaccharide-based inhibitors of tumor growth and metastasis using novel in vitro assays for angiogenesis and heparanase activity. Cancer. Res., 1999, 59, 3433-3441.
215. Peat, R. A.; Gecz, J.; Fallon, J. R.; Tarpey, P. S.; Smith, R.; Futreal, A.; Stratton, M. R.; Lamande, S. R.; Yang, N.; North, K. N.; Exclusion of biglycan mutations in a cohort of patients with neuromuscular disorders. Neuromuscul. Disord., 2008, 18 (8), 606-609.
216. Pejler, G.; Danielsson, A.; Bjõrk, I.; Lindahl, U.; Nader, H.B.; Dietrich, C.P.; Structure and antithrombin binding properties of heparin isolated from the clams Anomalocardia brasiliana and Tivela macroides. J. Biol. Chem, 1987, 262, 11413–11421.
217. Pellegrini, L.; Burke, D. F.; von Delft, F.; Mulloy, B.; Blundell, T. L.; Crystal structure of fibroblast growth factor receptor ectodomain bound to ligand and heparin. Nature, 2000, 407, 6807, 1029-1034.
218. Perlmutter, L. S.; Chui, H. C.; Saperia, D.; Athanikar, J.; Microangiopathy and the colocalization of heparan sulfate proteoglycan with amyloid in senile plaques of Alzheimer's disease. Brain. Res., 1990, 508 (1), 13-19.
219. Petitou, M.; Lormeau, J-C.; Perly, B.; Berthault, P.; Bonnesec, V.; Sié, P.; Choay, J.; Is there a unique sequence in heparin for interaction with heparin cofactor II? Structural and biological studies of heparin-derived oligosaccharides. J. Biol. Chem., 1988, 263, 8685–8690.
220. Petitou, M.; Jaurand, G.; Derrien, M.; Duchaussoy, P.; Choay, J.; A new, highly potent, heparin-like pentasaccharide fragment containing a glucose residue instead of a glucosamine. Bioorg. Med. Chem. Lett., 1991, 1, 95–98.
221. Petitou, M.; Herault, J.P.; Bernat, A.; Driguez, P.A.; Duchaussoy, P.; Lormeau, J.C.; Herbert, J.M.; Synthesis of thrombin-inhibiting heparin mimetics without side effects. Nature, 1999, 398, 417–422.
222. Petitou, M.; van Boeckel, C. A. A synthetic antithrombin III binding pentasaccharide is now a drug! What comes next? Angew. Chem. Int. Ed., 2004, 43, 3118–3133.
223. Petkova, A. T.; Ishii, Y.; Balbach, J. J.; Antzutkin, O. N.; Leapman, R. D.; Delaglio, F.; Tycko, R.; A structural model for Alzheimer's beta -amyloid fibrils based on experimental constraints from solid state NMR. Proc. Natl. Acad. Sci. U S A, 2002, 99 (26), 16742-16747.
224. Petkova, A. T.; Yau, W. M.; Tycko, R.; Experimental constraints on quaternary structure in Alzheimer's beta-amyloid fibrils. Biochemistry, 2006, 45 (2), 498-512.
225. Pimplikar, S. W.; Reassessing the amyloid cascade hypothesis of Alzheimer's disease. Int. J. Biochem. Cell Biol., 2009, 41 (6), 1261-1268.

226. Plotnick, M.I.; Mayne, L.; Schechter, N.M.; Rubin, H.; Distortion of the active site of chymotrypsin complexed with a serpin. Biochemistry, 1996, 35, 7586–7590.
227. Prydz, K; Dalen, K.T.; Synthesis and sorting of proteoglycans. J. Cell. Sci., 2000, 113, 193-205.
228. Ragazzi, M.; Ferro, D.M.; Provasoli, M.; A force-field study of the conformational characteristics of the iduronate rings. J. Comp. Chem., 1986; 7, 105-12.
229. Ragazzi, M.; Ferro, D. R.; Perly, B.; Torri, G.; Casu, B.; Sinay, P.; Petitou, M.; Choay, J.; Conformation of the pentasaccharide corresponding to the binding site of heparin to antithrombin-III. Carbohydr. Res., 1987, 165 (1), c1-c5.
230. Raman, R.; Venkataraman, G.; Ernst, S.; Sasisekharan, V.; Sasisekharan, R.; Structural specificity of heparin binding in the fibroblast growth factor family of proteins. Proc. Natl. Acad. Sci. USA, 2003, 100, 2357–2362.
231. Rezaie, A. R.; Calcium enhances heparin catalysis of the antithrombin-factor Xa reaction by a template mechanism. Evidence that calcium alleviates Gla domain antagonism of heparin binding to factor Xa. J. Biol. Chem., 1998, 273 (27), 16824-16827.
232. Riek, R.; Guntert, P.; Dobeli, H.; Wipf, B.; Wuthrich, K.; NMR studies in aqueous solution fail to identify significant conformational differences between the monomeric forms of two Alzheimer peptides with widely different plaque-competence, A beta(1-40)(ox) and A beta(1-42)(ox). Eur. J. Biochem., 2001, 268 (22), 5930-5936.
233. Rolls, A.; Avidan, H.; Cahalon, L.; Schori, H.; Bakalash, S.; Litvak, V.; Lev, S.; Lider, O.; Schwartz, M.; A disaccharide derived from chondroitin sulphate proteoglycan promotes central nervous system repair in rats and mice. Eur. J. Neurosci., 2004, 20 (8), 1973-1983.
234. Rong, J.; Nordling, K.; Björk, I.; Lindahl, U.; A novel strategy to generate biologically active neo-glycosaminoglycan conjugates. Glycobiology, 1999, 9, 1331–1336.
235. Rosenberg, R. D.; Damus, P. S.; The purification and mechanism of action of human antithrombin-heparin cofactor. J. Biol. Chem., 1973, 248 (18), 6490-6505.
236. Rosenfeld, L.; Danishefsky, I.; Location of specific oligosaccharides in heparin in terms of their distance from the protein linkage region in native proteoglycan. J. Biol. Chem, 1988, 263, 262–266.
237. Roychaudhuri, R.; Yang, M.; Hoshi, M. M.; Teplow, D. B.; Amyloid beta -protein assembly and Alzheimer's disease. J. Biol. Chem., 2008, 284 (8), 4749-4753.
238. Rudd, T. R.; Skidmore, M. A.; Guimond, S. E.; Cosentino, C.; Torri, G.; Fernig, D. G.; Lauder, R. M.; Guerrini, M.; Yates, E. A.; Glycosaminoglycan origin and structure revealed by multivariate analysis of NMR and CD spectra. Glycobiology 2009, 19 (1), 52-67.
239. Ruiz-Calero, V.; Saurina, J.; Galceran, M. T.; Hernandez-Cassou, S.; Puignou, L.; Potentiality of proton nuclear magnetic resonance and multivariate calibration methods for the determination of dermatan sulfate contamination in heparin samples. Analyst. 2000, 125 (5), 933-938.
240. Ruiz-Calero, V.; Saurina, J.; Hernandez-Cassou, S.; Galceran, M. T.; Puignou, L.; Proton nuclear magnetic resonance characterisation of glycosaminoglycans using chemometric techniques. Analyst, 2002, 127 (3), 407-415.
241. Ruiz-Calero, V.; Saurina, J.; Galceran, M. T.; Hernandez-Cassou, S.; Puignou, L.; Estimation of the composition of heparin mixtures from various origins using proton nuclear magnetic resonance and multivariate calibration methods. Anal. Bioanal. Chem., 2002, 373 (4-5), 259-265 [b].
242. Rusnati, M.; Tulipano, G.; Spillmann, D.; Tanghetti, E.; Oreste, P.; Zoppetti, G.; Giacca, M.;

Presta, M.; Multiple interactions of HIV-I Tat protein with size-defined heparin oligosaccharides. J. Biol. Chem., 1999, 274 (40), 28198-28205.

243. Sandwall, E.; O'Callaghan, P.; Zhang, X.; Lindahl, U.; Lannfelt, L.; Li, J. P.; Heparan sulfate mediates amyloid-beta internalization and cytotoxicity. Glycobiology, 2010, 20 (5), 533-541.
244. Sasisekharan, R.; Raman, R.; Prabhakar, V.; Glycomics approach to structure-function relationships of glycosaminoglycans. Annu. Rev. Biomed. Eng., 2006, 8, 181-231.
245. Sasisekharan, R.; Shriver, Z.; From crisis to opportunity: a perspective on the heparin crisis. Thromb. Haemost., 2009, 102 (5), 854-858.
246. Schlessinger, J.; Plotnikov, A. N.; Ibrahimi, O. A.; Eliseenkova, A. V.; Yeh, B. K.; Yayon, A.; Linhardt, R. J.; Mohammadi, M.; Crystal structure of a ternary FGF-FGFR-heparin complex reveals a dual role for heparin in FGFR binding and dimerization. Mol. Cell., 2000, 6 (3), 743-750.
247. Schleucher, J.; Schwendinger, M.; Sattler, M.; Schmidt, P.; Schedletzky, O.; Glaser, S. J.; Sorensen, O. W. and Griesinger, C.; A general enhancement scheme in heteronuclear multidimensional NMR employing pulsed field gradients. J. Biomol. NMR, 1994, 4 (2), 301-306.
248. Schreuder, H.A.; de Boer, B.; Dijkema, R.; Mulders, J.; Theunissen, H.J.M.; Grootenhuis, P.D.J.; Hol, W.G.J.; The intact and cleaved human antithrombin III complex as a model for serpin-proteinase interactions. Nat.Struct. Biol., 1994, 1, 48–54.
249. Serpell, L. C.; Alzheimer's amyloid fibrils: structure and assembly. Biochim. Biophys. Acta., 2000, 1502 (1), 16-30.
250. Sharma, A.; Askari, J. A.; Humphries, M. J.; Jones, E. Y.; Stuart, D. I.; Crystal structure of a heparin- and integrin-binding segment of human fibronectin. EMBO J., 1999, 18 (6), 1468-1479.
251. Sheehan, J. P.; Sadler, J. E.; Molecular mapping of the heparin-binding exosite of thrombin. Proc. Natl. Acad. Sci. U S A, 1994, 91 (12), 5518-5522.
252. Shen, C. L.; Scott, G. L.; Merchant, F.; Murphy, R. M.; Light scattering analysis of fibril growth from the amino-terminal fragment beta(1-28) of beta-amyloid peptide. Biophys. J., 1993, 65 (6), 2383-2395.
253. Shively, J. E. and Conrad, H. E.; Formation of anhydrosugars in the chemical depolymerization of heparin. Biochemistry, 1976, 15 (18), 3932-3942.
254. Shriver, Z.; Raman, R.; Venkataraman, G.; Drummond, K.; Turnbull, J.; Toida, T.; Linhardt, R.; Biemann, K.; Sasisekharan, R.; Sequencing of 3-O-sulfate containing heparin decasaccharides with a partial antithrombin III binding site. Proc. Natl. Acad. Sci. USA, 2000, 97, 10359–10364.
255. Shriver, Z.; Sundaram, M.; Venkataraman, G.; Fareed, F.; Linhardt, R.; Biemann, K.; Sasisekharan, R.; Cleavage of the antithrombin III binding site in heparin by heparinases and its implication in the generation of low molecular weight heparin. Proc. Natl. Acad. Sci. USA, 2000, 12, 71–77.
256. Silverman, G. A.; Bird, P. I.; Carrell, R. W.; Church, F. C.; Coughlin, P. B.; Gettins, P. G.; Irving, J. A.; Lomas, D. A.; Luke, C. J.; Moyer, R. W.; Pemberton, P. A.; Remold-O'Donnell, E.; Salvesen, G. S.; Travis, J.; Whisstock, J. C.; The serpins are an expanding superfamily of structurally similar but functionally diverse proteins. Evolution, mechanism of inhibition, novel functions and a revised nomenclature. J. Biol. Chem., 2001, 276 (36), 33293-33296.
257. Sitkowski, J.; Bednarek, E.; Bocian, W.; Kozerski, L.; Assessment of oversulfated chondroitin sulfate in low molecular weight and unfractioned heparins diffusion ordered nuclear magnetic

resonance spectroscopy method. J. Med. Chem., 2008, 51 (24), 7663-7665.
258. Sjoberg, I.; Fransson, L. A.; Structural studies on heparan sulphate from human lung fibroblasts. Characterization of oligosaccharides obtained by selective periodate oxidation of D-glucuronic acid residues followed by scission in alkali. Biochem. J., 1980, 191 (1), 103-110.
259. Skidmore, M. A.; Guimond, S. E.; Dumax-Vorzet, A. F.; Atrih, A.; Yates, E. A. and Turnbull, J. E.; High sensitivity separation and detection of heparan sulfate disaccharides. J. Chromatogr. A, 2006, 1135, 52-56.
260. Skinner, R.; Abrahams, J-P.; Whisstock, J.C.; Lesk, A.M.; Carrell, R.W.; Wardell, M.R.; The 2.6 Å structure of antithrombin indicates a conformational change at the heparin binding site. J. Mol. Biol., 1997, 266, 601–609.
261. Snow, A. D.; Wight, T. N.; Nochlin, D.; Koike, Y.; Kimata, K.; DeArmond, S. J.; Prusiner, S. B.; Immunolocalization of heparan sulfate proteoglycans to the prion protein amyloid plaques of Gerstmann-Straussler syndrome, Creutzfeldt-Jakob disease and scrapie. Lab. Invest., 1990, 63 (5), 601-611.
262. Somsen, G. W.; Tak, Y. H.; Torano, J. S.; Jongen, P. M.; de Jong, G. J.; Determination of over-sulfated chondroitin sulfate and dermatan sulfate impurities in heparin by capillary electrophoresis. J. Chromatogr. A, 2009, 1216 (18), 4107-4112.
263. Soto, C.; Branes, M. C.; Alvarez, J.; Inestrosa, N. C.; Structural determinants of the Alzheimer's amyloid beta-peptide. J. Neurochem., 1994, 63 (4), 1191-1198.
264. Spencer, J. A.; Kauffman, J. F.; Reepmeyer, J. C.; Gryniewicz, C. M.; Ye, W.; Toler, D. Y.; Buhse, L. F.; Westenberger, B. J.; Screening of heparin API by near infrared reflectance and Raman spectroscopy. J. Pharm. Sci., 2009, 98 (10), 3540-3547.
265. Spillmann, D.; Witt, D.; Lindahl, U.; Defining the interleukin-8-binding domain of heparan sulfate. J. Biol. Chem., 1998, 273 (25), 15487-15493.
266. Su, J. H.; Cummings, B. J.; Cotman, C. W.; Localization of heparan sulfate glycosaminoglycan and proteoglycan core protein in aged brain and Alzheimer's disease. Neuroscience, 1992, 51 (4), 801-813.
267. Sudo, M.; Sato, K.; Chaidedgumjorn, A.; Toyoda, H.; Toida, T.; Imanari, T.; (1)H nuclear magnetic resonance spectroscopic analysis for determination of glucuronic and iduronic acids in dermatan sulfate, heparin and heparan sulfate. Anal. Biochem., 2001, 297 (1), 42-51.
268. Sugumaran, G.; Silbert, J. E.; Sulfation of chondroitin. Specificity, degree of sulfation and detergent effects with 4-sulfating and 6-sulfating microsomal systems. J. Biol. Chem., 1988, 263 (10), 4673-4678.
269. Taylor, R.L.; Shively, J.E. and Conrad, H.E.; Stoichiometric reduction of uronic acid carboxyl groups in polysaccharides. Methods Carbohydr. Chem.; 1976, 7, 149-151.
270. Toida, T.; Hileman, R.E.; Smith, A.E.; Vlahova, P. I.; Linhardt, R.J.; Enzymatic preparation of heparin oligosaccharides containing antithrombin III binding sites. J. Biol. Chem., 1996, 271, 32040–32047.
271. Tollefsen, D.M.; The interaction of glycosaminoglycans with Heparin Cofactor II: structure and activity of a high-affinity dermatan sulfate hexasaccharide. In: Lane, D.A., Björk, I., Lindahl, U., eds. Heparin and Related Polysaccharides. New York: Plenum Press, 1992, vol. 425, 35–44, 167–176.
272. Tomski, S. J.; Murphy, R. M.; Kinetics of aggregation of synthetic beta-amyloid peptide. Arch. Biochem. Biophys., 1992, 294 (2), 630-638.
273. Tone, Y.; Kitagawa, H.; Imiya, K.; Oka, S.; Kawasaki, T.; Sugahara, K.; Characterization of

recombinant human glucuronyltransferase I involved in the biosynthesis of glycosaminoglycan-protein linkage region of proteoglycans. FEBS Lett, 1999, 459, 415-420.

274. Trehy, M. L.; Reepmeyer, J. C.; Kolinski, R. E.; Westenberger, B. J.; Buhse, L. F.; Analysis of heparin sodium by SAX/HPLC for contaminants and impurities. J. Pharm. Biomed. Anal., 2009, 49 (3), 670-673.
275. Triguero, L.; Singh, R.; Prabhakar, R.; Comparative molecular dynamics studies of wild-type and oxidized forms of full-length Alzheimer amyloid beta-peptides Abeta(1-40) and Abeta(1-42). J. Phys. Chem. B, 2008, 112, 23, 7123-7131.
276. Tsiang, M.; Jain, A. K.; Gibbs, C. S.; Functional requirements for inhibition of thrombin by antithrombin III in the presence and absence of heparin. J. Biol. Chem., 1997, 272 (18), 12024-12029.
277. Tycko, R.; Molecular structure of amyloid fibrils: insights from solid-state NMR. Q. Rev. Biophys., 2006, 31 (9), 1-55.
278. U.S. Food and Drug Administration, Information on Adverse Event Reports and Heparin. http://www.fda.gov/Drugs/DrugSafety/PostmarketDrugSafetyInformationforPatientsandProviders/ucm1 12669.htm.
279. U.S. Food and Drug Administration, Information on Heparin: Heparin Test Results < http://www.fda.gov/Drugs/DrugSafety/PostmarketDrugSafetyInformationforPatientsandProviders/ucm112597.htm>.
280. Urbanc, B.; Cruz, L.; Yun, S.; Buldyrev, S. V.; Bitan, G.; Teplow, D. B.; Stanley, H. E.; In silico study of amyloid beta-protein folding and oligomerization. Proc. Natl. Acad. Sci. U S A, 2004, 101 (50), 17345-17350.
281. Urbanc, B.; Cruz, L.; Ding, F.; Sammond, D.; Khare, S.; Buldyrev, S. V.; Stanley, H. E.; Dokholyan, N. V.; Molecular dynamics simulation of amyloid beta dimer formation. Biophys J., 2004, 87 (4), 2310-2321 [b].
282. Urbanyi, Z.; Forrai, E.; Sarvari, M.; Liko, I.; Illes, J.; Pazmany, T.; Glycosaminoglycans inhibit neurodegenerative effects of serum amyloid P component in vitro. Neurochem. Int., 2005, 46 (6), 471-477.
283. van Boeckel, C. A. A.; Petitou, M. The unique antithrombin III binding domain of heparin: a lead to new synthetic antithrombotics. Angew. Chem. Int. Ed., 1993, 32, 1671-1818.
284. van den Berg, R. A.; Hoefsloot, H. C.; Westerhuis, J. A.; Smilde, A. K. and van der Werf, M. J.; Centering, scaling and transformations: improving the biological information content of metabolomics data. BMC Genomics, 2006, 7, 142.
285. van Horssen, J.; Wesseling, P.; van den Heuvel, L. P.; de Waal, R. M.; Verbeek, M. M.; Heparan sulphate proteoglycans in Alzheimer's disease and amyloid-related disorders. Lancet Neurol., 2003, 2 (8), 482-492.
286. Verbeek, M. M.; Otte-Holler, I.; van den Born, J.; van den Heuvel, L. P.; David, G.; Wesseling, P.; de Waal, R. M.; Agrin is a major heparan sulfate proteoglycan accumulating in Alzheimer's disease brain. Am. J. Pathol., 1999, 155 (6), 2115-2125.
287. Viskov, C.; Just, M.; Laux, V.; Mourier, P.; Lorenz, M. Description of the chemical and pharmacological characteristics of a new hemisynthetic ultra-low-molecular-weight heparin, AVE5026. J. Thromb. Haemost., 2009, 7, 1143-1151.
288. Volpi, N.; Maccari, F.; Linhardt, R. J.; Quantitative capillary electrophoresis determination of oversulfated chondroitin sulfate as a contaminant in heparin preparations. Anal. Biochem., 2009, 388 (1), 140-145.

289. Walzer, M.; Lorens, S.; Hejna, M.; Fareed, J.; Hanin, I.; Cornelli, U.; Lee, J. M.; Low molecular weight glycosaminoglycan blockade of beta-amyloid induced neuropathology. Eur. J. Pharmacol., 2002, 445 (3), 211-220.
290. Wang, L.; Buchanan, S.; Meyerhoff, M. E.; Detection of high-charge density polyanion contaminants in biomedical heparin preparations using potentiometric polyanion sensors. Anal. Chem., 2008, 80 (24), 9845-7.
291. Watanabe, N.; Araki, W.; Chui, D. H.; Makifuchi, T.; Ihara, Y.; Tabira, T.; Glypican-1 as an Abeta binding HSPG in the human brain: its localization in DIG domains and possible roles in the pathogenesis of Alzheimer's disease. FASEB J., 2004, 18 (9), 1013-1015.
292. Wielgos, T.; Havel, K.; Ivanova, N.; Weinberger, R.; Determination of impurities in heparin by capillary electrophoresis using high molarity phosphate buffers. J. Pharm. Biomed. Anal., 2009, 49 (2), 319-326.
293. Xian, X.; Gopal, S.; Couchman, J. R.; Syndecans as receptors and organizers of the extracellular matrix. Cell Tissue. Res., 2010, 331 (1), 31-46.
294. Yamada, S.; Yoshida, K.; Sugiura, M.; Sugahara, K.; Khoo, K-K.; Morris, H.R.; Dell, A.; Structural studies on the bacterial lyase-resistant tetrasaccharides derived from the antithrombin III-binding site of porcine intestinal heparin. J. Biol. Chem., 1993, 268, 4780–4787.
295. Yan, D.; Lin, X.; Shaping morphogen gradients by proteoglycans. Cold Spring Harb. Perspect. Biol., 2009, 1 (3), 1-16.
296. Yan, S. D.; Chen, X.; Fu, J.; Chen, M.; Zhu, H.; Roher, A.; Slattery, T.; Zhao, L.; Nagashima, M.; Morser, J.; Migheli, A.; Nawroth, P.; Stern, D.; Schmidt, A. M.; RAGE and amyloid-beta peptide neurotoxicity in Alzheimer's disease. Nature, 1996, 382 (6593), 685-691.
297. Ye, J.; Rezaie, A. R.; Esmon, C. T.; Glycosaminoglycan contributions to both protein C activation and thrombin inhibition involve a common arginine-rich site in thrombin that includes residues arginine 93, 97 and 101. J. Biol. Chem., 1994, (269 (27), 17965-17970.
298. Yu, L.; Edalji, R.; Harlan, J. E.; Holzman, T. F.; Lopez, A. P.; Labkovsky, B.; Hillen, H.; Barghorn, S.; Ebert, U.; Richardson, P. L.; Miesbauer, L.; Solomon, L.; Bartley, D.; Walter, K.; Johnson, R. W.; Hajduk, P. J.; Olejniczak, E. T.; Structural characterization of a soluble amyloid beta-peptide oligomer. Biochemistry, 2009, 48 (9), 1870-1877.
299. Zang, Z.; Weiwer, M.; Li, B.; Kemp, M. M.; Daman, T. H.; Linhardt, R. J. Oversulfated chondroitin sulfate: impact of heparin impurity, associated with adverse events, on low-molecular-weight heparin preparation. J. Med. Chem., 2008, 51, 5498-5501.
300. Zhang, Z.; Li, B.; Suwan, J.; Zhang, F.; Wang, Z.; Liu, H.; Mulloy, B.; Linhardt, R. J.; Analysis of pharmaceutical heparins and potential contaminants using 1H-NMR and PAGE. J. Pharm. Sci., 2009, 98, 4017-4026.
301. Zhu, H.; Yu, J.; Kindy, M. S.; Inhibition of amyloidosis using low-molecular-weight heparins. Mol. Med., 2001, 7 (8), 517-522. Bae, J.; Desai, U. R.; Pervin, A.; Caldwell, E. E.; Weiler, J. M.; Linhardt, R. J.; Interaction of heparin with synthetic antithrombin III peptide analogues. Biochem. J., 1994, 301 (Pt 1), 121-129.
302. Zhu, H.; Yu, J.; Kindy, M. S.; Inhibition of amyloidosis using low-molecular-weight heparins. Mol. Med., 2001, 7 (8), 517-522.

Acknowledgements

9. Acknowledgements

When I started my Ph.D. I knew nothing about spectroscopy and very little about polysaccharides, now that this marvellous journey has finished I can say I know a little more than before. This great experience was possible because someone trusted in me, thus I really want to thank all the friends and the colleagues who have accompanied me.
My friend Dr Luca Mollica was the first one who trusted in my skills and without his help and friendship I would have never decided to start this Ph.D., now that I am succeeding: thank you so much Luca.
My gratitude is also directed towards my mother and my girlfriend, they have supported me for all the path: sometimes it was not simple helping me, but you both continue loving and caring for me.
I want to thank the person who practically gave me the possibility to approach the glycoscience and NMR world: Dr Marco Guerrini, even though he knew I lacked knowledge about NMR and heparin, he trusted in my will to succeed. He taught me most of my spectroscopic knowledge and now that I want to continue in this field, I can say that his help was fundamental to getting me to this point.
During these three years I solved and I tried to solve many problems, mostly related to NMR and I always found someone ready to listen me, to help me: that person was Cesare Cosentino. He conveyed how interesting it could be to see the molecules from the perspectives of a magnetic field, I also remember all the occasions spent speaking about photography... great moments.
I absolutely want to thank my English friends who gave me the opportunity to understand, see and live in that wonderful island called Britain and to "breath" in the English research environment: Drs Edwin Yates, Tim Rudd and Mark Skidmore.
Dr. Stefano Elli was not present at the start of my "journey", nevertheless I want to thank him for all the times spent speaking about science, the time spent at the coffee machine, times spent speaking about computers and for all the molecular modeling knowledge he tried to pass me.
I want also to thank Giorgio Eisele, for his contribution to the amyloid work, for the moments spent at the DLS working, laughing and speaking about politics and society.
I also need to thank the people in the lab who taught and helped me with chromatography and all the biochemical approach related to polysaccharides.
Dr. Annamaria Naggi and Dr. Sabrina Bertini were pillars for the entire period involving the DLS/amyloid experiments, I could overcame theoretical and practical hurdles thank to their tips and experiences.
Finally, Dr. Gianciacomo Torri, I would like to thank you for your support and constant encouragement.